Mechanisms and Therapeutic Applications of RNA Delivery by Small Extracellular Vesicles

Ryan Reshke

Thesis submitted to the University of Ottawa
in partial fulfillment of the requirements for the
Doctorate in Philosophy degree in Cellular and Molecular Medicine

Department of Cellular and Molecular Medicine
Faculty of Medicine
University of Ottawa

Abstract

MicroRNAs (miRNAs) are short non-coding RNA molecules that function in a ribonucleoprotein complex to silence gene expression through inhibition of translation and messenger RNA (mRNA) decay of complementary mRNAs. Short interfering RNAs (siRNAs) harness the same silencing machinery to enzymatically cleave complementary mRNAs leading to highly selective and potent reduction of gene expression. siRNAs represent a new class of therapeutics that have been approved for use against multiple disease-associated genes in the liver. Unfortunately, widespread use of siRNA therapeutics for the treatment of disorders in organs other than the liver has been hindered by difficulties delivering siRNAs into the cytoplasm of target cells. While existing delivery technologies have enabled reliable delivery in the liver, novel approaches are needed to unlock the full potential of siRNA therapeutics. Small extracellular vesicles (sEVs) are released from most cell types and travel through the body to deliver their contents, including microRNAs (miRNAs) into recipient cells. It has been suggested that they have evolved to be highly efficient at cargo delivery into a diverse population of tissues and cell types, making them an attractive option for delivery of siRNA therapeutics if they can be effectively packaged. This thesis is comprised of three manuscripts focusing on a novel mechanism for loading siRNAs into sEVs for therapeutic use.

The first manuscript (Reshke, Taylor, Savard *et al.* 2020) describes our discovery that an RNA structure can be applied to package siRNAs into sEVs for efficient delivery into target cells. Specifically, we show that pre-miR-451, which has a uniquely short pre-miRNA hairpin is highly enriched in sEVs in almost all cell types. Importantly, changing the sequence of the short pre-miR-451 hairpin to include siRNA sequences causes those sequences to be packaged into sEVs as well, confirming that the packaging is dependent on the pre-miR-451 hairpin structure. We produce cell

lines stably expressing siRNAs in the pre-miR-451 hairpin structure that release sEVs loaded with up to 30 copies of siRNA and use them to reduce target mRNA expression *in vitro* and in mice. We confirm that sEVs loaded with siRNA using the pre-miR-451 hairpin can deliver their siRNA cargo into cells of multiple organs beyond the liver including the kidney and small intestine, and do so more efficiently than synthetic lipid nanoparticles (LNPs) or sEVs loaded using other leading technologies like electroporation.

The second manuscript (Dutta, Reshke *et al.* Submitted 2022) explores the feasibility of using these siRNA-loaded sEVs as therapeutics. We show that tangential flow filtration (TFF) is an ideal method for sEV production as it increases yield over 10-fold versus ultracentrifugation, and generates an sEV product that shows no signs of immunogenicity or toxicity in cultured human blood or in mice. We demonstrate the clinical relevance of sEVs in three distinct mouse models of chronic kidney disease (CKD), showing that siRNA can be delivered into kidney glomeruli knocking down disease-associated TRPC6 and APOL1 leading to improved kidney function and pathology. Finally, we show that sEV treatment can be scaled to reduce targets in larger animal models like rabbits.

In the third manuscript (Reshke *et al.* in preparation 2023) we explore the mechanism that facilitates the active sorting of pre-miR-451 and other sequences in the pre-miR-451 hairpin structure into sEVs. We determine that the protein Midkine (MDK) is involved in this process and our data supports a model in which it shuttles pre-miR-451 into sEVs by physically binding to pre-miR-451 hairpins through a previously unknown RNA binding ability.

Together, data presented here demonstrates that novel RNA binding proteins (RBPs) can play important biological roles outside of their known functions. One of these functions, the sorting of pre-miR-451 hairpins into sEVs by MDK, can be repurposed to effectively load siRNA into

sEVs, generating a highly potent potential therapeutic that will hopefully unlock the capability of siRNA to treat a wide range of diseases in human patients.

Acknowledgements

As I reflect on the years I've spent working on this PhD, it is easy for me to see just how many people have played a part in the completion of this project.

I first want to thank my supervisor, Dr. Derrick Gibbings, for taking a chance on me when he hired me over seven years ago, for later encouraging me to pursue a PhD and, most of all, for providing knowledge, guidance, and support through it all. He has undoubtably helped me become a better scientist, and a better person. I would also like to thank the members of my thesis advisory committee, Dr. Stephen Ferguson, Dr. Tommy Alain, and Dr. Carolina Ilkow for their years of support and for always being available to lend advice and guidance. They always helped to remind me just how exciting science is.

I would like to thank all of the members of the Gibbings lab, past and present, who made it so that coming to the lab every day never felt like work. I have made lifelong friends in the lab, and I can't wait to see what else you all accomplish. A special thank you to Dr. James Taylor, Dr. Alexandre Savard, and Dr. Kallol Dutta, I couldn't have done this without each one of you. And to all of my co-authors and collaborators, this thesis would not tell the story that it does without each of your contributions, I am eternally grateful.

Thank you to all of my family and friends for always supporting me, it has never gone unnoticed; and especially to my parents and my sister who have always believed I could do anything I set my mind to. Finally, to Allison and Lorna, thank you for always encouraging me to learn, always understanding when evenings and weekends were spent at the lab, and for inspiring me every day. This is for you.

Table of Contents

List of Figures

List of Supplementary Figures

List of Tables

List of Abbreviations

32P	Phosphorus-32
AAV	Adeno-associated virus
ACE	Angiotensin-converting enzyme
ADR	Adriamycin
AEV	Autophagic extracellular vesicles
AF4	Asymmetric flow field-flow fractionation
AGO	Argonaute
AIMP	Aminoacyl TRNA Synthetase Complex Interacting Multifunctional Protein
ALIX	ALG-2 interacting protein X
ALT	Alanine transaminase
AMPK	AMP-activated protein kinase
ANOVA	Analysis of variance
APOL1	Apolipoprotein L1
AR	Angiotensin receptor
ARF6	ADP ribosylation factor 6
ARMMs	Arrestin domain-containing protein 1 (ARRDC1)-mediated microvesicles
ARRDC1	Arrestin domain-containing protein 1
ASGPR	Asialoglycoprotein receptor
αSMA	Alpha-smooth muscle actin
ASO	Antisense oligonucleotide
AST	Aspartate transaminase
ATP	Adenosine triphosphate
BACE1	Beta-site APP cleaving enzyme 1
BBB	Blood brain barrier
bp	Base pair
BSA	Bovine serum Albumin
BUN	Blood urea nitrogen
CAG	Chicken beta-actin promoter
cGMP	Current Good Manufacturing Practice
CKD	Chronic kidney disease
CLIP	Cross-linking and immunoprecipitation
c-MET	Mesenchymal-epithelial transition factor
CMV	Cytomegalovirus
CPP	ell penetrating peptide
Ct	Cycle threshold
Ctgf	Connective tissue growth factor
DAPI	4′,6-diamidino-2-phenylindole
DCP1A	mRNA-decapping enzyme 1A
DCP2	mRNA-decapping enzyme 2
DDX6	DEAD-Box Helicase 6

DIG	Digoxigenin
DiR	DiIC18(7); 1,1′-dioctadecyl-3,3,3′,3′-tetramethylindotricarbocyanine iodide
DMEM	Dulbecco's Modified Eagle Medium
DNA	Deoxyribonucleic acid
DNase	Deoxyribonuclease
DOX	Doxycycline
DPX	Dibutylphthalate polystyrene xylene
DTT	Dithiothreitol
ECL	Enhanced chemiluminescence
EDTA	Ethylenediaminetetraacetic acid
EGFP	Enhanced green fluorescent protein
EGFR	Epidermal growth factor receptor
eIF	Eukaryotic initiation factor
ELISA	Enzyme-linked immunosorbent assay
EM	Electron microscopy
EMR1	EGF-like molecule containing mucin-like hormone receptor 1
EMSA	Electrophoretic mobility shift assay
Eps15	Epidermal Growth Factor Receptor Pathway Substrate 15
ESCRT	Endosomal sorting complexes required for transport
ESRD	End stage renal disease
EV	Extracellular vesicle
FBS	Fetal bovine serum
FDA	The United States Food and Drug Administration
FISH	Fluorescence in situ hybridization
FSGS	Focal segmental glomerulosclerosis
GalNAc	N-Acetylgalactosamine
GAPDH	Glyceraldehyde 3-phosphate dehydrogenase
G-CSF	Granulocyte colony-stimulating factor
GFAP	Glial fibrillary acidic protein
GFP	Green fluorescent protein
GFR	Glomerular filtration rate
GM-CSF	Granulocyte-macrophage colony-stimulating factor
GTP	Guanosine triphosphate
GusB	Beta-glucuronidases
H&E	Hematoxylin and eosin stain
HAcO	Acetic acid
HA-ESKD	Hypertension-attributed end stage kidney disease
HEPES	4-(2-hydroxyethyl)-1-piperazineethanesulfonic acid
HIVAN	HIV-associated nephropathy
hnRNPA2B1	Heterogeneous Nuclear Ribonucleoprotein A2/B1
HRP	Horseradish peroxidase
Hrs	hepatocyte growth factor-regulated tyrosine kinase substrate
HuB	ELAV Like RNA Binding Protein 2

HuR	ELAV Like RNA Binding Protein 1
IFN	Interferon
IgG	Immunoglobulin G
IL	Interleukin
IP	Immunoprecipitation
IP-10	Interferon gamma-induced protein 10
IRES	Internal ribosome entry site
ISG15	Interferon-stimulating gene 15
IV	Intravenous
IVIS	In vivo imaging system
kb	Kilobases
KH	K-homology domain
KRAS	Kirsten rat sarcoma virus
LBP	Laminin binding protein precursor
LCMS	Liquid chromatography–mass spectrometry
LNA	Locked nucleic acid
lncRNA	Long noncoding RNA
LNP	Lipid nanoparticle
LRP	Low-density lipoprotein receptor related protein
MDK	Midkine
MEF	Mouse embryonic fibroblast
MEM/HBSS	Minimum Essential Medium - Eagle with Hank's Balanced Salts
MHC	Major histocompatibility complex
MIP-1a	Macrophage Inflammatory Protein 1 alpha
miRNA	MicroRNA
M-MuLV	Moloney Murine Leukemia Virus
mRNA	Messenger ribonucleic acid
MS	Mass spectrometry
MSC	Mesenchymal stem cell
Mtpn	Myotrophin
MVB	Multivesicular body
MVP	Major Vault Protein
NS	Not significant
nSMase2	Neutral sphingomyelinase 2
nt	Nucleotide
NTA	Nanoparticle Tracking Analysis
OCT	Optimal cutting temperature compound
PABPC	Poly(A)-binding protein
PAGE	Polyacrylamide gel electrophoresis
PAK4	Serine/threonine-protein kinase PAK 4
PAS	Periodic Acid-Schiff
P-bodies	Processing bodies

PBS	Phosphate-buffered saline
PCSK9	Proprotein convertase subtilisin/kexin type 9
PEG	Polyethylene glycol
PFA	Paraformaldehyde
PI3P	Phosphatidylinositol-3-phosphate
PMO	Phosphorodiamidate morpholino oligomer
PNK	T4 Polynucleotide Kinase
PS	Phosphorothioate
PTBP1	Polypyrimidine tract-binding protein 1
PTM	Post-translational modification
PTN	Pleiotrophin
qPCR	Quantitative polymerase chain reaction
RA	Retinoic Acid
RAC1	Ras-related C3 botulinum toxin substrate 1
RBD	RNA-binding domain
RBP	RNA binding protein
RISC	RNA-induced silencing complex
RNA	Ribonucleic acid
RNAi	RNA interference
RNase	Ribonuclease
RNP	Ribonucleoprotein
RRM	RNA recognition motif
RT-qPCR	reverse transcription quantitative real-time polymerase chain reaction
SDS	Sodium dodecyl sulfate
SEC	Size exclusion chromatography
s.e.m	Standard error of the mean
sEV	Small extracellular vesicle
SF	Serum free
siRNA	Short interfering RNA
SNAP	Soluble N-ethylmaleimide-sensitive fusion attachment protein
SNARE	soluble N-ethylmaleimide-sensitive fusion attachment protein receptor
snRNA	Small nuclear RNAs
SOD1	Superoxide dismutase 1
SSC	Saline-sodium citrate
STAM	Signal transduction adaptor molecule
STAU1	Staufen Double-Stranded RNA Binding Protein 1
SUMO	Small ubiquitin-related modifiers
SYNCRIP	Synaptotagmin-binding, cytoplasmic RNA-interacting protein
T_A	Melting temperature
TBE	Tris/Borate/EDTA
TBST	Tris-buffered saline with Tween-20
TetR	Tet Repressor protein

TFA	Trifluoroacetic acid
TFF	Tangential Flow Filtration
Tfrc	Transferrin Receptor
TMB	3,3',5,5'-Tetramethylbenzidine
TNF	Tumor necrosis factor
TRBP	transactivation response element RNA-binding protein
TRIM25	Tripartite Motif Containing protein 25
tRNA	Transfer RNA
TRPC6	Transient Receptor Potential Cation Channel 6
TSG101	Tumor susceptibility gene 101
TTR	Transthyretin
UBL	ubiquitin-like modifiers
UTR	Untranslated region
UUO	Unilateral ureteral obstruction
UV	Ultraviolet
VEGF	Vascular endothelial growth factors
VPS4	Vacuolar protein sorting-associated protein 4
VTA1	Vesicle Trafficking protein 1
WT	Wild-type
XRN1	5’ to 3’ exonuclease 1
YBX-1	Y-Box Binding Protein 1

Chapter 1 - Introduction

1.1 RNA interference

RNA interference (RNAi) is a conserved process through which small noncoding RNA molecules can regulate gene expression. The first such small RNA to be identified, *lin-4*, was found in *Caenorhabditis elegans* by Lee *et al.* in 1993[1]. The *lin-4* gene was found to produce two short RNA products, one approximately 22 nucleotides (nt) in length, and one stem loop of approximately 61 nt that had sequence complementarity to regions of the *lin-14* 3'- untranslated region (UTR) and controlled LIN-14 protein levels through translational repression[1, 2]. In 1998, Fire *et al.* showed that injecting exogenous, double stranded RNAs with sequence complementarity to RNAs from numerous different genes causes a specific reduction of protein products from those genes[3, 4]. Though they weren't termed as such at the time, these two seminal studies discovered the two key non-coding RNA types involved in RNAi: microRNA (miRNA) and short interfering RNA (siRNA), respectively.

1.1.1 MicroRNA

Canonical miRNAs are generated from an RNA stem loop, or hairpin, structure through two cleavage events. First, in the nucleus, the Ribonuclease (RNase) III endonuclease Drosha cleaves approximately 11 base pairs (bp), or one helical turn of a double stranded RNA, from the base of the hairpin removing it from the transcript and forming a pre-miRNA of approximately 65 nt[5]. The pre-miRNA hairpin is then exported to the cytoplasm, typically by the karyopherin Exportin-5 and GTP-binding nuclear protein, Ran-GTP where the second cleavage event occurs[6]. Recently, it was shown that Exportin-5 is not critical in this process, and in its absence alternative mechanisms can facilitate nuclear export[6, 7]. The second cleavage event, by the RNase III endonuclease Dicer, cuts approximately 22 bp, or two helical turns of a double stranded RNA,

from the 3' overhang left by Drosha processing, producing a double stranded RNA of approximately 22 nt with a 5' phosphate and a 3' overhang of 2 nt[5, 8]. In almost all cases, this cleavage removes the loop portion of the hairpin. The transactivation response element RNA-binding protein (TRBP), a tightly associated Dicer effector, assists with RNA binding and discrimination of substrates to ensure that Dicer cuts double stranded RNAs containing the 2 nt 3' overhang[9].

Dicer and TRBP then load the RNA duplex onto one of four Argonaute (AGO) proteins, AGO1-4, forming a ribonucleoprotein complex, the RNA-induced silencing complex (RISC)[10]. After loading, the passenger strand of the RNA duplex is removed either through cleavage, when the two strands are perfectly complementary in the central region of the duplex, or through unwinding and subsequent degradation. AGO2 was long thought to be the only Argonaute protein that possesses the slicing activity that enables passenger strand removal by cleavage, though it is now recognized that AGO1 is also able to remove passenger strands through slicing[8, 11]. Guide versus passenger strand selection is determined by thermodynamic stability, specifically the strand with the less stable 5' end typically becomes the guide strand, as it binds more readily to the 5' miRNA binding pocket of Argonautes[12]. Removal of the passenger strand leaves the RISC in its active form where base complementarity of the remaining miRNA strand, particularly bases 2-8 which represent the seed region, determine the target mRNAs[8].

In almost all cases in mammals, miRNAs have non-complete base complementarity with regions within the 3' UTR of many target mRNAs and guide RISC to the site to facilitate translational repression and/or mRNA degradation. Effective mRNA translation relies on the interaction of the Eukaryotic initiation factor 4F (eIF4F) complex (consisting of three proteins, eIF4A, eIF4E and eIF4G) with the mRNA 5' cap and binding of the mRNA poly(A) tail by the

cytoplasmic poly(A)-binding protein (PABPC). Interaction between eIF4G and PABPC brings the two ends of the transcript together, circularizing the mRNA. This greatly increases translation efficiency by promoting recruitment of the 40S and 60S ribosomal subunits by eIF4E and the eukaryotic translation initiation factor 3 (eIF3)[5, 13]. RISC binding to mRNA can cause translational repression prior to initiation through multiple mechanisms including direct competition with eIF4E for 5' cap binding, repression of 60S ribosome recruitment through interaction of AGO proteins with eIF6, a critical protein for maturation of 60S ribosomal subunits, and deadenylation of the poly(A) tail, which inhibits PABPC binding to the tail and subsequent circularization of the mRNA[5, 13]. Translational repression can also occur post-initiation, whereby RISC binding to the 3'-UTR stimulates ribosomes to drop from the translating mRNA[14, 15]. The promoter used to transcribe the target mRNA plays a role in determining through which mechanism RISC will facilitate translational repression[16]. Alternatively, RISC can also induce degradation of the target mRNA. In this case, the miRNA-loaded AGO protein interacts with GW182, a trinucleotide-repeat-containing protein, that subsequently binds PABPC at the poly(A) tail and promotes deadenylation by the CAF1-CCR4-NOT complex and decapping by the mRNA decapping enzyme DCP2. Deadenylated and decapped mRNAs are rapidly degraded by the 5' to 3' exonuclease, XRN1[13, 17, 18]. Mounting evidence suggests that the primary mechanism of gene silencing by miRNA is through degradation of target mRNAs, with translation inhibition being a secondary, less common mechanism[19].

It is estimated that over 60% of human protein-coding genes are regulated by miRNA silencing[20]. The first biological control attributed to miRNA was in *C. elegans*, where *lin-4* RNA regulates levels of Lin-14 protein, leading to changes in protein expression over the course of development, and controlling the timing of different developmental stages[21]. Indeed, miRNA has

now been implicated in the tuning of transcript levels through different stages of development in worms, flies, fish and mammals[22]. miRNAs can also act as cell fate switches, particularly during development. For example, following granulocyte differentiation during granulopoiesis, miR-223 expression is induced, which suppresses the transcription factor NFI-A, itself a negative regulator of miR-223. This feedback loop prevents the cells from returning to an undifferentiated state[23]. While miRNAs can help reduce protein levels to undetectable levels in cells that no longer require it during development, for example, their effects on target levels are often much more subtle, usually causing less than 2-fold reduction, allowing for tuning of protein levels[24]. This is seen in pancreatic islets where miR-375 targets Myotrophin (*Mtpn*). Repression must be finely tuned, as Myotrophin plays a critical role in insulin secretion and thus levels must not deviate far from acceptable levels[25]. These levels must be maintained through adulthood. Overall, regulation of protein output by miRNA is implicated in virtually all biological processes, and generally helps to maintain biological robustness[22, 26]. The dysregulation of miRNAs is seen in multiple neurodegenerative diseases[27] and is often associated with cancer progression. This is observed in patients with myelodysplastic syndrome and acute myeloid leukaemia where loss of miR-29 results in overexpression of DNA methyltransferases, silencing of tumour suppressors and increased tumour proliferation[28].

1.1.2 Short interfering RNA

siRNAs are a second class of short, non-coding RNAs that facilitate RNAi and are structurally and functionally highly similar to miRNA with some notable differences. Unlike miRNA, which are transcribed in the nucleus as long hairpins with imperfect base pairing and are exported to the cytoplasm to be cleaved by Dicer, the precursors for siRNA are perfectly paired, double stranded RNAs in the cytoplasm that can have a number of different origins. In rare cases,

these double stranded RNAs can arise endogenously from genomic regions, like transposons, that produce transcripts containing inverted repeat structures that can form perfectly paired double stranded mRNAs, or through antisense transcription[29, 30]. More frequently, cytoplasmic double stranded RNAs of exogenous origin, such as virus-derived RNAs, are the precursor to siRNAs[31, 32]. Much like miRNA hairpins, these long double stranded RNAs are cleaved into short duplexes of approximately 22 nt in length with 2 nt 3' overhangs by Dicer in the cytoplasm. Alternatively, siRNAs are commonly added to cells exogenously in the lab as research tools by introducing synthetic 22 nt double stranded RNAs into the cytoplasm using techniques like electroporation, or transfection via interactions with cationic polymers[33].

These short double stranded RNAs are then loaded into the AGO proteins, forming the RISC complex. When the RISC complex is formed with AGO1 or AGO2, the passenger strand is removed by slicing, since base complementarity is perfect through the entire duplex, forming the active RISC. Unlike miRNA, which facilitate RNA silencing by RISC through translational repression and mRNA degradation, siRNA facilitates silencing through direct cleavage of its target mRNA, since base complementarity with its target mRNA is perfect. The remaining mature siRNA strand guides RISC to its target mRNA where AGO2, previously the only AGO protein thought to possess slicing activity, cleaves the phosphodiester bond between bases of the mRNA strand complementary to nucleotides 10 and 11 of the siRNA[5]. While it is able to slice siRNA passenger stands, AGO1 is not able to enzymatically cleave mRNA transcripts in a similar fashion to AGO2[11]. AGO3, on the other hand, was recently shown to cleave target mRNAs, similar to AGO2, though only when activated by a very specific set of guide RNAs that are 18 nt or less, which is shorter than most miRNA or siRNA guide strands[34, 35]. For this reason, siRNA-mediated cleavage of mRNA targets is generally considered to be mainly mediated by AGO2. The cleaved mRNA is

subsequently removed from RISC and targeted for further degradation by exonucleases while the active RISC can proceed to silence additional targets[32].

siRNA can achieve highly specific and potent levels of target knockdown of mRNA transcribed from virtually any gene, and importantly, could be used to knock down any disease-causing gene, including those that have not been druggable with other small molecules. This has led to it being widely studied as a potential therapeutic for numerous disorders, with over 20 drugs advancing to clinical trials by 2017[36]. siRNA is not the only RNA-based therapeutic in clinical- and pre-clinical trials, however, so the question arises: what makes a good RNA therapeutic, and is siRNA better than the competition?

1.2 RNA Therapeutics

In order for an RNA therapeutic to be efficient in human patients, it must be non-toxic and non immunogenic, avoid excretion and degradation, have the ability to enter tissues of interest, escape the endosome once taken up by cells and finally, if all of these barriers are overcome, must exert the desired function on its target[37]. Needless to say, with all of these constraints and requirements therapeutic development is not a trivial task.

While many obstacles have been overcome, and though some still remain, in the past decade significant progress has been made in bringing RNA therapeutics to the clinic. As of early 2022 there are 16 RNA therapeutics approved by the United States Food and Drug Administration (FDA)[38]. Eight are antisense oligonucleotide (ASO) treatments, four are siRNA, two are aptamers and two are mRNA vaccines. Additionally, there are three approved Adeno-associated virus (AAV)-based gene replacement therapies[39]. Meanwhile, 28 additional RNA therapeutics are in phase II or III of clinical trials, and countless others are in the pre-clinical development phase[38]. There has been significant excitement around the potential of these therapeutics to treat previously

untreatable diseases, however each comes with its own set of barriers and drawbacks. Here, the focus will be on ASOs, currently the most prominent type of RNA therapeutic on the market, as well as on siRNA therapeutics, a rapidly emerging area of interest.

1.2.1 Antisense oligonucleotides

ASOs are short (typically 8-50 nt long), synthetic, single stranded oligonucleotides that bind to target mRNA sequences through complementary base pairing[40]. When the ASO is made of DNA, or a mixture of DNA and RNA, target binding causes the mRNA target to be cleaved by endogenous RNase H and subsequently degraded by exonucleases. mRNA binding by ASOs composed entirely of RNA causes post-transcriptional regulation of protein synthesis by sterically blocking ribosome recruitment[39]. Importantly, certain ASOs can enter the nucleus to bind pre-mRNA targets. ASOs that bind nuclear targets at splice recognition sites can cause alternative splicing or allow for the specific elimination of particular disease-associated splice variants[41].

Unfortunately, examples of early ASOs were easily degraded by endo- and exonucleases, and therefore turned over too quickly within cells and were largely unsuccessful at knocking down their target mRNAs. This muted much of the early excitement over their potential as a therapeutic platform that might be able to alter a wide range of targets in the body. Since then, significant efforts have been put toward chemically modifying ASOs to increase their resistance to nucleases, increase stability in serum, increase hybridization with target mRNAs, and reduce their toxicity. The first modification was Phosphorothioate (PS) modification of the inter-nucleotide phosphate group. PS-modified ASOs have greatly increased half lives, are nuclease resistant, and interact with plasma proteins, reducing renal clearance. The second class of modifications consists of a series of ribose sugar modifications like 2′-OMe, 2′-MOE, or 2′-fluoro modifications. These modifications increase target binding affinity and again improve nuclease resistance. A third set

of modifications include nucleobase modifications like methylation of 5' cytosines, or incorporation of locked nucleic acids (LNAs), which contain a restrictive methylene linkage between the 2' and 4' carbons of the ribose sugar. These modifications greatly enhance binding to target mRNAs and improve resistance to exonucleases. The most recent ASO therapeutics are phosphorodiamidate morpholino oligomer (PMO) ASOs, which contain some or all of the previously mentioned modifications, as well as an alternative backbone structure consisting of neutral morpholino rings linked through phosphorodiamidate bonds. This modification confers improved efficacy, and greatly reduced toxicity[40, 42].

This work led to the eventual FDA approval of several ASO therapeutics targeting a range of diseases including familial hypercholesterolemia, spinal muscular atrophy, Duchenne muscular dystrophy and familial amyloid polyneuropathy.

The main drawback to ASO therapies is their restricted bioavailability to tissues of interest. To date, systemic administration allows only a small portion of ASOs to reach tissues for cellular uptake, and significant uptake is only observed in the liver and kidneys, while targeted intrathecal administration is required to achieve delivery to the nervous system[40]. Because of this, administered doses needed to achieve target knockdown tend to be high, which can lead to other adverse effects like kidney toxicity, for example[43, 44]. This has left their potential largely untapped, and work is ongoing to try to improve these characteristics in the next generation of ASOs.

1.2.2 siRNA therapeutics

In their Nobel-prize winning 1998 study, Fire *et al.* demonstrated that double stranded RNAs downregulate their target mRNAs more effectively than either of the single strands are capable of individually[3]. This represented the first evidence that siRNAs (double stranded) might represent a better platform for human therapeutics than ASOs (single stranded). However, the first

ASO to receive FDA approval did so in 1998, and four ASO therapeutics received approval before the first siRNA did. This apparent competitive edge for ASOs can partially be explained by the fact that ASOs were first discovered in 1978, 20 years before siRNA[45]. Interestingly, the first ASO therapeutic was approved by the FDA in 1998, 20 years after the discovery of ASOs, while the first siRNA therapeutic received approval in 2018, 20 years after their discovery. However, it took 15 years before the next ASO therapeutic was approved, while four siRNA therapeutics were approved between 2018 and 2021.

The four FDA approved siRNA therapeutics are Patisiran, Givosiran, Lumasiran and Inclisiran, treatments for Transthyretin (TTR) amyloidosis, acute hepatic porphyria, primary hyperoxaluria and atherosclerotic cardiovascular disease, respectively.

ASO- and siRNA-based therapeutics both have their merits, and their emergence is allowing for the treatment of a variety of different diseases. Considering they alter gene expression through distinct mechanisms, continued development of both classes of drugs should allow for the development of many more treatments for seemingly untreatable genetic disorders. This thesis is primarily focused on siRNA therapeutics. To date, siRNA therapeutics have shown clinical ability to knock down Proprotein convertase subtilisin/kexin type 9 (PCSK9) and *Ttr* mRNA targets in patients by over 80% for six months with a single injection[46, 47]. This is particularly important considering the low efficacy of other lipid-lowering therapies available for PCSK9-associated atherosclerotic cardiovascular disease, and the overall lack of available treatments for TTR amyloidosis. The only previously available treatment for TTR amyloidosis was the small molecule Tafamidis, which provided modest improvements in patient survival during a Transthyretin Cardiomyopathy clinical trial and is cost prohibitive for many patients[48, 49].

Unfortunately, siRNA therapeutics share many of the same barriers to clinical implementation as ASOs, though the most significant hurdle is that of delivery into cells of interest.

1.3 Delivery of siRNA therapeutics

siRNAs are relatively large, negatively charged molecules, which makes it very difficult for them to enter cells across the cell membrane. Furthermore, if siRNAs are taken up by a cell, they still need to escape the endosome before they reach the cytoplasm where they can bind their targets and mediate mRNA degradation. This major barrier has led to failure of many research and development efforts and caused numerous clinical trials to be shut down in recent years[50, 51]. There have been varying reports of the number of siRNA copies required in the cytoplasm of a cell to elicit efficient target knockdown, but numbers range from 300 copies per cell to more than 10,000 copies per cell to obtain at least 50% knockdown in gene expression[52-54]. Considering these numbers and the difficulty with which siRNAs enter the cytoplasm, it is not feasible for siRNA, in its native form, to be used as a therapeutic in human patients.

With these constraints in mind, the siRNA therapeutics field has focused over the past two decades on identifying novel delivery strategies and vehicles to deliver siRNAs safely and efficiently into the cytoplasm[37, 55-57]. These vehicles are being designed with the goal of protecting siRNAs from nuclease degradation, allowing them to remain in circulation longer before being excreted via glomerular filtration, reducing or eliminating their immunogenic and toxic properties, and increasing their ability to enter cells and escape the endosome[57].

While other delivery strategies like viruses[58] and polymer-based polyplexes[59] are being investigated, currently the two most common siRNA delivery vehicles are lipid nanoparticles (LNPs) and N-acetylgalactosamine (GalNAc) conjugates. Of the FDA approved siRNA

therapeutics, Patisiran is an LNP-contained siRNA, while Givosiran, Lumasiran and Inclisiran are all GalNAc conjugated siRNAs.

1.3.1 Lipid nanoparticles

Cationic and ionizable lipids can form nanoparticle structures, or liposomes, when they interact with negatively charged RNA through electrostatic interactions. This leads to the formation of spherical structures typically less than 100nm in diameter, with positively charged lipid bilayers that encapsulate the RNA[60]. Typically, lipids used in these nanoparticles have an amine head group, a linker group and hydrophobic tails and the exact design of the lipids can be tweaked to produce the best-acting delivery vehicle[61]. These nanoparticle structures serve many functions in siRNA delivery. They protect the siRNA within from degradation by exonucleases and can increase their time in circulation as they are less readily absorbed through the glomeruli[62]. Their most important function is to increase the ability for their siRNA contents to be taken up into cells and escape the endosome through fusion with the endosomal membrane, allowing for release of contents[62]. Ionizable LNPs have been shown to lower the siRNA dose required to knockdown targets in the liver by 100-fold[63].

Another desirable feature of LNPs is their ability to be tuned with different lipids and ligands. For example, adding polyethylene glycol (PEG) to LNPs prevents aggregation and reduces their uptake by red blood cells, while adding cholesterol facilitates fusion with other membranes, and thus, improves endosomal escape[62, 64]. Alternatively, incorporating phytosterols in place of cholesterol allowed for 10-fold more frequent endosomal fusion events[65]. LNPs can be decorated with targeting ligands to alter biodistribution and uptake. Adding retinol binding protein, for example, to LNPs causes an increased uptake by hepatic stellate cells expressing the Retinol binding protein receptor[66].

There are, however, multiple drawbacks to LNP use for siRNA delivery: immunogenicity, biodistribution and delivery efficacy. First, LNPs are immunogenic. PEG-lipids have been shown to activate the complement system[67] while cationic and ionizable lipids can activate Toll-like receptors, stimulating release of pro-inflammatory cytokines[68]. For this reason patients typically require dosing with a corticosteroid to limit adverse reactions[69]. Next, due to their size and surface composition, following injection, LNPs accumulate almost exclusively in the liver, in large part due to decreased blood flow rate and discontinuous, highly fenestrated vasculature making the liver sponge-like in nature, limiting the dose that can reach other sites[70, 71]. It is for this reason that virtually all LNP-based siRNA therapeutics in clinical trials target liver-associated genes. Finally, while LNPs allow for siRNA delivery into the cytoplasm of cells that would not be achievable by naked, unencapsulated siRNA, it has been shown that they actually deliver less than 1% of their siRNAs cargos into the cytoplasm, therefore requiring high siRNA doses to achieve significant target knockdown[72]. New LNP formulations, or novel delivery vehicles will be needed to deliver clinically relevant doses of siRNA to tissues beyond the liver.

1.3.2 GalNAc conjugates

Many of the siRNAs used in LNPs are altered using similar chemical modifications that were used earlier in ASO design. Specifically, chemical modification allows for the incorporation of 2'-O-methyl, or 2'-fluoro modified bases, LNAs and phosphorothioate modifications into the siRNA backbone. These chemical modifications allow siRNAs to avoid degradation by nucleases, avoid recognition by the immune system, and greatly increase the half life of the molecules, increasing potency and duration of target knockdown while not interfering with the RNAi machinery[73, 74]. It is these chemical modifications that allowed early siRNA therapeutics to achieve extended target knockdown for up to six months[46, 47].

The success of chemically modified siRNAs in largely avoiding degradation and immune activation is what drove the field toward conjugates of naked siRNAs. The question became: Are there ways to conjugate certain molecules onto a naked, chemically modified, siRNA to achieve cellular uptake without the need for lipid encapsulation? The answer, for hepatocytes in the liver at least, came in the form of GalNAc conjugates.

GalNAc is an amine-containing sugar derivative of galactose and is a ligand for the Asialoglycoprotein receptor (ASGPR). ASGPR is expressed on the surface of liver hepatocytes and when it is bound by GalNAc, it rapidly leads to clathrin-mediated endocytosis of the ligand[74]. This phenomenon has been exploited over the past several decades as researchers have been able to force the hepatic uptake of different molecules by fusing them to GalNAc, or similar derivatives[75-77]. The first chemically modified siRNA to be conjugated to GalNAc was effectively taken up by hepatocytes and led to a target reduction of approximately 80%[78]. Since then, three GalNAc conjugated siRNA therapeutics have received FDA approval, highlighting their potential.

Unfortunately, as is the case with LNPs, based on the biology of GalNAc mediated uptake, which is reliant on receptors specifically expressed on liver hepatocytes, GalNAc conjugated siRNAs are only able to reduce target mRNAs in the liver. There is a continuing need for novel delivery vehicles that will allow siRNAs to knock down targets throughout the body, unlocking their full potential to combat genetic disorders.

1.4 Small Extracellular Vesicles

Extracellular vesicles (EVs) are membrane bound particles released by most cell types that are found in virtually all biological fluids as well as cell-conditioned culture medium. There are three widely studied classes of EVs that differ in their mode of biogenesis, size, and cargo: exosomes, microvesicles and apoptotic bodies.

1.4.1 Nomenclature

Until recently, in the field of EV biology, strict boundaries were drawn between exosomes, microvesicles and apoptotic bodies. Exosomes were described as small (40-120nm), membrane bound vesicles with an endosomal origin. They form through the inward budding of the late endosome, forming a multivesicular body (MVB), and are subsequently released into the extracellular space upon fusion of the MVB with the plasma membrane[79]. Unlike exosomes, microvesicles have been described to bud directly from the plasma membrane and are typically larger than exosomes, ranging from 100-1,000nm. Finally, apoptotic bodies are larger than exosomes and microvesicles, ranging in size from approximately 300-5,000nm and are released by plasma membrane budding specifically from cells undergoing apoptosis[79-81]. Recently, a number of other classes of small extracellular vesicles that are not as well characterized have been identified. Arrestin domain-containing protein 1 (ARRDC1)-mediated microvesicles (ARMMs) are a type of small (~40-100 nm) EV dependent on functions of ARRDC1 to facilitate direct budding from the plasma membrane[82]. Autophagic extracellular vesicles (AEVs) form when the autophagasome, the membrane-bound structure where cellular components are gathered prior to shuttling to the lysosome during autophagy, fuses with the late endosome, forming the amphisome[83]. AEVs are released upon amphisome fusion with the plasma membrane and are distinct from classical exosomes[84]. Matrix vesicles are a subset of vesicles ranging in size from 20 to 2000 nm that bud directly from the plasma membrane and are involved in modulation of the extracellular matrix[85]. Exomeres are small (30-50 nm) nanoparticles released from cells that are not membrane bound, unlike other small EVs, and are enriched in proteins including Argonautes, and enzymes involved in glycolysis[86, 87].

Typically, EV populations are separated based on their size, density, or surface proteins. Considering the overlap in size and, frequently, surface proteins of extracellular vesicles of endosomal origin or of different varieties of EVs that bud directly from the plasma membrane, current isolation and characterization techniques do not readily allow for the absolute separation of the different types of small vesicles. For this reason, it has become accepted practice in the field to refer to this population as "small extracellular vesicles (sEVs)"[88, 89]. Henceforth in this thesis, "sEV" will be used to describe extracellular vesicles of ~50-150nm, isolated using ultracentrifugation and filtration techniques, with primarily endosomal origin as well as direct plasma membrane origin.

1.4.2 Biogenesis

Biogenesis of sEVs of endosomal origin is largely regulated by a family of proteins called endosomal sorting complex responsible for transport (ESCRT), which form four complexes, ESCRT-0, -I, -II and -III that interact with accessory proteins like Vacuolar protein sorting-associated protein 4A (VPS4), Vacuolar protein sorting-associated protein (VTA1) and ALG-2 interacting protein X (ALIX)[79, 90]. Each of the ESCRT complexes has a distinct role in sEV formation; ESCRT-0 interacts with the Signal transduction adaptor molecule (STAM), Epidermal growth factor receptor substrate 15 (Eps15) and clathrin to gather ubiquitinated protein cargoes to phosphatidylinositol-3-phosphate (PI3P) enriched endosomes. ESCRT-I and ESCRT-II then facilitate entrapment of those cargos into forming vesicles through bending of the membrane, and finally ESCRT-III mediates pinching off of the newly formed vesicles[79, 90, 91]. ALIX is responsible for the recruitment of ESCRT-III, and a complex of VSP4 and VTA1 for its recycling[92, 93]. This process leads to ubiquitinated cellular cargo situated near the membrane of the endosome to be

encapsulated into the inward-budding vesicles[91]. Mechanisms of cargo loading will be discussed in more detail in section 1.4.4.

Interestingly, knocking down key proteins from each of the four ESCRT complexes does not completely eliminate the formation of endosomal sEVs[94]. This is likely due to the existence of a number of other ESCRT-independent biogenesis mechanisms, which are dependent on the sphingolipid ceramide[95] and the tetraspanin CD63[96]. It has been suggested that the sEVs formed through these different mechanisms result in subpopulations with distinct, though overlapping, sizes and cargoes[81, 97]. Another subpopulation of endosomal sEVs can be released specifically when the heparan sulphate proteoglycan-binding protein Syntenin-1 connects syndecans to Alix, facilitating ESCRT-dependent biogenesis[98]. MVB shuttling to the plasma membrane is mediated by the RAB GTPase Rab27. Rab27a has been implicated in docking of the MVB to the plasma membrane in multiple cell types and influences sEV size, while Rab27b is involved in the intracellular trafficking of the MVB[99]. Other RAB proteins Rab11, Rab35 and Rab7 may also be required for MVB trafficking, though their exact roles in the process are not clearly defined[91]. Once at the plasma membrane, MVB fusion, and subsequent release of sEVs is mediated by soluble N-ethylmaleimide-sensitive fusion attachment protein (SNAP) receptor (SNARE) proteins[79, 100].

The release of sEVs through direct budding of the plasma membrane is mediated by changes in the composition of lipids and proteins at particular sites within the plasma membrane. Lipid rearrangement is mediated by an inward directed pump, flippase, an outward-directed pump, floppase, and a lipid scramblase. Under the control of these three players, lipid rearrangement leads to the reshaping of the membrane to form vesicle structures[101]. The Ras GTPase, ADP ribosylation factor 6 (ARF6), then plays an important role in recruiting and activating kinases that contract the

membrane, facilitating fission of the vesicles[102]. Interestingly, a subset of sEVs that bud directly from the membrane, ARMMs, are dependent on the action of Tumor susceptibility gene 101 (TSG101), one of the key proteins of the ESCRT-I complex and VSP4, both key proteins involved in the formation of sEVs of endosomal origin, again illustrating the overlap between biogenesis mechanisms of different subtypes of sEVs [82].

1.4.3 Isolation techniques

sEVs are most often purified based on their size. The gold standard in sEV isolation is differential ultracentrifugation, where supernatants are spun at increasing speeds to pellet out various contaminants like whole and damaged cells, organelles and larger EVs prior to pelleting the sEVs themselves at speeds upwards of 100,000 g[103]. sEVs isolated in this way are frequently shown to be of expected size when measured by Nanoparticle tracking analysis (NTA) and electron microscopy (EM) and possess many typical markers by Western blot, like TSG101, Flotillin-2, Alix, and CD63, while not containing cell specific markers like Calnexin and Tomm20[88]. While differential ultracentrifugation is the most common means for isolation, it does come with drawbacks especially in the context of developing sEV therapeutics. First, reproducibility is a concern since the use of different rotors has been shown to introduce significant variability in pellet size while increased spin lengths increases yield but can increase protein contamination in the pellet[104]. Secondly, long ultracentrifugation spins have been shown to induce aggregation of sEVs[105] and introduce contaminants into the isolation[106]. Finally, when compared to other isolation methods that are gaining in popularity, like filtration based techniques, sEV yield is low and processing time relatively high by differential ultracentrifugation, with each rotor typically holding less than 200mL and spinning for upwards of 2 hours[107-109]. Together, these drawbacks will likely lead to significant challenges translating sEV therapies to the clinic.

Tangential flow filtration (TFF) may be a well-suited technique to overcome many of the hurdles faced by differential ultracentrifugation. TFF is a filtration process based on size exclusion where sEV-conditioned cell culture media, previously cleared of large contaminants by low-speed centrifugation and/or dead-end filtration, is continuously passed parallel to a filter under mild back pressure. This allows for media, and components within it, that are smaller than the molecular weight cut-off of the filter to pass through into a permeate, while larger particles, like sEVs in this case, are concentrated within the retained sample[108]. Studies have shown that TFF allows for the isolation of sEVs with faster processing time, reduced user handling, higher yield, scalability and purity, improved reproducibility and better process sterility as compared to ultracentrifugation[104, 108, 110-113].

A number of other isolation techniques also exist that are not as commonly used. PEG-based precipitation allows for relatively fast isolation of sEVs from small volumes, though tends to produce a relatively impure product as many contaminants coprecipitate with the sEVs[114, 115]. Immunoaffinity capture isolates sEVs through antibody interaction with specific surface markers, like tetraspanins. This allows for very rapid isolation of a highly pure subset of sEVs, however may lead to biased results since specific subgroups of sEVs that lack the particular surface protein may be excluded, while sEVs rich in the protein may be enriched[115]. Size exclusion chromatography (SEC)[116], Asymmetric flow field-flow fractionation (AF4)[86] and density gradient isolation[97, 117] isolate sEVs with the highest degree of purity in the lab setting, but do not lend themselves well to potential scale up that would be required for clinical scale sEV production.

Overall, the different isolation techniques are more or less suitable for specific applications since compromises must be made between sample volumes, isolation time, purity, sterility, and

yield. Careful consideration will need to be given to the specific technique used as sEV-based therapeutics move toward the clinic.

1.4.4 sEV cargo

sEVs contain an array of different cargoes including proteins[91, 118], lipids[119], DNA[120], mRNA[121] and miRNAs[122]. Importantly, the cargoes do not represent a random assortment of cellular components, but rather a highly specific subset of cargoes that suggests active mechanisms of cargo sorting are involved.

Proteins - sEVs contain diverse protein cargo. Proteins involved in the biogenesis of sEVs like ESCRT proteins, tetraspanins like CD9, CD,63 and CD81 that are important in membrane trafficking, and annexins that are involved in membrane fusion are all commonly observed in sEV isolations and are used as general markers of sEVs[123], though new studies are shedding light on the fact that certain subpopulations of sEVs may not contain certain sets of these typical markers[81]. Other protein cargoes are dependent on the origin of the parental cell. As outlined in section 1.4.2, many protein cargoes are loaded into actively forming sEVs through Ubiquitin- and ESCRT-dependent mechanisms. Specifically, the hepatocyte growth factor-regulated tyrosine kinase substrate (Hrs), a subunit of the ESCRT-0 complex, recognizes ubiquitinylated cargoes and sorts them into endosomes through interaction with PI3P[124]. sEV-associated epidermal growth factor receptor (EGFR) is an example of ESCRT-dependent, ubiquitinated protein cargo[124]. Interestingly, the level of ESCRT proteins like TSG101 sorted into the forming sEVs can also be altered based on ubiquitination[125]. Other post-translational modifications (PTMs) are also associated with ESCRT-mediated cargo loading. These PTMs include ubiquitin-like modifiers (UBLs), like small ubiquitin-related modifiers (SUMO) and interferon-stimulating gene 15 (ISG15) modifications [123, 124]. For example, the presence of α-Synuclein in sEVs from cerebrospinal fluid is dependent on

sumoylated protein recruitment by ESCRT proteins TSG101, VPS4 and Alix[126]. ISGylation, on the other hand, renders proteins less likely to be sorted into sEVs and instead promotes lysosomal degradation[127]. Other PTMs appear to be involved in protein cargo sorting into sEVs, though the mechanisms behind these effects remain unclear[124].

ESCRT-independent mechanisms of sEV protein cargo sorting have also been uncovered. Lipid rafts are regions of the plasma membrane enriched in cholesterol and sphingolipids that are present on sEV membranes. Certain proteins like Flotillin-1 are sorted to sEVs owing to their high affinity for lipid rafts[128]. Additionally, it has been shown that reduction of the enzyme that turns sphingolipid to ceramide, sphingomyelinase, greatly reduces the protein content of sEVs independently of the ESCRT machinery suggesting it represents a separate control mechanism for sorting certain protiens[95].

Lipids - The sEV lipid membrane is not simply a miniaturized replica of the cellular plasma membrane. Cholesterol, sphingomyelin, glycosphingolipids, ceramide, and phosphatidylserine are all enriched in sEVs, while phosphatidylcholines are relatively more abundant on the sEV-producing cells[129]. The mechanisms behind active sorting of lipids to sEVs remain poorly understood, though it has been suggested that lipid cargo sorting is likely independent of protein sorting[130].

DNA - sEVs also contain a range of nucleic acids. While the DNA content of sEVs is not as well studied as RNA, there is consensus in the field that sEVs can carry single stranded DNA, double stranded DNA, and mitochondrial DNA both inside the lumen and on the surface of the membrane[131, 132]. Cancer cell-derived sEVs were shown to contain fragments of double stranded DNA of up to 20 kilobases (kb) that represents the whole genome, and this DNA can function as a biomarker of cancer and metastasis since it reflects the mutational status of the producing cells[120,

[133]. The mechanism for DNA loading into sEVs is not well understood, but appears to be independent of the ESCRT machinery. The most well-described mechanism involves budding of micronuclei from the nucleus in response to DNA damage. These micronuclei contain DNA that are released into the cytoplasm following rupture of the micronuclei, that are then seen to colocalize with endosomal and sEV markers[134]. It has been proposed that DNA release by sEVs is required to eliminate harmful cytoplasmic DNA, thus maintaining cellular homeostasis[135], though this contrasts with the observation that DNA delivered by sEVs into recipient cells can increase coded mRNA and protein expression[136]. The presence of DNA within sEVs of non-cancerous origin is not well characterized, and one recent study has proposed that double stranded DNA is present in the amphisome and is released alongside AEVs, but is not actually contained within AEVs or other sEVs[84].

mRNA and long noncoding RNA (lncRNA) - Similar to what is observed with proteins and lipids, the RNA content of sEVs is not random. Certain RNAs are highly over- or under-abundant in sEVs, as compared to the cells that release them. In the case of long RNAs, 609 of the 10,761 mRNAs detected in sEVs were found to be enriched in sEVs versus the cells that produced them, while 680 were found to be relatively depleted. Similarly, in the case of lncRNAs, 72 of 6544 detected were enriched, while 123 were depleted in sEVs[137]. These RNAs can be present inside of sEVs as fragments, or full length transcripts. mRNA sorting into sEVs can be facilitated by binding of the heterogeneous nuclear ribonucleoprotein A2B1 (hnRNPA2B1) to specific sequences within their 3' UTRs[137, 138].

miRNA and other small RNAs - Various types of small RNA have now been observed in sEVs, including transfer RNAs (tRNAs)[139], small nuclear RNAs (snRNAs)[140], Y RNAs[141] and vault RNAs[142], though miRNA are by far the most widely studied RNA cargo in sEVs. Multiple

reports have shown that 30-50% of sEV-associated miRNAs are over- or under enriched in sEVs as compared to the cells that produced them, suggesting that they too are actively sorted[143-145]. To date, several mechanisms have been provided that control this sorting. The sphingolipid ceramide is involved in the biogenesis of a subset of sEVs, and protein sorting to those sEVs, as discussed above[95]. It has also been implicated in miRNA sorting. Specifically, decreasing the activity of neutral sphingomyelinase 2 (nSMase2), a regulator of ceramide biosynthesis, with chemical inhibitors was shown to greatly reduce the sorting of certain miRNAs including miR-16 and miR-146a into sEVs, while overexpressing nSMase2 had the opposite effect[146]. Increased sEV sorting was not tied to changes in cellular levels, and was independent of the ESCRT machinery.

Several miRNA sequence motifs have been identified that are overrepresented in sEVs. These motifs are recognized by at least two different RNA binding proteins (RBPs), hnRNPA2B1[147] and synaptotagmin-binding cytoplasmic RNA-interacting protein (SYNCRIP)[148] for sEV sorting in T-lymphocytes or hepatocytes respectively. In both cases, sumoylated forms of the proteins were shown to bind directly to a variety of miRNA molecules at these sequence motifs, driving them into sEVs. Alternatively, the Y-box protein 1 (YBX1) has been shown to shuttle miR-223 into sEVs from HEK293 cells[149], Lupus La protein sorts miR-122 into MDA-MB-231 sEVs[150], Human antigen R (HuR) protein sorts miR-122 into sEVs in hepatocytes[151] and the major vault protein (MVP) shuttles different miRNAs into sEVs from both HEK293 cells[152] and colon cancer CT26 cells[153].

These studies present a common thread: Many miRNAs are actively sorted into sEVs through direct interaction with RBPs. Approximately 25% of the protein content of sEVs is made up of RBPs[154]. Canonical RBPs contain one or more RNA-binding domains (RBD) such as the RNA recognition motif (RRM), the K-homology (KH) domain, zinc fingers, PAZ domains and

others, that bind to particular RNA structures and sequence motifs through a variety of biochemical mechanisms and can be arranged to hold RNAs in specific topologies[155]. RNA binding by RBPs forms ribonucleoproteins (RNPs), which can affect processing, nuclear export, cellular localization, and translation of the RNAs[155]. It is, however, becoming clear that many previously unidentified RBPs exist that do not possess traditional RBDs[156]. These unconventional RBPs bind RNAs at sites previously thought to be only associated with other functions like DNA- and protein-binding and enzymatic function[156].

The first and only study to date to show how an RBP binds a miRNA for sEV packaging was published in 2018 and focused on SYNCRIP[157]. The study showed that while SYNCRIP does have multiple canonical RRM domains, it actually binds miRNA targets for sorting into sEVs at a non-canonical RBD that was previously thought to strictly play a role in protein-protein interaction[157]. This opens the possibility that other sEV-enriched miRNAs could be bound by and be shuttled into sEVs by proteins with unconventional RBDs. The exact mechanisms through which RBPs shuttle miRNAs into sEVs remains to be uncovered but, at least in some cases, post-translational modification of the RBPs is required[147, 148].

1.4.5 Cargo delivery

The most commonly proposed biological role for sEVs is in intercellular communication, whereby sEVs released from one cell can fuse with another cell and deliver contents into the cytoplasm to modulate the recipient cell, allowing sEVs to play important roles in a multitude of biological processes. The mechanism of sEV uptake into recipient cells is still not well understood, though it is becoming apparent that interactions between sEVs of diverse cellular origin or subtype and different recipient cells drives uptake through unique mechanisms; there does not appear to be one single global regulator or mechanism of sEV uptake by recipient cells[158]. Tetraspanins[159],

integrins[160] and proteoglycans[161] have all been implicated in helping sEVs of different origins target and dock with different recipient cells. Following targeting, sEVs can release their contents into the cell by directly fusing with the plasma membrane[162, 163], or can be taken up through either clathrin- or caveola-mediated endocytosis[91, 164, 165]. Once internalized by endocytosis, sEVs can fuse with the endosomal membrane, in an acidification-dependent manner, to release cargoes into the cytoplasm[166]. Alternatively, in some cases sEVs have been shown to be re-released from cells through re-fusion of the endosome with the plasma membrane[167].

Numerous studies have identified endogenous sEV-contained miRNAs as key modulators of recipient cell mRNA in sEV mediated intercellular communication[168-172]. This innate ability for sEVs to travel throughout the body and deliver their contents, miRNA specifically, into other cells is what makes them an obvious candidate for use as siRNA delivery vehicles.

1.4.6 sEVs as delivery vehicles for siRNA

As discussed previously in the context of ASOs and other siRNA delivery vehicles like LNPs and GalNAc conjugates, there are several hurdles that need to be overcome for a delivery strategy to be deemed promising as a therapeutic. These hurdles include being nontoxic and non immunogenic, effectively reaching tissues of interest, facilitating cargo delivery into recipient cells, and having the desired effect on target genes.

Within the past decade, in the field of cell-based therapies, especially using mesenchymal stem cells (MSCs) for regenerative medicine, it has been observed that many of the benefits of whole cell therapy can be achieved by delivering the sEVs from those cells with significantly improved safety profiles over delivering the cells themselves[173, 174]. For example, pre-clinical studies have shown injected sEVs from MSCs improve kidney function in models of acute and chronic kidney damage[175, 176], improve hepatic regeneration in chronic liver failure[177], improve

lung function following acute ischemia injury[178] and improve post-stroke neuroregeneration[179]. Additionally, a systematic study of sEVs from three different cellular origins showed that sEVs build up in multiple tissues beyond the liver, including spleen, lungs, gastrointestinal tract, pancreas, and others following multiple routes of injection[180]. Together, these studies suggest that siRNA-loaded sEVs should be able to reach multiple interesting tissues and organs that LNPs and GalNAc conjugates cannot. sEVs also remain in circulation longer than LNPs, in part due to the presence of CD47 on their surface, which acts as a negative uptake signal for monocytes and macrophages[181]. sEVs can also be engineered to express a specific range of surface markers to improve organ and cellular tropism[182]. Importantly, unaltered sEVs have been shown to be non-inflammatory and non-toxic, resulting in minimal or no cytokine response, no adverse effect on tissue histopathology or changes in blood cell counts or organ function[183, 184]. sEVs engineered to deliver siRNA have been found to be similarly safe in multiple studies[185-187]. Furthermore, clinical scale production of sEVs adhering to current good manufacturing practices (cGMP) has been shown to be feasible with the use of bioreactors to grow producing cells at high density[187] and the use of high throughput isolation methods like TFF[112]. All of these features, plus their innate ability to deliver miRNA contents into recipient cells has pushed them to the forefront of the siRNA delivery field.

While certain hydrophobic substances like doxorubicin[188] and curcumin[189] can be incorporated inside of sEVs through simple incubation, siRNAs cannot actively pass through the membrane and must be actively inserted into the sEVs. This can be accomplished after isolation of the sEVs using a number of approaches including electroporation[181, 182], hydrophobic modification by cholesterol conjugation[190, 191] and transfection with commercial reagents to form sEV-liposome complexes[192]. sEVs loaded with siRNA using these techniques have been used to

reduce pre-clinical targets including pancreatic cancer targets KRAS[181] and PAK4[193], Alzheimer's disease associated BACE1[182], Huntington's disease associated Huntingtin[190] and numerous others. Currently the only ongoing clinical trial featuring siRNA-loaded sEVs is based on the electroporation of siRNA against mutated KRAS in pancreatic cancer[194].

Each of these methods come with significant drawbacks. First and foremost, they each alter the sEV surface which could interfere with lipid and protein structure of the membrane, potentially impeding delivery. A thorough investigation of this possibility is required. It has also been shown that electroporation causes not only aggregation of sEVs, potentially reducing their efficiency, but also causes naked siRNA to aggregate and copurify with the sEV-loaded siRNA, which can disguise the *de facto* action of the sEV-loaded siRNA[195]. Transfection with commercial reagents, meanwhile, presents a serious issue of component separation. It has been shown that transfection with lipid-based transfection reagents creates complexes that copurify with sEVs during isolation and thus makes interpretation of results in these studies questionable, and could introduce immunogenic components into otherwise non-immunogenic sEV isolations[196]. Transfection has also been shown to impair the ability of sEVs to deliver RNA cargoes[196].

The alternative to these post-isolation loading techniques is to alter the producing cell, hijacking the endogenous loading machinery. In the simplest case, cells can be transfected with siRNAs that they then load into sEVs prior to their secretion. This technique has been used in pre-clinical studies to load siRNAs against KRAS for treatment of pancreatic cancer[197], and against c-Met to combat chemotherapeutic resistance in gastric cancer[198] amongst many others. Unfortunately, transfecting cells brings with it many of the same issues that transfecting sEVs directly does. Lipid-based transfection complexes that are transfected into cells are subsequently released back into the media and copurify with sEVs, contaminating sEV products, and once again

confounding any findings that effects are, in fact, caused by the sEVs and not transfection complexes containing siRNA[196]. Additionally, most endogenous miRNAs are present at very low levels in sEVs, less than one copy per 100 sEVs on average, with specific subsets being highly enriched, suggesting simple overexpression of an siRNA in cells will likely not lead to very efficient loading into sEVs through endogenous packaging mechanisms[199].

This begs the question: Which endogenous miRNAs are highly abundant in sEVs, and is there a way to use our knowledge of these miRNAs to facilitate effective siRNA loading into sEVs without having to modify them post-isolation?

1.5 miR-451

miR-451 is a miRNA with a primary proposed role in erythropoiesis[200-202]. It is expressed in a limited number of cell types and tissues including neutrophils, B cells, monocytes, erythroblasts, cerebellum and placenta[203] and targets *14-3-3ζ*[202, 204] and *Rac1*[205] mRNA. It is one of the most highly enriched miRNAs in sEVs[143]. In this context, "enriched" means that the level of miR-451 in sEVs is relatively high compared to the cells that produce them. Thus, even in cases where cellular expression of miR-451 is low, there is a relatively large amount in the released sEVs. This suggests that miR-451 is likely packaged into sEVs through an active mechanism, similar to the other miRNAs discussed in section 1.4.4.

1.5.1 Biogenesis

Mature miR-451 is generated through a non-canonical pathway, in contrast to the canonical pathway described in section 1.1.1 herein. This unique biogenesis was described in three reports all published in 2010[206-208]. At the transcript level, miR-451 and miR-144, a canonical miRNA, are located approximately 100 bp apart and form a miRNA cluster. When Drosha cleaves the pre-miR-451 stem loop structure from the transcript, it produces a 42 nt hairpin, which is unusually

short compared to the average length of canonical miRNA, approximately 65 nt. Like other miRNAs, the pre-miR-451 hairpin is exported to the cytoplasm by Exportin-5 where Dicer cleavage would normally occur. However, Dicer requires the stem of a miRNA to be at least 19 nt long to bind and cleave the hairpin into the double stranded form of approximately 22 nt long. The pre-miR-451 stem is only 17 nt long, inhibiting its processing by Dicer. Instead, the short hairpin is bound directly by Ago2, which cleaves one side of the stem, generating a product of approximately 34 nt. The 3' end is then progressively trimmed by nucleases resulting in the eventual generation of a mature product of approximately 22 nt. This trimming was demonstrated by the appearance of miR-451 intermediates of progressively smaller size from approximately 34 nt to 22 nt in Dicer knockout cells[206-208]. Interestingly, as a result of this biogenesis, the final mature strand of miR-451 includes bases through the loop region, while canonically, mature miRNAs are found only within the stem region of the pre-miRNA[206-208].

1.5.2 Reprogramming

When the sequence of the short pre-miR-451 hairpin is changed to contain other sequences but maintain the uniquely short hairpin structure, those sequences are also processed through the non-canonical Dicer-independent pathway[208]. Importantly, these alternatively processed forms of miRNAs retain their ability to reduce target mRNA levels. Given this fact, and the evidence that miR-451 is highly enriched into sEVs[143], we hypothesize that siRNA sequences inserted into this pre-miR-451 hairpin structure may also be enriched into sEVs. This would allow for the generation of cell lines that package siRNA into sEVs without the need for any cellular transfection or post-isolation modifications to the sEVs. Though, if that were to be the case, the unknown mechanism that preferentially drives pre-miR-451 hairpins into sEVs would need to retain that function when

the RNA sequence is changed, similar to how the biogenesis pathway appears to be sequence independent.

1.6 Rationales and hypotheses

Results presented in this thesis is divided into three chapters, each comprised of a published, submitted, or prepared manuscript related to the use of reprogrammed pre-miR-451 for the sorting of siRNAs into sEVs to produce potential therapeutics. The first manuscript explores the feasibility of this endeavour. The second manuscript focuses on the safety of siRNA-loaded sEVs and their use in pre-clinical models of kidney disease. The third manuscript delves into the mechanism behind pre-miR-451 sorting into sEVs that makes the first two chapters possible.

1.6.1 Reduction of the therapeutic dose of silencing RNA by packaging it in extracellular vesicles via a pre-microRNA backbone

Rationale: sEVs are natural carriers and delivery vehicles for miRNA throughout the body[122], but altering them can limit their ability to deliver their cargo[195]. Reprogramming the uniquely short hairpin of pre-miR-451 with other miRNA sequences forces those sequences to be processed into their mature form through the same non-canonical Dicer-independent pathway that matures endogenous miR-451[206-208]. Meanwhile, miR-451 is one of the most highly enriched miRNAs in sEVs, suggesting that its packaging into sEVs is an active process[143].

Hypothesis: Inserting siRNA sequences into the pre-miR-451 hairpin structure will cause them to be actively packaged into sEVs. These sEVs will be able to deliver their siRNA cargo to reduce targets *in vitro* and *in vivo* more effectively than other siRNA delivery methods or other types of sEV technologies.

1.6.2 Safe, scalable delivery of silencing RNAs with small extracellular vesicles in models of chronic kidney diseases

Rationale: Multiple known gene variants are associated with different forms of Chronic kidney disease (CKD) including variants of Apolipoprotein L1 (*Apol1*)[209, 210] and Transient Receptor Potential Cation Channel 6 (*Trpc6*)[211-213]. Reduction of these variants leads to improved kidney function in pre-clinical studies[214-216] and sEVs have been shown to deliver functional cargo to kidney cells in CKD models[176]. Furthermore, TFF has been used to produce cGMP-compatible sEV products with a high yield and therapeutic efficacy in pre-clinical models[111-113].

Hypothesis: sEVs loaded with siRNAs targeting *Trpc6* or *Apol1*, isolated by TFF, will safely reduce targets in the kidney, leading to improved renal function in models of CKD without showing signs of toxicity or immunogenicity and will be functional in larger animal models.

1.6.3 Midkine binds pre-miR-451 derivatives for active sorting into small extracellular vesicles

Rationale: Changing the RNA sequence of pre-miR-451 while maintaining its unique hairpin structure allows for the selective packaging of siRNAs into sEVs, as seen in chapter two and three. Multiple RBPs are responsible for sorting miRNAs into sEVs from diverse cell types[147-153] and the interaction between RBPs and their sEV-associated miRNA partners is not necessarily through canonical RNA binding domains[157].

Hypothesis: One or more RBPs are responsible for sorting pre-miR-451 or siRNAs inserted into the pre-miR-451 hairpin structure into sEVs. We hypothesize that RBP binding is based on the unique structure of the hairpin, possibly through a nonconventional RNA binding domain.

Chapter 2 - Manuscript #1

Reduction of the therapeutic dose of silencing RNA by packaging it in extracellular vesicles via a pre-microRNA backbone

Publication information:

Ryan Reshke*, James A. Taylor*, Alexandre Savard*, Huishan Guo, Luke H. Rhym, Piotr S. Kowalski, My Tran Trung, Charles Campbell, Wheaton Little, Daniel G. Anderson and Derrick Gibbings. Reduction of the therapeutic dose of silencing RNA by packaging it in extracellular vesicles via a pre-microRNA backbone. Nature Biomedical Engineering. **4**, 52-68 (2020).

* These authors contributed equally to this work

Author Contributions:

Designed experiments: RR, JAT, AS, LHR, PSK, WL, DGA, DG. Performed experiments: RR, JAT, AS, HG, LHR, PSK, MT, CC. Analyzed data: RR, JAT, AS, DG. Conceived the study: DG. Wrote the manuscript: RR, JAT, AS, DG.

RR contributions by figure: Figure 1b, f, i, Figure 2e, Figure 3c, e, f, g, i, Figure 4a-d, Figure 5a, b, c, g-j, Figure 8a, b, Supplementary Figure 1 b, c, Supplementary Figure 2a, h-m, Supplementary Figure 4d.

Reduction of the therapeutic dose of silencing RNA by packaging it in extracellular vesicles via a pre-microRNA backbone

Ryan Reshke[1,2,3,7], James A. Taylor[1,2,7], Alexandre Savard[1,2,7], Huishan Guo[1,2], Luke H. Rhym[4], Piotr S. Kowalski[4], My Tran Trung[1,2], Charles Campbell[1,2], Wheaton Little[5], Daniel G. Anderson[4] and Derrick Gibbings[1,2,3,6*]

[1]Department of Cellular and Molecular Medicine, University of Ottawa, Ottawa, Canada.

[2]Ottawa Institute of Systems Biology, University of Ottawa, Ottawa, Canada.

[3]Éric Poulin Center for Neuromuscular Disease, University of Ottawa, Ottawa, Canada.

[4]The Koch Institute for Integrative Cancer Research, Massachusetts Institute of Technology, Cambridge, MA, USA.

[5]Central Nervous System Disorders Drug Discovery Unit, Takeda Pharmaceuticals, Cambridge, Ma, USA.

[6]Brain and Mind Research Institute, Ottawa, Canada

[7]These authors contributed equally: Ryan Reshke, James A. Taylor, Alexandre Savard

* Corresponding author. Email: gibbings@uottawa.ca

2.1 Abstract

A small percentage of the short interfering RNA (siRNA) delivered via passive lipid nanoparticles and other delivery vehicles reaches the cytoplasm of cells. The high doses of siRNA and delivery vehicle that are thus required to achieve therapeutic outcomes can lead to toxicity. Here, we show that the integration of siRNA sequences into a Dicer-independent RNA stem–loop based on pre-miR-451 microRNA—which is highly enriched in small extracellular vesicles secreted by many cell types—reduces the expression of the genes targeted by the siRNA in the liver, intestine and kidney glomeruli of mice at siRNA doses that are at least tenfold lower than the siRNA doses typically delivered via lipid nanoparticles. Small extracellular vesicles that efficiently package siRNA can significantly reduce its therapeutic dose.

2.2 Introduction

Canonically, pre-microRNAs (pre-miRNAs) are 60–120 nucleotide (nt) stem–loop structures that are cleaved by the ribonuclease (RNase) III enzyme Dicer into short, approximately 21 nt double-stranded (ds) RNAs[8]. This 21 nt dsRNA complex binds the microRNA effector Argonaute (Ago). After removal of one RNA strand, the Ago–miRNA complex represses translation of target genes by translational repression and mRNA degradation[8]. siRNAs are designed to mimic Dicer-processed dsRNA that bind Ago and are used therapeutically. When siRNAs are perfectly complementary to mRNA targets, Ago2 can enzymatically cleave target mRNA[46, 47], conferring remarkable potency and specificity to these drugs.

For therapeutic applications, delivery of siRNA into the cytoplasm of cells is a perennial challenge[62, 217]. Quantitative analysis has shown that 300–2,000 copies of siRNA that catalytically cleave mRNA are required in the cytoplasm of each cell to silence target mRNAs[52-54]. For example, 300 copies of siRNA per cell were required to silence target expression by 50% when siRNA was microinjected directly into the cytoplasm[54]. Alternatively, 800 copies of siRNA loaded into Ago2 were required to silence a target mRNA effectively in the liver[53]. Measured in cultured cells or in the liver of mice, current delivery vehicles such as lipid nanoparticles enable only between 0.05% and 1% of siRNA to enter the cytoplasm of cells[52, 53, 72, 218]. For this reason, high doses of siRNA and their delivery vehicles are required to reach a therapeutic dose in patients; this can lead to toxicity, which has halted multiple clinical trials of silencing RNAs[51]. Lipid nanoparticles and siRNA accumulate predominantly in the liver. Consequently, most siRNA therapeutics target proteins expressed in the liver. siRNA delivery to the liver with lipid nanoparticles reduces target expression in patients by more than 80% for over 6 months with a single dose[46, 47], and was recently

approved for treatment of transthyretin amyloidosis. Delivery of siRNA to other organs remains a major challenge.

Extracellular vesicles, and in particular small extracellular vesicles, have been proposed as a delivery vehicle for siRNA. Small extracellular vesicles (sEVs) can be produced by budding from the plasma membrane or by budding of 60–120 nm vesicles into the lumen of late endosomes. These late endosomes can subsequently fuse with the plasma membrane, releasing the sEVs inside them into the extracellular space[79]. Studies showed that extracellular vesicles and sEVs contain miRNA and can transfer miRNA activity into other cells[121, 122, 219-222]. A hypothesis has emerged that sEVs have an evolved ability to deliver small RNAs or other molecules between cells and that this capacity could be captured for efficient drug delivery. Despite the attention on sEVs, the efficiency with which they deliver their cargoes into the cytoplasm has not been directly evaluated. Indeed, in some cases, target silencing was indistinguishable whether siRNA was electroporated into sEVs or injected directly into mice[182]. In other cases, where siRNA was electroporated with sEVs or coated onto the sEV surface, the siRNA doses required to knockdown target expression markedly exceeded that required for siRNA in lipid nanoparticles[181, 190]. This suggests that sEVs may actually have little inherent capacity to deliver RNAs.

Studies of siRNA delivery using sEVs to date may not, however, test the actual delivery efficiency of sEVs. Topologically, siRNA on the sEV exterior will not enter the cytoplasm if sEVs fuse with target cells, but will rather remain trapped in endosomes or on the exterior of the cell, and thus inactive. Also, electroporating sEVs with siRNA may not actually introduce siRNA into sEVs, but rather precipitate siRNA, which then co-purifies with sEVs[195]. Electroporation or otherwise altering the sEV surface may also interfere with the membrane architecture of sEVs

required for fusion with target cell membranes. For this reason, the actual delivery efficiency of sEVs still requires testing.

miRNAs are sparse in sEVs, with an absolute copy number ranging from one copy of a specific miRNA per 10^6 sEVs to one copy per sEV[199]. This underscores that any attempt to deliver RNA therapeutics using sEVs will probably require a means of packaging more RNA into sEVs. However, sEVs are loaded with a highly selective subset of RNAs from the cells that produce them[121, 149, 222]. For example, specific miRNAs that are similarly abundant in cells are found with a 10^6-wide range of relative quantity in sEVs[199]. This suggests that simply overexpressing a miRNA may not enable its packaging into sEVs. Sequence motifs are probably not an adequate solution, as they result in modest enrichment in sEVs[147, 151] and are difficult to insert into a small siRNA.

Pre-miR-451 is an exception to the canonical pre-miRNA biogenesis cascade[223]. The stem–loop of pre-miR-451, after processing by Drosha, is only 42 nt long and too short to be bound and cleaved by Dicer. Instead, pre-miR-451 binds directly to Ago2[206-208]. Ago2 cleaves the distal strand of the pre-miR-451 stem–loop. This generates a 34 nt product that is progressively trimmed by exonucleases to produce an approximately 21 nt miRNA[206-208]. Notably, if the structure of the pre-miR-451 stem–loop is maintained, it can be reprogrammed with other miRNA sequences, which will be processed through the same Dicer-independent, Ago2-dependent pathway into mature effective miRNA[206-208].

Here, we demonstrate that integration of siRNA into an RNA backbone derived from pre-miR-451, but not a canonical pre-miRNA, enables robust packaging into sEVs. sEVs packaged with siRNA in this manner can efficiently reduce expression of target genes in primary cells in

culture and also in mice. sEVs packaged with siRNA can knockdown targets with at least tenfold less siRNA than lipid nanoparticles, suggesting that sEVs are highly efficient delivery vehicles.

2.3 Results

Pre-miR-451 products are selectively enriched in sEVs

sEVs were enriched by differential centrifugation from supernatants of mouse embryonic fibroblasts (MEFs), MDA-MB-231 human breast cancer cell line and NSC-34 motor neuron-like cell line grown in sEV-depleted media. These preparations were enriched in sEV markers Tsg101 and flotillin 2 and contained small to moderate amounts of Ago2. As expected, tubulin and a mitochondrial protein (Tomm20) were undetectable in these preparations (Fig. 2.1a and Supplementary Fig. 2.1a). Particles in sEV preparations had a median size (100–120 nm) and size distribution consistent with sEVs (Fig. 2.1b and Supplementary Fig. 2.1b).

Following recent reports of siRNA delivery by sEVs in mice[181, 182], we attempted to electroporate siRNA into sEVs. Using a protocol and instrument identical to the one described[181, 182], we electroporated sEVs and siRNA targeted against superoxide dismutase (SOD1). Whether siRNA was electroporated in the presence or absence of sEVs, siRNA was similarly pelleted by a standard protocol to isolate sEVs by ultracentrifugation (Fig. 2.1c). This suggests that electroporation may cause siRNA to aggregate or precipitate. Consistent with this suggestion, whereas free siRNA was degraded by RNase A, electroporated siRNA was resistant to digestion by RNase A whether sEVs were present or not in the electroporation cuvette (Fig. 2.1c). In agreement with ref. [195], this suggests that siRNA is not introduced into sEVs by electroporation but precipitates outside sEVs and copurifies with them on ultracentrifugation. We sought an alternative method to package siRNA into sEVs by harnessing cellular mechanisms of packaging RNAs into sEVs.

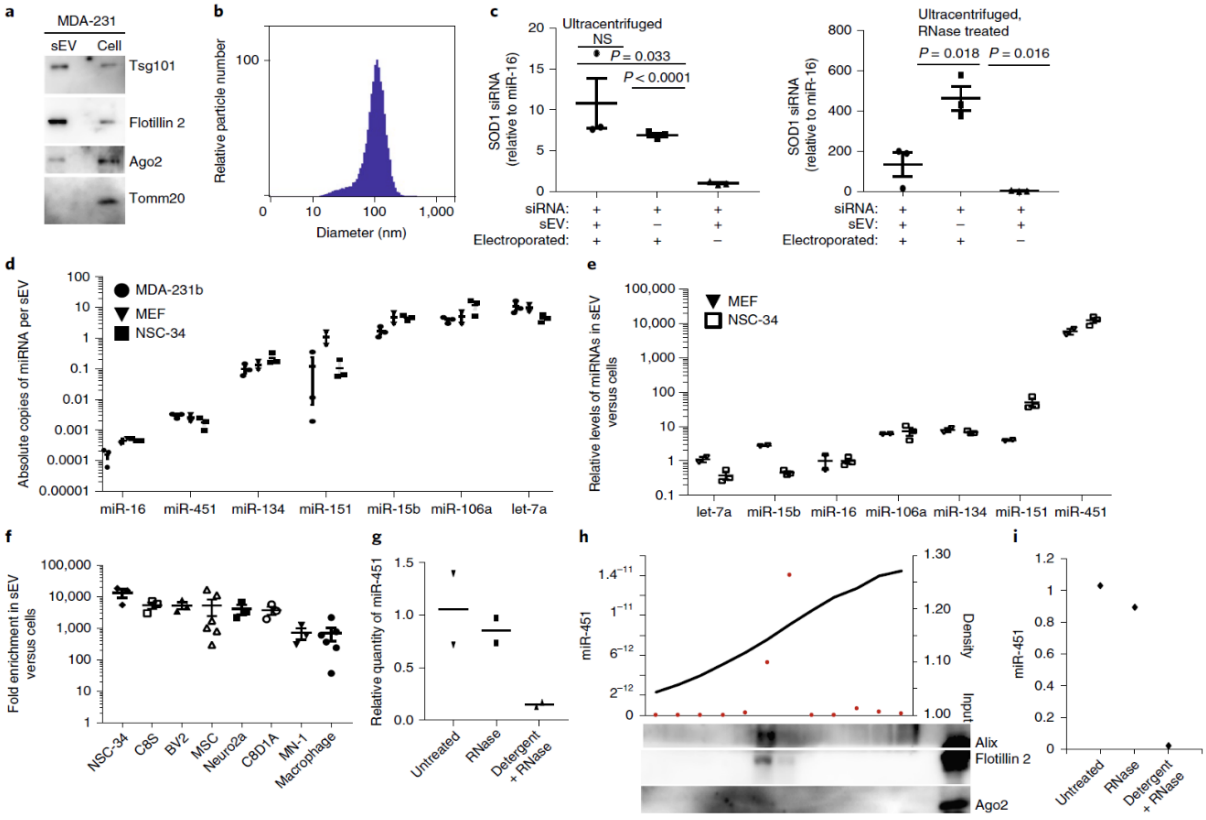

Figure 2.1. sEVs contain few miRNAs and are enriched in miR-451 compared with cells. a, Western blot of equal amounts of proteins from cells and the sEVs they produce for markers of sEVs (Tsg101 and flotillin 2), proteins excluded from sEVs (mitochondrial Tomm20) and Ago2. **b**, Nanoparticle tracking analysis of sEVs. Representative plot of particle number (y axis) versus diameter in nm (x axis) of sEV preparations from NSC-34 cells. **c**, Left, RT–qPCR of SOD1 siRNA recovered by ultracentrifugation after electroporation with or without sEVs. Unpaired two-tailed t-test; n = 3 for all groups. Right, RT–qPCR of SOD1 siRNA recovered by ultracentrifugation and then treated with RNase A and RNase T1 after electroporation with or without sEVs (NSC-34). Repeated measurements one-way analysis of variance (ANOVA) with Holm–Sidak correction; n = 3. **d**, Absolute copy numbers of miRNAs in sEVs measured by standard curve RT–qPCR analysis in sEVs produced by three cell types (MDA-MB-231 (n = 3), MEF (n = 2) and NSC-34 (n = 3)). **e**, Enrichment of miRNAs in sEVs, expressed as the level of the respective miRNA in total sEV RNA relative to its level in total cell RNA as measured by RT–qPCR, normalized to miR-16. MEF (n = 2) and NSC-34 (n = 3)). **f**, Enrichment of miR-451 in sEVs versus its level in cells in the listed cell types. n = 6 (mesenchymal stem cell (MSC) and macrophage) and n = 3 (all others). **g**, RT–qPCR to measure relative quantity of miR-451 in sEVs (NSC-34) left untreated, treated with RNase or treated with detergent and RNase. n = 2. **h**, Sucrose density gradient fractionation of sEVs produced by NSC-34 cells. Top: densities of fractions measured by refractometry (black line) and quantity of miR-451 (red dots, RT–qPCR, 2^{-Ct} without normalization) in these fractions. Western blot for Ago2 was performed on a separate membrane with the same fractions as western blots for Alix and flotillin 2. **i**, RT–qPCR analysis of combined fractions 6 and 7 from **h** either left untreated, treated with RNase A and RNase T1, or RNase A/T1 and 0.5% Triton X-100. Full blot images from **a** and **h** are presented in Supplementary Information. Data are mean ± s.e.m. NS, not significant.

We evaluated the absolute copy number of endogenous miRNA per sEV. Nanoparticle tracking enabled counting of 100 nm polystyrene particles of known concentration with high accuracy and reproducibility across a range that coincided closely with that recommended by the instrument's software (Supplementary Fig. 2.1c). sEVs were diluted into this range for quantification in all experiments. To estimate the number of miRNA per sEVs, standard curves of quantitative PCR (qPCR) products were used correcting for efficiency of qPCR with reverse transcription (RT–qPCR) (Supplementary Fig. 2.1d). An independent method, digital droplet PCR, demonstrated that the standard curve method quantified miRNA with an error of less than 20% over a wide range of concentrations (Supplementary Fig. 2.1e). Some miRNAs were present at 1 to 10 copies per sEV (Fig. 2.1d), in agreement with studies which quantified the most abundant miRNAs in sEVs[224]. By contrast, many miRNAs, such as miR-16, miR-451 and miR-134, were present at extremely low numbers in sEVs (1 copy per 10,000 sEVs to 1 copy per 10 sEVs; Fig. 2.1d), in line with previous studies[199]. The relative abundance in sEVs of several of the miRNAs tested did not differ greatly from their abundance in sEV-producing cells (Fig. 2.1e), suggesting that they are randomly packaged into sEVs. Notably, despite its low copy number in sEVs (Fig. 2.1d), miR-451 was 500 to 10,000-fold enriched in sEVs compared with its levels in the respective cells (Fig. 2.1e,f). miR-451 was similarly enriched in sEVs normalized to U6 RNA and produced in serum-free Ultraculture medium (Lonza) (Supplementary Fig. 2.1f).

miR-451 is abundant in fetal bovine serum (FBS), and trace amounts of miR-451 and sEVs may persist even in sEV-depleted FBS[225, 226]. These sources of miR-451 could attach to or be internalized by cells and be maintained across cell culture passages. This suggests the possibility that the observed enrichment of miR-451 in sEVs could be due to contamination with residual miR-451 from FBS. Whereas miR-451 was abundant in FBS, more than 99.99% of this was

eliminated by ultracentrifugation for 18 h and total amounts of miR-451 in sEVs increased approximately 32-fold when sEV-depleted medium was incubated with cells (Supplementary Fig. 2.2a). In addition, culture of three cell types in serum-free medium continuously for six weeks or eightfold dilution of cells into serum-free medium did not deplete miR-451 in cells or sEVs, or impact its enrichment in sEVs (Supplementary Fig. 2.2b–m). This demonstrates that miR-451 is being continuously expressed by many cell types and is strongly enriched in sEVs released by these cells.

miR-451 was similarly enriched in sEVs when normalized to miR-16 (Fig. 2.1e,f) which exhibits similar abundance to miR-451 in the sEVs tested (Fig. 2.1d), or to U6 RNA (Supplementary Fig. 2.1f). Finally, miR-451 was present inside sEVs as it was only sensitive to RNase treatment after pre-treatment with detergent (Fig. 2.1g). Similarly, when sEVs were isolated by sucrose density gradient centrifugation, miR-451 abundance peaked with sEV-containing fractions at a density of 1.10–1.18 g ml^{-1} (Fig. 2.1h). miR-451 in these fractions was only sensitive to RNase degradation after permeabilization of sEVs with detergent (Fig. 2.1i). Furthermore, miR-451 was not digested with RNase even when sEVs were pre-treated with proteinase K to release any RNA from proteins or protein aggregates co-purifying with sEVs, whereas a spiked-in siRNA was degraded even without detergent (Supplementary Fig. 2.3a,b). This demonstrates that miR-451 is selectively packaged inside sEVs compared with other cellular miRNAs.

New siRNAs in pre-miR-451 structures are enriched in sEVs

The stem–loop hairpin of pre-miR-451 binds directly to Ago2, which cleaves the distal strand of RNA in the stem region[206-208]. Exonucleases then trim pre-miR-451 to around 22 nt, producing a mature miRNA (Fig. 2.2a). Other miRNA sequences can be integrated into the pre-miR-451 hairpin and processed through the same Dicer-independent pathway[206-208] (Fig. 2.2a). We

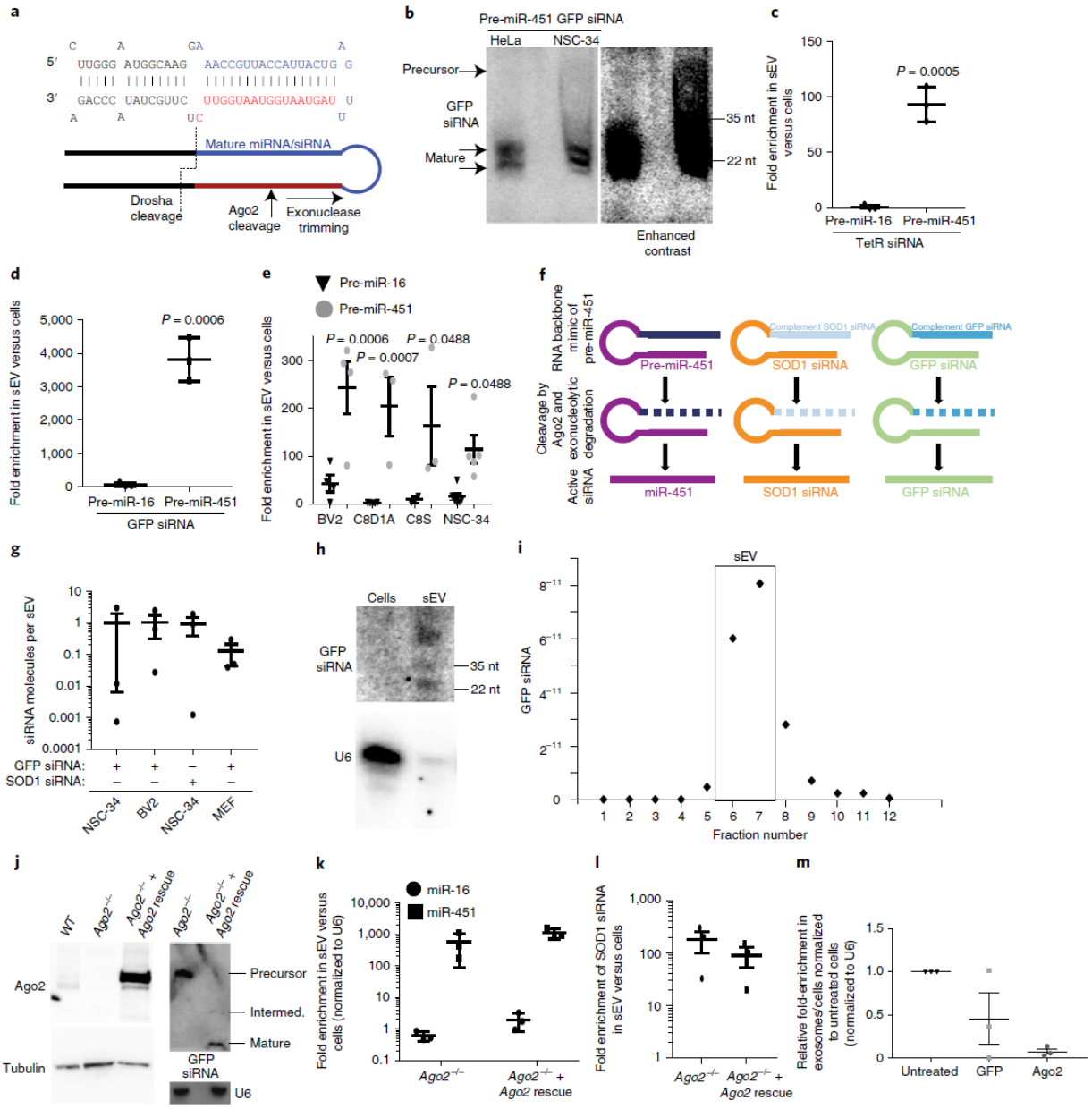

Figure 2.2. Reprogramming the pre-miR-451 backbone with siRNAs causes their enrichment in sEVs. a, Schematic of the predicted pre-miR-451 secondary structure, detailing its cleavage by Drosha, Ago2 and subsequent trimming by exonucleases. **b**, Northern blot of GFP siRNA produced from the pre-miR-451 backbone in HeLa and NSC-34 cells. **c**,**d**, RT–qPCR measuring enrichment of TetR (**c**) or GFP (**d**) siRNA in sEVs versus their levels in cells when these were integrated in either the pre-miR-451 backbone or the pre-miR-16 backbone (control) and transiently expressed in MEF. Two-tailed unpaired t-test; n = 3. **e**, RT–qPCR measuring enrichment of SOD1 siRNA in sEVs versus the level in cells when SOD1 siRNA was integrated in either the pre-miR-451 backbone or the pre-miR-16 backbone (control) and transfected into the indicated cell types. One-way ANOVA with Holm–Sidak correction; n = 4, 3, 2 and 6 for BV2, C8D1A, C8S and NSC-34 pre-miR-16 control transfected, respectively; n = 4, 3, 3, and 5 for the same cell types, respectively, transfected with pre-miR-451. **f**, Schematic portraying the

reprogramming of the pre-miR-451 hairpin structure with siRNA targeting SOD1 or GFP siRNA. **g**, Copy number of GFP or SOD1 siRNA in sEVs after stable expression from the pre-miR-451 backbone in the indicated cell types. n = 3. **h**, Northern blot of GFP siRNA or U6 (control) in equal amounts of RNA from cells or sEVs from MEFs. **i**, RT–qPCR analysis of GFP siRNA processed integrated in the pre-miR-451 backbone in fractions of density gradient in Fig. 2.1k using the 2^{-Ct} method without normalization. **j**, Western blot of Ago2 and tubulin (loading control) in WT, *Ago2*$^{-/-}$ or *Ago2*$^{-/-}$ cells stably rescued with Ago2. Right: northern blot of GFP siRNA programmed into the pre-miR-451 backbone or U6 (loading control) in cellular RNA of *Ago2*$^{-/-}$ cells or *Ago2*$^{-/-}$ cells stably rescued with Ago2. Intermed., intermediate. **k**,**l**, RT–qPCR of miR-16 and miR-451 (**k**) or SOD1 siRNA integrated in the pre-miR-451 hairpin structure (**l**) in sEVs versus cells, using *Ago2*$^{-/-}$ or *Ago2*$^{-/-}$ cells stably rescued with Ago2. Enrichment in sEVs versus cells normalized to U6 (**k**) or miR-16 (**l**) RNA. n = 3. **m**, RT–qPCR to measure fold change in enrichment in sEVs versus cells of miR-451 after transiently expressing GFP (control) or Ago2. Full blot images from **b**, **g** and **k** are presented in the Supplementary Information. One-way ANOVA with Holm–Sidak multiple comparison, unless otherwise mentioned. Data are mean ± s.e.m. the pre-miR-451 hairpin are enclosed inside sEVs and are not substantially in protein aggregates (Supplementary Fig. 2.3a,b,e,f).

hypothesized that integrating siRNA into the pre-miR-451 backbone would cause these siRNA to be enriched in sEVs. We integrated a siRNA targeting GFP into the pre-miR-451 backbone. As expected, this was processed into a mature siRNA of about 22 nt in cells (Fig. 2.2b). Integration of siRNA targeting GFP, tetracycline repressor (TetR) or SOD1 into the pre-miR-451 backbone caused these siRNA, like miR-451, to be enriched from 58-fold to more than 7,000-fold in sEVs produced by multiple cell types (Fig. 2.2c–e and Supplementary Fig. 2.3c,d). This was independent of over-expression, as integration of the same siRNA in pre-miR-16 did not result in comparable enrichment in sEVs measured as relative enrichment or absolute copy number (Fig. 2.2c–e and Supplementary Fig. 2.3c,d). When produced from the pre-miR-451 hairpin, siRNA targeting GFP or SOD1 were enriched up to one copy per sEV on average (Fig. 2.2g and Supplementary Fig. 2.3d), similar to the level of the most abundant miRNA in sEVs[199] (Fig. 2.1d). Finally, miR-451 (Fig. 2.1h,i) and GFP-targeted siRNA expressed from the pre-miR-451 hairpin separated with sEVs on sucrose density gradients (Fig. 2.2h,i). Ago2, like proteins inside sEVs including Alix and Tsg101 were only sensitive to proteinase K digestion when sEVs were treated with detergent (Supplementary Fig. 2.3e). Similarly, GFP siRNA in sEVs purified by sucrose density gradient

resisted RNase digestion when these sEVs were pre-treated with proteinase K, but were rendered sensitive to RNase digestion after treatment of sEVs with detergent (Supplementary Fig. 2.3f). This provides strong evidence that Ago2, miR-451 and siRNA expressed from the pre-miR-451 hairpin are enclosed inside sEVs and are not substantially in protein aggregates (Supplementary Fig. 2.3a,b,e,f).

Pre-miR-451 structures are packaged independently of Ago2

The evidence described above shows that siRNA of unrelated sequences can be integrated in the pre-miR-451 structure, leading to their enrichment in sEVs (Fig. 2.2b–g). This suggests that it is the structure of the pre-miR-451 hairpin and not a specific siRNA sequence that is required for packaging into sEVs. Low levels of Ago2 are present in sEVs, even when purified by sucrose density gradient[227] (Fig. 2.1a,h and Supplementary Figs. 2.1a,2.3e). This suggests that once packaged into sEVs, pre-miR-451 hairpins approximately 42 nt in length may be processed there by Ago2 into mature miRNAs in the hours to days between generation of sEVs vesicles in late endosomes, their release from cells and isolation[228]. In agreement, whereas in cells, mature forms of GFP-targeted siRNA of about 21 nt integrated into pre-miR-451 dominate (Fig. 2.2b), in sEVs, these RNAs are highly abundant at sizes corresponding to pre-miR-451 precursors (approximately 42 nt), intermediate processing products (24–34 nt) and mature siRNA (about 22 nt; Fig. 2.2h). This confirms, independently of RT–qPCR analysis, the enrichment in sEVs of siRNAs built into the pre-miR-451 structural mimic and suggests that precursor forms of pre-miR-451 structural mimics rather than mature forms are preferentially packaged into sEVs.

To test directly whether the precursor form of miR-451 is packaged into sEVs, we used *Ago2*$^{-/-}$ cells, which arrest processing of pre-miR-451 or its structural mimics at the 42 nt-hairpin stage[206-208]. Confirming this arrest, only the 42 nt form of GFP-targeting siRNA integrated in the

pre-miR-451 hairpin was detected by northern blot in *Ago2*$^{-/-}$ cells and sEVs, whereas a mature approximately 21 nt form was detected in cells rescued with wild-type (WT) Ago2 (Fig. 2.2j and Supplementary Fig. 2.2g). This means that in *Ago2*$^{-/-}$ cells, only the approximately 42 nt precursor of pre-miR-451 structural mimics is available for packaging into sEVs. To determine the relative length of pre-miR-451 structural mimics in sEVs by an independent method, we used an RT–qPCR kit (miScript, Qiagen) that preferentially amplifies either the ~ 22 nt mature miRNA or siRNA (specific buffer) or longer precursors (flexible buffer). Validating this assay with synthetic RNAs, 42 nt pre-miR-451 structural mimics were amplified more quickly with the flexible buffer, whereas the corresponding 21 nt mature siRNA was amplified more quickly with the specific buffer (Supplementary Fig. 2.3h). This enables the relative enrichment of pre-miR-451 precursors versus mature forms to be expressed as a ratio of RNA abundance measured by flexible versus specific buffers. In sEVs produced by WT cells, SOD1 siRNA produced from a pre-miR-451 structural mimic was amplified at similar cycle numbers with either the flexible or specific buffers (Supplementary Fig. 2.3i), suggesting that the SOD1 siRNA exists in WT sEVs as a mixture of mature siRNA and longer pre-miR-451 structural mimics, as demonstrated by northern blot data (Fig. 2.2h and Supplementary Fig. 2.3g). By contrast, sEVs produced by *Ago2*$^{-/-}$ cells were strongly enriched in long forms of pre-miR-451 structural mimics (Supplementary Fig. 2.3i), closely resembling amplification of the 42 nt synthetic version of pre-miR-451 structural mimics (Supplementary Fig. 2.3h). This reinforces northern blot data showing that *Ago2*$^{-/-}$ cells (Fig. 2.2j) only contain 42 nt versions of pre-miR-451 structural mimics for packaging into sEVs.

Of note, the relative enrichment in sEVs of pre-miR-451 or a pre-miR-451 structural mimic containing SOD1 siRNA were not significantly changed in the absence of Ago2 despite these cells only containing 42 nt precursors of these (Fig. 2.2j–l). Similarly, over-expression of Ago2 in WT

cells did not significantly change the enrichment of pre-miR-451 derivatives in sEVs (Fig. 2.2m). Ago2 expression appears to slightly reduce packaging of pre-miR-451 derivatives into sEVs (Fig. 2.2j–m), although these effects were not statistically significant. This suggests that binding of pre-miR-451 derivatives to Ago2 may retain them in cells and pre-miR-451 hairpins are robustly packaged into sEVs independent of Ago2. Once inside sEVs, low levels of Ago2 there (Fig. 2.1a,h and Supplementary Figs. 2.1a, 2.3e) may process pre-miR-451 structural mimics into shorter versions. Cumulatively, this suggests that the 42 nt pre-miR-451 structural mimics can account for all selective packaging into sEVs rather than a mature version of the miRNAs or siRNAs produced from it. At the same time, the data cannot exclude that approximately 20–24 nt forms of miR-451 or siRNA derived from pre-miR-451 structural mimics are also packaged into sEVs in WT cells.

Hairpins in RNAs inhibit processivity of reverse transcriptase, compete for primer binding and can impede PCR. Our data confirm this as, equimolar amounts of synthetic mature siRNA (21 nt) were amplified much earlier in RT–qPCR reactions than a similar amount of the same siRNA embedded in a 42 nt pre-miR-451 structural mimic that contains a hairpin (Supplementary Fig. 2.3h). This suggests that the presented RT–qPCR analyses may underestimate the enrichment of pre-miR-451 structural mimics in sEVs (where longer forms with secondary structure are abundant) compared with their levels in cells where mature approximately 21 nt versions of these RNAs predominate.

Select sEVs deliver siRNA to primary motor neurons

We sought to test whether sEVs loaded with siRNA reprogrammed into the pre-miR-451 backbone could efficiently deliver these siRNA. sEVs from NSC-34 cells that were packaged with either siRNA targeting GFP or a control siRNA expressed from the pre-miR-451 backbone were incubated with primary mixed motor neuron cultures from GFP transgenic mice. siRNA detected

by fluorescence in situ hybridization (FISH) accumulated in motor neurons and colocalized with target GFP mRNA and a marker of P-bodies (DDX6, also known as RCK) (Fig. 2.3a,b). This suggests the siRNA packaged in sEVs has reached the cytoplasm and engaged its target in RNA silencing. GFP knockdown in mixed motor neuron cultures measured by RT–qPCR peaked at a ratio of 1,000 sEVs per cell (Fig. 2.3c). We used FISH capable of detecting single mRNA molecules as an orthogonal method to quantify GFP mRNA. Similar to RT–qPCR results, both FISH for GFP mRNA and GFP protein fluorescence exhibited peak knockdown at ratios of 1,000 sEVs per cell (Fig. 2.3d). Free siRNA administered to mixed motor neurons at the same dose had no effect on GFP expression (Fig. 2.3e). Knockdown of GFP in primary mixed motor neurons did not require sEV-producing cells to express Ago2, demonstrating that siRNA in the pre-miR-451 hairpin can be packaged into sEVs equivalently in the absence of Ago2, and delivered into target cells in the precursor form (Fig. 2.3f). sEVs produced by a distinct neuronal cell line, Neuro2a, and loaded with GFP siRNA also reduced GFP mRNA expression (Fig. 2.3g,h, and Supplementary Fig. 2.4a), whereas vesicles produced by BV2 microglia cells did not (Fig. 2.3i,j and Supplementary Fig. 2.4b), despite both being packaged with GFP siRNA to the same level as sEVs produced by NSC-34 cells (1 copy per sEV-like vesicle; Fig. 2.2g). This demonstrates that the cell source of sEVs can determine whether siRNA delivery is effective. This suggests that sEVs deliver siRNA to targeted, specific cell types.

Multiple previous studies have together established that between 300 and 2,000 copies of a siRNA are required to elicit target knockdown in cells[52-54]. If sEVs at a dose of 1,000 siRNAs per cell cause target knockdown (Fig. 2.3c–e), then sEVs would appear to deliver a large proportion of their siRNA contents into the cytoplasm, compared with 0.05–1% of siRNA for lipid nanoparticles[52, 218]. However, as previously reported[229, 230], recovery of spiked-in RNA of 21 nt

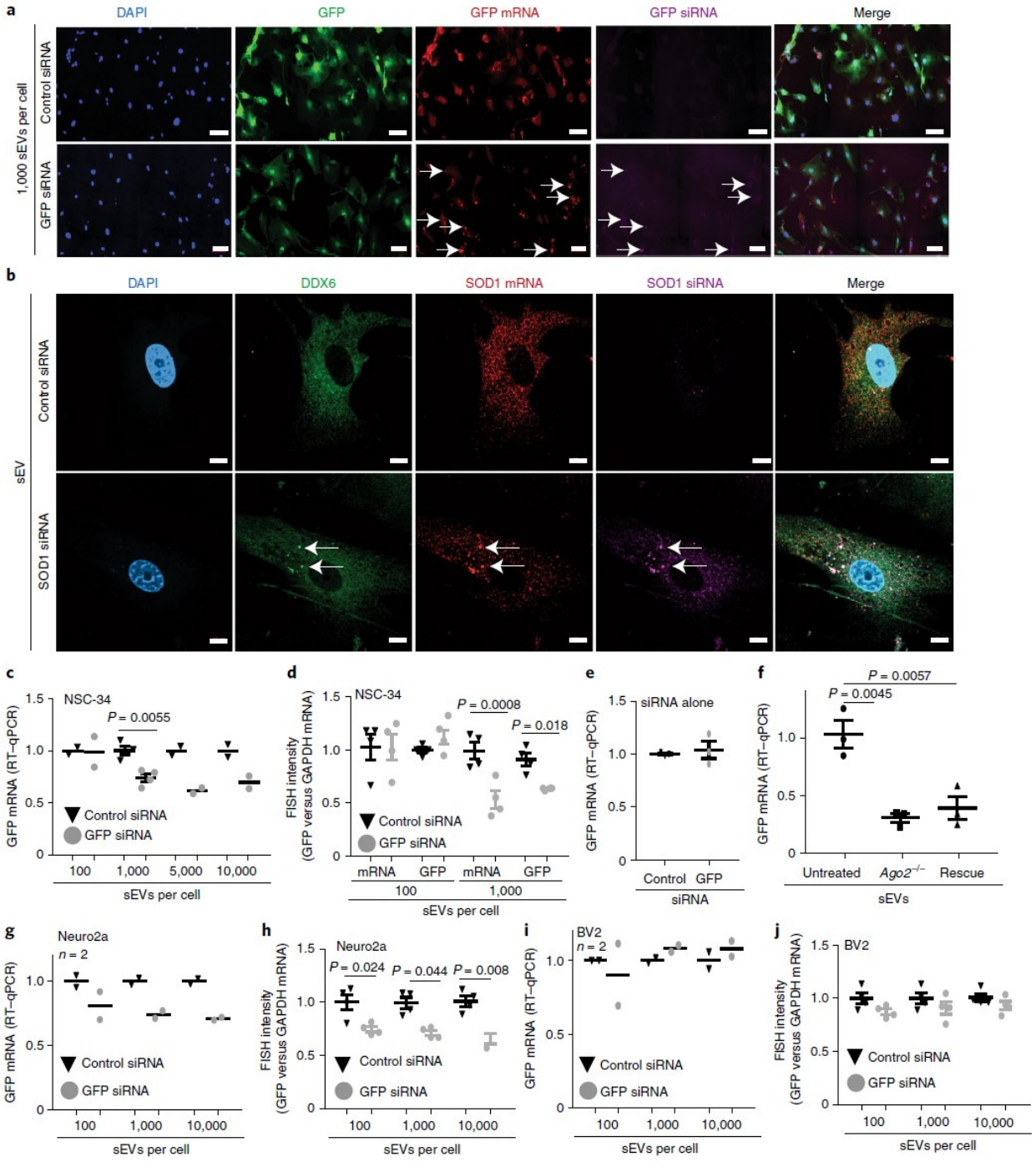

Figure 2.3. sEVs loaded with siRNA integrated in the pre-miR-451 backbone efficiently deliver siRNA to primary motor neurons. a, Confocal microscopy of GFP fluorescence, GFP mRNA (FISH) and siRNA targeting GFP (FISH) in primary mouse motor neurons from GFP transgenic mice after incubation with sEVs produced by NSC-34 cells and loaded with the indicated siRNA integrated in the pre-miR-451 backbone. Scale bars, 100 μm. White arrows highlight co-localization of siRNA and target mRNA. **b**, Confocal microscopy of DDX6 (P-body marker), SOD1 mRNA (FISH) and siRNA targeting SOD1 (FISH) in primary mouse motor neurons from human SOD1(G93A) transgenic mice after incubation with sEVs loaded with the

indicated siRNA integrated in the pre-miR-451 backbone. Scale bars, 10 μm. White arrows highlight co-localization of siRNA and target mRNA in P bodies. **c**, RT–qPCR for GFP mRNA in primary mixed motor neuron cultures of GFP transgenic mice after incubation with the indicated doses of sEVs produced by NSC-34 cells. n = 4 at 1,000 sEVs per cell, n = 2 all others. **d**, Quantification of GFP fluorescence and GFP mRNA in primary mixed motor neuron cultures of GFP transgenic mice after incubation with the indicated doses of sEVs produced by NSC-34 cells. **e**, RT–qPCR for GFP mRNA in primary mixed motor neuron cultures of GFP transgenic mice after incubation with amounts of siRNA alone equivalent to that in 1,000 sEVs per cell. n = 3. **f**, RT–qPCR for GFP mRNA in primary mixed motor neuron cultures from GFP transgenic mice after incubation with sEVs produced by MEF cells produced by *Ago2*$^{-/-}$ or *Ago2*$^{-/-}$ cells stably rescued with *Ago2*. n = 3. **g**,**i**, RT–qPCR for GFP mRNA in primary mixed motor neuron cultures of GFP transgenic mice after incubation with the indicated doses of sEVs produced by Neuro2a cells (**g**) or BV2 cells (**i**). Reference mRNAs were averaged GAPDH, GusB and TfrR. n = 2. **h**,**j**, Quantification of GFP fluorescence and GFP mRNA in primary mixed motor neuron cultures of GFP transgenic mice after incubation with the indicated doses of sEVs produced by Neuro2a cells (**h**) or BV2 cells (**j**). One-way ANOVA with Holm–Sidak multiple comparison. For microscopy analysis, fields of view containing approximately 100 cells were quantified (4 per slide, n = 4 slides, ~1,600 cells in total). Data are mean ± s.e.m.

was lower than 10% when small amounts of RNA were used, as in sEVs preparations (Supplementary Fig. 2.4c). The poor recovery of small RNAs with limited amounts of RNA input has not been accounted for in previous studies of miRNA copy number in sEVs. This suggests that estimates of siRNA and miRNA copy number in sEVs here (Figs. 2.1–3) and in the literature may be underestimated by 10- to 30-fold, and the delivery efficiency of sEVs may be correspondingly lower.

SEVs deliver siRNA to multiple organs in mice

We tested whether sEVs could deliver siRNA in mice. sEVs labelled with the far-red dye DiR and injected intravenously distributed broadly to many tissues including liver, kidneys, spleen, intestines and lungs (Fig. 2.4a). By contrast, DiR alone, subjected to the identical labelling method but without sEVs, resulted in negligible signals in mice (Fig. 2.4a). sEVs packaged with GFP-targeted siRNA at approximately 1–30 copies per sEV (Fig. 2.2g and Supplementary Fig. 2.4c) or control siRNA (10^{10} sEVs) were injected intravenously into mice constitutively expressing GFP

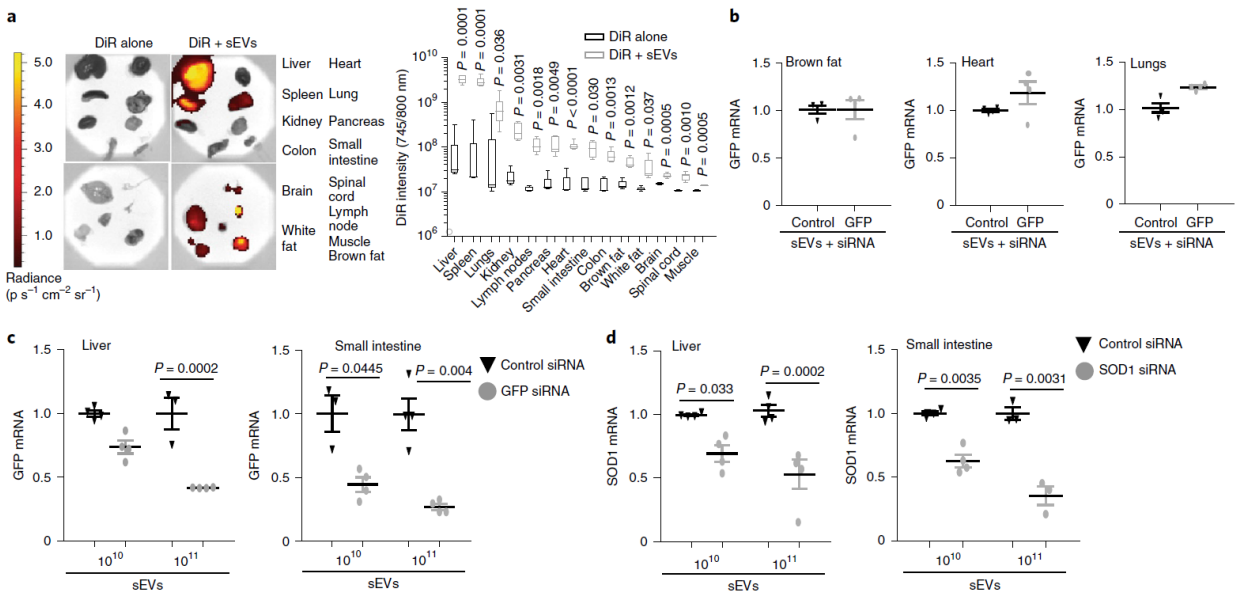

Figure 2.4. Intravenously injected sEVs loaded with siRNA integrated in the pre-miR-451 backbone knock down target expression in mouse liver and small intestine. a, Left: Imaging of organs collected from mice injected with sEVs (NSC-34) labelled with DiR or DiR prepared similarly without sEVs. Right: quantification of fluorescence in organs of intravenously injected mice. n = 5 mice. Box plot shows median value, box edges represent the 25th and 75th percentiles and whiskers span the maximum and minimum values. Two-tailed unpaired t-test with Welch's correction. **b**, RT–qPCR of GFP mRNA in brown fat, heart and lungs 3 d after injection of 10^{10} sEVs (NSC-34) packaged with GFP siRNA or control siRNA. n = 4 mice per group. Two-tailed unpaired t-test with Welch's correction. **c**, RT–qPCR of GFP mRNA in liver and small intestine of GFP transgenic mice 3 d after injection of 10^{10} or 10^{11} sEVs (NSC-34) packaged with GFP siRNA or control siRNA. n = 4 mice per group for liver and control groups, n = 6 for small intestine GFP siRNA. **d**, RT–qPCR of SOD1 mRNA in liver and small intestine of SOD1 (G93A) mice 3 d after injection of 10^{10} or 10^{11} sEVs (NSC-34) packaged with SOD1 siRNA or controls (equal numbers of untreated mice and mice treated with sEVs packaged with control siRNA). n = 4 mice per group. One-way ANOVA with Holm–Sidak multiple comparison, unless otherwise mentioned. Data are mean ± s.e.m. except in **a**.

from a ubiquitous promoter. Despite the accumulation of sEVs in heart, lungs and brown fat (Fig. 2.4a), no knockdown of targets was detected in these organs at an estimated siRNA dose of 10–300 ng kg^{-1} (Fig. 2.4b). By contrast, in the small intestine and liver, sEVs packaged with GFP siRNA decreased GFP expression by approximately 50% (Fig. 2.4c). Similar knockdowns in liver and small intestine were observed if sEVs packaged with SOD1 siRNA by reprogramming the pre-miR-451 hairpin were injected intravenously into mice transgenic for human SOD1(G93A) mutant (Fig. 2.4d). Increasing by tenfold the dose of sEVs (10^{11}) and siRNA (estimated 100–3,000

ng kg^{-1}) increased knockdown in liver to 50–60% and small intestine to 70–75% (Fig. 2.4c,d). This demonstrates that sEVs can deliver siRNA to specific organs and knock down targets in a dose-dependent manner.

The half-life of miRNA or siRNA in non-dividing cells is estimated at between one and four weeks[231, 232]. This suggests that target knockdown induced by unmodified siRNA delivered by sEVs may similarly last for multiple weeks[231, 232]. In agreement, knockdown of GFP mRNA after injection of sEVs packaged with GFP siRNA persisted for 12 d in liver, where cell turnover is slow[233] (Fig. 2.5a). By contrast, epithelium and other cells in the intestine turn over in less than a week[233]. In agreement, knockdown of GFP mRNA in the small intestine had dissipated by 12 d (Fig. 2.5b). This suggests that the effects of unmodified siRNA delivered by sEVs can persist for extended periods of time in tissues with slow rates of cellular turnover.

Enhanced delivery efficiency compared with other vehicles

Testing sEVs delivery of siRNA on primary motor neurons suggested that sEVs may be highly efficient delivery vehicles. To test this *in vivo*, we compared sEVs packaged with siRNA using the pre-miR-451 backbone to lipid nanoparticles. As expected, InVivoFectamine lipid nanoparticles (ThermoFisher) at a high dose (1 mg kg^{-1}) of mature standard siRNA of the same sequence as in sEVs decreased target mRNA expression in the liver by > 80% and by approximately 55% in small intestine (Fig. 2.5c). sEVs packaged with approximately 10–300 ng kg^{-1} siRNA elicited knockdown in liver and small intestine, whereas InVivoFectamine lipid nanoparticles with the same dose of siRNA had no effect on target mRNA levels (Fig. 2.5c). We compared sEVs with advanced C12–200 lipid nanoparticles capable of silencing targets in liver at doses of 0.003 mg kg^{-1} and 0.03 mg kg^{-1} (ref. 41). At 0.3 mg kg^{-1}, C12–200 lipid nanoparticles elicited 60% silencing of GFP in liver at 3 d, while sEVs at a siRNA dose 10- to 300-fold lower

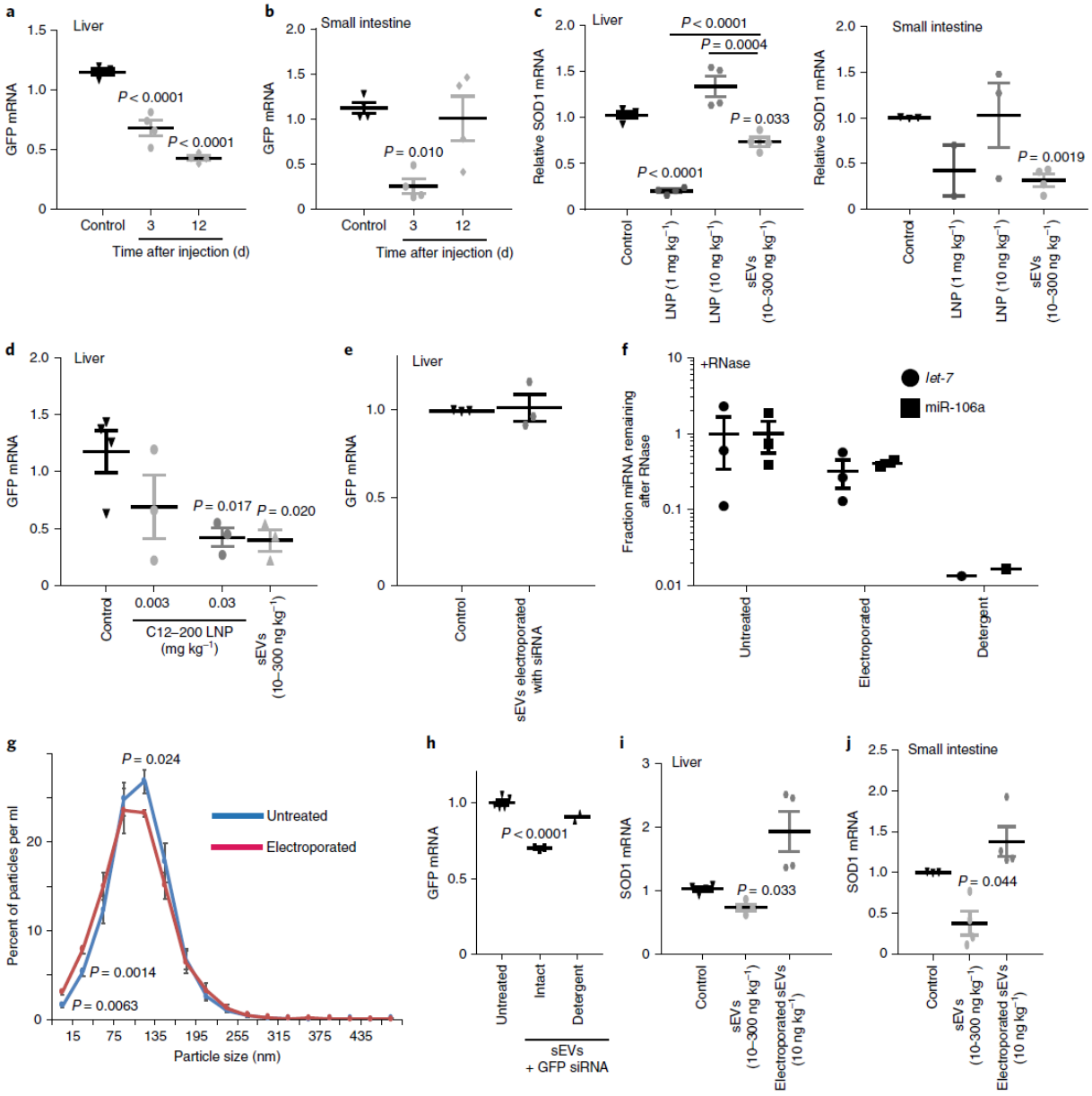

Figure 2.5. sEVs loaded with siRNA integrated in the pre-miR-451 backbone knock down target expression with lower doses than lipid nanoparticles or electroporated sEVs. a,**b**, RT–qPCR of GFP mRNA in liver (**a**) and small intestine (**b**) of GFP transgenic mice 3 d or 12 d after injection of 10^{10} sEVs packaged with GFP siRNA or control siRNA. n = 4 mice per group at 3 d, n = 3 mice per group at 12 d. **c**, RT–qPCR of SOD1 mRNA in liver and small intestine of SOD1(G93A) mice 3 d after injection of InvivoFectamine lipid nanoparticles packaged with 1 mg kg^{-1} siRNA, 10 ng kg^{-1} siRNA or 10^{10} sEVs packaged with 10–300 ng kg^{-1} of the identical SOD1 siRNA. n = 4 mice per group. LNP, lipid nanoparticles. **d**, RT–qPCR of GFP mRNA in liver 3 d after intravenous injection of C12–200 lipid nanoparticles or sEVs packaged with GFP siRNA at the indicated doses. n = 3 mice for control siRNA, n = 4 mice per group of sEVs or lipid nanoparticle treatments. **e**, RT–qPCR of GFP mRNA in liver of GFP transgenic mice 3 d after injection of sEVs electroporated with GFP siRNA using previously published conditions[181]. n = 3 mice per group. **f**, RT–qPCR of let-7 and miR-106 after treatment of sEVs pellets with RNase A

and RNase T1 after sEVs were left untreated, electroporated as described[181], or treated with detergent. n = 3 or n = 2 experiments as shown. **g**, Size distribution of sEVs after electroporation measured by nanoparticle tracking analysis. n = 6 sEVs preparations. **h**, RT–qPCR of GFP mRNA in mixed motor neurons after incubation for 2 d with sEVs (10,000 per cell) left intact or disrupted with detergent. n = 5 untreated, n = 3 for intact sEVs and n = 2 for detergent-treated sEVs. **i**,**j**, RT–qPCR of SOD1 mRNA in liver (**i**) and small intestine (**j**) after treatment of mice with sEVs packaged with control siRNA or sEVs that were left untreated or electroporated after packaging with SOD1 siRNA using the pre-miR-451 hairpin. n = 4 mice per group. All sEVs were derived from NSC-34 cells. One-way ANOVA with Holm–Sidak multiple comparison. Data are mean ± s.e.m

elicited similar silencing in liver (Fig. 2.5d). This reinforces the notion from experiments on primary mixed motor neuron cultures that sEVs deliver siRNA at least tenfold more efficiently than lipid nanoparticles.

Others have proposed electroporation as a strategy to load siRNA into sEVs. In agreement with previous literature[195], our data suggests that siRNA is not packaged inside sEVs by electroporation, but is precipitated and co-purifies with them (Fig. 2.1c). Nonetheless, we used the electroporation instrument and settings as published[181, 182] to test the ability of sEVs electroporated with siRNA to deliver cargoes in mice. Mice were injected with sEVs electroporated with 10 ng kg^{-1} of siRNA. At this dose, intact sEVs packaged with the pre-miR-451 backbone elicit 35–50% knockdown in liver (Figs. 2.4c, 5a), but sEVs electroporated with siRNA failed to decrease target expression (Fig. 2.5e).

Electroporated cells often die due to excessive membrane permeabilization. Electroporation of sEVs rendered miR-106a and let-7a endogenously present inside sEVs sensitive to degradation by RNase A nearly to the same extent as sEVs permeabilization with detergents (Fig. 2.5f). Furthermore, analysis of electroporated sEVs by nanoparticle tracking demonstrated a significant loss of sEV-sized particles and an accumulation of smaller sized particles, consistent with sEV fragments, after electroporation (Fig. 2.5g), even if median particle size was unchanged

(Supplementary Fig. 2.4d). This suggests that sEV membrane integrity is disrupted by electroporation and this could compromise the ability of sEVs to deliver siRNA. Confirming this, when the sEV membrane was disrupted by pre-treating sEVs with detergent their ability to deliver GFP siRNA into mixed motor neurons was abrogated (Fig. 2.5h). Similarly, electroporation of sEVs abolished their ability to deliver siRNA in mice. sEVs packaged with SOD1 siRNA using the pre-miR-451 hairpin reduced target expression in the liver and small intestine, but the same sEVs that had undergone electroporation did not (Fig. 2.5i,j). This suggests that electroporation disrupts sEV membrane integrity and the capacity of sEVs to efficiently deliver siRNA.

sEV source-dependent tissue- and cell-specific delivery

Not all cell types produced sEVs capable of delivering siRNA to primary motor neurons (Fig. 2.3). sEVs may deliver cargoes to specific cell types. To investigate siRNA delivery and target knockdown in specific tissue regions or cell types we utilized a FISH method capable of detecting single mRNAs with a linear quantification method. We validated that this FISH method closely replicated target mRNA knockdown assessed by RT–qPCR in liver and small intestine (Fig. 2.6). We then used FISH to quantify target knockdown in specific regions and cell types of these organs. In small intestine, when total GFP mRNA was decreased by 55% by GFP siRNA delivered by sEVs (Fig. 2.6c,d), loss of GFP mRNA and GFP fluorescence was 50% in villi and 80–85% in submucosa (Fig. 2.7a–c and Supplementary Fig. 2.5a,b). In liver, when total tissue GFP fluorescence and mRNA was decreased by 35–50% (Figs. 2.6g,h, 2.7d,e), GFP mRNA and GFP fluorescence in hepatocytes, Kuppfer cells and macrophages ($F4/80^+$), and stellate cells (glial fibrillary acidic protein ($GFAP^+$)) was reduced by 60–70%, 20% and 0%, respectively (Fig. 2.7d,f–i and Supplementary Fig. 2.5c–f). We also assessed siRNA target knockdown in specific regions of the kidney by FISH; at the whole-tissue level, only marginal target knockdown was observed

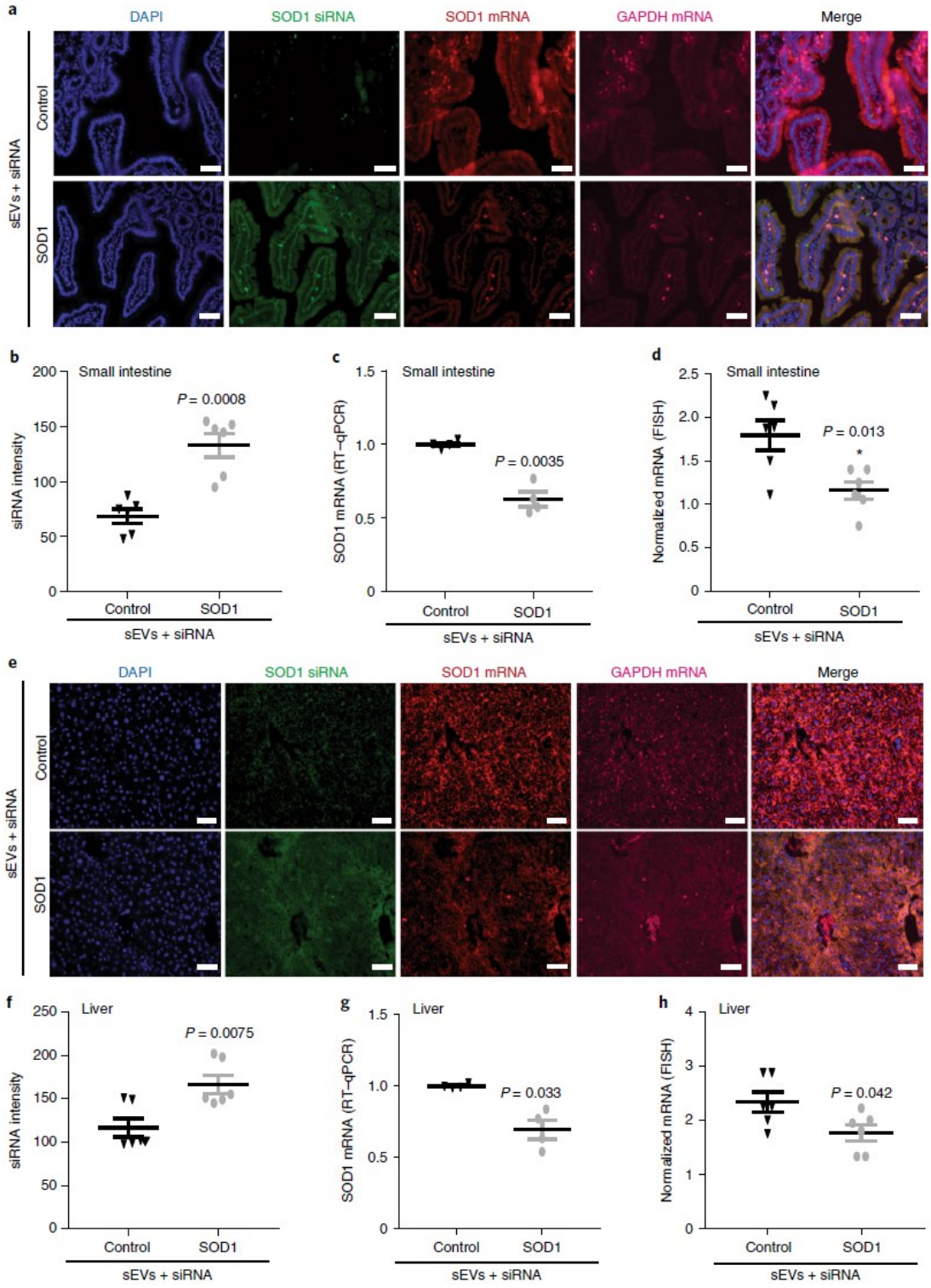

Figure 2.6. Quantitative FISH accurately measures mRNA in mouse tissues. a,**e**, Confocal microscopy of SOD1 siRNA (FISH) and SOD1 mRNA (FISH) versus GAPDH mRNA (normalization control) in sections of mouse liver and small intestine 3 d after injection of sEVs loaded with control siRNA or SOD1 siRNA integrated in the pre-miR-451 backbone. Scale bars, 50 μm. **b**,**f**, Quantification of SOD1 siRNA by FISH in liver and small intestine sections 3 d after

intravenous injection of sEVs loaded with control siRNA or SOD1 siRNA integrated in the pre-miR-451 backbone. **c**,**g**, RT–qPCR of SOD1 mRNA in liver and intestine 72 h after intravenous injection of sEVs loaded with control siRNA or SOD1 siRNA integrated in the pre-miR-451 backbone. n = 5 mice per group. **d**,**h**, Quantification of SOD1 mRNA by FISH in liver and small intestine sections 3 d after intravenous injection of sEVs loaded with control siRNA or GFP siRNA integrated in the pre-miR-451 backbone. Two-tailed unpaired t-tests with Welch's correction; n = 6 animals per experimental group. All sEVs were derived from NSC-34 cells. Two pieces of tissue per slide (duplicates) were analysed in two randomly selected areas (four in total per animal per tissue). n = 4 mice per group for RT–qPCR data. Data are mean ± s.e.m.

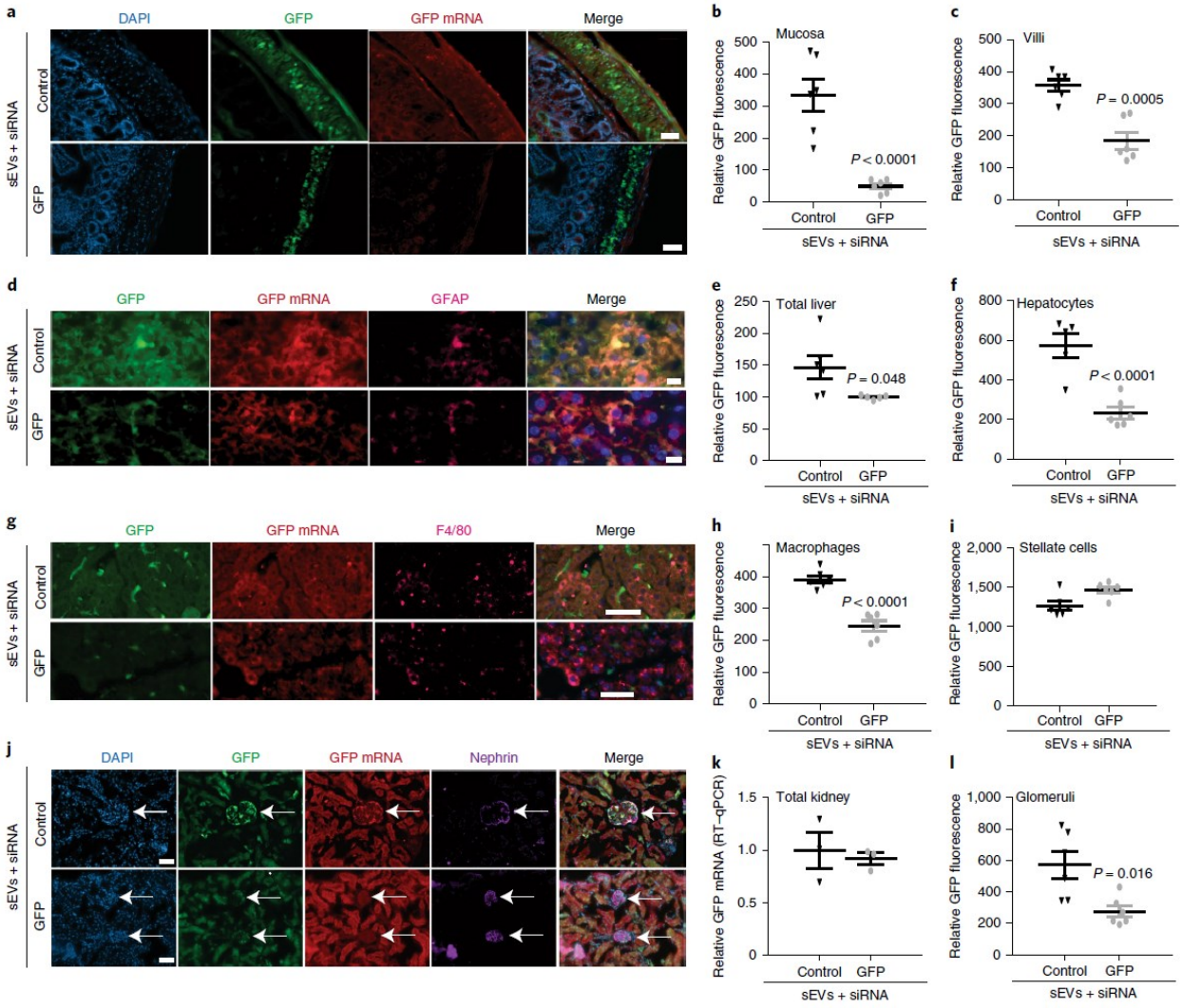

Figure 2.7. sEVs packaged with siRNA knock down target genes in specific regions and cell types of liver, small intestine and kidney. a–l, Experiments were performed on tissues of GFP transgenic mice 3 d after injection of 10^{10} sEVs (low dose) packaged with GFP siRNA or control siRNA using the pre-miR-451 backbone. **a**,**d**,**g**,**j**, Confocal microscopy of GFP fluorescence and GFP mRNA (FISH) in sections of small intestine (**a**; scale bars, 50 μm); liver stained for GFAP, a marker for stellate cells (**d**; scale bars, 10 μm); macrophages (**g**; scale bars, 50 μm); or kidney

stained for nephrin (white arrows), a podocyte marker (**j**; scale bars, 10 μm for control siRNA, 50 μm for GFP siRNA). **b**,**c**,**e**,**f**,**h**,**i**,**l**, Quantification of GFP fluorescence in small intestine submucosa (**b**) and villi (**c**), in total liver (**e**), hepatocytes (**f**), liver macrophages (F4/80) (**h**), liver stellate cells ($GFAP^+$) (**i**) and kidney podocytes ($nephrin^+$) (**l**). **k**, RT–qPCR of GFP mRNA in total kidney 3 d after injection of sEVs packaged with GFP siRNA or control siRNA using the pre-miR-451 backbone. n = 4. Two-tailed unpaired t-test with Welch's correction; n = 6 animals per experimental group. Two pieces of tissue per slide (duplicates) were analysed in two randomly selected areas (four total per animal per tissue). For cell-specific analysis, 3–5 cells positive for the label were quantified per image in 2–3 images per tissue slice and 2 tissue slices per animal. All sEVs were derived from NSC-34 cells. Data for whole-liver and whole-small intestine knockdown contain results from three mice also used in Fig. 2.6, in addition to data from three more mice included only in Fig. 2.7. Data are mean ± s.e.m.

(Fig. 2.7j,k). Notably, in $Nephrin^+$ glomeruli, GFP mRNA and GFP fluorescence were reduced by approximately 50%, whereas knockdown outside these cells was not noticeable (Fig. 2.7j,i and Supplementary Fig. 2.5g). This demonstrates that sEVs exhibit delivery of siRNA to specific cell types and tissue regions in mice.

Of note, in many cell types, such as Kuppfer cells, GFP siRNA delivered by sEVs was abundant; however no knockdown of GFP mRNA was observed. This suggests that in many cell types, sEVs and their cargoes are internalized but rarely fuse with the target cell membrane to deliver their cargoes.

Reduction of transthyretin expression with low siRNA doses

To evaluate the therapeutic potential of siRNA delivery by sEVs, we selected a validated target expressed in a cell type to which delivery had been detected above. Patisiran (trade name Onpattro) was recently approved to treat patients with transthyretin amyloidosis by delivering siRNA targeting the transthyretin (TTR) gene, which is expressed predominantly in liver hepatocytes. siRNA targeting transthyretin was integrated into the pre-miR-451 backbone for packaging into sEVs. It would be preferable to treat patients with sEVs derived from human cells. sEVs produced by primary human fibroblasts or by the human 293T cell line and packaged with

siRNA using the pre-miR-451 backbone elicited knockdown of mRNA targets in liver by > 80% at an estimated siRNA dose of 10–300 ng kg^{-1} (Fig. 2.8a,b and Supplementary Fig. 2.6a,b). sEVs (10^{10}) from human fibroblasts containing an estimated dose of 10–300 ng kg^{-1} siRNA targeting transthyretin or a non-silencing siRNA were injected intravenously. This reduced levels of transthyretin protein in blood in a time course, reaching knockdown of more than 85% at 7 d (Fig. 2.8c,d).

Collectively, these data demonstrate that pre-miR-451 is selectively packaged into sEVs, and integrating siRNA into the hairpin structure of pre-miR-451 can induce their selective packaging into sEVs. By leaving sEVs intact, this strategy enables sEVs to deliver their siRNA cargoes and knock down targets in specific cell types and tissues in mice with siRNA doses that are magnitudes lower than with lipid nanoparticles or other sEVs technologies.

2.4 Discussion

The data presented in this study uses four independent methods to demonstrate that pre-miR-451 and RNAs with unrelated sequences but the same secondary structure are robustly packaged into sEVs (Figs. 2.1, 2.2). Cleavage and maturation of pre-miR-451 is arrested in *Ago2*$^{-/-}$ cells[206-208] at the stage of the 42 nt precursor as confirmed by northern blot and RT–qPCR (Fig. 2.2j and Supplementary Fig. 2.3h,i). Despite this, in *Ago2*$^{-/-}$ cells, pre-miR-451 or a pre-miR-451 structure containing SOD1 siRNA was still similarly enriched in sEVs (Fig. 2.2k–m). In addition, sEVs produced by WT and *Ago2*$^{-/-}$ cells similarly knocked down GFP siRNA targets in primary motor neurons (Fig. 2.3f). These two independent methods demonstrate that the 42 nt hairpin that structurally resembles pre-miR-451 can account entirely for enrichment in sEVs of the studied miR-451 or siRNAs expressed from the pre-miR-451 hairpin.

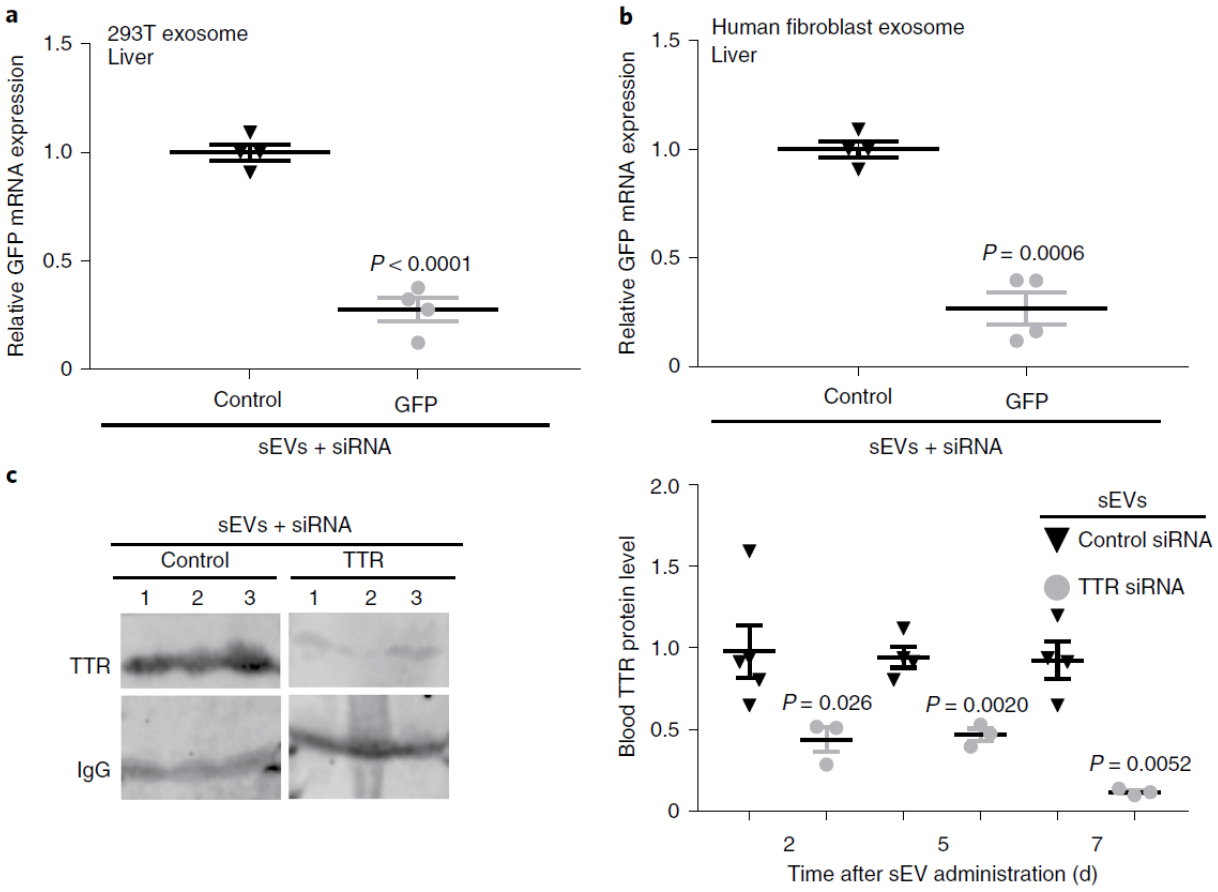

Figure 2.8. sEVs packaged with siRNA targeting TTR reduce TTR levels in blood by more than 85%. a,**b**, RT–qPCR of GFP mRNA 3 d after injection of 10^{10} sEVs produced by 293T cells (**a**) or human primary neonatal fibroblasts (**b**), and packaged with about 10–300 ng kg^{-1} GFP siRNA using the pre-miR-451 backbone, compared with untreated mice. n = 4 mice per group. Experiments in **a** and **b** were performed in parallel with the same control mice. **c**, Left: Western blot of TTR from blood (versus IgG loading control) 7 d after injection of 10^{10} sEVs produced by human primary neonatal fibroblasts and packaged with about 10–300 ng kg^{-1} control siRNA or TTR siRNA using the pre-miR-451 backbone. Right: quantification of TTR levels in blood at 2, 5 and 7 d after sEV administration. n = 4 mice in control group, n = 3 in TTR siRNA group. In **a** and **b**, two-tailed unpaired t-test with Welch's correction. In **c**, one-way ANOVA with Holm–Sidak multiple comparison. Data are mean ± s.e.m. Full blot images from (**c**) are shown in the Supplementary Information.

The sequence of the pre-miR-451 structural mimic is completely changed when a siRNA against a new target is built into it (Fig. 2.2a; GFP, SOD1 or TetR). Nonetheless, these RNAs are highly enriched in sEVs much like pre-miR-451 derivatives (Fig. 2.2). This also strongly suggests that the packaging of these RNAs into sEVs requires the shared structure of the pre-miR-451

hairpin and not mature siRNAs of approximately 21 nt, each with distinct sequences (Figs. 2.1 and 2.2).

Mature, approximately 20–24 nt lengths of GFP siRNA expressed from the pre-miR-451 backbone are the predominant species found in cells (Fig. 2.2b), whereas precursors with lengths of about 42 nt and about 34 nt are abundant in sEVs along with the mature GFP siRNA (Fig. 2.2h). This also suggests that the approximately 42 nt hairpins are selectively packaged into sEVs. Why matured 21–34 nt forms of these RNAs are found in sEVs is less clear. It is possible that these matured forms are also sorted into sEVs in an independent process. An alternative explanation is also possible: sEVs collected from cell medium may have been present in late endosomes for substantial periods before release, and sEVs may remain in cell culture medium for hours before collection. During this time, 42 nt hairpins structurally resembling pre-miR-451 may undergo maturation by low levels of Ago2 packaged inside sEVs[227, 228] (Figs. 2.1a,h, 2.2g, Supplementary Fig. 2.3e). This would account for the ability of only the 42 nt pre-miR-451 structural mimics to drive packaging into sEVs in *Ago2*$^{-/-}$ cells and the relative abundance of matured forms of pre-miR-451 structural mimics in sEVs.

Sequence motifs can also influence packaging of RNAs into sEVs. For example, sequence motifs that bind heterogeneous nuclear riboprotein A2B1 (hnRNPA2B1), YBX1 and HuR have all been shown to promote inclusion of small RNAs into sEVs[147, 149, 151]. While the driving force behind packaging of RNA hairpins with the structure of pre-miR-451 into sEVs is the secondary hairpin structure, these types of sequence motifs may also influence packaging of these hairpins into sEVs.

For years the major physiological role of sEVs was hypothesized to be in expelling proteins from cells or activating receptors on target cells. These effects did not assume the ability of sEVs

to deliver their cargoes into the cytoplasm of target cells. Cells internalize many inert and biological particles, including lipid nanoparticles, apoptotic cells and pathogens, and traffic them to lysosomes for degradation. Therefore, it is important to distinguish sEVs internalization from a more complex and possibly rare event in which sEVs fuse with target cells and deliver their luminal contents into the cytoplasm. We observed that, in some circumstances, cells internalized sEVs and accumulated siRNA but exhibited no signs of siRNA delivery measured as target knockdown (stellate cells in liver or sEVs produced by BV2 cells on primary motor neurons (data not shown)). This highlights that sEV internalization by cells does not always lead to delivery of sEV contents. Cells expend considerable resources to establish and maintain differentiated states and these are critical for tissue specialization in multicellular organisms. sEVs, by transferring RNA contents between cells have the capacity to disturb or overthrow the identity and function of target cells. Our evidence emphasizes that delivery by sEVs is targeted to specific cell types. Biologically, this may help prevent widespread loss of cell identity and function.

Several studies have shown that sEVs contain RNA and that target cells exhibited signs of using siRNA, miRNA or mRNA from sEVs[121, 219, 221, 222]. This has led to the emergence of the model that sEVs escape from endolysosomal degradation to fuse with target cell membranes and deliver their cargoes into the cytoplasm of cells. However, even naked RNAs, incubated with cells at high enough doses, will enter the cytoplasm in sufficient quantities to be active, and this can be substantially improved to the extent that liposomes and lipid nanoparticles can deliver up to 1 in every 100 to 1,000 siRNAs that they contain[52, 62, 218]. In this context, when sEVs were used in previous studies to deliver siRNA, the siRNA doses required were much higher than that of lipid nanoparticles[62, 181, 182, 190], suggesting that sEVs loaded in these manners were relatively inefficient delivery vehicles[53, 218]. This leaves open the possibility that sEVs may have no natural propensity

to fuse with target cells and deliver RNA. Therefore, whether sEVs are actually efficient at delivering RNA into target cells has not been rigorously tested to our knowledge and many experimental effects observed with sEVs could be due to supraphysiological doses of sEVs or excessive amounts of siRNA loaded onto sEVs.

Using absolute quantification of siRNA and sEVs, we have tested the efficiency of sEVs in delivering siRNA into target cells both *in vitro* and *in vivo*. Previous quantitative analyses has shown that 300–2,000 copies of siRNA that catalytically cleave mRNA are required in the cytoplasm of each cell to silence target mRNAs[52-54]. Our results demonstrate that sEVs containing 1,000 to 30,000 copies of siRNA per cell are sufficient to silence target mRNAs in recipient cells. This suggests that between 3–30% of siRNA inside intact sEVs is delivered into the cytoplasm. Supporting this claim, sEVs knock down targets in liver and intestine at siRNA doses at least tenfold lower than lipid nanoparticles or other best-in-class engineered delivery vehicles that only deliver about 1 in every 100 to 1,000 siRNA they contain into cells[52, 53, 218]. This suggests that sEVs are probably between 10- to 300-fold better at delivering siRNA that is packaged inside them into recipient cells than contemporary engineered vehicles. This provides evidence that sEVs are highly efficient delivery vehicles and may have evolved this efficiency to fulfil biological roles in targeted intercellular communication. At the same time, this suggests that the majority of sEVs (70–97%) do not deliver their contents into target cells and are probably degraded in lysosomes. An increasing number of studies have described subpopulations of sEVs differentiated by surface markers and size[86, 234, 235]. It is possible that one subpopulation of sEVs is exceptionally efficient in delivering contents including RNA into the cytoplasm whereas other subpopulations of vesicles are internalized and degraded by cells.

Lipid nanoparticles contain much more siRNA per particle than most miRNA or siRNA in sEVs. Consequently, to inject similar amounts of siRNA requires injecting substantially larger numbers of sEVs than lipid nanoparticles. It is possible that this excess of sEVs (compared to lipid nanoparticles) saturates non-productive pathways of particle entrapment or uptake. Saturating such 'sinks' for particles with an excess of sEVs could theoretically contribute to their enhanced delivery efficacy.

We found that electroporating sEVs ablated their ability to deliver siRNA and knockdown targets in mouse liver and small intestine. Similarly, according to previous studies and our data, sEVs electroporated with siRNA or coated with siRNA required much higher doses of siRNA (ranging from 0.04 mg kg^{-1} (ref. [181]) to 6 mg kg^{-1} (ref. [182])) to elicit target knockdown in mice compared with siRNA packaged inside sEVs endogenously using the pre-miR-451 hairpin (10–300 ng kg^{-1}) or lipid nanoparticles[62]. Adhering to standard models of lipid membrane fusion in cell biology, this suggests that sEVs must remain intact to fuse with target cells and deliver their cargoes.

As previously reported[199], results here demonstrate that miRNA are present at low copy number in sEVs. Accounting for RNA recovery from standard sEV samples (Supplementary Fig. 2.4c), miRNAs, or siRNA packaged into sEVs with the pre-miR-451 backbone may be present in sEVs at up to 30–300 copies per sEVs (Fig. 2.1d and Supplementary Fig. 2.3g). Many other miRNA are detectable in sEVs, but they occur at 100- to 10,000-fold lower copy number per sEV. miRNA have more subtle effects on mRNA degradation and translational inhibition than siRNA used here, which enzymatically cleave their targets. Consequently, our results suggest that only the most abundant miRNAs in sEVs could feasibly have biological effects *in vivo*. Expression or inhibition of miRNAs in sEV-producing cells will have a wide spectrum of effects on lipids,

proteins and small molecules that are released in sEVs with miRNA, and in some cases may account for effects observed in recipient cells independent of the delivery of miRNA by sEVs. Measuring absolute quantities of miRNAs in sEVs rather than relative levels can establish the plausibility that observed effects are due to miRNA in sEVs.

The current results demonstrate that sEVs are highly efficient delivery vehicles, providing evidence to support previous speculation. This suggests that harnessing sEVs to deliver siRNA may enable siRNA doses in patients to be reduced by orders of magnitude. To bring this possibility to practical application will require a method to robustly package siRNA inside sEVs and manufacture them at a feasible scale. The current results show that integration in the pre-miR-451 backbone can enrich an siRNA of choice to the level of the most abundant miRNA in sEVs and thereby reduce volumes required to manufacture sEV delivery vehicles by 100- to 10,000-fold. This suggests that the pre-miR-451 backbone may be the foundation for a method for the manufacture and delivery of therapeutic siRNA.

2.5 Materials and Methods

sEVs isolation

All cells were grown to 70–80% confluence to produce sEVs, except human fibroblasts, which reached 90–100% confluence before collection. sEVs were collected from cells grown in DMEM (Wisent Bioproducts; catalogue no. 319–015-CL; 4.5 g l^{-1} glucose) with 10% sEV-depleted heat-inactivated FBS (Wisent Bioproducts, catalogue no. 080–150) prepared as described[236], or alternatively cultured for 18–24 h in serum-free UltraCULTURE medium (catalogue no. 12–725F, Lonza). sEVs were produced using two methods: differential ultracentrifugation, or tangential flow filtration and ultracentrifugation.

For differential ultracentrifugation, sEVs containing media was spun at 300g for 10 min and supernatants were subsequently centrifuged at 2,000g for 10 min, 10,000g for 30 min (SW-32Ti rotor, Beckman-Coulter Life Sciences; polycarbonate tubes, catalogue no. 355631, Beckman-Coulter Life Sciences) and 100,000g for 2 h (SW-32Ti rotor). sEV pellets were washed by resuspending in 1 ml 1× PBS (Wisent Bioproducts; catalogue no. 311–010-CL) and centrifuged at 100,000g for 30 min (TLA-100.3, Beckman-Coulter Life Sciences; polypropylene microfuge tubes, catalogue no. 357448, Beckman-Coulter Life Sciences).

HEK293T and human fibroblast sEVs were isolated using tangential flow filtration and ultracentrifugation. sEVs-conditioned media was spun at 300g for 10 min and supernatants were subsequently spun at 2,000g for 10 min. Supernatants were passed through a 0.22 μm filter (Thermo-Scientific, catalogue no. 09–741–04) and concentrated to a final volume of 15 ml using the KR2i tangential flow filtration system (Spectrum Labs) with a 75 cm2 modified polyethersulfone hollow fibre column with 500 kDa cut-off (Spectrum, D02-E500- 10-S) at a flow rate of 140 ml min^{-1} and transmembrane pressure 2.5 psi to achieve a shear rate of 2,000 s^{-1}. The concentrated media underwent 10× buffer exchange in 1× PBS before being pelleted at 100,000g for 30 min (TLA-100.3 rotor). All sEVs were resuspended in 50 μl 1× PBS and were quantified using nanoparticle tracking analysis on the ZetaView (ParticleMetrix).

Nanoparticle tracking analysis

Nanoparticle tracking analysis was performed on a ZetaView PMX-110 (ParticleMetrix). The ZetaView nanoparticle tracking instrument (ParticleMetrix) was calibrated for experiments following every instrument start-up. Focusing and alignment are performed automatically using 102 nm polystyrene beads (Microtrac, catalogue no. 900383). sEVs samples were diluted in PBS into the range determined by the instrument to be accurate for measurement (typically 1:10,000–

1:500,000). One millilitre of sample was injected into the machine and allowed to equilibrate until it reached an acceptable level according to the built in particle-drift sensor. Once the sample fell within the acceptable reading concentration range, video acquisition and analysis were performed using the parameters outlined in Table 2.1. Undiluted concentration and median size based on concentration are reported. The acceptable measurement range was determined using serial dilutions of 110 nm polystyrene beads of known concentration (5.0×10^{12} particles per ml) (Microtrac, catalogue no. 400168). Table 2.1 shows settings used for nanoparticle tracking analysis.

Table 2.1. Settings used for measuring sEV by Nanoparticle Tracking (Zetaview, ParticleMetrix)

Pre-Acquisition parameters	
Sensitivity	85
Shutter Speed	40
Frame Rate (fps)	30
Resolution	Highest
Camera Gain	770
Positions Measured	11
Post-Acquisition Parameters	
Minimum Brightness	15
Minimum Size (pixels)	10
Maximum Size (pixels)	500

Measurement of enrichment of miRNA and siRNA in sEVs relative to cells

RNA was prepared from cells or their sEVs using Trizol reagent (ThermoFisher Scientific, catalogue no. 15596018) as described by the manufacturer, and using 5 µg of glycogen (ThermoFisher Scientific, catalogue no. R0551) as a carrier in the alcohol precipitation step. RNA was quantified by spectrophotometry and 250 ng were added to a reverse transcription reaction using the miScript II microRNA reverse transcription kit using the Flex buffer option (Qiagen, catalogue no. 218161). Reverse transcription was performed as described by the manufacturer using the miScript SYBR Green PCR kit (catalogue no. 218075, Qiagen). qPCR was performed

using the miScript qPCR kit (Qiagen, catalogue no. 218076) on a Bio-Rad CFX-384 or Bio-Rad CFX-96 instrument using 12.5 µl or 25 µl reaction volumes, respectively. Primer sequences are included in the table below. Optimization of the reaction melting temperatures (TA) was performed such that reaction efficiency was between 95–105%. For all subsequent reactions TA was 55 °C except GFP siRNA reactions, where TA was 58 °C. Fold enrichment was measured using the ΔΔCt method comparing query miRNA levels in sEVs versus cells to miR-16 or U6 (reference) levels in sEVs versus cells. Please refer to Table 2.2 for primer sequences used for RT–qPCR.

Table 2.2. RT-qPCR Primers

Primer target	Sequence (5'-3')
GFP siRNA	atgaacttcagggtcagcttgc
SOD1 siRNA	Ttcagtcagtcctttaatgctt
mir-451	aaaccgttaccattactgagtt
TetR siRNA	tcttgatcttccaatacgcaac
mir-16	tagcagcacgtaaatattggcg
let-7	tgaggtagtaggttgtatagtt
mir-15b	tagcagcacatcatggtttaca
mir-106a	aaaagtgcttacagtgcaggtag
mir-134	tgtgactggttgaccagagggg
mir-151	tcgaggagctcacagtctagt
mir-155	ttaatgctaatcgtgatagggt

Measurement of copy number of miRNAs per sEV

RNA was prepared from known numbers of sEVs (quantified by nanoparticle tracking) and reverse transcribed using the miScript system (Qiagen) as described above. qPCR was performed on sEV samples, simultaneously with qPCR reactions using purified products of known concentration as templates to generate a standard curve. Correlation of sample Ct values with standard curve Ct values enabled measurement of the number of molecules in the reverse transcription reaction. As the number of sEVs in the original sample was known, this allowed calculation of the number of molecules of specific miRNAs per sEV.

Mice

All experiments performed using mice were approved by the Animal Care Committee of the University of Ottawa under protocol CMM-2273 and performed according to guidelines of the Canadian Council on Animal Care and the International Guiding Principles for Biomedical Research Involving Animals. Mice transgenic for eGFP under the expression of the ubiquitous chicken β-actin enhancer and cytomegalovirus promoter[237] (C57BL/6-Tg(CAG-EGFP)1Osb/J, The Jackson Laboratory, catalogue no. 003291)) were bred and females were used between the ages of 15 and 18 weeks. Mice expressing a low copy number of human SOD1 G93A[238] (C57/B6.Cg-Tg(SOD1*G93A)dl1Gur/J, The Jackson Laboratory, catalogue no. 002299) were also bred and males between the ages of 15 and 18 weeks (25–30 g) were used. Groups of mice were matched for littermates for intravenous injections. For intravenous injections mice were warmed with a heat lamp, restrained (Braintree Scientific restrainer, catalogue no. NC0690443) and injected in the lateral tail vein (U-100 insulin syringe 28G half inch needle, Beckton-Dickinson, catalogue no. 329424) with a 5 ml kg^{-1} (100–150 μl) suspension of sEVs (10^{10}–10^{11} particles as specified) in PlasmaLyte A (Baxter, catalogue no. JB2544) after a 10× diafiltration from the tangential flow filtration system with PlasmaLyte A. Mice were euthanized with intraperitoneal sodium pentobarbital (120 mg kg^{-1}, Bimeda-MTC, catalogue no. 8015E) and perfused with PBS (10 ml) before tissue collection. Those performing injections and tissue collection were blinded to the treatment.

Cell lines

The following cell lines were used: NSC-34 (CLU140, Cedarlane), MDA-MB-231 (ATCC), C8S (CRL-2535, ATCC), C8D1A (CRL-2541, ATCC), MN-1 (gift from J. Cote, University of Ottawa), Neuro2a (CCL-131, ATCC), 293T (CRL-3216, ATCC), MSC-TERT

(Cedarlane), and Human neonatal dermal fibroblasts (Lonza, CC-2509). BV2 cells were a gift from D. Park (University of Ottawa). Bone marrow-derived macrophages were generated from femurs of WT C57/B6 mice selected by adherence and matured in GM-CSF for one week. Cell lines were not authenticated. Cell lines were verified to be free of mycoplasma contamination by assessing for cytoplasmic 4,6-diamidino-2- phenylindole (DAPI) staining. All cell culture was performed at 37 °C in 5% CO2 in humidified incubators.

Mixed motor neurons extraction and culture

Mice embryos were collected from pregnant mice between embryonic day (E)13.5 and E14.5. Spinal cords were dissected using a Zeiss Stereo Discovery V20 microscope (Carl Zeiss, Oberkochen, Germany). The clean spinal cords were placed in dissection buffer (sucrose 40 g l^{-1}, dextrose 1 g l^{-1} and HEPES 2.4 g l^{-1} in 1× PBS), minced with scissors and incubated with trypsin (Sigma-Aldrich) for 30 min at 37 °C. The cells were separated using a 1 ml pipette and placed in NFeed neuronal culture medium (MEM/HBSS, Hyclone, catalogue no. SH3002402), insulin 10 μg ml^{-1} (Sigma-Aldrich, catalogue no. I-6634), transferrin 200 μg ml^{-1} (USBiologicals, catalogue no. T8205-47-1G), BSA 10 μg ml^{-1} (Sigma, catalogue no. A9418), putrescine 32 μg ml^{-1} (Sigma, catalogue no. P-5780), selenium 26 ng ml^{-1} (Sigma-Aldrich, catalogue no. S-1382), T3 20 ng ml^{-1} (Sigma-Aldrich, catalogue no. T-6397), hydrocortisone 9.1 ng ml^{-1} (Sigma-Aldrich, catalogue no. H-0888), progesterone 13 ng ml^{-1} (Sigma-Aldrich, catalogue no. P-8783) and 2.5S nerve growth factor 5 ng ml^{-1} (EMD Millipore, catalogue no. 01-125), horse serum 1.3% (Invitrogen Life Technologies, catalogue no. 16050-015) and 1% antibiotic-antimycotic (Gibco, catalogue no. 15240062). Cells were counted and seeded at 300,000 cells per well in 12-well plates pre-treated with poly-d-Lysine 1 mg ml^{-1} (Sigma-Aldrich, catalogue no. P7280,) and Matrigel 0.5% (Corning,

VWR, catalogue no. 354234,). After 4–7 d, mitotic cells were killed using arabinofuranosylcytosine 1.4 μg ml^{-1} (EMD Millipore, catalogue no. 251010).

FISH

Tissues were collected from mice and placed in 4% PFA in 1× PBS for 24 h. PFA was replaced by 1× PBS with 30% sucrose until the tissues sank to the bottom of tubes. Tissues were then placed in optimal cutting temperature solution (OCT, 23-730-571, Fisher) and frozen on dry ice. Tissue sections of 5 μm were collected on slides and placed at −80 °C. Slides were heated to room temperature before staining. Slides were placed in 4% PFA in PBS for 10 min at ambient temperature. They were washed with 1× PBS and placed at 37 °C for 20 min in permeabilization buffer (10 μg ml^{-1} proteinase K, 0.2% Triton X-100 in PBS). Slides were returned to room temperature, washed in PBS and blocked for 1 h with 1% BSA, 100 μg ml^{-1} salmon sperm DNA and 250 μg ml^{-1} yeast extract RNA in PBS. Slides were washed with 1× PBS and treated for autofluorescence reduction with NaBH4 0.1% in water for 1 h. Slides were washed with Stellaris wash A buffer (LGC Biosearch Technologies, catalogue no. SMF-WA1-60) and incubated with Stellaris fluorescent mRNA probes (LGC Biosearch Technology, SOD1 (custom assay), GFP (VSMF- 1014-5), GAPDH (SMF-3002-1), β-actin) and DIG-coupled siRNA probes (SOD1 siRNA, GFP siRNA and negative control siRNA; Integrated DNA Technologies) in hybridization buffer (90% Stellaris hybridization buffer, catalogue no. SMFHB1– 10, 10% formamide). Slides were incubated with the probes in the dark at 37 °C overnight. Slides were returned to room temperature and washed with wash A buffer and incubated with a sheep anti-DIG antibody (Enzo Life Sciences, catalogue no. ENZ-ABS266–0100) diluted 1:100 in blocking solution for 1 h. Slides were washed with wash A buffer and incubated with a donkey anti-sheep AlexaFluor488 or 647 antibody (Life Technologies, catalogue no. A-21448) diluted 1:500 in blocking solution for 1h.

Slides were washed with wash A buffer and incubated with DAPI (Life Technologies) 1:10,000 in PBS for 5 min. A final wash was performed with Stellaris wash B buffer and slides were mounted with Citifluor AF3 antifade solution (Electron Microscopy Sciences, catalogue no. AF3–25) and sealed with nail polish. Where specific cell types were stained antibodies used were: macrophages (anti-EMR1 (F4/80) Santa-Cruz, catalogue no. sc-365340), Stellate cells (anti-GFAP, DAKO, catalogue no. Z0334).

Production of stable cell lines

We adapted published siRNA sequences to reprogram pre-miR-451 to target GFP[239], Sod1[240], TetR[241] and Ttr (US patent US9399775). Where published siRNA sequences contained less complementary sequence than the length of the 22 nt mature miR-451, we added bases complementary to the targets at the 3′ end of the antisense strand. The mature antisense strands were designed as follows: Gfp 5′ - atgaacttcagggtcagcttgc; Sod1 5′ - ttcagtcagtcctttaatgctt; TetR 5′ - tcttgatcttccaatacgcaac; Ttr 5′ - ttatagagcaagaacactgttt. Pre-miR-451 reprogrammed to express GFP siRNA or TetR siRNA were generated as a G-block (Integrated DNA Technologies DNA) with the following sequences: GFP siRNA, AGATCTTACTGACTGCCAGGGCACTTGGGAATGGCAAGGATGAACTTCAGGGTCAG CTTGCGTTGACCCTGAAGTTCATTCTTGCTATACCCAGAAAACGTGCCTTTTTGGTAC CAAGCTT; TetR siRNA, AGATCTTACTGACTGCCAGGGCACTTGGGAATGGCAAGGTCTTGATCTTCCAATACG CAACCGTGTTGGAAGATCAAGCTCTTGCTATACCCAGAAAACGTGCCTTTTTGGTAC CAAGCTT; Ttr siRNA, GGATCCTACTGACTGCCAGGGCACTTGGGAATGGCAAGGTTATAGAGCAAGAACAC

TGTTTAGTGTTCTTGCTTTATATTCTTGCTATACCCAGAAAACGTGCCTTTTTGGTAC CAAGCTT.

These were cloned between the BamHI and HindIII sites of pSilencer 2.1-U6(Puro) (Invitrogen, catalogue no. AM5762M) as a BglII–HindIII fragment with the exception of the Ttr siRNA construct, which was cloned as a BamHI– HindIII fragment.

Further constructs were generated from these plasmids by inverse PCR using the following primer pairs: SOD1 siRNA, AGCATTAAAGGACTGACTGAACCTTGCCATTCCCAAGTGC and TTTTAAAGGACTGACTGACTCTTGCTATACCCAGAAAAC.

Reprogrammed pre-miR-16 constructs were generated by inverse PCR using the human pre-miR-16 sequence cloned as a BamHI–HindIII fragment in pSilencer 2.1-U6(Puro) (as template with the following primer pairs: GFP siRNA, GAATCTTAAGCAAGCTGACCCTGAAGTTCATGGATCCCGCGTCCTTTCC and TAAAATTATGTAAGCTGTCCTCTGAAGTTCATTTTTTTGGAAAAGCTTGGCAC; TetR siRNA GAATCTTAAGTTGCGTATTGGAAGATCAAGAGGATCCCGCGTCCTTTCC and TAAAATTATGTTGCGTAATGTGAAGATCAAGATTTTTTGGAAAAGCTTGGCAC; SOD1 siRNA GAATCTTAAAAGCATTAAAGGACTGACTGAAGGATCCCGCGTCCTTTCC and TAAAATTATAAGCATTAAAGTGACTGACTGAATTTTTTGGAAAAGCTTGGCAC.

Constructs encoding reprogrammed pre-miR-451 in pSilencer were moved into a vector allowing production of lentiviral particles. In brief, the following DNA fragments were amplified by PCR using Herculase II DNA polymerase (Agilent, catalogue no. 600677) as recommended by the manufacturer and combined into a single vector by Gibson assembly (NEB, catalogue no. E2611S): The region coding reprogrammed miR-451, amplified using oligonucleotide primers 5′–

TACAGAATCGTTGCCTGCACTTTCTTGGGTAGTTTGCAGTTT and 5′–ATGCAACAAGACACGAGACGGTTTTCCCAGTCACGACGTT; a fragment of pGIPZ (Dharmacon) encoding all components of a lentiviral transfer vector, amplified using oligonucleotide primers 5′–CGTCTCGTGTCTTGTTGCAT and 5′–GGTGGCAGATCCTCTAGTAG; a fragment of pXPAC-luc (Systems Biosciences) encoding the luciferase gene, amplified using oligonucleotide primers 5′–CTACTAGAGGATCTGCCACCGTGGGCCAGTCCTCTGATAG and 5′–GCGGCCGCTACTTGTACACTTGAAGGCGTGCTGGTACT; and a fragment of pGIPZ encoding an IRES site and puromycin resistance gene, amplified using oligonucleotide primers 5′–TGTACAAGTAGCGGCCGC and 5′–GTGCAGGCAACGATTCTGTA. The resulting vector enabled transduction of cells in cell culture to produce stable cell lines expressing luciferase, puromycin resistance and the reprogrammed miR-451 construct from a CAG-enhanced CMV promoter. Lentiviral particles were produced using standard methods from transfected HEK293T cells and were concentrated by ultracentrifugation. Dilutions of these lentiviral particle stocks were added to cell growth media and after 3 d, cells were spilt into media containing puromycin to select for transduced cells. Transduction was confirmed by measurement of luciferase activity within the cells.

Fluorescent labelling of sEVs

For biodistribution studies, sEVs were labelled with XenoLight DiR Fluorescent Dye (PerkinElmer, catalogue no. 125964). sEVs were incubated with 41.5 μg μl^{-1} DiR in a total volume of 1 ml 1× PBS at room temperature on a rotator for 30 min. sEVs were then centrifuged at 100,000g for 30 min (TLA-100.3 rotor) and resuspended in an appropriate volume for injection.

PBS (1×) was treated with the same concentration of dye and centrifuged and resuspended identically to sEVs to produce an sEVs-free dye only control.

Mixed motor neuron transfer

siRNA-containing sEVs were quantified by nanoparticle tracking analysis (Zetaview) and added to mixed motor neuron cultures at a concentration of 1,000 sEVs per cell in 12-well plates containing 300,000 cells per well on removable coverslips. After 72 h, coverslips were removed from the wells for FISH analysis. The remaining cells in the well were lysed using Trizol (Life Technologies, catalogue no. 15596026) for qPCR analysis.

In other experiments, siRNA-containing sEVs from *Ago2*$^{-/-}$ MEFs and WT rescued MEFs were quantified by nanoparticle tracking analysis (Zetaview) and added to mixed motor neuron cultures at a concentration of 10,000 sEVs per cell in 24-well plates. Untreated wells were used as naive controls. After 72 h, cells were lysed using Trizol for qPCR analysis.

qPCR analysis of mixed motor neurons and mouse organs

Cells or mouse tissues were homogenized in Trizol (Sigma-Aldrich) and RNA was extracted following the Tri-Reagent isolation protocol. Reverse transcription was conducted with the M-MuLV enzyme (NEB, catalogue no. M0253S) and 18 nt oligoDT primer (Integrated DNA Technologies, custom synthesis). Taqman qPCR was performed using probes from ThermoFisher for GFP (Mr04097229_mr), human SOD1 (Hs00533490_m1) and mouse housekeeping genes Gusb (Mm01197698_m1), Pgk1 (Mm00435617_m1), Gapdh (Mm99999915_g1) and Tfrc (Mm00441941_m1) (ThermoFisher) on a CFX-384 instrument (Bio-Rad).

Image analysis

ZEN 2.3 analysis software (Carl Zeiss, Oberkochen, Germany) was used for FISH image analysis. Briefly, images were acquired by confocal microscopy (Zeiss LSM800 AxioObserverZ1 mot, Carl Zeiss, Oberkochen, Germany) with a ×63 Plan-Apochromat 1.4 Oil lens. Colours were added after acquisition. Analyses were done blindly. Mean intensity of the whole image or specific cell types (GFAP or Iba1) were measured with the software. Mean intensity average and s.e.m. were calculated and statistical analyses were performed using Graphpad Prism (GraphPad Software).

For experiments on mixed motor neuron cultures fields of view with approximately 100 cells were analysed. Four randomly selected fields of view were analysed per slide and two slides from two independent wells were analysed in each of two independent experiments (~1,600 cells in total).

RNase treatment of sEVs

Where described, sEVs suspended in PBS + 0.25 M sucrose were treated with 10 µg RNase A (ThermoFisher-Scientific, catalogue no. EN0531) or the same amount of RNase A + 0.5% Triton X-100.

DNase I, proteinase K and RNase A treatment.

Reactions of 10^{10} sEVs purified on sucrose density gradients and containing GFP siRNA were suspended in 0.25 M sucrose in PBS. These were spiked with 1 µg plasmid DNA and 100 pg single guide strand SOD1 siRNA (Integrated DNA Technologies, custom synthesis) to control for DNAse and RNase activity, respectively. Reactions that received DNase I, proteinase K or RNase A treatments were first treated with 10 µg DNase I (Roche, catalogue no. 10104159001) for 10 min at 37 °C. Reactions that received detergents were then treated with 0.5% SDS or Triton X-

100. Reactions that received DNase I, proteinase K and RNase A treatments were then treated with proteinase K (Sigma- Aldrich, catalogue no. P2308) to a final concentration of 100 μg ml^{-1} for 10 min at 37 °C. All reactions were then treated with PMSF at a final concentration of 5 mM for 10 min at room temperature. Reactions that received DNase I, proteinase K and RNase A treatments were then treated with 10 μg RNase A for 10 min at 37 °C. All reactions were then split into three equal parts for western blot, RT–qPCR or DNA analysis. RNA was extracted with 0.5 ml Trizol, whereas DNA was extracted with an equal volume of phenol:chloroform:isoamyl alcohol and the aqueous portion was run on an agarose gel and stained with ethidium bromide to visualize the spiked DNA. Identical methods were used for analysis of ultracentrifuged sEVs by RT–qPCR. For western blot analysis of ultracentrifuged sEVs in Supplementary Fig. 2.3f, a proteinase K concentration of 10 μg ml^{-1} was used.

Northern blots

RNA preparations were separated on 17.5% polyacrylamide gels in 0.5× TBE (Wisent Bioproducts, catalogue no. 880-545-CL) and electroblotted (TurboBlot, Bio-Rad) onto positively charged nylon membranes (GE Healthcare, catalogue no. 1417240) also in 0.5× TBE. RNAs were crosslinked to membranes by UV using a Stratalinker delivering 240 mJ to each side of the membrane. Membranes were prehybridized for 1 h in 10 ml PerfectHyb buffer (Sigma-Aldrich, catalogue no. H7033) at 40 °C and hybridized with labelled probe overnight under the same conditions. Membranes were washed twice in 5× SSC + 0.1 % SDS and once in 1× SSC + 0.1% SDS before exposure to storage phosphor screens (GE Healthcare). Screens were imaged using a Typhoon Trio machine (GE Healthcare). Custom probe oligonucleotides (Integrated DNA Technologies) were labelled as follows: 18 pmol of oligonucleotide was labelled with 30 μCi of [γ-32P]-ATP (PerkinElmer, catalogue no. BLU002A500UC) using T4 PNK (NEB, catalogue no.

M0201S) as recommended by the manufacturer. Labelled probes were separated from unincorporated nucleotides by ethanol precipitation using 10 µg glycogen (ThermoFisher, catalogue no. R0551) as a carrier. Oligonucleotide probe sequences were as follows: GFP siRNA probe 5′-GCAAGCTGACCCTGAAGTTCAT and U6 probe 5′-AGGGGCCATGCTAATCTTCT.

Western blot

Blood (20–50 µl) was collected from the tail vein at different time points in heparinized tubes (Greiner Bio-One, 450477). Whole blood was separated by centrifugation at 3,500g for 15 min. An equal amount of serum (5 µl) was collected and diluted in water and 4× Laemmli sample buffer (Bio-Rad, 161–0747) with 10% β-mercaptoethanol (Bio-Rad, 1610710) and boiled for 5 min at 99 °C. Samples were separated by SDS–PAGE (10% acrylamide) at 100 V for 10 min and 150 V for 1 h 15 min. Samples were transferred on a positively charged nylon membrane (Roche, 1417240) for 1 h 15 min at 100 V. Membranes were washed with 1× TBST (3 × 5 min) and blocked with 1× TBST + 5% milk for 1 h. Membranes were incubated at 4 °C overnight with the primary antibody (rabbit anti-mouse TTR, Invitrogen, PA5-80197). Membranes were washed with TBST (3 × 5 min) and incubated for 1 h with secondary antibody (Li-Cor Odyssey, goat anti-rabbit IRdye 800 (TTR), 926–32211, donkey anti-mouse IRDye 680 (IgG, loading control), 925–68072). Membranes were washed with 1× TBST (3 × 5 min) and imaged with Li-Cor Odyssey Fc imaging system (Li-Cor Biotechnology). Images were analysed using Image Studio software (Li-Cor Biotechnology). Table 2.3 presents details about the antibodies used.

Table 2.3. List of antibodies used for Western blot

Antibody (clone)	**Company**	**Catalog #**
Alix (3A9)	Cell Signaling Technology	2171S
Ago2 (C34C6)	Cell Signaling Technology	2897S
B-Actin (AC-15)	Sigma-Aldrich	A5441

Flotillin2 (C42A3)	Cell Signaling Technology	3436S
GFP (GF28R)	eBiosciences	14-6674-82
Tomm20 (FL-145)	Santa-Cruz Biotechnology	sc-11415
TSG101 (4A10)	GeneTex	GTX70255
TTR (Polyclonal)	ThermoFisher	PA5-80197
Tubulin (DM1A)	Sigma-Aldrich	T6199
Anti-Mouse HRP	Jackson ImmunoResearch	115-035-174
Ant-Rabbit HRP	Jackson ImmunoResearch	111-035-144

Electroporation of sEVs

siRNA, sEVs or a mixture of both were electroporated as described[181]. In brief, 10^9 sEVs isolated as described above and/or 1 µg siRNA (custom synthesized *in vivo* grade siRNA, Dharmacon) were resuspended in 400 µl electroporation buffer (1.15 mM potassium phosphate pH 7.2, 25 mM potassium chloride, 21% Optiprep), transferred to a 4 mm electroporation cuvette (VWR) and pulsed in a Gene Pulser Xcell (Bio-Rad). The following electroporation settings were used: 400 V, 125 µF and ∞ Ω. After pulsing, the cuvette was immediately transferred to ice. The electroporated mixture was recovered from the cuvette, centrifuged at 100,000g for 30 min in a TLA-100.3 rotor (Beckman), resuspended in 1 ml PBS and recentrifuged as above before final resuspension in 20 µl 1× PBS.

Digital droplet PCR

Digital droplet PCR (ddPCR) was performed using the Bio-Rad QX200 system (QX200 droplet generator, C1000 Thermotouch thermal cycler and QX200 droplet reader) following the manufacturer's recommendations, using the QX200 ddPCR EvaGreen Supermix (Bio-Rad) and the QX200 droplet generation oil for Evagreen (Bio-Rad, catalogue no. 186–4034). PCR was performed using the SOD1 siRNA primer and the miScript Universal primer from the miScript kit described above (Qiagen) both present at 0.5 µM in the reaction. Optimal primer annealing

temperatures (57 °C) and template dilutions were determined empirically as previously described[242]51. PCR activation was performed as recommended for the QX200 ddPCR EvaGreen Supermix. PCR cycling conditions were otherwise those recommended for the miScript qPCR system (Qiagen).

Quantification of miR-451 in sEVs after long-term culture in serum-free media

NSC-34, HEK293 and human neonatal fibroblast cells were cultured in DMEM + 10% FBS or in Serum-free media (Lonza UltraCULTURE + 1% penecillin-streptomycin + 1% l-glutamine) for six weeks. Cells were passaged at a sub-cultivation ratio of 1:10 approximately every 5 d. Cells were centrifuged at 300g for 10 min and resuspended in media at each passage. Following six weeks of culture, cells at 80% confluence were washed with 1× PBS and media (either DMEM + 10% FBS or Lonza Ultraculture serum-free media) was replaced with serum-free media for sEVs collection. sEVs were isolated by differential ultracentrifugation. miR-451 levels in sEVs were quantified by RT–qPCR.

Quantification of miR-451 in sEV-depleted medium with and without exposure to cells

sEV-depleted DMEM prepared by ultracentrifugation as above was used to collect sEVs from 80% confluent NSC-34 cells (sEVs-conditioned media). sEVs were isolated by differential ultracentrifugation from equal volumes of standard DMEM + 10% FBS, sEVs-depleted DMEM, and sEVs-conditioned medium. Pellets obtained from the final 100,000g spin were used to quantify miR-451 by RT–qPCR.

MiR-451 quantification in cells and sEVs after serial dilution of cells

Cell lines were grown in DMEM + 10% FBS + penicillin-streptomycin and were washed extensively with PBS before collecting with trypsin. Indicated dilutions of cells were then seeded

in serum-free Ultraculture (Lonza) in 10 cm plates, with the most concentrated plates receiving 2 × 10^6 cells. Medium was replaced with fresh Ultraculture daily. Once each dilution reached approximately 80% confluence, medium that had been on the plates for 20 h was collected for sEVs collection and quantification of miRNA levels by RT–qPCR.

Preferential detection of short and long forms of pre-miR-451

RNA from sEVs from *Ago2*$^{-/-}$ and *Ago2*$^{-/-}$ cells rescued with Ago2 was isolated and subjected to reverse transcription using the miScript RT kit (Qiagen) with either the specific or flexible buffers. Specific buffer is designed to preferentially produce short amplicons corresponding to mature miRNA, whereas flexible buffer produces both short and long amplicons. To verify the preferences of these buffers, synthetic RNAs mimicking the mature 22 nt strand or Drosha-processed 42 nt strand were included in separate reactions (sequences 5′-UUCAGUCAGUCCUUUAAUGCUU or 5′-UUCAGUCAGUCCUUUAAUGCUUAUUAAAGGACUGACUGAUUC, respectively; Integrated DNA Technologies). qPCR using the miScript system was then used to assess the fold change in product levels of flexible to specific buffer.

Measurement of RNA recovery from sEVs samples

To determine the efficiency with which small approximately 22 nt single-stranded RNAs are recovered in Trizol preparations, a synthetic RNA mimicking the fully processed SOD1 siRNA was spiked into sEVs. Final cell RNA preparations contained approximately 50 µg or 1 µg RNA, while sEVs preparations contained approximately 1 µg RNA (measured by spectrophotometry). In brief, cell and sEVs pellets in 1 ml of Trizol were spiked with 5 µl of 2 nM ssRNA and RNA was prepared according to the manufacturer's instructions, including the addition of 10 µg

glycogen (RNA grade, ThermoFisher Scientific, catalogue no. R0551) to the isolated aqueous phase to aid RNA precipitation. After alcohol precipitation RNA was resuspended in 50 µl RNase free water. Five microlitres of the 2 nM ssRNA was similarly diluted to serve as the input sample. Recovery of the siRNA versus SOD1 was quantified using absolute copy numbers with a standard curve as above.

Sucrose density gradient

sEVs produced from NSC-34 cells transduced with pre-miR-451 hairpin vectors with GFP siRNA integrated were isolated by differential ultracentrifugation. sEVs pellets were resuspended in 1.85 ml of 0.95 M sucrose solution. The 0.95 M sucrose solution containing sEVs was inserted in a sucrose step gradient composed of six 1.85 ml layers with sucrose concentrations of 2.0 M, 1.65 M, 1.30 M, 0.95 M, 0.6 M and 0.25 M. The sucrose step gradient was centrifuged at 200,000g for 20 h at 4 °C. Twelve fractions of 0.925 ml were collected and their density was measured with a refractometer (No.16046 ERMA). About 250–500 µl of fractions was diluted to 30 ml in cold 1× PBS and centrifuged at 100,000g at 4 °C for 70 min. The pellets were resuspended in 25 µl of cold 1× PBS and used for western blotting.

Fraction RT–qPCR and RNase A–RNaseT1 treatment

Trizol LS (ThermoFisher, catalogue no. 10296028) was used to isolate RNA from 250 µl of each fraction and RT–qPCR was performed with the miSCRIPT kit (Qiagen). For RNase A–RNase T1 treatments, equal volumes of fractions 6 and 7, which contained more than 80% of the sEV markers (flotillin 2 and Tsg101), were combined. Fifty microlitres of these combined fractions was used for each reaction in a total volume of 75 µl. Fractions were treated with RNase A–RNase

T1 Mix (1.5 µl at 2 mg ml^{-1} of RNase A and 5,000 U ml^{-1} RNase T1; ThermoFisher, catalogue no. EN0551,) at 37 °C for 10 min with or without 0.5% Triton X-100 in 1× PBS.

Lipid nanoparticles

In some experiments, lipid nanoparticles were produced using InvivoFectamine 3.0 (ThermoFisher, catalogue no. IVF3001) loaded with synthetic siRNA versus SOD1 (Integrated DNA Technologies) without chemical modifications according to the manufacturer's instructions. The SOD1 siRNA represents a canonical double-stranded siRNA with 3′ overhangs and the targeting sequence is identical in sequence to that produced by the SOD1 siRNA integrated into the pre-miR-451 hairpin above. In other experiments C12–200 lipid nanoparticles were prepared and loaded with siRNA targeting GFP (Qiagen, GFP-22 siRNA positive control). The targeting sequence of GFP-22 siRNA is identical to that produced by the GFP siRNA integrated into the pre-miR-451 hairpin elsewhere. C12–200 lipid nanoparticles were produced as previously described[243].

Statistics

In all cases where sample size is mentioned, measurements were taken from distinct samples. Statistics were calculated in GraphPad Prism.

Reporting Summary

Further information on research design is available in the Nature Research Reporting Summary linked to this article online.

Data availability

The main data supporting the results of this study are available within the paper and its Supplementary Information. The raw and analysed datasets are too numerous to be readily shared publicly, but can be obtained for research purposes from the corresponding author on reasonable request.

Received: 22 January 2018; Accepted: 4 December 2019;

Published online: 14 January 2020

2.6 Acknowledgements

The authors acknowledge E. Lai (Memorial Sloan-Kettering Cancer Center) for providing mouse embryonic fibroblast cell lines (WT, *Ago2*$^{-/-}$ and *Ago2*$^{-/-}$ rescued with Ago2). R.R. was funded in part by a scholarship in translational research from the Centre for Neuromuscular Disease and the University of Ottawa Brain and Mind Research Institute. This research was funded by grants from the Canadian Institutes of Health Research (proof of principle grant, PPP-141720), the National Research and Engineering Council of Canada (discovery grant no. 436104), The Quebec Consortium for Drug Discovery (CQDM Explore grant) and the ALS Association Treat Program (grant no. 15-LGCA-290) awarded to D.G.

Author contributions

J.A.T. performed cloning, lentivirus production, northern blots, analysis of RNA enrichment in sEVs and absolute quantification of RNA in sEVs. A.S. maintained mouse colonies, performed injections and tissue collections, helped analyse sEVs distribution, performed western blots of sEVs, generated cultures of primary mixed motor neurons, performed some RT–qPCR and performed and analysed microscopy. R.R. produced sEVs, performed nanoparticle tracking analysis, performed tissue collections, labelled sEVs and analysed their distribution, and analysed

RNA enrichment in sEVs and mRNA target knockdown by RT–qPCR. M.T.T. maintained mouse colonies, generated mouse protocols, genotyped mice and performed injections and tissue collections. C.C. helped establish protocol for primary mixed motor neuron culture and performed some analyses of miRNA levels in sEVs. H.G. performed western blots of sEVs and density gradient analyses of sEVs. L.H.R. and P.S.K. helped design lipid nanoparticle experiments and produced C12–200 lipid nanoparticles. D.G.A. helped design lipid nanoparticle experiments and supervised L.H.R. and P.S.K. W.L. helped design experiments. J.A.T., A.S. and R.R. analysed experiments and helped design experiments. D.G. conceived the project, designed experiments and wrote the manuscript.

Competing interests

J.A.T. and D.G. are inventors on a filed patent that claims the use of the pre-miR-451 backbone for enrichment of small RNAs in sEVs. The remaining authors declare no competing interests.

Additional information

Supplementary information is available for this paper at https://doi.org/10.1038/s41551-019-0502-4. Correspondence and requests for materials should be addressed to D.G.

Reprints and permissions information is available at www.nature.com/reprints.

Publisher's note Springer Nature remains neutral with regard to jurisdictional claims in published maps and institutional affiliations.

2.7 Supplementary Figures

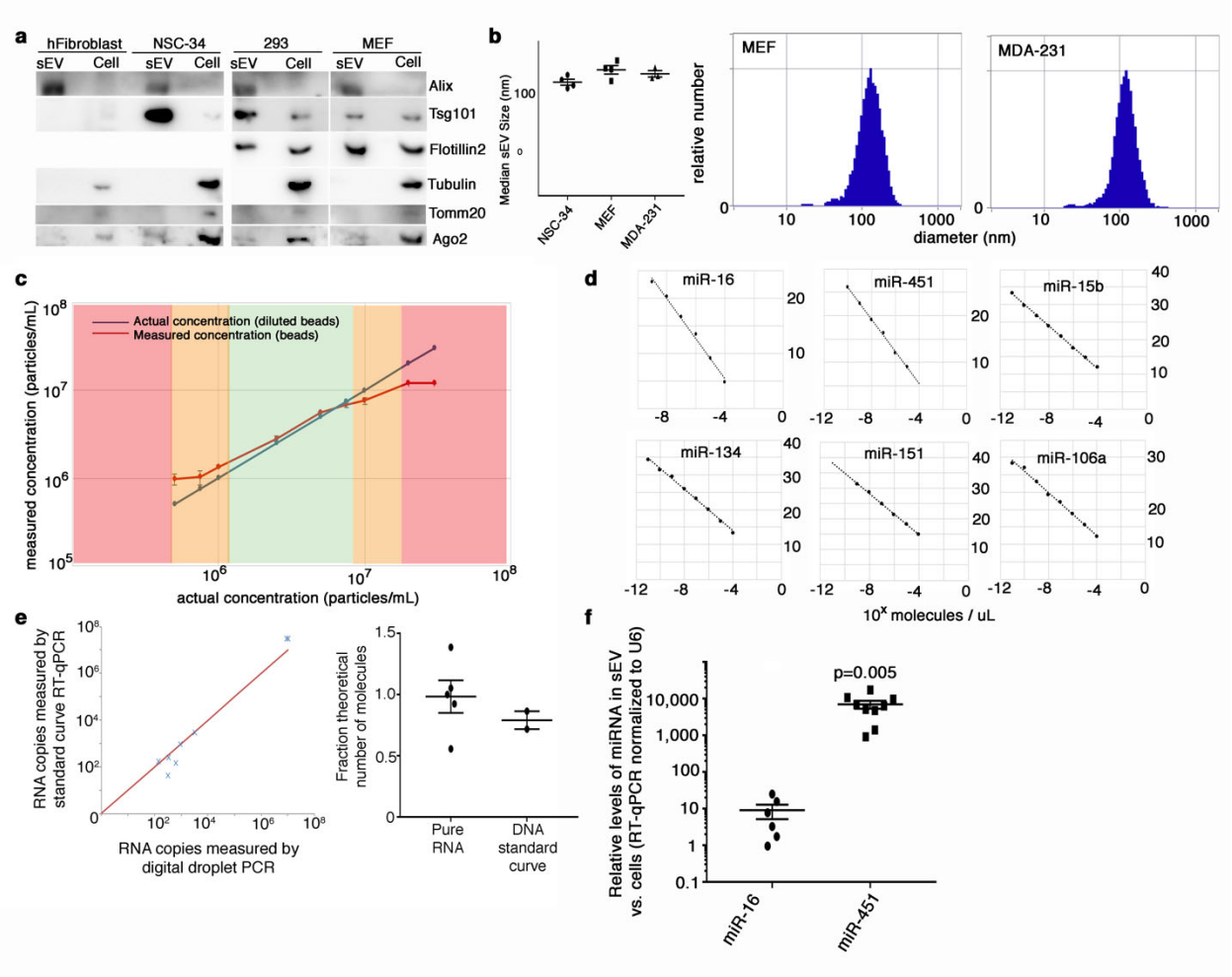

Supplementary Fig. 2.1. Characterization of sEV and their RNA contents. a, Western blot of equal amounts of proteins from sEV or cells produced by human primary fibroblasts, NSC-34, 293 or MEF cells for markers of sEV (Alix, Tsg101, Flotillin2), cellular markers (Tomm20, Tubulin) and Ago2. **b,** Nanoparticle tracking analysis of sEV. Left, median diameter of sEV measured over 3 or 4 sEV preparations from the indicated cell lines as shown. Right, representative plot of particle number (y-axis) vs. diameter (x-axis, nm) of sEV preparations produced by MDA-MB-231 and MEF cells. **c,** Plot of measured (y-axis) vs. actual (x-axis) particle concentration of 100 nm polystyrene beads measured by Nanoparticle tracking analysis using settings used for measurements of sEV in two independent trials. **d,** Representative standard curves used to calculate copy number of miRNA in sEV generated using RT-qPCR of serial dilutions of PCR reaction products. **e,** Left, Correlation plot of copy number of siRNA of defined concentration measured by RT-qPCR standard curve method vs. digital droplet PCR. Right, Graph of copy number of siRNA of defined concentration measured by RT-qPCR standard curve method vs. digital droplet PCR. **f,** Enrichment of miR-451 and miR-16 in sEV vs. their levels in MEF cells grown in serum-free Ultraculture media (normalized to U6 RNA). Statistics are derived from a two tailed unpaired ttest. N=3.

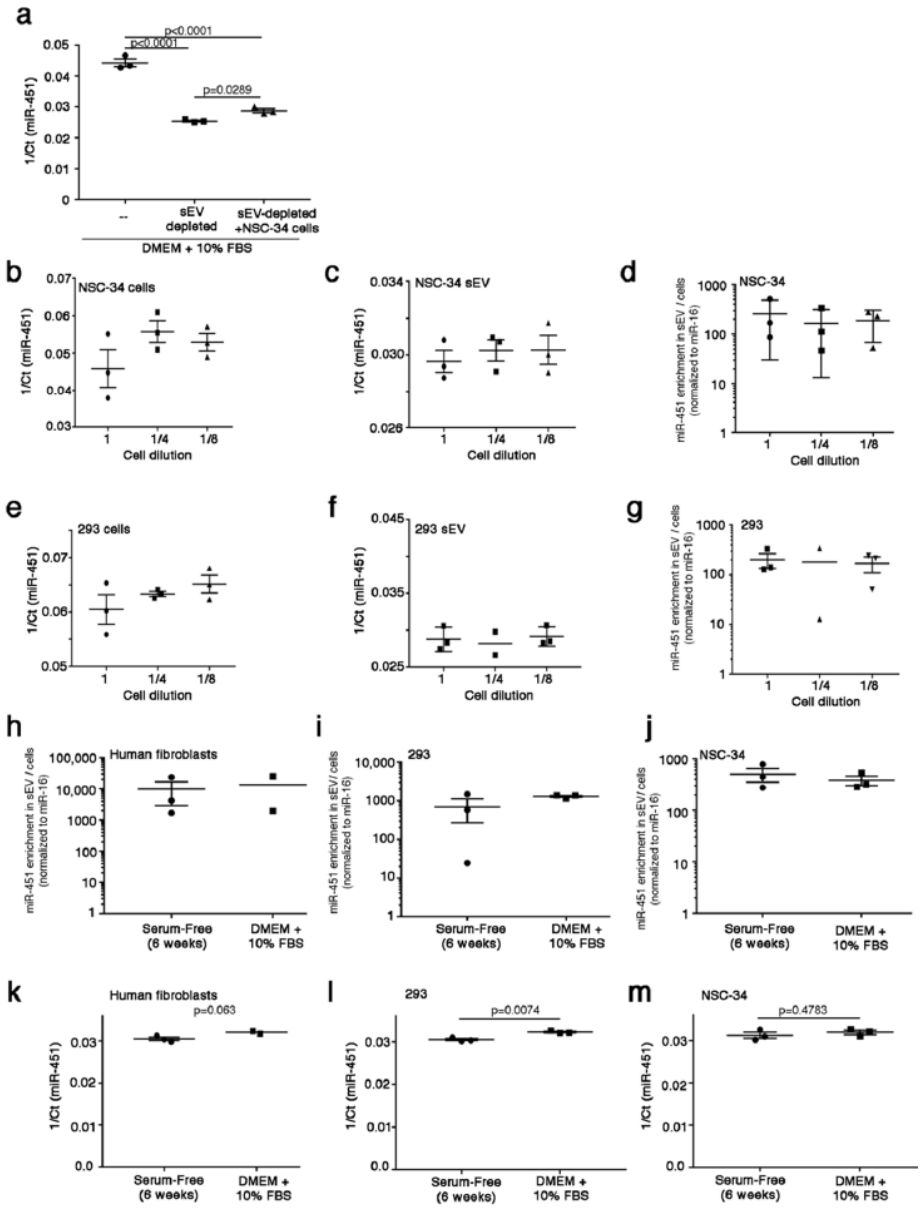

Supplementary Fig. 2.2. miR-451 is produced by cell lines independent of contamination with fetal bovine serum. **a**, 1/Ct values of RT-qPCR of miR-451 in sEV purified from DMEM including 10% FBS, the same media depleted of sEV by ultracentrifugation or the same sEV-depleted media incubated with NSC-34 cells. N=3. 1 way ANOVA with Holmes-Sidack multiple comparison was used for statistical analysis. **b-g**, RTqPCR of miR-451 (1/Ct) in cells (**b,e**) or sEV (**c,f**) or the enrichment of miR-451 in sEV / cells (**d,g**) after serial dilution of NSC-34 (**b-d**) or 293 cells (**e-g**) into serum-free media (Ultraculture). N=2 or N=3 as shown. **h-m**, RT-qPCR of miR-451 enrichment in sEV / cells (**h-j**) or miR-451 (1/Ct) (**k-m**) after passage of human neonatal primary fibroblasts (**h,k**) 293 (**i,l**) or NSC-34 cells (**j,m**) in serum-free Ultraculture media or DMEM including 10% FBS for six weeks. N=3. Statistics for (**k-m**) used a two-tailed unpaired ttest with Welch's correction. Where error bars are shown, the center value is the mean and the bars show the standard error in the mean.

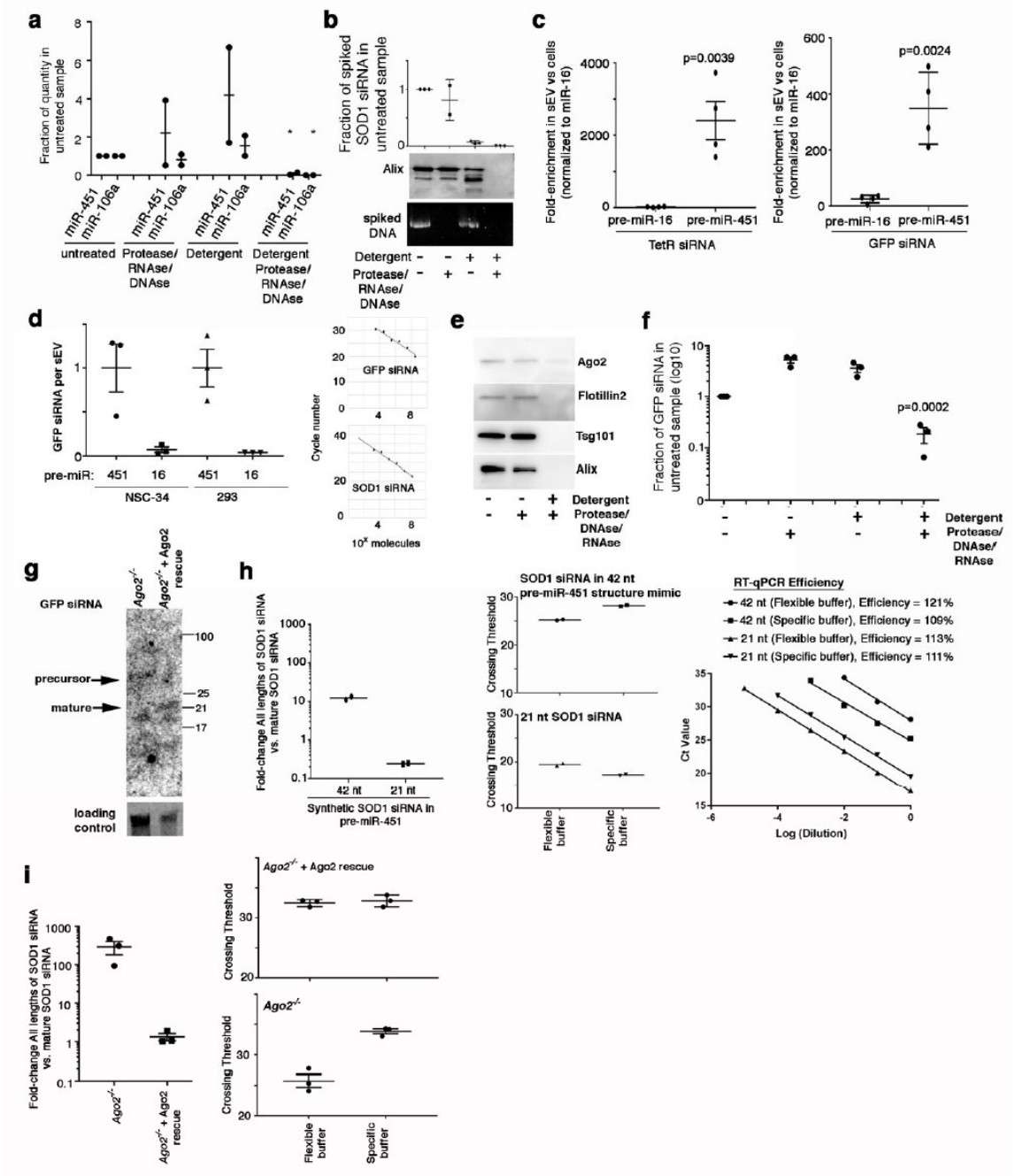

Supplementary Fig. 2.3. Quantification of pre-miR-451 and derivatives in sEV. **a**, Quantification of miR-451 in sEV purified by ultracentrifugation after treatment with Proteinase K, RNAse A and DNAse with or without detergent. Statistics are derived from a repeated measurements one way ANOVA with Holmes-Sidack correction. N=2. **b**, Validation of efficacy of RNAse, Proteinase K and DNAse treatments in **(a)** by degradation of spiked-in SOD1 siRNA, Alix and spiked-in plasmid DNA respectively in the same samples as **(a)**. 1 way ANOVA with Holmes-Sidack correction was used for statistical analysis. **c**, RT-qPCR measuring enrichment of TetR or GFP siRNA in sEV vs. their levels in cells when these were integrated in either the pre-miR-451 backbone or the pre-miR-16 backbone (control) and transiently transfected in MDA-MB-231. Statistics are derived from a two-tailed unpaired ttest. N=3. **d**, Absolute copy number of GFP

siRNA in sEV when this was integrated in either the pre-miR451 backbone or the pre-miR-16 backbone (control). Right, Representative standard curves used to calculate copy number of siRNA in sEV generated using RT-qPCR of serial dilutions of PCR reaction products. **e**, Validation of efficacy of Proteinase K treatments in **(f)** by degradation of Alix, Flotillin2, Tsg101 and Ago2 in the same samples as **(f)**. **f**, Quantification of miR-451 in sEV purified by sucrose gradient after treatment with Proteinase K, RNAse A and DNAse with or without detergent. Statistics are derived from a repeated measurements one way ANOVA with Holmes-Sidack correction. N=3. **g**, Northern blot for GFP siRNA in $Ago2^{-/-}$ or $Ago2^{-/-}$ cells rescued with wild-type Ago2. Loading control is non-specific band from top of gel. **h**, RT-qPCR of synthetic versions of the 42 nt pre-miR-451 hairpin structure reprogrammed with SOD1 siRNA, or the 21 nt SOD1 siRNA sequence using Specific or Flexible buffers provided by the manufacturer. Left, Y-axis represents the ratio of RNA quantity (2- Ct) measured using the Flexible buffer (detects long and short RNAs) divided by RNA quantity measured using the Specific buffer (preferentially detects ~21 nt RNAs). Middle, RT-qPCR Ct (Crossing-threshold) values used to generate the ratios in graph on the left. Right, graphs of Ct values over dilution series of synthetic 21 and 42 nt RNAs used to calculate RT-qPCR efficiency for Supplementary Fig. 2.3h and i. N=2. **i**, Ratio of SOD1 siRNA reprogrammed in the pre-miR-451 structure detected by RT-qPCR with Flexible / Specific buffers in sEV produced by $Ago2^{-/-}$ cells or $Ago2^{-/-}$ cells rescued with wild-type Ago2. Right, RT-qPCR Ct (Crossing-threshold) values used to generate the ratios in graph on the left. N=3. Where error bars are shown, the center value is the mean and the bars show the standard error in the mean. Full blot images from **(b, e, g)** are available in Supplementary Information.

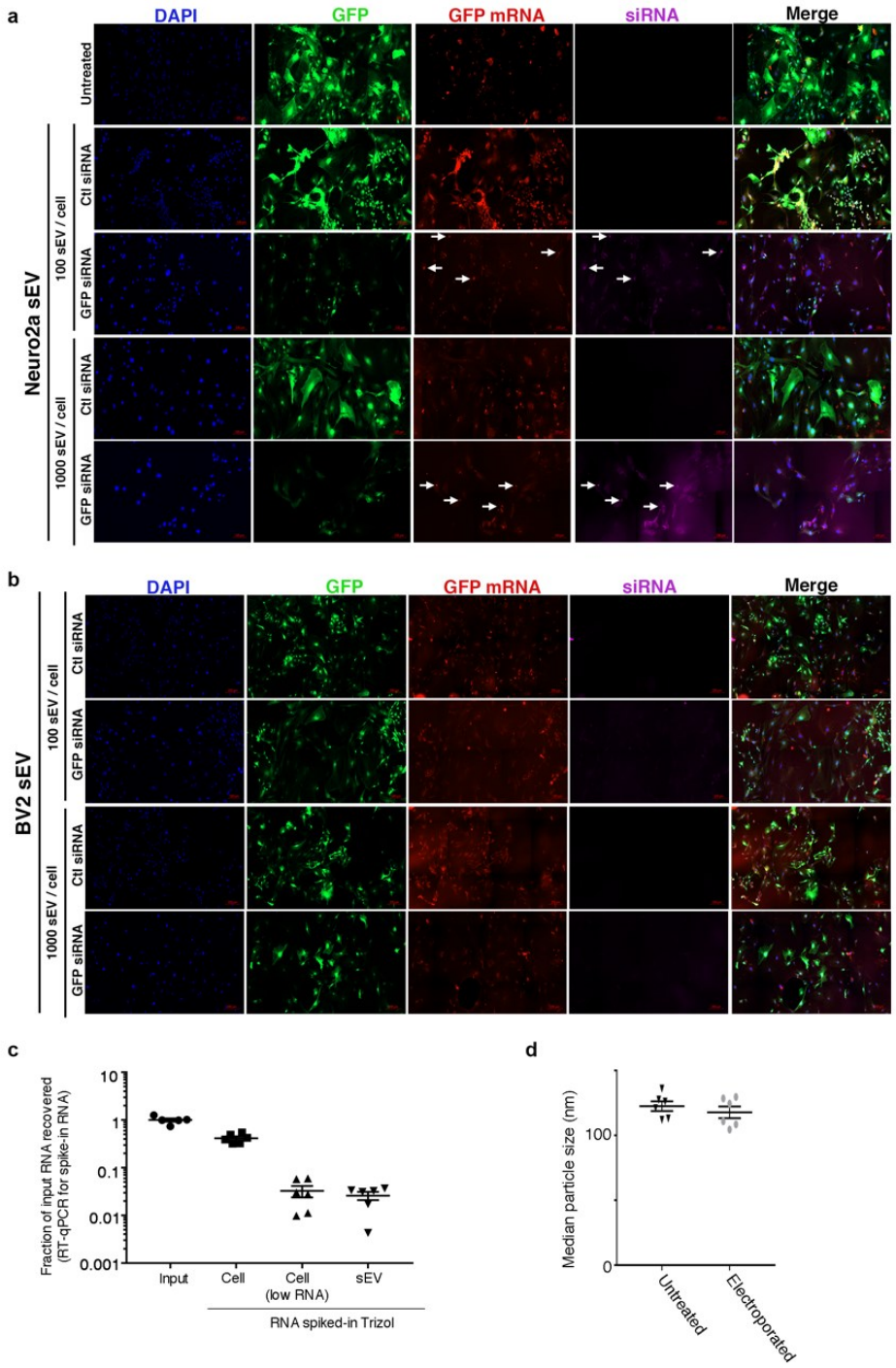

Supplementary Fig. 2.4. siRNA delivery is determined by the cell source of sEV, RNA recovery by Trizol extraction and effect of electroporation on sEV size. a, Fluorescent microscopy of GFP fluorescence, GFP mRNA (FISH) and siRNA targeting GFP (FISH) in primary mouse motor neurons from GFP transgenic mice after incubation with sEV produced by Neuro2a cells and loaded with the indicated siRNA integrated in the pre-miR-451 backbone. **b,** Fluorescent microscopy of GFP fluorescence, GFP mRNA (FISH) and siRNA targeting GFP (FISH) in primary mouse motor neurons from GFP transgenic mice after incubation with sEV

produced by BV2 cells and loaded with the indicated siRNA integrated in the pre-miR-451 backbone. Images were acquired with a Zeiss AxioScan at 40x. **c,** Recovery of 21 nt SOD1 siRNA spiked into Trizol containing approximately 50 µg of cell RNA, low amounts of cell RNA (1 µg) or sEV RNA from an average sized preparation (1 µg of sEV RNA). Normalized to 21 nt SOD1 siRNA spiked directly into reverse transcription reaction. N=6. **d,** Median size of sEV with or without electroporation as measured by Nanoparticle tracking analysis. N=6. Where error bars are shown, the center value is the mean and the bars show the standard error in the mean.

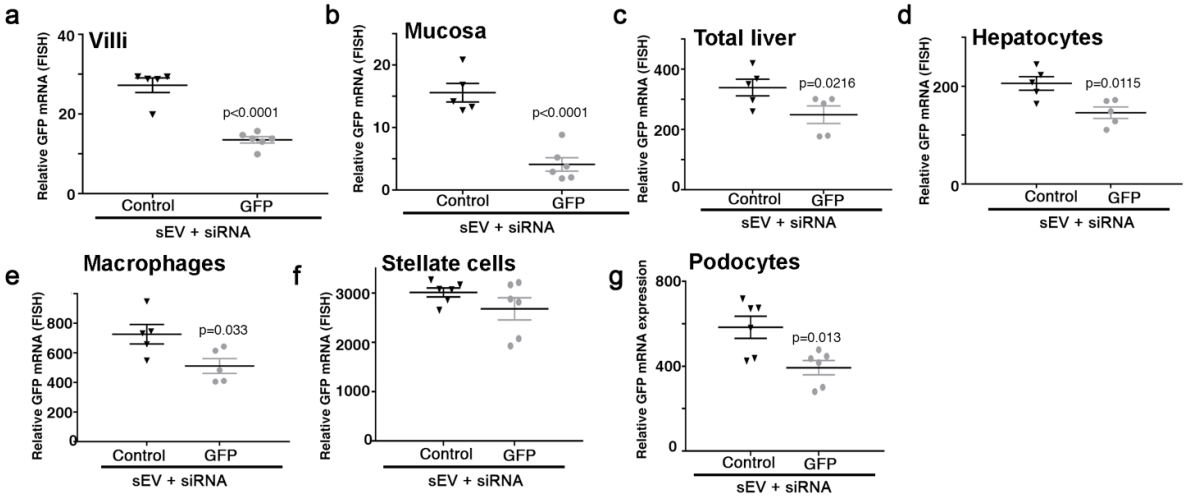

Supplementary Fig. 2.5. Quantification of GFP mRNA by FISH in specific regions and cell-types of small intestine, liver and kidney after administration of sEV packaged with GFP siRNA. Quantification of GFP mRNA in small intestine villi **(a)** and submucosa **(b)**, in total liver **(c)** hepatocytes **(d)** liver macrophages (F4/80) **(e)** liver stellate cells (GFAP) **(f),** and kidney podocytes (Nephrin) **(g)** three days after injection of sEV packaged with GFP siRNA or control siRNA using the pre-miR-451 backbone. Two-tailed unpaired t-test with Welch's correction was used for shown statistics. N=6 animals per experimental group. Two pieces of tissue per slide (duplicates) were analyzed in two randomly selected areas (4 total per animal per tissue). Where error bars are shown, the center value is the mean and the bars show the standard error in the mean.

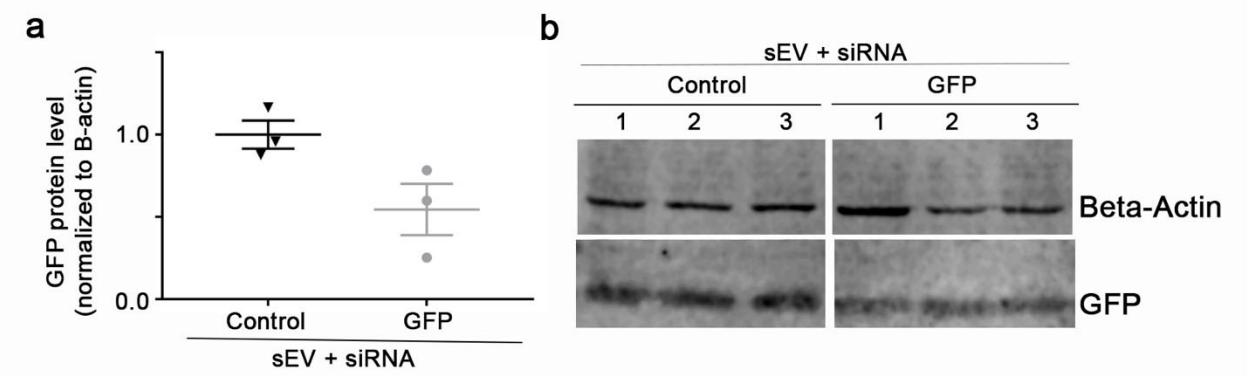

Supplementary Fig. 2.6. Quantification of GFP in Liver After Injection of SEV Packaged with GFP siRNA Using the Pre-miR-451 Hairpin Structure. (a,b) Quantification of GFP protein levels in liver by western blot after IV injection of sEV packaged with GFP siRNA or control siRNA by expression in the pre-miR-451 hairpin structure. **(b)** Fluorescent western blot of Beta-Actin and GFP (with anti-GFP antibody) captured using a LiCoR Odyssey. N=3 mice per group. For error bars, the center value is the mean and the bars show the standard error in the mean.

Chapter 3 - Manuscript #2

Safe, scalable delivery of silencing RNAs with small extracellular vesicles in models of chronic kidney diseases

Publication information:

Kallol Dutta*, Ryan Reshke*, Alexandre Savard, Junnan Wu, James A. Taylor, Adnie Etienne, Ergi Duli, Huishan Guo, Bibek Poudel, Mathieu Lemaire, Katalin Susztak and Derrick Gibbings. Safe, Scalable Delivery of Silencing RNAs with Small Extracellular Vesicles in Models of Chronic Kidney Diseases. Reviewed at Science Translational Medicine. (2022).

* These authors contributed equally to this work

Author Contributions:

Designed experiments: KD, RR, AS, JW, ML, KS, DG. Performed experiments: KD, RR, AS, JW, JAT, AE, ED, HG, BP. Analyzed data: KD, RR, AS, JW, ED, KS, DG. Conceived the study: DG. Wrote the manuscript: RR, DG.

RR contributions by figure: Figure 1a-c, g, Figure 2 b-f, Figure 3d, e, Figure 7c, d, Supplementary Figure 1 NTA profiles, Supplementary Figure 2.

Safe, scalable delivery of silencing RNAs with small extracellular vesicles in models of chronic kidney diseases

Kallol Dutta[1,2†], Ryan Reshke[1,2†], Alexandre Savard[1,2], Junnan Wu[3], James A. Taylor[1,2], Adnie Etienne[1,2], Ergi Duli[4,5], Huishan Guo[1,2], Bibek Poudel[3], Mathieu Lemaire[4,5], Katalin Susztak[3] and Derrick Gibbings[1,2*]

[1]Department of Cellular and Molecular Medicine, Faculty of Medicine, University of Ottawa; Ottawa, Canada K1H 8M5.

[2]Eric Poulin Centre for Neuromuscular Disease, Faculty of Medicine, University of Ottawa; Ottawa, Canada, K1H 8M5.

[3]Department of Medicine and Genetics, Perelman School of Medicine, University of Pennsylvania; Philadelphia, PA, USA 19104.

[4]Division of Nephrology, Hospital for Sick Children; Toronto, Ontario, Canada, M5G 0A4.

[5]Institute of Medical Sciences, Faculty of Medicine, University of Toronto; Toronto, Canada, M5S 1A4

* Corresponding author. Email: gibbings@uottawa.ca

† These authors contributed equally to this work

One Sentence Summary: Small extracellular vesicles packaged with silencing RNAs limit pathology in multiple models of chronic kidney diseases and scale by mass into larger animals.

3.1 Abstract

Chronic kidney disease (CKD) affects nearly 10% of the global population. Treatments for CKD may control the symptoms of CKD but cannot stop its progression toward end-stage renal disease. Multiple genetic risk factors are associated with glomerular kidney disorders, including *APOL1* and *TRPC6*, and these represent promising therapeutic targets. Short interfering RNAs (siRNAs) capitalize on endogenous RNA silencing machinery to therapeutically ablate expression of target genes. siRNA therapeutics are approved for use in several diseases where target genes are expressed in the liver. Inefficient delivery of siRNA into the cytoplasm and dose-limiting toxicity have combined to limit use of this drug class for CKD. We recently demonstrated that small extracellular vesicles (sEVs) can be highly efficient delivery vehicles for siRNA. Here, we show that small extracellular vesicles (sEVs) loaded with siRNA by stably expressing it in the pre-miR-451 backbone can deliver this siRNA to kidney glomeruli, and silence *TRPC6* or *APOL1* leading to improved kidney function in multiple models of kidney disease. These sEVs can be manufactured in a scalable tangential flow filtration system, exhibit no signs of toxicity at elevated doses, and efficiently silence target genes in large animals including rabbits. Our data suggest that sEVs are a scalable, safe and highly effective siRNA delivery vehicle for various forms of CKD.

3.2 Introduction

Chronic kidney disease (CKD) is a progressive disease with multiple known causes characterized by glomerular pathology, fibrosis, and reduced glomerular filtration rate (GFR)[244, 245]. Close to 10% of the global population is affected by CKD, with 1.2 million people dying of the disease in 2017 alone[246]. Focal segmental glomerulosclerosis (FSGS) is a chronic glomerular disorder characterized by progressive scarring of glomeruli leading to CKD and end-stage renal disease (ESRD)[247]. Currently available treatments for CKD, including angiotensin-converting enzyme (ACE) inhibitors and angiotensin receptor (AR) blockers, are aimed at controlling symptoms and slowing the progression of the disease but do not stop the eventual development of ESRD[248]. There remains an urgent need for new treatments to slow progression of kidney diseases.

Several gene variants are associated with FSGS. Variants of *Apolipoprotein L1* (*APOL1*) called G1 and G2 are prevalent in African Americans and provide protection from *Trypanosomes* which are endemic in western Africa. G1 and G2 alleles of *APOL1* are also associated with nearly 40% of all ESRD in this population[209]. *APOL1* risk variants are associated with increased risk of CKD in patients with FSGS, hypertension-attributed end stage kidney disease (HA-ESKD), and HIV-associated nephropathy (HIVAN)[210]. The expression of *APOL1* risk alleles in mice induces glomerular pathology and filtration defects reproducing the major characteristics of FSGS[214, 249], suggesting *APOL1* variants cause FSGS through a toxic gain of function. Humans with the G0 *APOL1* variant and *APOL1*-null humans have no apparent disease suggesting therapeutic inhibition of *APOL1* would be safe.

Another rare form of FSGS is caused by a heterozygous pathogenic variant in *Transient Receptor Potential Cation Channel 6* (*TRPC6*)[211-213]. *In vitro* experiments revealed that variants of TRPC6 proteins associated with FSGS exhibit increased cation fluxes when compared to wild-

type TRPC6[213, 250]. This suggests that *TRPC6* variants cause FSGS through a toxic gain-of-function phenomenon. Accordingly, the expression of TRPC6 variants in mice induces proteinuria as in FSGS[251, 252]. Interestingly, overexpression of wild-type TRPC6 channels was noted in a wide range of proteinuric kidney diseases, including FSGS, minimal change disease, and membranous nephropathy[253]. Blocking TRPC6 channels, or reducing their expression, led to less severe pathology in several rodent models of glomerular diseases and kidney fibrosis[216, 254]. These data reinforce the idea that inhibiting glomerular TRPC6-dependent cation fluxes may be beneficial to a group of patients that is much broader than those with FSGS who carry *TRPC6* risk alleles.

MicroRNAs (miRNAs) are short non-coding RNAs that regulate the expression of partially complementary mRNAs through translational inhibition and mRNA decay[5, 36]. MiRNAs are formed by the consecutive cleavage of endogenous pri-miRNA and pre-miRNA into 21-23 nt miRNAs. Therapeutic siRNAs are perfectly complementary to their targets and appropriate the endogenous miRNA effector Argonaute 2 (AGO2) to enzymatically cleave its mRNA targets. siRNA can achieve specific knockdown of target mRNAs in liver by over 80% in patients, making them, in principle, an attractive therapeutic modality for disorders like *APOL1* and *TRPC6*-associated FSGS[36]. Current siRNA delivery strategies for liver like lipid nanoparticles and GalNAc conjugates deliver approximately 0.1% of the siRNA they carry into the cytoplasm of cells where it is active[37, 53]. This has been sufficient to enable the approval of siRNA therapeutics for Transthyretin amyloidosis, Hyperoxaluria type 1, and Acute Hepatic Porphyria. However, lipid nanoparticles administered intravenously usually require patients to be pre-treated with corticosteroids and anti-histamines to control adverse responses to them. Lipid nanoparticles and other RNA delivery vehicles induce nephrotoxicity that has limited the use of siRNA in kidney

diseases[44, 255]. For example, siRNA delivery vehicles and related Anti-Sense Oligonucleotides (ASO) induce elevated serum creatinine [256] and renal tubular toxicity during clinical trials[43, 257].

Small extracellular vesicles (sEVs) are 40-120 nm membrane-bound vesicles which are naturally released by most cells[79]. sEVs released from one cell can fuse with another cell to deliver contents into the cytoplasm of recipient cells, making them a potential delivery vehicle for siRNA[121, 122]. Numerous groups have harnessed sEVs to deliver siRNA in pre-clinical models of disease, loading the siRNA exogenously by electroporation[181, 182] and hydrophobic modification[190]. These studies often required higher doses of siRNA than lipid nanoparticles, suggesting that when manipulated in these ways sEVs are poor delivery vehicles. Alternatively, we have shown that sEVs can be endogenously loaded with siRNA by integrating it into the stem-loop backbone of pre-miR-451[258]. This eliminates the need for any modifications to be made to the sEVs after purification and allows sEVs to deliver approximately 300-fold more of their siRNA cargoes than lipid nanoparticles[258]. These sEVs could deliver siRNA targeting *GFP* mRNA and silence GFP in the kidney glomeruli of transgenic mice[258], evoking their therapeutic potential for glomerular kidney disease.

The use of sEVs therapeutically in patients must address key issues related to scaling. First, limitations on distribution can increase as body size scales. These restrictions can be more acute and unpredictable for biologicals that bind proteins, are actively targeted or transported, or are subject to renal excretion[259]. sEVs are subject to all of these: they can be coated with a protein corona in the blood[260, 261], the cell types targeted by sEVs are driven by the expression of cell surface receptors, including integrins[160, 262] and CD47[181], and sEVs are abundant in the urine, suggesting that they can be filtered at the glomerulus and are not completely reabsorbed along the nephron[263, 264].

The second issue relevant to scaling into larger animals and patients is inter-species differences in cell composition of organs[265, 266], or immune cells[267] and their receptors which may bind and internalize sEVs. These differences may render the scaling of sEV therapies into larger animals unpredictable. These factors likely underlie, for example, challenges in scaling of adeno-associated viruses (AAV) into larger animals[268]. Whereas intravenous administration of AAV in mouse models is usually sufficient for expression in the central nervous system, clinical trials in patients have had to use stereotactic injections of AAV directly near the brain lesion (e.g., Voyager (VY-AADC) and UniQure (AMT-130)). The number of AAV particles required to achieve an outcome in larger species similar to mice has frequently not scaled well by body mass either[269]. For example, when compared to mice, AAV doses scaled based on body mass had 20- and 60-fold lower transduction rates in hepatocytes from non-human primates or humans, respectively[269].

Finally, manufacturing of sEVs for larger animals will require isolation from large volumes of culture media. Differential ultracentrifugation has been the standard method for sEV isolation, however, it poses several challenges including difficulties with reproducibility[104], aggregation of sEVs[105], low yield and difficulty maintaining sterile and endotoxin-free preparations[106-109]. In contrast, tangential flow filtration (TFF) can be scaled to allow concentration of sEVs from media in a fast, controlled, and sterile manner[108].

Here, we use TFF to purify sEVs loaded with siRNA via the pre-miR-451 backbone. We show that TFF isolation generates an sEV product that causes no signs of toxicity or immune activation. We produce sEVs packaged with siRNA targeting *TRPC6* and *APOL1*, and using three distinct mouse models of kidney disease, we show that siRNA-loaded sEVs silence target mRNAs in the kidney glomeruli and significantly improve kidney pathology and function. Finally, siRNA-loaded sEVs knockdown targets in rat liver and rabbit kidney at doses which scale with body mass.

3.3 Results

TFF increases the yield and delivery efficiency of sEVs

We compared the sEVs produced by a standard differential ultracentrifugation protocol and by TFF on several key parameters to demonstrate their safety, identity, strength, purity, and quality. These two methods produced sEVs with a similar median size according to nanoparticle tracking analysis (NTA) (Fig. 3.1a), however, the yield of sEV-sized particles using the ultracentrifugation protocol was reduced by over 90% (Fig. 3.1b). To compare the siRNA delivery activity of sEVs produced using the two protocols, sEVs were produced from NSC-34 motor neuron-like cells stably expressing an siRNA targeting *GFP* in a stem-loop structure identical to pre-miR-451, or a control siRNA expressed from the same structure and vector[258]. We hypothesized that the ultracentrifugation protocol which exposes sEVs to 100,000 g force may damage them and reduce their capacity to deliver siRNA. The sEVs produced by TFF silenced *GFP* mRNA in a dose-dependent manner in primary mixed motor neuron cultures from *GFP* transgenic mice. A dose of 2,000 sEVs produced by TFF achieved maximal *GFP* silencing in this assay, demonstrating their potency. In contrast, even 100-fold more sEVs produced by ultracentrifugation did not reach similar levels of silencing (Fig. 3.1c, Supplementary Fig. 3.1). Together these data demonstrate that TFF increases sEV yield by 10-fold and these sEVs retain siRNA delivery efficiency over 100-fold greater than that of sEVs produced by ultracentrifugation.

TFF produces sEVs with minimal inflammatory or toxic responses

To establish a protocol for scalable and sterile manufacturing of sEVs, sEV-producing cells were cultured in defined serum-free media. After removing the cells, a 0.22 μm filter was used to exclude larger vesicles and contaminants. The filtered product was concentrated by TFF,

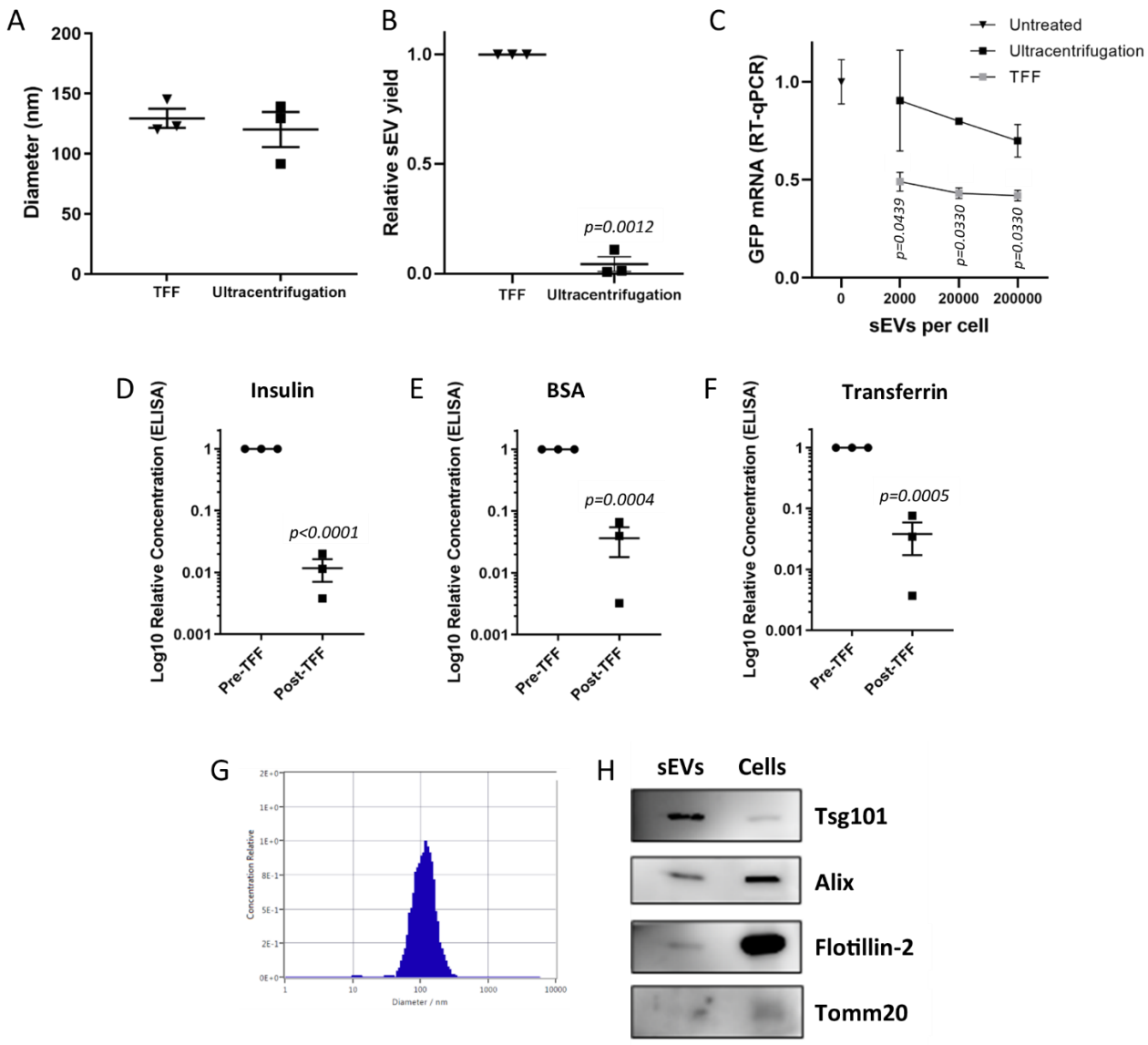

Figure 3.1. Tangential flow filtration (TFF) increases yield, delivery efficiency and purity of sEVs. (**A**) sEVs prepared from conditioned cell culture medium by either TFF or differential ultracentrifugation produce particles with similar median size measured by NTA (n=3). (**B**) Particle yield, measured by NTA, is reduced by >90% when sEVs are prepared via differential ultracentrifugation as compared to TFF (n=3). (**C**) GFP siRNA-loaded NSC-34-derived sEVs prepared by either TFF or differential ultracentrifugation were dosed onto mixed motor neuron cultures from GFP+ transgenic mice. TFF-prepared sEVs can reduce target expression, quantified by RT-qPCR, at lower doses of sEVs than ultracentrifuged sEVs even with doses 100-fold lower (n=3). (**D** to **F**) The TFF protocol to prepare sEVs, including 10x diafiltration with PlasmaLyte, reduces the presence of soluble contaminating proteins insulin (D), BSA (E), and transferrin (F) in conditioned culture media from fibroblasts by >96%, measured by ELISA (n=3). (**G**) TFF produces an sEV product that demonstrates a typical size distribution, measured by NTA. (**H**) TFF-prepared sEVs demonstrate a western blot marker profile typical of sEVs, containing EV-associated proteins Tsg101, Alix and Flotillin-2 while lacking the mitochondrial protein, Tomm20.

Significant differences between groups were determined by a two-tailed, unpaired t test with Welch's correction (B, D to F) or by ordinary One-Way ANOVA Holm-Šídák's multiple comparisons test (C).

diafiltered on TFF columns to reduce levels of soluble contaminants and concentrated further by TFF. Soluble media contaminants including insulin, bovine serum albumin, and transferrin were quantified in input cell culture media and the sEV product. Levels of each were reduced by >96% (Fig. 3.1d-f), demonstrating substantial purification of sEVs. TFF-isolated sEV preparations displayed identifying characteristics of sEV including size distributions peaking between 100 and 120nm as measured by NTA (Fig. 3.1g). sEV markers including Flotillin2, Tsg101, and Alix were abundant in these sEV preparations while the mitochondrial protein Tomm20 was undetectable (Fig. 3.1h).

Some reports have found that sEV preparations cause inflammatory reactions. These could be due to the production of sEVs from inflammatory cells, such as primed dendritic cells[270]. The standard protocol for producing sEVs by differential ultracentrifugation employs tubes and rotors that are frequently neither sterile nor clean. This risks contamination with endotoxin and other environmental inflammatory stimuli. The TFF process used above utilizes exclusively sterile and clean materials and is performed in a biosafety cabinet. Endotoxin levels in sEVs prepared with this method were 0.04 EU/mL on average, well below the Food and Drug Administration standard for intravenous injection of <0.25 EU/ml (Fig. 3.2a).

To test directly whether these sEV preparations instigated inflammatory responses, sEVs were incubated with human whole blood to reproduce a potentially distinct human response. One thousand sEVs per cell are sufficient to silence a gene *in vitro*[258], so we added sEVs at a 10-fold higher dose to human whole blood. This dose of 10,000 sEVs per cell is also greater than the ratio of sEVs per white blood cell in mice after an intravenous injection. sEVs from primary neonatal

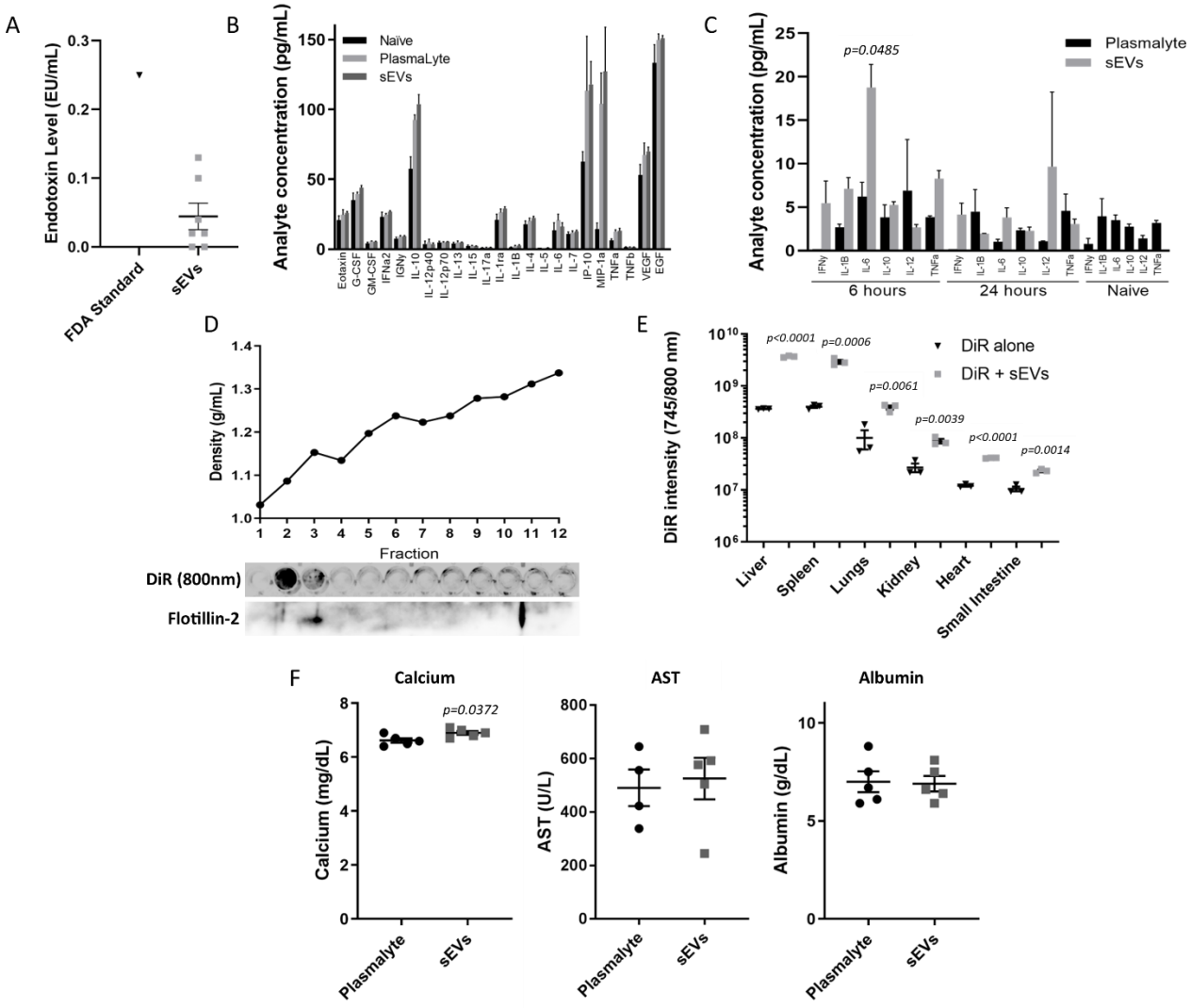

Figure 3.2 TFF produces sEVs with minimal inflammatory or toxic response. (**A**) TFF-prepared sEVs for injection into animals contain endotoxin levels of 0.04 EU/mL on average, well below the FDA standard for water suitable for intravenous injection of <0.25 EU/mL (n=7). (**B**) A dose of siRNA-loaded, fibroblast-derived sEVs 10x greater than needed to achieve target knockdown from three distinct TFF preparations was incubated with blood from two human donors in duplicate revealing no significant differences between vehicle and sEV treatments across a panel of 23 cytokines and chemokines, measured by milliplex assay (n=4 for naïve and PlasmaLyte, n=12 for sEVs). (**C**) siRNA-loaded, fibroblast-derived sEVs were injected into mice at a dose 10x higher than required to achieve maximum target knockdown and blood was analyzed using a milliplex assay. A small increase in IL-6 levels was seen at 6h, and no other significant differences were seen between the sEVs and vehicle across a panel of 6 cytokines (n=3 for PlasmaLyte, n=6 for sEVs: 3 distinct TFF preparations in 2 mice each). (**D**) Primary human fibroblast sEVs were labelled with the far-red fluorescent lipophilic membrane dye, DiR and separated by iodixanol (Optiprep) gradient. The gradient was separated into 12 fractions. DiR fluorescence, excited at 800nm, is present alongside the sEV marker Flotillin-2 in fractions two and three, which are the expected density of sEVs, 1.05-1.19 g/mL. (**E**) sEVs stained with the

lipophilic dye, DiR, were injected into mice, and organs were removed and imaged in the IVIS Spectrum after 6 hours. sEVs were observed primarily in the liver, spleen, lungs, and kidney (n=3). (**F**) A dose 10x higher than required to achieve maximum target knockdown was injected into mice and serum was used in a comprehensive blood chemistry panel (n=5). Significant differences between groups were determined by two-tailed, unpaired t-test with Welch's correction (G) or by ordinary One-Way ANOVA Holm-Šídák's multiple comparisons test (B-F).

fibroblasts from three distinct TFF preparations were incubated with whole blood from two donors. No significant differences were found between the vehicle (Plasmalyte) or sEV treatments across 23 cytokines and chemokines representing Th1, Th2, and other responses (Fig. 3.2b). We then injected sEVs from primary human fibroblasts intravenously into mice at a dose 10-fold higher (10^{12} sEVs) than that necessary to elicit maximal knockdown of siRNA targets in the liver and kidney[258]. IL-6 levels increased from approximately 6 pg/mL in vehicle-treated animals to 15-20 pg/mL in sEV-treated mice at 6 h and returned to the background at 24 h. For perspective, 1000 pg/mL of IL-6 is associated with sepsis[271]. Otherwise, no significant differences between the vehicle (Plasmalyte) and sEV injected samples were observed across a panel of 6 other cytokines including TNFα, IL-1β, IL-12, IL-10, or IFNγ (Fig. 3.2c).

We analyzed the distribution of sEVs released by human neonatal fibroblasts injected intravenously in mice. The lipophilic dye, DiR (tetramethylindotricarbocyanine Iodide) was used to label sEVs. DiR partitioned with an sEV marker in fractions at the expected density of sEV, from 1.05 to 1.19 g/mL (Fig. 3.2d). Injection of DiR-labeled sEVs led to their accumulation predominantly in the liver, spleen, lungs, and kidney (Fig. 3.2e). Comprehensive toxicology panels were performed on blood 24 hours after mice were injected with a 10-fold higher dose (10^{12} sEVs) than used to attain maximal target knockdown with siRNA-loaded sEVs. A small, but significant increase in serum calcium levels, well within the normal range of blood calcium, was observed after sEV injection, otherwise, no significant differences were observed between vehicle or sEV injected mice across a panel of 16 analytes including albumin and markers of hepatoxicity (AST,

ALT, bilirubin) and nephrotoxicity (BUN) (Fig. 3.2f, Supplementary Fig. 3.2). Pathological analysis was performed by a registered veterinary pathologist on hematoxylin and eosin (H&E) stained slides and revealed no observable differences in kidney, liver, lung, small intestine, or spleen between vehicle- or sEV-injected mice (Supplementary Fig. 3.3). These data together suggest that TFF produces sEVs that elicit minimal toxicity or immune responses.

siRNA delivered by sEV reduces target expression in the kidney

We previously showed the ability of sEVs isolated from engineered mouse cell lines to deliver siRNA targeting *GFP* mRNA to the glomeruli of the kidney[258]. To test the efficacy of TFF isolated sEVs of human origin in delivering siRNA in mouse kidney glomeruli, we targeted *GFP* and *SOD1* as a proof-of-concept. Transgenic mice expressing *EGFP* or *SOD1 G93A* were intravenously injected with human neonatal fibroblast sEVs (10^{11}) carrying siRNA targeting *GFP* or *SOD1*, respectively. Control-treated mice were injected with sEVs derived from the same cell type, loaded with off-target siRNA. Seven days later the kidneys were harvested, sectioned, and probed for protein levels by immunofluorescence and for mRNA expression by quantitative Fluorescence *In Situ* Hybridization (FISH). In transgenic mice ubiquitously expressing *GFP*, sEVs containing *GFP* siRNA reduced GFP protein expression in glomerular cells by 70% (Fig. 3.3a,b, Supplementary Fig. 3.1). Similarly, FISH showed a 75% decrease in glomerular *GFP* mRNA levels (Fig 3.3c). Interestingly, glomerular cells with reduced *GFP* expression included, but were not limited to, podocytes (co-stained for nephrin). Similar results were observed after injection with sEVs derived from a separate human cell line, HEK293T (Supplementary Fig. 3.4a-c, Supplementary Fig. 3.1). Knockdown was dose-dependent (Fig. 3.3d) and increased significantly when kidneys were harvested 12 days after sEV injection, compared to 3 days after injection (Fig. 3.3e). For comparison, sEVs loaded with siRNA against Transthyretin (*Ttr*), a gene expressed

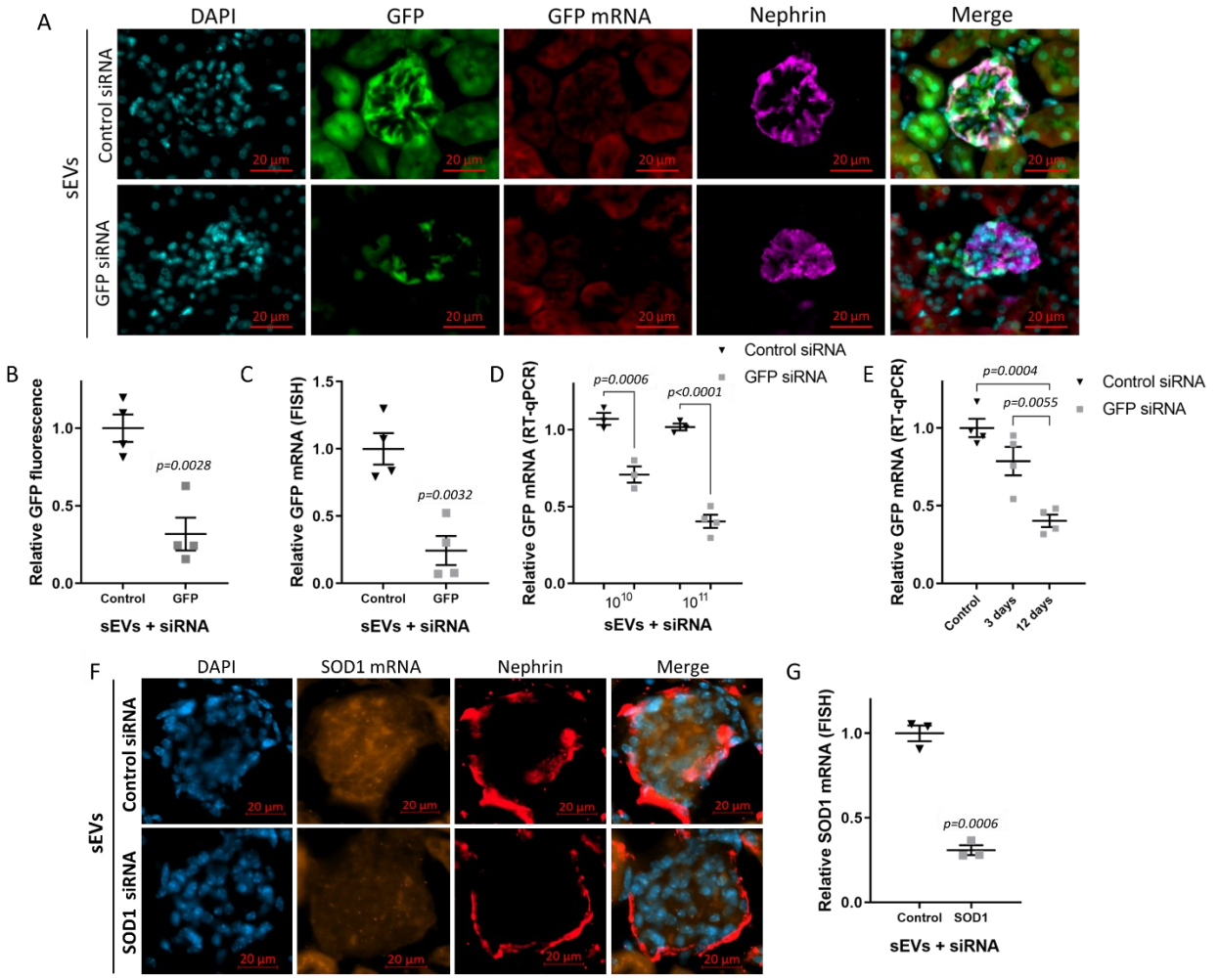

Figure 3.3 siRNA delivered by sEV reduces target expression in the kidney. (**A** to **C**) 10^{11} sEVs containing siRNA targeting *GFP* (or containing an off-target siRNA as control) from human fibroblasts were injected into mice ubiquitously expressing *GFP* and kidneys were harvested seven days after injection. Immunofluorescence revealed a decrease in GFP expression in Nephrin-positive glomeruli of 70% (A and B) and quantitative FISH revealed a reduction of *GFP* mRNA of 75%. Magnification is 20X; the scale bar represents 20 µm (A and C) (n=4). (**D**) A dosing experiment showed that increasing the injected dose of sEVs from 10^{10} to 10^{11} sEVs increases the observed target knockdown (n=4 for 10^{11} sEV dose, n=3 for other groups). (**E**) Kidneys from mice that had been injected as above were harvested after either 3 or 12 days and knockdown was observed to increase when harvested after 12 days, as compared to 3 days (n=4). (**F** and **G**) 10^{11} sEVs containing siRNA targeting *SOD1* (or containing an off-target siRNA as control) were injected into transgenic *SOD1 G93A* mice and quantitative FISH revealed a reduction of *SOD1* mRNA expression of 70% in Nephrin-positive glomeruli (n=3). Significant differences between groups were determined by a two-tailed, unpaired t-test with Welch's correction (B, C, G) or by ordinary One-Way ANOVA Holm-Šídák's multiple comparisons test (D and E).

primarily in hepatocytes that is the target of the siRNA therapeutic Patisiran (trade name Onpattro)

for the treatment of transthyretin amyloidosis, were injected into mice and TTR levels in the blood

were monitored over time. A single injection of sEVs (10^{11}) reduced blood TTR levels after only 3 days and knockdown peaked after 7 days, returning to baseline levels after 15 days (Supplementary Fig. 3.4d, Supplementary Fig. 3.1). When mice were injected weekly for 3 weeks, TTR silencing was sustained at 70% for the full 21 days of the experiment (Supplementary Fig. 3.4e). In kidneys from transgenic *SOD1 G93A* mice injected with sEV carrying siRNA targeting *SOD1*, FISH demonstrated a reduction in mRNA expression of ~70% in glomeruli (Fig. 3.3f,g, Supplementary Fig. 3.1).

sEV-delivered siRNAs demonstrate therapeutic efficacy in *APOL1* model of nephropathy in mice

Dose-limiting toxicity has limited attempts to use siRNA or antisense oligonucleotides (ASOs) to treat glomerular diseases in patients[255, 257, 272, 273]. The capacity of siRNA-loaded sEVs to knockdown transgenes in kidney glomeruli with minimal toxicity suggests that sEVs may enable the treatment of chronic kidney diseases with siRNA. To evaluate the potential efficacy of sEVs packaged with siRNA in treating glomerular diseases, we first evaluated an siRNA targeting *APOL1.* This was done in a published mouse model with inducible expression of the *APOL* risk variant G2 (G2 APOL1) from a podocyte-specific promoter (*NPHS1rtTA/TRE-APOL1-G2*)[249]. Two days after the induction of *APOL1* transgene expression, sEVs containing siRNA targeting *APOL1,* or targeting *GFP* as a control, were administered on two consecutive days, every week for three weeks (Fig. 3.4a, Supplementary Fig. 3.1). siRNA targeting *APOL1* accumulated in kidney glomeruli. No signal was present in glomeruli from mice that were treated with sEVs loaded with control siRNA, demonstrating that the *APOL1* siRNA was specifically detected (Fig. 3.4b). RT-qPCR demonstrated a 90% reduction in *APOL1* mRNA in the kidneys of mice receiving sEVs containing siRNA against *APOL1* vs. control siRNA (Fig. 3.4c). Immunofluorescent staining

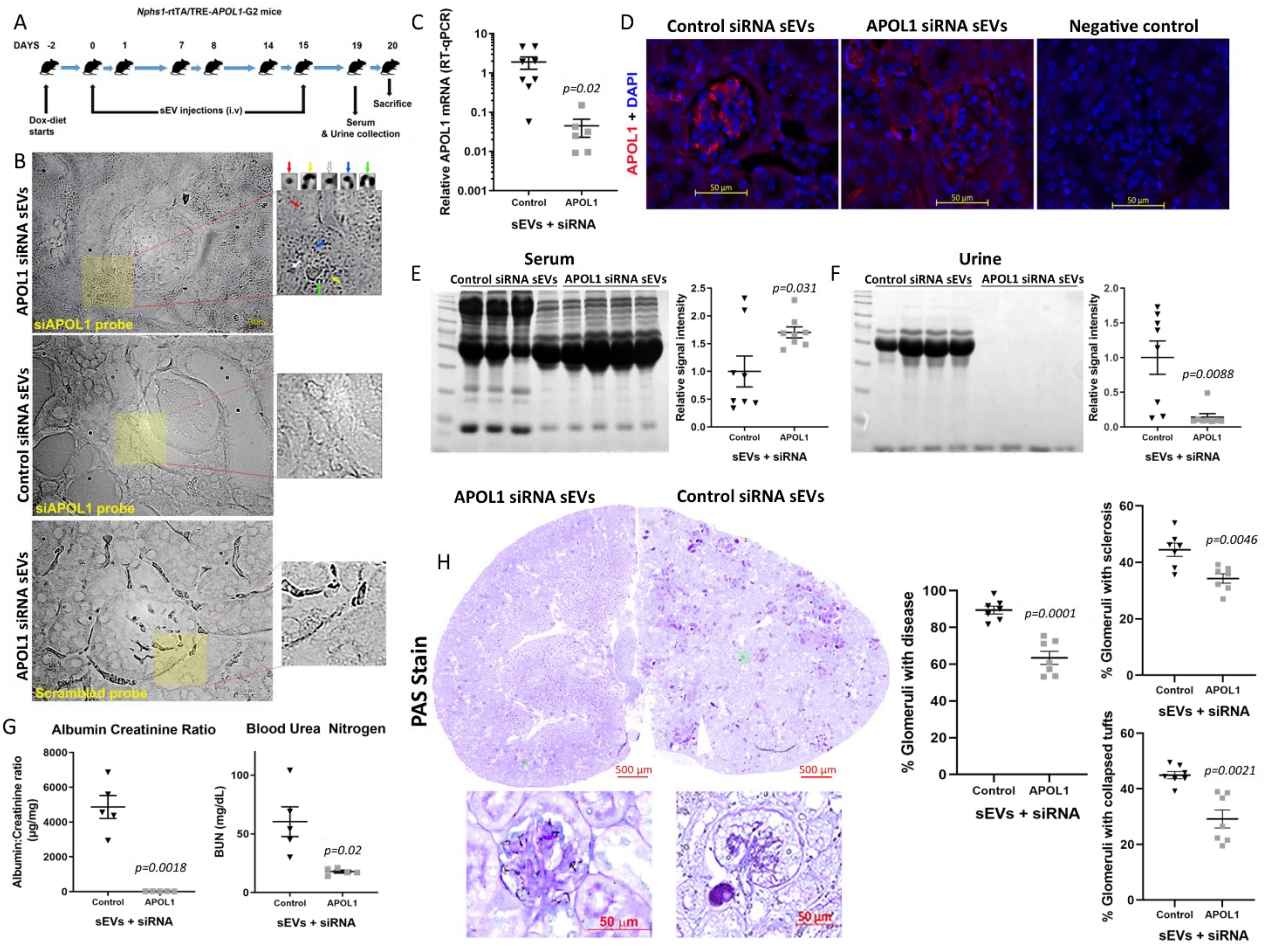

Figure 3.4. sEV-delivered siRNAs demonstrate therapeutic efficacy in an APOL1 mouse model of nephropathy. (**A**) NPHS1rtTA/TRE-APOL1-G2 mice were administered a dose of $5x10^{11}$ human fibroblast-derived sEVs containing siRNA targeting *APOL1* (or an off-target siRNA as control), on two consecutive days, weekly for three weeks. Animals were euthanized five days after the last dose. (**B**) The RNAscope hybridization system was used to detect the presence of APOL1 siRNA delivered to the kidney ultrastructure. Kidney sections from *APOL1* or control siRNA treated groups were incubated with probes against *APOL1* siRNA and dark puncta (marked by coloured arrows) representative of siRNA particles are observed only in the APOL1 siRNA treated kidney section (Inset shows marked area at 200% zoom). A scramble probe was used to rule out non-specific signals. (Images are representative of 3 animals per group. Magnification is 40X; the scale bar represents 20 µm). (**C**) RT-qPCR revealed a reduction of *APOL1* mRNA expression of >90% in sEV-treated mice (n=8, two data points in the *APOL1* siRNA-treated group were statistical outliers as determined by the Rout test in GraphPad Prism). (**D**) Immunofluorescent staining shows a reduction of *APOL1* expression in kidney glomeruli of mice treated with sEVs containing *APOL1* siRNA. A control without primary antibody did not show non-specific fluorescence. Magnification is 20X; the scale bar represents 50 µm . (**E** to **F**) Representative Coomassie staining of gels shows serum and urine albumin levels from the treated and control groups. Bands were quantified using FIJI with background correction and revealed an increase in serum levels of 1.7-fold and a decrease in urine levels of >85% (n=8). (**G**) In control-treated animals, serum and urine chemistry panels reveal increased urinary albumin creatinine ratio and

elevated BUN as compared to APOL1 siRNA treated animals, indicative of acute kidney damage (n=4 control, n=5 treated). (**H**) PAS staining of kidney sections from control and *APOL1* siRNA treated kidneys shows pathological changes. Magnification is 20X; the scale bar represents 500 μm. Boxed regions on the images are magnified for a clearer depiction of glomerular changes, scale bar represents 50 μm. Glomeruli were categorized into groups with disease, sclerosis or collapsed tufts by an expert observer. Significantly fewer glomeruli were observed in each case in mice treated with sEVs containing siRNA targeting *APOL1* (n=7). Significant differences between groups were determined by a two-tailed, unpaired t-test with Welch's correction (C, E, F, G, H).

of kidneys confirmed the lower APOL1 protein expression in the glomeruli of treated mice (Fig. 3.4d).

Previous work showed that induction of the *APOL1* risk variant in podocytes was responsible for glomerular pathology, including proteinuria, azotemia, and glomerulosclerosis[249]. In mice treated with siRNA targeting *APOL1* serum albumin levels were significantly higher compared to their control siRNA-treated counterparts (Fig. 3.4e). Urine albumin levels and the urine albumin/creatinine ratio, measures of the integrity of the glomerular barrier, were reduced by >85% in the animals receiving siRNA against *APOL1* (Fig. 3.4f,g). Mice treated with *APOL1* siRNA exhibited improved kidney function parameters including lower blood urea nitrogen levels compared to control treated mice (Fig. 3.4g). Pathological examination of the kidneys using Periodic Acid Schiff (PAS) staining identified a significant decrease in glomeruli with sclerosis, collapsed tufts or signs of disease in the group treated with sEVs loaded with siRNA against *APOL1* (Fig. 3.4h). Similar results were independently obtained by a blinded observer (Supplementary Fig. 3.5a). Taken together, these data demonstrate that sEVs packaged with siRNA targeting *APOL1* deliver their cargoes to glomeruli, reduce *APOL1* expression, and prevent much of the APOL1-induced glomerular dysfunction and damage.

sEV-delivered siRNAs demonstrate therapeutic efficacy in models of *TRPC6*-dependent nephropathy in mice

We evaluated the capacity of sEVs to deliver siRNAs against *TRPC6,* which may have therapeutic benefits in a broader group of patients with proteinuric kidney disease. We initially tested siRNA against *Trpc6* in mice subjected to unilateral ureteral obstruction (UUO), an experimental model of the fibrotic response in chronic kidney disease (Fig. 3.5a). A single dose of sEVs containing siRNA targeting murine *Trpc6* was injected intravenously 48 hours prior to UUO surgery. Mice were euthanized 5 days post-surgery and qPCR revealed a reduction of *Trpc6* expression in kidneys of ~70% in mice that received sEVs containing *Trpc6* siRNA compared to mice that received sEVs containing control siRNA (Fig. 3.5b, Supplementary Fig. 3.1). Similarly, injection of sEVs loaded with siRNA against *Trpc6* significantly reduced levels of mRNAs encoding proteins involved in the fibrotic response such as *Alpha-Smooth Muscle Actin (αSma)*, *Collagen 1,* and Connective tissue growth factor (*Ctgf*) (Fig. 3.5c). Immunofluorescent staining of αSma protein, and staining with aniline to reveal collagenous deposits, were both reduced to levels comparable to that of a sham kidney (Fig. 3.5d,e). PAS stained kidney tissue was assessed for gross histopathological changes. It showed a significant reduction in the number of diseased glomeruli only in mice treated with sEVs containing *Trpc6* siRNA (Fig. 3.5f). Similar results were independently obtained by a blinded observer using the same rules (Supplementary Fig. 3.5b). These results suggest that the extent of interstitial damage in kidneys subjected to UUO was reduced by exposure to siRNA-loaded sEVs.

For further validation of the effectiveness of *Trpc6* siRNA delivered by sEVs, we used Adriamycin (ADR; Fig. 3.6) to induce glomerulosclerosis that is known to depend on *Trpc6* expression[274, 275]. Mice were intravenously injected once per week with sEVs packaged with *Trpc6* siRNA or GFP siRNA as a control. Mice were also treated with Adriamycin once per week for three weeks to induce glomerulosclerosis and increase Trpc6 expression (Fig. 3.6a). In mice

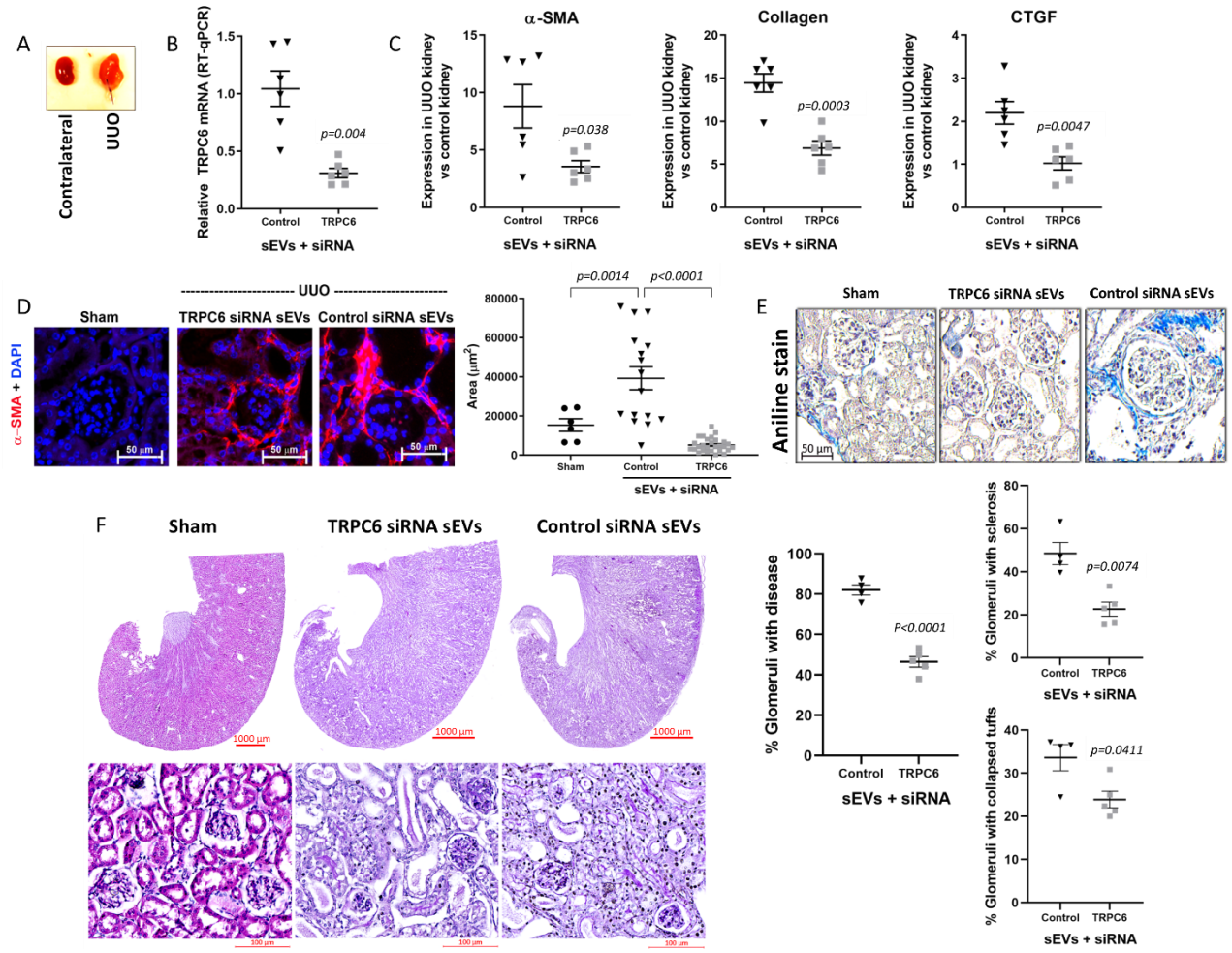

Figure 3.5. sEV-delivered siRNAs demonstrate therapeutic efficacy in mice subjected to unilateral ureteral obstruction, a TRPC6-dependent model of fibrotic response in chronic kidney disease. (**A**) Unilateral ureteral obstruction (UUO) was performed on mice to induce hydronephrotic changes. A stark anatomical difference was visible between the obstructed and unobstructed kidneys at 7 days post-surgery. (**B**) $5x10^{11}$ human fibroblast-derived sEVs containing siRNA targeting *Trpc6* (or an off-target siRNA as control) were injected into mice following UUO surgery, and led to a reduction of *Trpc6* mRNA expression by ~70%, as measured by RT-qPCR (n=6) (**C**) The relative mRNA expression of alpha-smooth muscle actin, collagen, and connective tissue growth factor, that are markers associated with fibrotic changes in the kidney following UUO surgery, were all significantly reduced in mice that received sEVs containing siRNA targeting *Trpc6*, as measured by RT-qPCR (n= 6) (**D**) Immunofluorescent staining performed to detect alpha-smooth muscle actin expression in kidneys following sham-operated mice or UUO mice that received treatment sEVs reveals a decrease in signal in treated mice as compared to control-treated counterparts. The total area of regions containing alpha-smooth muscle actin was evaluated using FIJI. Data is representative of at least 2 sections per mouse. Magnification is 20X; the scale bar represents 50 µm; (n=3 for sham, n=6 for treated and control UUO groups). (**E**) Aniline blue staining shows prominent fibrotic regions in UUO mice treated with off-target control siRNA, as compared to UUO mice treated with siRNA targeting *Trpc6* or sham. Magnification is 20X; the scale bar represents 50 µm. Figures representative of 3 mice per group. (**F**) PAS staining

of kidney sections from sham, or UUO mice receiving *Trpc6* or control siRNA sEVs shows pathological changes. Magnification is 20X; the scale bar represents 500 µm. Specific regions on the images were magnified for the clearer depiction of glomerular changes, scale bar represents 50 µm. Glomeruli were categorized into groups with disease, sclerosis or collapsed tufts by an expert observer. Significantly fewer glomeruli were observed in each case in mice treated with sEVs containing siRNA targeting *Trpc6* (n=4 for control, n=5 for treated). Significant differences between groups were determined by a two-tailed, unpaired t-test with Welch's correction (B, C, F) or ordinary One-Way ANOVA Holm-Šídák's multiple comparisons test (D).

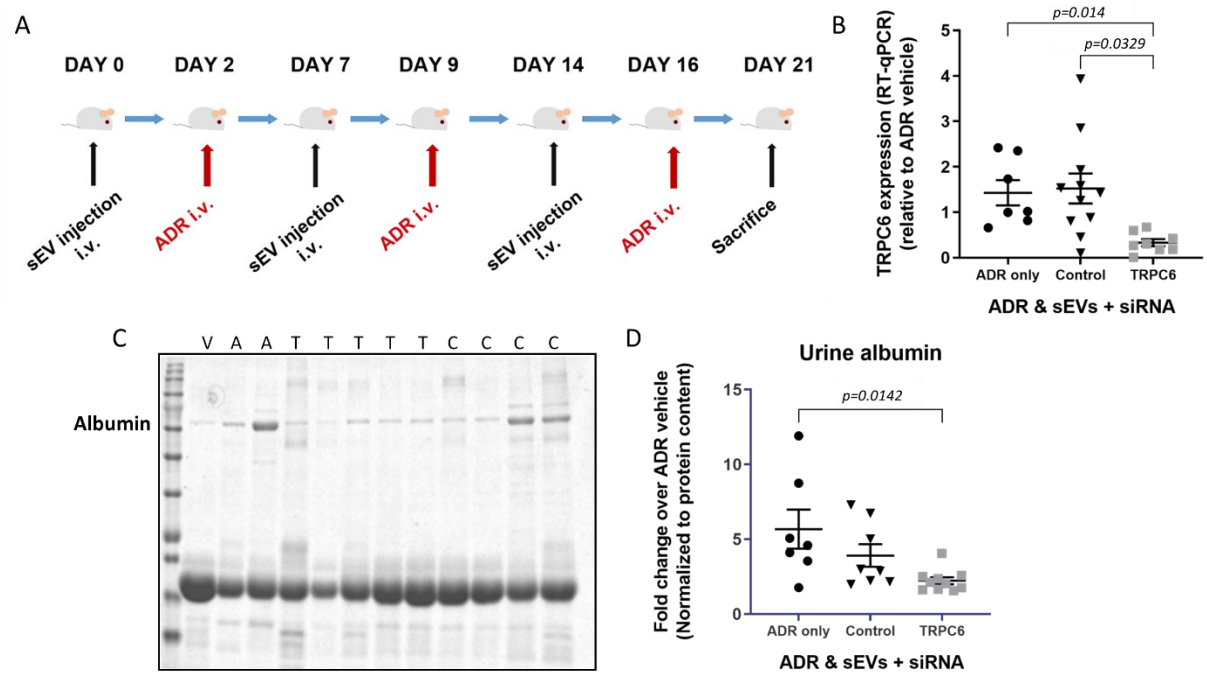

Figure 3.6. sEV-delivered siRNAs demonstrate therapeutic efficacy in mice treated with Adriamycin, a model of TRPC6-dependent glomerulosclerosis. (**A**) Adriamycin-(shortened to ADR for the brand name, Adriamycin, in the figure)-induced nephropathy model was established by weekly intravenous injections (5 mg/kg body weight) for 3 consecutive weeks. $5x10^{11}$ human fibroblast-derived sEVs containing siRNA targeting *Trpc6* (or off-target siRNA as control) were administered 48hours prior to each Adriamycin injection. Animals were euthanized 5 days after the final Adriamycin injection. (**B**) RT-qPCR shows a reduction of *Trpc6* mRNA following siRNA-loaded sEV treatment of nearly 80% as compared to the control siRNA-treated group or the group that received Adriamycin injections and no sEV injections (n=7 for ADR only, n=11 for control and *Trpc6* siRNA groups). Three statistically significant outliers were identified and removed following Rout's analysis using GraphPad Prism. (**C** and **D**) Representative Coomassie staining of urine samples collected from injected mice post-mortem. Albumin bands were quantified using FIJI. siRNA-loaded sEV treatment led to a significant reduction of albumin in the urine. V=ADR vehicle; A=ADR only; T=ADR+sEVs containing *Trpc6* siRNA; C=ADR+ sEVs containing control siRNA. (n=7 for ADR only, n=11 for control and *Trpc6* siRNA groups, lower number of data points is owing to a failure to collect enough volume of sample at the time of necropsy). Significant differences between groups were determined by ordinary One-Way ANOVA Holm-Šídák's multiple comparisons test (B and D).

treated with Adriamycin, expression of *Trpc6* mRNA expression in the kidney was only significantly reduced in mice exposed to sEVs loaded with *Trpc6* siRNA (Fig. 3.6b). Since mice exposed to Adriamycin typically exhibit more proteinuria than control mice[276], we evaluated the impact of sEVs packaged with *Trcp6* siRNA on this parameter. We found that treatment with sEVs containing siRNA against *Trpc6* led to a reduction in urine albumin levels of nearly 50% (Fig. 3.6c,d). Treatment with sEVs containing *Trpc6* siRNA also appeared to increase serum albumin levels when compared to sEVs packaged with control siRNA (Supplementary Fig. 3.6).

siRNA-loaded sEVs knockdown clinical targets in large animal models

Many types of drugs and delivery vehicles including ASOs and AAV lose efficacy as they are scaled into larger animals[269]. For ASOs injected into the spinal cord, the limitation may be the increased distance to travel before reaching tissues like the hippocampus[277]. To evaluate the scaling of sEVs into larger mammals, we first tested the ability of sEVs produced by human neonatal fibroblasts to knockdown Transthyretin (*Ttr*) in rats. A dose of 10^{11} sEVs reduced TTR protein levels in the blood by 70% in mice weighing on average 20-25 g (Supplementary Fig. 3.4d,e). In rats weighing 400 g, we administered an approximately 10-fold higher dose of $1.4x10^{12}$ sEVs containing the same siRNA targeting a region of the *Ttr* mRNA which is identical in mice and rats. sEVs packaged with *Ttr* siRNA reduced the levels of TTR in the blood by ~50% (Fig. 3.7a). The reduction of TTR in rats was dose-dependent (Fig. 3.7b). These results suggest that an sEV dose approximately 10x larger is effective in knocking down targets in an animal approximately 15-20-fold larger, suggesting siRNA delivery with sEV scales with body mass.

To evaluate target knockdown outside the liver in larger animals, we used the *Trpc6* siRNA that recognizes a region conserved in rabbit *Trpc6.* In rabbits, sEVs from neonatal human

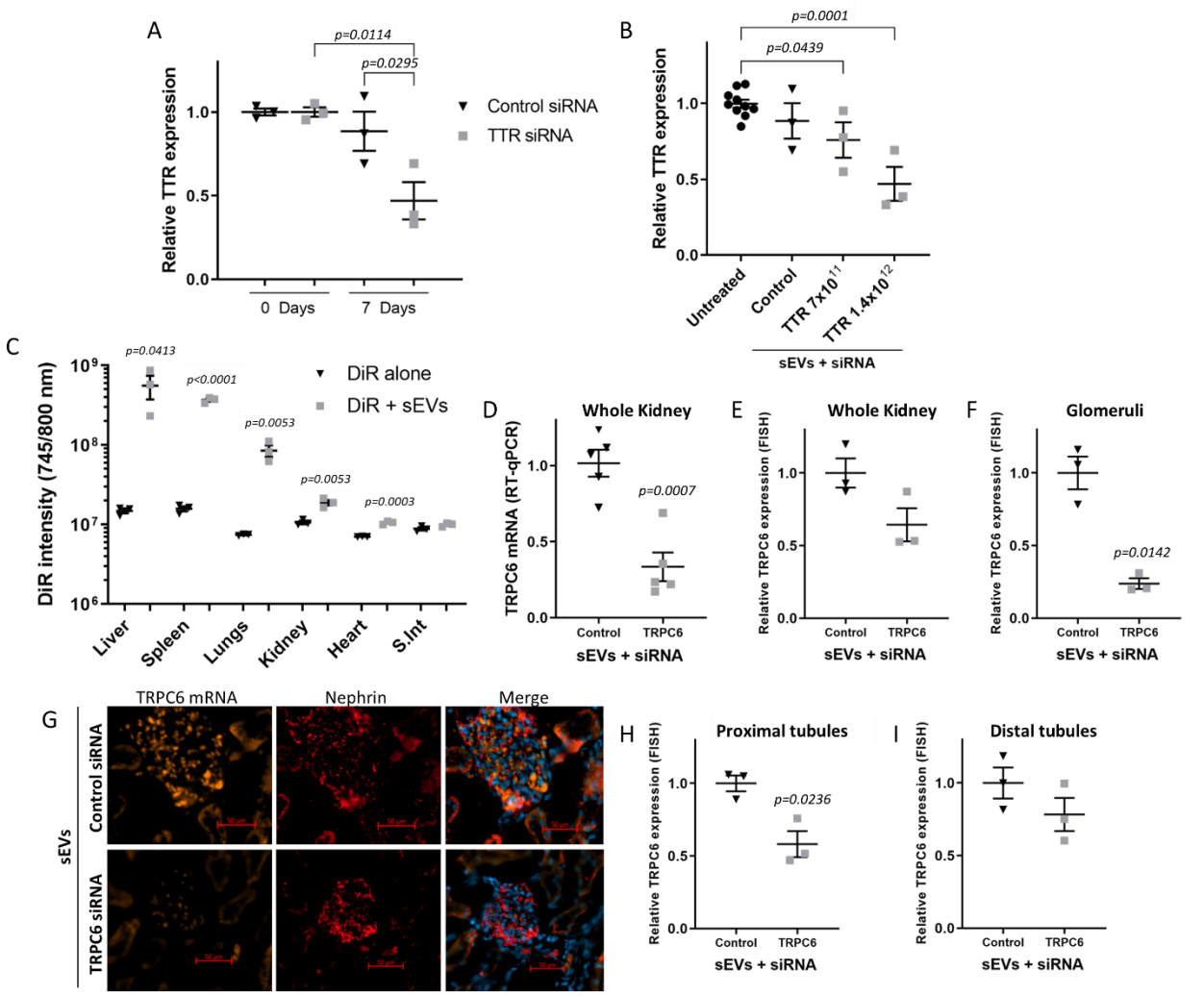

Figure 3.7. siRNA-loaded sEVs knockdown clinical targets in large animal models. (A) 1.4x10^{12} sEVs containing siRNA targeting *Ttr* were injected into rats and led to a reduction in TTR levels in the blood of ~50% (n=3). (**B**) TTR knockdown by sEV-derived siRNA in rats is dose-dependent, with target knockdown reaching 25% with 7x10^{11} sEVs and 50% with 1.4x10^{12} sEVs (n=3 for treated rats, n=10 naïve rats). (**C**) In rabbits, sEVs stained with the lipophilic dye, DiR, were injected and organs were removed and imaged in the IVIS Spectrum after 24 hours. sEVs were observed primarily in the liver, spleen, lungs, and kidney (n=3). (**D** to **I**) 10^{13} human fibroblast-derived sEVs containing siRNA targeting *Trpc6* (or off-target siRNA as control) were injected into rabbits and kidneys were harvested after 7 days. RT-qPCR revealed a decrease in *Trpc6* mRNA in the kidney of 75% (n=5) (D), while quantitative FISH revealed a decrease of ~40% in the whole kidney (n=3) (E). Using quantitative FISH to specifically examine Nephrin-positive glomeruli reveals a decrease of *Trpc6* mRNA of >70%. Magnification is 20X; the scale bar represents 50 µm (n=3) (F and G). Quantitative FISH revealed a decrease of *Trpc6* mRNA in proximal tubules of ~40% (n=3) (H) and no significant reduction in distal tubules (n=3) (I). Significant differences between groups were determined by a two-tailed, unpaired t-test with Welch's correction (D to J) or by an ordinary One-Way ANOVA Holm-Šídák's multiple comparisons test (A to C).

fibroblasts stained with DiR distributed to tissues in a similar pattern to mice, with predominant signals in the liver, spleen, lungs, and kidneys (Fig. 3.7c). 10^{13} sEVs packaged with siRNA against *Trpc6* or control siRNA were injected intravenously into rabbits weighing 3-4 kg and kidneys were harvested after 7 days. Whole kidney *Trpc6* mRNA expression was decreased when quantified by RT-qPCR (Fig. 3.7d). Quantitative FISH revealed a ~40% reduction in *Trpc6* mRNA in the whole kidney (Fig. 3.7e), and >70% reduction in glomeruli (Fig. 3.7f,g). Quantitative FISH also showed a ~40% reduction of *Trpc6* mRNA in proximal tubules (Fig. 3.7h), but not in distal tubules (Fig. 3.7i). These data suggest that sEV delivery of siRNAs in the rabbit kidney occurs mostly in the glomeruli and the first segment of the nephron, the proximal tubule. Together, these results demonstrate that the efficacy of siRNA-loaded sEVs scales with body mass into large mammals.

The results presented here demonstrate that TFF can be used to produce safe and potent sEVs packaged with siRNAs using the pre-mIR-451 backbone. These sEVs deliver siRNAs to enable effective silencing of target mRNAs in glomeruli of both mice and rabbits, improving pathology and proteinuria, suggesting their potential application for the treatment of chronic kidney diseases.

3.4 Discussion

sEVs are capable of highly efficient delivery of cargoes such as siRNA into the cytoplasm of target cells[258, 278]. This suggests that sEV membranes fuse with the membrane of target cells. In known fusion events involving vesicles, organelles, cells, and viruses a particular lipid composition, curvature and fluidity are often required alongside specific receptors. Ultracentrifugation is a standard method of enriching sEVs, but subjects them to a force of 100,000 g and vigorous pipetting for resuspension, which is likely to damage membranes and possibly proteins involved in sEV fusion. Exposure of viruses to similar ultracentrifugation compromises

viral particles and their infectivity markedly[279, 280]. Similarly, we observed that ultracentrifugation protocols led to the recovery of 10-fold fewer sEVs than TFF, and these sEVs exhibited severely impaired delivery of siRNA to target cells compared to the same number of sEVs prepared by TFF. Therefore, TFF enables both a 10-fold increased yield of sEV and a substantially increased delivery capacity or potency per sEV, compared to ultracentrifugation protocols. These advantages of TFF reduce by approximately 100-fold the volumes of cell culture media required for effective doses, and also decrease the risk of toxicity associated with sEVs. For example, on average 1 L of media from standard cell culture of the fibroblasts used here, generates sufficient sEVs for 3-10 effective doses for a 4 kg rabbit. These data provide concrete support for the proposal that TFF offers numerous benefits compared to other sEV isolation techniques including higher yield, scalability, reproducibility, purity, and process sterility[104, 108, 110-113].

The immune systems of rodents and humans have diverged significantly to adapt to their distinct environmental exposures[281]. Therefore, immune responses to therapeutics like sEVs are better modeled on human immune cells. To address these limitations of the current literature, we exposed human whole blood or mice to sEV doses that were 10-fold higher than that required to achieve knockdown of siRNA targets (Fig. 3.2b, c) and observed no substantial cytokine responses. Importantly, siRNA-loaded sEVs can be injected multiple times over a multi-week dosing schedule, resulting in prolonged depletion of targets and no incidence of adverse events (Fig. 3.4, 3.6, Supplementary Fig. 3.4). This raises the possibility that sEVs packaged with siRNA and produced using TFF could be a safe delivery vehicle for sustained treatment of various diseases.

Studies using sEVs purified by ultracentrifugation incur a major risk of contaminating sEV preparations with endotoxin that cannot be removed or neutralized by most sterilization or cleaning

protocols[282, 283]. This kind of contamination of sEV preparations could account for some of the inflammatory responses attributed to sEVs. In contrast, TFF, which can be performed in a sterile closed-loop, is likely to produce a safer sEV product considering native, unaltered sEVs have been shown to result in minimal or no cytokine response, tissue histopathology, or change in blood cell counts or organ function after intravenous administration[183, 184].

We previously showed that sEVs loaded with siRNA using the pre-miR-451 backbone can deliver functional siRNA in mice and knockdown targets with doses of siRNA much lower than lipid nanoparticles[258]. Here, we show that siRNA delivered by sEVs can knockdown targets in glomeruli in multiple models of kidney disease leading to improved glomerular function and reduction of kidney pathology (Fig. 3.4-3.6). siRNA delivered by sEV accumulated in glomeruli (Fig. 3.4b). sEVs range in size from 40-120 nm, but atomic force microscopy studies demonstrate they have a deformable, compressible shape which can be driven by binding of sEVs to surfaces[284]. Under glomerular filtration pressure, and interacting with receptors at the glomerular barrier, sEVs may be small enough to pass from the blood into the glomeruli to deliver contents into podocytes. As sEVs are complex, large biological delivery vehicles it is possible that the inflammation and pathology occurring in models of glomerulosclerosis would cause sEVs to be neutralized or phagocytosed, or otherwise limit their penetration into the glomeruli. The consistent ability of sEV to deliver siRNA demonstrated across three models of kidney pathology with diverse triggers suggests that sEVs are resilient in these situations.

The use of most RNA therapeutics in the kidney is limited by toxicity[255, 257, 272, 273]. For example, antisense oligonucleotides accumulate in the kidney in the proximal tubules, which results in substantial nephrotoxicity[255]. While ASO targeting *APOL1* can reduce expression in the kidney, it has been shown to only reduce its expression by 50% and this required weekly doses

each over 10-fold higher than the dose required to silence a target in the liver[214, 215]. Doses of ASO required to supress liver targets can already cause substantial toxicity in patients and have led to multiple halts of clinical trials, suggesting that using a 10-fold higher dose in patients with CDK would be challenging. Our data suggests sEVs may be able to deliver siRNA to the kidney with minimal toxicity, a comparable dosing schedule, while also eliciting more profound target mRNA reductions.

Moving from mice as a model organism to larger animals and eventually to humans is not straightforward. Scaling of production can be complicated, and in some cases scaling into larger animals reduces the distribution and potency of the product. For example, scaling AAV-based therapeutics can activate host immune response that decreases transgene expression, reducing therapeutic potency[285]. Here, to assess scalability we tested the siRNA-loaded sEVs in two large animal models: rats and rabbits. In rats, an sEV dose 10 times greater than that used in mice was effective in knocking down targets in an animal ~20-fold larger, while in rabbits, a dose only 100 times greater than that used in mice was sufficient to knockdown targets in an animal ~200-fold larger. This provides evidence that sEV delivery vehicles scale into larger species by body mass in a predictable manner. Targeting and delivery of siRNAs by sEVs may rely on specific sEV receptors which could be absent or lack conservation in other species. The ability of sEVs to deliver siRNAs across three species suggests that critical sEV delivery processes are relatively conserved.

To our knowledge, this is the first study to show that sEVs loaded with siRNA (using the pre-miR-451 backbone, in this case) and isolated by TFF can safely knockdown multiple targets leading to improved outcomes in multiple disease models in organs beyond the liver in mice and

larger animal models. This suggests that these sEVs represent a safe and effective delivery vehicle for siRNA and could be beneficial for treating chronic kidney disease.

3.5 Materials and Methods

Study design

This study was designed to evaluate whether sEVs could deliver siRNAs and limit pathology in models of chronic kidney diseases in a safe, scalable manner. Stable cell lines, from multiple sources, were engineered to express siRNA within the pre-miR-451 backbone, which causes them to be packaged into sEVs released into cell culture media[258]. sEVs were prepared from culture media using TFF, and all experiments examining purity of preparations were performed at least three separate times. Experiments comparing TFF to ultracentrifugation were performed three separate times using the same batch of conditioned media for the two methods in each trial. We previously identified 10^{11} sEVs as the dose of siRNA-loaded sEVs required to achieve maximal knockdown of targets in multiple organs in mice[258]. Here, to examine the safety profile of sEVs prepared by TFF we administered a dose 10-fold higher (10^{12}) from three distinct TFF batches to two BALB/c mice each and analyzed cytokine/chemokine responses using multiplex assays, blood toxicology panels, and pathology across tissues. Injections and analyses were performed by blinded individuals. These sEVs were similarly incubated with blood from two distinct human donors and multiplex analyses were performed by blinded individuals. sEVs were then injected into a series of mice from different mouse models to test their ability to knockdown targets in the kidney and reduce disease pathology. All mouse injections, tissue harvests and analyses including RT-qPCR, quantitative FISH, glomerular scoring and blood chemistry analysis were performed by blinded individuals. sEVs containing siRNA targeting *GFP*, *SOD1*, *APOL1*, and *Trpc6* were injected into the appropriate transgenic (*GFP*: C57BL/6-Tg(CAG-EGFP)1Osb/J, *SOD1*:

C57BL/6.Cg-Tg(SOD1*G93A)dl1Gur/J or *APOL1*: NPHS1rtTA/TRE-APOL1-G2) or wild-type mice (*Trpc6*) at a dose (10^{11}) previously identified to be functional in multiple organs[258]. In all cases, sEVs containing off-target siRNA, loaded into sEVs in the same manner were used as negative controls. Control and therapeutic sEVs were injected into litter matched animals; at least three mice per group were used, with larger groups being injected when mice of appropriate litter and genotype were available. To confirm the robustness of our target knockdown measurements, we used two distinct techniques to measure *GFP* knockdown in transgenic mice, RT-qPCR and quantitative FISH. In the *APOL1* model, sEVs were administered on two consecutive days once per week for three weeks, to keep maximal knockdown over time. In the UUO model, sEVs were injected into mice two days prior to surgery and kidneys were harvested five days after surgery. In the Adriamycin model, Adriamycin and sEVs were injected every seven days, offset by two days for three weeks. Mice with a C57BL6/J background were used in all experiments except the Adriamycin induced nephropathy model, where BALB/c mice were used, as multiple studies have shown that C57BL6/J mice are resistant to Adriamycin induced nephropathy. In rats and rabbits, sEVs were injected into three animals per group by blinded individuals at doses 10- and 100-fold higher than those used in mice, respectively. Animals were euthanized within seven days following injection to be consistent with the timing for maximal target knockdown we observed in mice. Tissues harvest, RT-qPCR and quantitative FISH were performed by blinded individuals.

Cell culture

The following cell lines were used: HEK293T (ATCC; catalogue no. CRL-3216), Human neonatal dermal fibroblasts (Lonza; catalogue no. CC-2509), and NSC-34 (Cedarlane; catalogue no. CLU140). Versions of these cell lines stably expressing siRNA against GFP, SOD1, and TTR in the pre-miR-451 backbone used here were described previously[258]. We reprogrammed pre-miR-

451 as previously described[258] to encode the fully mature sequences 5' – UAAGCUAUUCUGGAGAAACUUA or 5' – UUGUCUUGCAAGGUUGUCCAGA, targeting mouse *Trpc6* or human *APOL1* respectively. These reprogrammed pre-miR-451 cassettes were inserted separately into a lentiviral transfer vector generated in the lab and called pOL. pOL contains GFP-IRES-puroR expressed under the CMV promoter, with pre-miR-451 cassettes inserted downstream of puroR. Lentiviral particles were produced using these vectors by transiently transfecting HEK293T cells and lentivirus was concentrated by ultracentrifugation. Dilutions of lentiviral stocks were added to cell media in the presence of 10 μg/ml polybrene. Three days later, puromycin was added for selection. Transduction was confirmed by the visualization of GFP fluorescence in these cells.

All cell culture was performed at 37 °C in 5% CO_2 in humidified incubators. For expansion of cell lines, HEK293T and NSC-34 cells were grown to 70–80% confluence and human fibroblasts to 90–100% confluence in DMEM (Wisent Bioproducts; catalogue no. 319–015-CL; 4.5 g l^{-1} glucose) with 10% heat-inactivated FBS (Wisent Bioproducts, catalogue no. 080–150) and 1% penicillin-streptomycin (Wisent Bioproducts, catalogue no. 450-201-EL) prior to sEV collection. For production of sEVs, cells were washed once with 1× PBS (Wisent Bioproducts; catalogue no. 311–010-CL) and cultured for up to 72h in serum-free UltraCULTURE medium (Lonza, catalogue no. 12–725F) with 1% penicillin-streptomycin and 1% L-Glutamine (ThermoFisher Scientific, catalogue no. 25030081) or DMEM supplemented with PeproGrow-1 Serum-Free Cell Culture Supplement (PeproTech, catalogue no. 700-C100). sEV-containing media was collected every 24 hours for up to 3 days and combined for preparation of sEV.

sEV preparation by TFF

sEV-containing media was centrifuged at 300 g for 10 min and supernatants were subsequently centrifuged at 2,000 g for 10 min. Supernatants were passed through a 0.22 μm filter (Thermo-Scientific, catalogue no. 09–741–04) and loaded into a bioprocess sample bag (Sartorius Stedim, catalogue no. FFB103547) for TFF concentration. Samples were concentrated 10x using the KR2i tangential flow filtration system (Repligen) with a 75 cm^2 modified polyethersulfone hollow fiber column with 500 kDa cut-off (Repligen, catalogue no. D02-E500- 10-S) at a flow rate of 140 ml min^{-1} and transmembrane pressure 2.5 psi to achieve a shear rate of 2,000 s^{-1}. The concentrated media underwent 10X buffer exchange in PlasmaLyte A (Baxter, catalogue no. JB2544) to reach a final volume of ~12 mL. sEVs were then quantified by nanoparticle tracking analysis prior to injections.

sEV preparation by differential ultracentrifugation

sEV-containing media was centrifuged at 300 g for 10 min and supernatants were subsequently centrifuged at 2,000 g for 10 min, 10,000 g for 30 min (SW-32Ti rotor, Beckman-Coulter Life Sciences; polycarbonate tubes, catalogue no. 355631, Beckman-Coulter Life Sciences) and 100,000 g for 2 h (SW-32Ti rotor). sEV pellets were washed by resuspending in 1 ml 1X PBS (Wisent Bioproducts; catalogue no. 311–010-CL) and finally centrifuged at 100,000 g for 30 min (TLA-100.3 rotor, Beckman-Coulter Life Sciences; polypropylene microfuge tubes, catalogue no. 357448, Beckman-Coulter Life Sciences). sEVs pellets were resuspended in 50 μl 1X PBS.

Nanoparticle tracking analysis

Nanoparticle tracking analysis was performed on a ZetaView PMX-110 (ParticleMetrix). The instrument was calibrated for experiments following every instrument start-up. Focusing and

alignment were performed automatically using 102 nm polystyrene beads (Microtrac, catalogue no. 900383). sEV samples were diluted in PBS into the range determined by the instrument to be accurate for measurement (typically 1:10,000–1:500,000). One milliliter of the sample was injected into the machine and allowed to equilibrate until it reached an acceptable level according to the built-in particle-drift sensor. Once the sample fell within the acceptable concentration range, video acquisition and analysis were performed using the following pre-acquisition parameters: Sensitivity 85, shutter speed 40, frame rate 30 fps, resolution highest, camera gain 770, positions measured 11, and the following post-acquisition parameters: minimum brightness 15, minimum size 10 pixels, maximum size 500 pixels. Undiluted concentration and median size based on concentration are reported.

Animal studies

All experiments performed using animals were approved by the Animal Care Committee of the University of Ottawa under protocol CMM-3367, CMM-3376, CMM-3377, CMM-3119 and CMM-3429 and performed according to guidelines of the Canadian Council on Animal Care and the International Guiding Principles for Biomedical Research Involving Animals. Mice transgenic for eGFP under the expression of the ubiquitous chicken β-actin enhancer and cytomegalovirus promoter (C57BL/6-Tg(CAG-EGFP)1Osb/J, The Jackson Laboratory, catalogue no. 003291)) were bred and females were used between the ages of 15 and 18 weeks. Mice expressing a low copy number of human SOD1 G93A (C57BL/6.Cg-Tg(SOD1*G93A)dl1Gur/J, The Jackson Laboratory, catalogue no. 002299) were also bred and males between the ages of 15 and 18 weeks (25–30 g) were used. Littermates were randomized between groups of mice for intravenous injections. Eight week old BALB/c male mice (Charles River) and C57BL/6 male mice (Charles River) were used for the Adriamycin injection and UUO models, respectively. For

intravenous injections mice were warmed with a heat lamp, restrained (Braintree Scientific restrainer, catalogue no. NC0690443), and injected in the lateral tail vein (U-100 insulin syringe 28G half-inch needle, Beckton-Dickinson, catalogue no. 329424) with a 5 ml kg−1 (100–150 μl) suspension of sEVs (10^{11} particles as specified) in PlasmaLyte A (Baxter, catalogue no. JB2544).

For experiments in APOL1 mice, sEVs were produced as above and shipped to the Susztak lab for injection in NPHS1rtTA/TRE-APOL1-G2 mice which they previously generated as described[249, 286, 287]. Mice were kept in a pathogen free environment 12 hours light and dark cycle. Transgenic animals were identified by tail PCR. Animals were placed on doxycycline diet (200 mg/kg, BioServ) at 6 weeks of age to induce G2-APOL1 transgene expression. Members of the Susztak lab were blinded to the treatment groups. Mice received two doses of $5x10^{11}$ sEVs (*APOL1* or control siRNA) intravenously on two consecutive days, weekly for three weeks. Four days following the last injection, serum and urine were harvested and the following day animals were euthanized and kidneys were excised and processed for histochemical as well as protein and RNA analysis. The studies were approved by the Animal Care Committee of the University of Pennsylvania.

The unilateral ureteral obstruction (UUO) model was based on previously established protocols[288] with minor modifications. Briefly, 4-6 weeks old C57BL/6J mice were randomly assigned to sham or UUO surgery groups. The animals assigned for the surgery were again divided into 2 groups: one receiving $5x10^{11}$ sEVs loaded with siRNA against *Trpc6* and the other receiving sEVs loaded with off-target siRNA. sEVs were administered intravenously 48 hours prior to the surgery. Mice in the sham group received only PlasmaLyte, the sEV vehicle. On the day of surgery, the animals were anesthetized under isoflurane. Under aseptic conditions, midline laparotomy followed by incision of the avascular linea alba was performed to gain access to the peritoneal

cavity. The left ureter was exposed and ligated twice with sterile braided silk sutures between the bladder and renal pelvis. The peritoneal cavity was closed with blanket stiches and skin approximated using metallic skin clips. Animals in the sham group underwent the same surgical procedures except the UUO. Post-operative care was administered as per the requirements and guidelines of the Animal Care Committee of The University of Ottawa. Five days post-surgery, the animals were euthanized, and kidneys were harvested.

The Adriamycin (ADR)-induced nephropathy model was developed based on review of previously published reports[276] and consultations with the veterinarian at the Animal Care and Veterinary Service (ACVS) of the University of Ottawa. Based on dose-response studies it was observed that larger single doses of Adriamycin (Cayman chemicals; catalogue no. 15007) resulted in higher mortality rates. In contrast, a 5 mg/kg dosage administered intravenously once per week for 3 consecutive weeks had 100% survival rate along with observable pathological changes in the kidney. $5x10^{11}$ sEVs carrying siRNA against *Trpc6* or an off-target control siRNA were administered intravenously 48hrs prior to ADR administration. Animals in the ADR-only group received PlasmaLyte, the sEV vehicle. Animals were euthanized 5 days following the last ADR injection and kidneys were harvested.

Mice were euthanized with intraperitoneal sodium pentobarbital (120 mg kg−1, Bimeda-MTC; catalogue no. 8015E) and perfused with PBS (10 ml) before tissue collection. Those performing injections and tissue collection were blinded to the treatment groups. Male Sprague-Dawley rats (400-500g, Charles River) received intravenous injections of sEVs containing siRNA targeting *TTR*. Rats were anesthetized with 5% isoflurane and maintained under isoflurane for the procedure (2%). Three hundred µL of sEV suspension (10^{12} particles) was injected into the tail vein. Blood was collected pre-injection and 7 days post-injection. New-Zealand white male rabbits

(2 kg, Charles River) were used for sEV distribution and TRPC6 experiments. Rabbits were anesthetized with 5% isoflurane and maintained under isoflurane during handling (2%). Five mL of sEV suspension (10^{13} particles) was injected via the ear vein. Six days later, half of the rabbits were injected a second time with DiR-stained sEVs. Rabbits were euthanized 24 hours later and tissues were collected.

Mixed motor neuron isolation and culture

Mice embryos were collected from pregnant mice between embryonic days I13.5 and E14.5. Spinal cords were dissected using a Zeiss Stereo Discovery V20 microscope (Carl Zeiss, Oberkochen, Germany). The clean spinal cords were placed in dissection buffer (sucrose 40 g l−1, dextrose 1 g l−1, and HEPES 2.4 g l−1 in 1X PBS), minced with scissors, and incubated with trypsin (Sigma-Aldrich) for 30 min at 37 °C. The cells were separated using a 1 ml pipette and placed in NFeed neuronal culture medium (MEM/HBSS, Hyclone, catalogue no. SH3002402), insulin 10 μg ml−1 (Sigma-Aldrich, catalogue no. I-6634), transferrin 200 μg ml−1 (USBiologicals, catalogue no. T8205-47-1G), BSA 10 μg ml−1 (Sigma, catalogue no. A9418), putrescine 32 μg ml−1 (Sigma, catalogue no. P-5780), selenium 26 ng ml−1 (Sigma-Aldrich, catalogue no. S-1382), T3 20 ng ml−1 (Sigma-Aldrich, catalogue no. T-6397), hydrocortisone 9.1 ng ml−1 (Sigma-Aldrich, catalogue no. H-0888), progesterone 13 ng ml−1 (Sigma-Aldrich, catalogue no. P-8783) and 2.5S nerve growth factor 5 ng ml−1 (EMD Millipore, catalogue no. 01-125), horse serum 1.3% (Invitrogen Life Technologies, catalogue no. 16050-015) and 1% antibiotic-antimycotic (Gibco, catalogue no. 15240062). Cells were counted and seeded at 300,000 cells per well in 12-well plates pre-treated with poly-d-Lysine 1 mg ml−1 (Sigma-Aldrich, catalogue no. P7280,) and Matrigel 0.5% (Corning, VWR, catalogue no. 354234,). After 4–7 d,

mitotic cells were killed using arabinofuranosylcytosine 1.4 μg ml−1 (EMD Millipore, catalogue no. 251010).

Mixed motor neuron transfer

GFP siRNA-containing sEVs from mouse motor neuron-like cell line, NSC-34, were isolated by either TFF or ultracentrifugation and quantified by nanoparticle tracking analysis (Zetaview). sEVs isolated by either method were added to mixed motor neuron cultures at concentrations of 2,000, 20,000, or 200,000 sEVs per cell in 12-well plates containing 300,000 cells per well. After 72 h cells were washed once with 1x PBS and lysed using Trizol (Life Technologies, catalogue no. 15596026) for RT-qPCR analysis.

ELISA

ELISA assays for Bovine Transferrin and Bovine Serum Albumin were performed using commercial kits according to manufacturer instructions (Transferrin; Cygnus Technologies, catalogue no. F120. BSA, Cygnus Technologies, catalogue no. F030). Briefly, 50 µl of standards, controls and samples were added into respective wells. 100 µl of anti-bovine Transferrin:HRP or anti-BSA:HRP was added to the wells and the plate was incubated on an orbital shaker at 500rpm for 1 hour at room temperature. The liquid was then discarded, and wells were washed with 350 µl of provided wash solution. Next, 100 µl TMB substrate was added to wells and incubated for 30 minutes at room temperature. The reaction was stopped by adding 100 µl of stop solution. Absorbance was measured at 450/650nm. Similarly, the ELISA assay for human Insulin was performed using a commercial kit according to manufacturer instructions (ThermoFisher scientific, catalogue no. KAQ1251). Briefly, 50 µl of standards, samples, or controls were added to respective wells, followed by 50 µl of anti-Insulin:HRP. The plate was covered and incubated

for 30 minutes at room temperature. Wells were then washed three times with the provided 1X wash buffer and 100 µl of stabilized chromogen was added to each well within 15 minutes. The plate was then covered and incubated for 15 minutes at room temperature. The reaction was stopped by adding 100 µl stop solution to the wells. Absorbance was measured at 450nm.

Western blot for sEV markers

Cells or sEV lysates were diluted in 4x Laemmli buffer (Bio-Rad, catalogue no. 161-0747) with 10% 2-mercaptoethanol (Sigma-Aldrich, catalogue no. M3148-100ML) and were incubated for 5 min at 95°C before being loaded on a 10% polyacrylamide gel. Samples were run at 150 V and were then transferred to a PVDF membrane (Millipore Sigma, catalogue no. IPVH00010) using a wet transfer system (Bio-Rad) at 100 V for 1.5 hours at room temperature. The membrane was blocked in 5% skimmed milk (Santa Cruz Biotechnology, catalogue no. sc-2324) in TBST for 1 hour. The membrane was then incubated with primary antibodies diluted in TBST overnight at 4°C and washed three times (10 minutes each) with TBST. Incubation with secondary antibodies diluted at 1:7500 in PBST was done at room temperature for 1 hour. Finally, membranes were washed 3 times (10 minutes each) in TBST and incubated with ECL Western HRP Chemiluminescence Substrates Crescendo (Fisher Scientific, catalogue no. WBLUR0500). The chemiluminescence signal was recorded using a GE ImageQuant LAS4010 system. The membrane was stripped using 0.2N NaOH for 30mins when necessary. Antibodies are listed in table 3.1.

Table 3.1. List of antibodies used for Western blots

Antibody	**Company**	**Catalogue Number**
Flotillin2	Cell Signaling Technology	3436S
Tsg101	Genetex	GTX70255
Syntenin-1	Abcam	ab133267
Tomm20	Thermo Fisher Scientific	ab133267
Calnexin	Cell Signaling Technology	2679S
Alix	Cell Signaling Technology	2171S

	BD Transduction Laboratories	611621 (mixed together)

RT-qPCR analysis of cells and animal organs

Cells or animal tissues were homogenized in Trizol (Life Technologies, catalogue no. 15596026) and RNA was extracted following the Trizol isolation protocol. Reverse transcription was conducted with the M-MuLV enzyme (NEB, catalogue no. M0253S) and 18 nt oligoDT primer (Integrated DNA Technologies, custom synthesis). All qPCR reactions were run on a CFX-384 instrument (Bio-Rad). Taqman qPCR was performed using probes from ThermoFisher for APOL1 (HS01066280_m1), GFP (Mr04097229_mr), human SOD1 (hs00533490_m1), and housekeeping genes Gusb (Mm01197698_m1), Pgk1 (Mm00435617_m1), Gapdh (Mm99999915_g1) and Tfrc (Mm00441941_m1) (ThermoFisher). RT-qPCR on samples from mouse TRPC6 experiments were performed using GoTaq qPCR (Promega) using the following primers obtained from IDT in table 3.2.

Table 3.2. RT-qPCR Primers

TRPC6	Forward	CTCTCTAAAGGCTGCCCCTG
	Reverse	TTCATTACCCCGGAAGCTGG
αSMA	Forward	CTGACAGAGGCACCACTGAA
	Reverse	CATCTCCAGAGTCCAGCACA
Collagen 1	Forward	GAGCGGAGAGTACTGGATCG
	Reverse	GTTCGGGCTGATGTACCAGT
CTGF	Forward	CCCTAGCTGCCTACCGACTG
	Reverse	TTAGAACAGGCGCTCCACTC
β-Actin	Forward	ACTGCCGCATCCTCTTCCTC
	Reverse	GGATGCCACAGGATTCCATACC

Similarly, RT-qPCR on samples from rabbit TRPC6 experiments was performed using GoTaq qPCR (Promega) using the following primers obtained from IDT in table 3.3.

Table 3.3. Rabbit RT-qPCR Primers

TRPC6	Forward	ACATCCTGCTTCTCATGGATGG
	Reverse	CCACTTAATCCTAGCAAAATCAAGC
β-Actin	Forward	GGGACATCAAGGAGAAGCTG
	Reverse	ACTCCATGCCCAGGAAGG
Gapdh	Forward	TCGGAGTGAACGGATTTGGC
	Reverse	TTCCCGTTCTCAGCCTTGAC

Endotoxin test

Quantitative endotoxin measurements were performed using the Pierce™ Chromogenic Endotoxin Quant Kit (ThermoFisher, catalogue no. A39552) as recommended by the manufacturer.

Fluorescent labelling of sEVs and biodistribution

For biodistribution studies, sEVs were labelled with XenoLight DiR Fluorescent Dye (PerkinElmer, catalogue no. 125964). sEVs were incubated with 41.5 μg μl^{-1} DiR in a total volume of 1 ml 1× PBS at room temperature on a rotator for 30 min. sEVs were then centrifuged at 100,000 g for 30 min (TLA-100.3 rotor) and resuspended in an appropriate volume for injection. PBS (1×) was treated with the same concentration of dye and centrifuged and resuspended identically to sEVs to produce an sEVs-free dye only control. Animals or *ex-vivo* organs were imaged in the IVIS Spectrum In Vivo imaging system (Perkin Elmer) and analyzed using the Living Image Software Version 4.3.1 (Perkin Elmer).

FISH and image analysis

Tissues were collected from mice and placed in 4% PFA in 1X PBS for 24 h. PFA was replaced by 1X PBS containing 30% sucrose until the tissues sank to the bottom of the tubes. Tissues were then placed in optimal cutting temperature solution (Fisher Scientific, catalogue no.

23-730-571) and frozen on dry ice. Tissue sections of 5 μm were collected on slides and placed at −80 °C. Slides were heated to room temperature before staining. Slides were placed in 4% PFA in PBS for 10 min at ambient temperature. They were washed with 1X PBS and placed at 37 °C for 20 min in permeabilization buffer (10 μg ml^{-1} proteinase K, 0.2% Triton X-100 in PBS). Slides were returned to room temperature, washed in PBS, and blocked for 1 h with 1% BSA, 100 μg ml^{-1} salmon sperm DNA and 250 μg ml^{-1} yeast extract RNA in PBS. Slides were washed with 1× PBS and treated for autofluorescence reduction with NaBH4 0.1% in water for 1 h. Slides were washed with Stellaris wash A buffer (LGC Biosearch Technologies, catalogue no. SMF-WA1-60) and incubated with Stellaris fluorescent mRNA probes (LGC Biosearch Technology, SOD1 (custom assay), GFP (VSMF-1014-5) or TRPC6 (custom assay)) in hybridization buffer (90% Stellaris hybridization buffer, catalogue no. SMFHB1–10, 10% formamide). Slides were incubated with the probes in the dark at 37 °C overnight. Slides were returned to room temperature and washed with wash A buffer. Slides were incubated with DAPI (Life Technologies, 1:10,000) in PBS for 5 min. A final wash was performed with Stellaris wash B buffer and slides were mounted with Citifluor AF3 antifade solution (Electron Microscopy Sciences, catalogue no. AF3–25) and sealed with nail polish. The following Nephrin antibody was used in certain cases: Nephrin (R&D Systems, catalogue no. AF3159).

Milliplex Multiplex assay

All research conducted using blood from human subjects was approved by the Ottawa Hospital Research Institute Ethics Board (Ottawa, ON, Canada) and conforms to the provisions of the Declaration of Helsinki. Informed consent was obtained from all participating subjects. 15 mL of peripheral blood was collected in 100 i.u./mL heparin (LEO Pharma Inc., Thornhill, ON, Canada) from healthy volunteers. 200 μL of whole human blood was incubated at 37 °C with 800

μL of Iscove's Modified Dulbecco's Medium (Invitrogen, catalogue no. 12440053) in wells of a 24-well plate. 24 hours later, sEVs from primary human fibroblasts packaged with siRNA against GFP were then added into the cultures at a dose of 10,000 sEVs per blood cell. PlasmaLyte was used as a negative control and DH5-Alpha E. coli that had been boiled at 99°C for 10 minutes was used as a positive control. sEVs from three distinct TFF preparations were incubated with blood from two distinct donors in duplicate. After 24 hours, supernatant was collected and centrifuged at 3000 g for 15 minutes. In mice, 10^{12} sEVs from primary human fibroblast containing siRNA targeting GFP, or PlasmaLyte as a negative control, were intravenously injected into BALB/c mice and blood was drawn six and 24 hours later, and centrifuged at 3000 g for 15 minutes. Milliplex assays were set up according to the manufacturer's instructions using the human cytokine/chemokine magnetic bead panel (Millipore Sigma, catalogue no. HCYTOMAG-60K) or mouse high sensitivity T cell magnetic bead panel (Millipore Sigma, catalogue no. MHSTCMAG-70K). Plates were read on a Magpix Multiplexing Instrument (Luminex Corporation) running the Luminex xPONENT software, version 4.2. Analysis was performed with Milliplex Analyst version 5.1 using four-parameter curve fitting (log scale).

Blood chemistry panel

10^{12} human fibroblast-derived sEVs containing siRNA targeting GFP, or PlasmaLyte as a negative control, were intravenously injected into BALB/c mice and blood was drawn 24 hours later. Blood was centrifuged at 3000 g for 15 minutes to isolate serum before being frozen at -20°C and shipped to IDEXX BioAnalytics for analysis as a service. Analysis was performed on the AU680 Clinical Chemistry Analyzer (Beckman-Coulter Life Sciences).

Optiprep Gradients

Optiprep gradients were performed as described previously[289]. Briefly, DiR-labelled sEVs were resuspended in 3 mL PBS, to which 9 mL of 60% iodixanol (Optiprep) was added. This solution was added to the bottom of an ultracentrifuge tube. Iodixanol solutions of 30%, 23%, 18% were layered on top and the tube was ultracentrifuged for 16 h at 150,000 g in a SW32 Ti swinging bucket rotor (Beckman-Coulter, k-factor 239). Twelve fractions were collected. Density was measured using a refractometer. 100µL of each fraction was plated in a 96 well plate and fluorescence signal was imaged at 800nm using the Li-Cor Odyssey Fc imaging system (Li-Cor Biotechnology, Lincoln, USA). Half of each fraction was ultracentrifuged to pellet sEVs for analysis by western blot.

Fluorescent western blot

Mouse blood (20-50 uL) was collected from the tail vein at different time points in heparinized tubes (Greiner Bio-one, catalogue no. 450477). Whole blood was separated by centrifugation at 3500 g for 15 minutes. An equal amount of serum (5 uL) was collected and diluted in water and Laemmli sample buffer 4x (Bio-Rad, catalogue no. 161-0747) with 10% 2-Mercaptoethanol (Bio-Rad, catalogue no. 1610710) and boiled for 5 minutes at 99ºC. Samples were loaded on an SDS-PAGE gel (10% acrylamide). Samples were stacked at 100V for 10 min and separated at 150V for 1h 15 min. Samples were transferred to a positively charged nylon membrane (Roche, catalogue no. 1417240) for 1h 15 min at 100V. Membranes were washed with TBST (3x5 min) and blocked with TBST + 5% skim milk for 1h. Membranes were incubated at 4ºC overnight with the primary antibody (rabbit anti-mouse TTR, Invitrogen, catalogue no. PA5-80197). Membranes were washed with TBST (3x5 min) and incubated 1h with secondary antibody (Li-Cor Odyssey, goat anti-rabbit IRdye 800 (TTR), catalogue no. 926-32211, donkey anti-mouse IRDye 680 (IgG, loading control), catalogue no. 925-68072). Membranes were washed with TBST

(3x5 min) and imaged with Li-Cor Odyssey Fc imaging system (Li-Cor Biotechnology, Lincoln, USA). Images were analyzed using Image Studio software (Li-Cor Biotechnology, Lincoln, USA).

H&E staining and analysis

PFA fixed tissues from sEV-injected mice were paraffin-embedded, cut in 5 µm thick slices, put on slides, and stained with H&E by the histology department (Louise Pelletier Histology Core Facility, University of Ottawa, Ottawa, Canada). Slides were analyzed by a pathologist (Dr. Manijeh Daneshmand) for cell infiltration, tissue morphology irregularities, or any signs of tissue damage.

RNAscope assay

miRNAScope (Red) assay (Advanced Cell Diagnostics) was used to visualize siRNA molecules that were delivered by sEVs based on the manufacturer's protocol[290]. Briefly, deparaffinized and hydrated kidney sections were incubated overnight in 10% neutral buffered formaldehyde, at room temperature. The following day, sections were rinsed with distilled water and dried at room temperature. The dried sections were covered with RNAscope hydrogen peroxide solution (ACD, catalogue no. 322335) and incubated for 10 min at room temperature followed by repeated washes in distilled water. Antigen retrieval was performed by incubating the sections in RNAscope 1X target antigen retrieval buffer (ACD, catalogue no. 322000), in a steamer for 15 minutes. Post antigen retrieval, the sections were washed with distilled water, rinsed with 100% ethanol, and dried at room temperature. Slides were then loaded onto an ACD EZ-Batch slide holder, the sections were covered with RNAscope protease III (ACD, catalogue no. 322337), and placed in a pre-warmed HybEZ humidity control tray. The tray was then placed inside the hybridization oven set at 40°C and incubated for 30 minutes. Post incubation, slides were washed

with distilled water and re-incubated with the APOL1 siRNA (ACD, catalogue no. 1100691-S1) or scrambled probe (ACD, catalogue no. 727881-S1) at 40°C for 2 hrs. Slides were then washed with the RNAscope wash buffer (ACD, catalogue no. 310091) and incubated sequentially with the amplification reagents 1-6 (ACD, catalogue no. 324510) as indicated in the manual. Sections were then incubated with a working Red solution (ACD, catalogue no. 324517/324518; 1:60 ratio of Fast Red B to Fast Red A) for 10 minutes at room temperature. The Red solution was washed away using the wash buffer, then slides were briefly dipped into fresh xylene, mounted with VectaMount (Vector laboratories, catalogue no. H-5000), and visualized under a bright field in a Zeiss epifluorescent microscope. Images were processed with FIJI.

PAS Staining and glomerular scoring

Mouse kidney sections were stained with Periodic acid-Schiff (PAS, Sigma Aldrich catalogue no. 395B-1KT). Briefly, sections were deparaffinized and hydrated in deionized water. The slides were then incubated in periodic acid solution for 5 minutes at room temperature, followed by several rinses in distilled water. The slides were then immersed in Schiff's reagent for 15 minutes at room temperature. Post incubation, the slides were washed in running tap water for 5 minutes, counterstained with hematoxylin, dehydrated by passing through graded alcohol, cleared with xylene, and mounted with dibutylphthalate polystyrene xylene (DPX) mountant. One entire kidney section on each slide was scanned using the Zeiss Axio Scan.Z1 slide scanner. Glomeruli were categorized as unaffected, sclerotic, or with collapsed tufts. Sclerotic glomeruli encompassed non-specific, perihilar, cellular, and segmental sclerosis[291].

Immunofluorescent stain for APOL1 and α-SMA

Kidney sections were deparaffinized and hydrated followed by antigen retrieval with sodium citrate buffer (10 mM tri-Sodium citrate dihydrate, 0.05% Tween-20, pH 6.0). The sections were blocked with 10% goat serum and incubated with primary antibodies against APOL1 (Proteintech, catalogue no. 66124-1-Ig) and α-Smooth Muscle Actin (GeneTex, catalogue no. GTX100034) overnight at 4℃. The next day, following multiple washes with 1X TBS, sections were incubated with fluorophore-conjugated secondary antibodies at room temperature for 90 minutes. Post-incubation, the slides were washed with 1X TBS and mounted with DAPI-containing mounting medium (Vector Laboratories, catalogue no. H-1200). Images were acquired with a Zeiss epifluorescent microscope and processed using the Zen software (Zeiss). The total area of Smooth Muscle Actin deposits in the kidneys was analyzed using FIJI. The images were converted to 8-bit grayscale followed by threshold adjustments so that fluorescent signal area was entirely covered. The area was measured after setting the appropriate scales. The area was measured from at least 2 kidney sections per animal and all the data points were plotted using Graphad Prism.

Aniline stain

To visualize collagen deposition in kidney sections, aniline staining was performed. Briefly, sections were deparaffinized, hydrated in deionized water, and then incubated overnight with a mordant (Bouin's solution- Ricca chemical company, catalogue no. 1120-16). On the following day, slides were washed under running tap water, and placed in Hematoxylin solution Gill No. 3 (Millipore Sigma, catalogue no. GHS332-1L) for 5 minutes at room temperature. The slides were washed again in running tap water, incubated in working Phosphotungstic/Phosphomolybdic acid solution (25% Phosphotungstic acid [Sigma Aldrich, catalogue no. HT152], 25% Phosphomolybdic acid [Sigma Aldrich, catalogue no. HT153], 50%

deionized water) for 5 minutes, followed by another 5 minute incubation in Aniline Blue solution (Sigma Aldrich, catalogue no. HT154). The slides were then placed briefly in 1% glacial acetic acid solution before repeated washes with deionized water, dehydrated through graded alcohol, cleared in xylene, and mounted with DPX. The sections were visualized with a bright field in a Zeiss epifluorescent microscope.

Coomassie staining for detection of serum and urine albumin

Mouse urine and serum samples were diluted 10-fold with sterile PBS. Equal volumes of the samples were electrophoretically separated by SDS-PAGE. Gels were incubated in Coomassie staining solution (0.5% Brilliant Blue R-250 [Sigma Aldrich, catalogue no. 27816-25G] in 50% methanol and 10% acetic acid) for 15 minutes at room temperature. After discarding the dye solution, gels were destained in a solution containing 40% methanol and 10% acetic acid until clean bands were visible. Gels were imaged in a Gel Doc XR+ System (Biorad) and bands were quantified using FIJI.

Statistics

Sample size is noted in the figure legends with *n* denoting measurements taken from distinct samples. Statistical analyses performed are listed in figure legends and were calculated in GraphPad Prism. In cases where two groups are compared, a two-tailed, unpaired t-test with Welch's correction was performed. Where more than two groups were compared, an ordinary One-Way ANOVA Holm-Šídák's multiple comparisons test was performed. Significant P values are shown in all cases. Error bars indicate s.e.m.

3.6 Acknowledgements

The authors acknowledge the University of Ottawa Faculty of Medicine Cell Biology and Image Acquisition core facility and the University of Ottawa Faculty of Medicine Louise Pelletier Histology Core facility for assistance with tissue staining, sample imaging and processing. We thank Stephanie Burke Schinkel for running the Magpix instrument for Milliplex assays. We also thank Dr. Manijeh Daneshmand for assistance with the pathological analysis of tissues and Dr. Moises Freitas-Andrade and Dr. Baptiste Lacoste for assistance in setting up the RNAscope assay.

Funding: Natural Sciences and Engineering Research Council of Canada (NSERC) Postgraduate Scholarship-Doctoral (RR). R01 DK105821/DK/NIDDK NIH HHS/United States (KS). NSERC Discovery grant (DG), NSERC Discovery Accelerator Supplement (DG).

Author Contributions:

Conceptualization: KD, RR, AS, DG, KS, JW
Methodology: KD, RR, AS, JT, ML, KS, DG, KS, JW, BP
Investigation: KD, RR, AS, JW, JT, HG, AE, JW, ED, BP
Formal analysis: KD, RR, AS, KS, JW, ED
Visualization: KD, RR, AS
Funding Acquisition: DG, KS
Project administration: DG, KS
Supervision: ML, KS, DG
Writing – original draft: RR, DG
Writing – Review and Editing: KD, RR, AS, JW, ED, BP, ML, KS, DG

Competing Interests: JT and DG are inventors on a filed patent that claims the use of the pre-miR-451 backbone for the enrichment of small RNAs in sEVs. The remaining authors declare no competing interests.

Data and materials availability: Data supporting the results of this study are available within the paper and its Supplementary Information. Raw and analysed datasets can be obtained for research purposes from the corresponding author on reasonable request.

3.7 Supplementary Figures

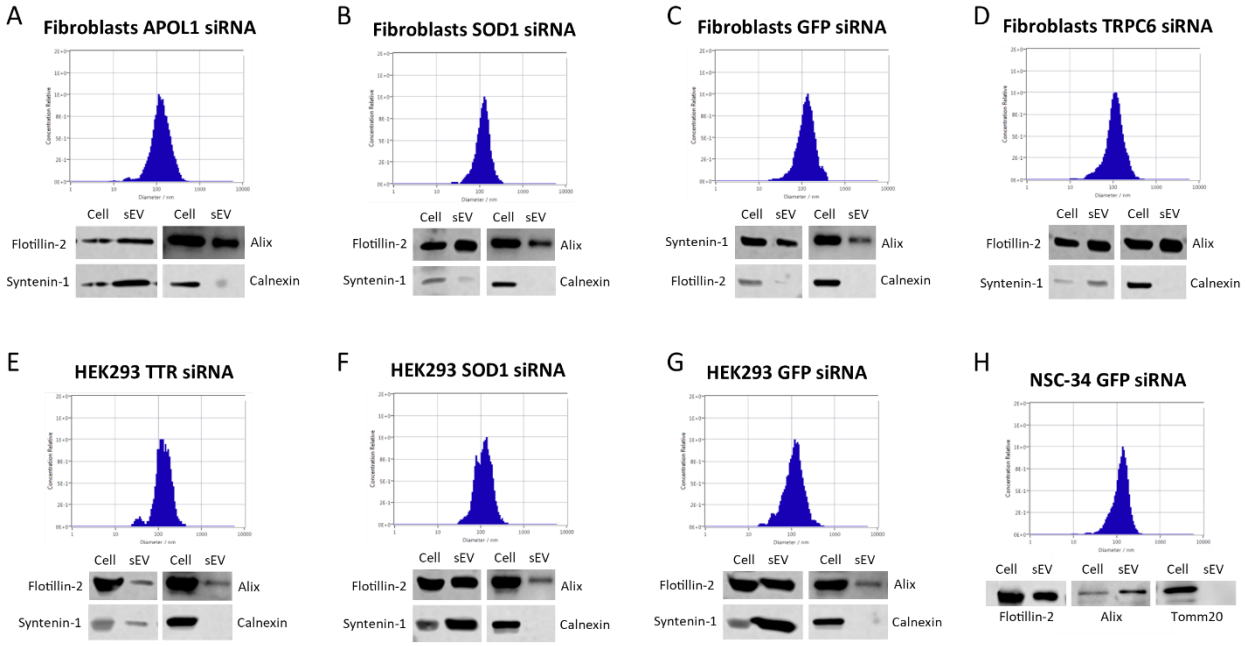

Supplementary Fig. 3.1. siRNA-loaded sEVs from all cell lines used in this study show characteristic NTA and western blot profiles. (**A to D**) sEVs derived from primary human fibroblasts containing siRNA targeting APOL1 (A), SOD1 (B), GFP (C), or Trpc6 (D) all display characteristic NTA size profiles centering around ~100 nm and contain sEV markers Flotillin2, Syntenin-1 and Alix, but do not contain the negative marker, calnexin. (**E** to **G**) sEVs derived from HEK293T cells containing siRNA targeting Ttr (E), SOD1 (F), or GFP (G) all display characteristic NTA size profiles centering around ~100 nm and contain sEV markers Flotillin2, Syntenin-1, and Alix, but do not contain the negative marker, calnexin. (**H**) sEVs derived from mouse motor neuron-like cell line, NSC-34, containing siRNA targeting GFP display a characteristic NTA size profile centering around ~100 nm and contain sEV markers Flotillin2, and Alix, but do not contain the negative marker, Tomm20.

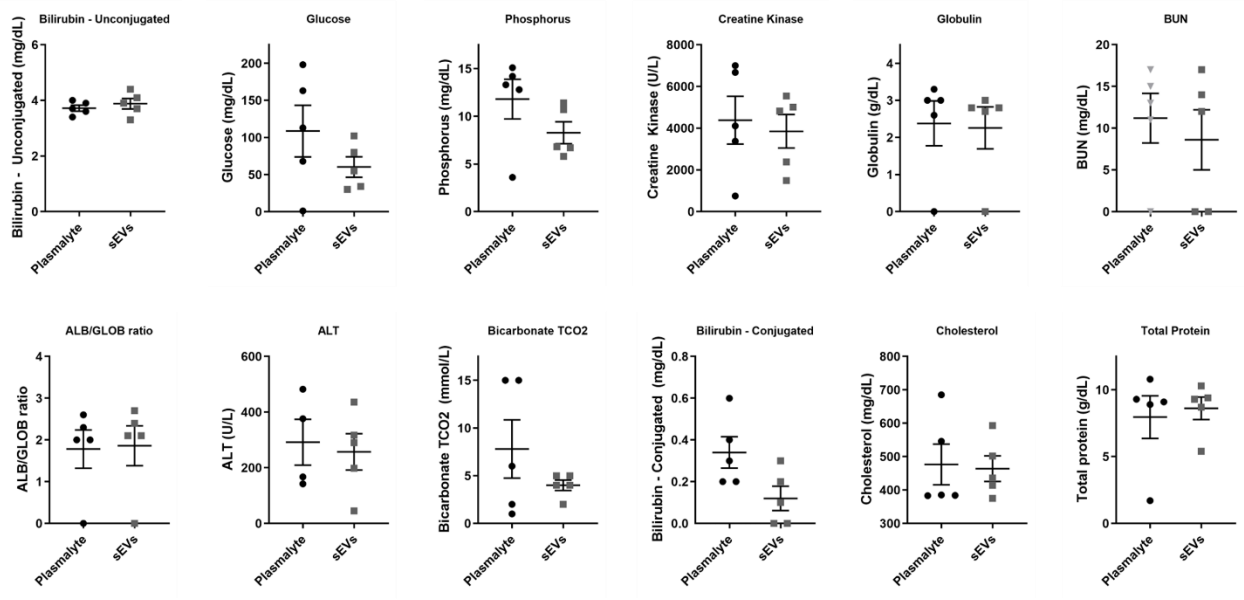

Supplementary Fig. 3.2. TFF-isolated sEVs do not induce a toxic response in mice. A comprehensive toxicology panel was performed on blood 24 hours after injecting mice with a 10-fold higher dose than used to attain maximal target knockdown with siRNA-loaded sEVs and revealed no significant differences between sEV- or PlasmaLyte-injected mice across a panel of 12 markers (n=5). A two-tailed, unpaired t-test with Welch's correction was used for statistical analysis.

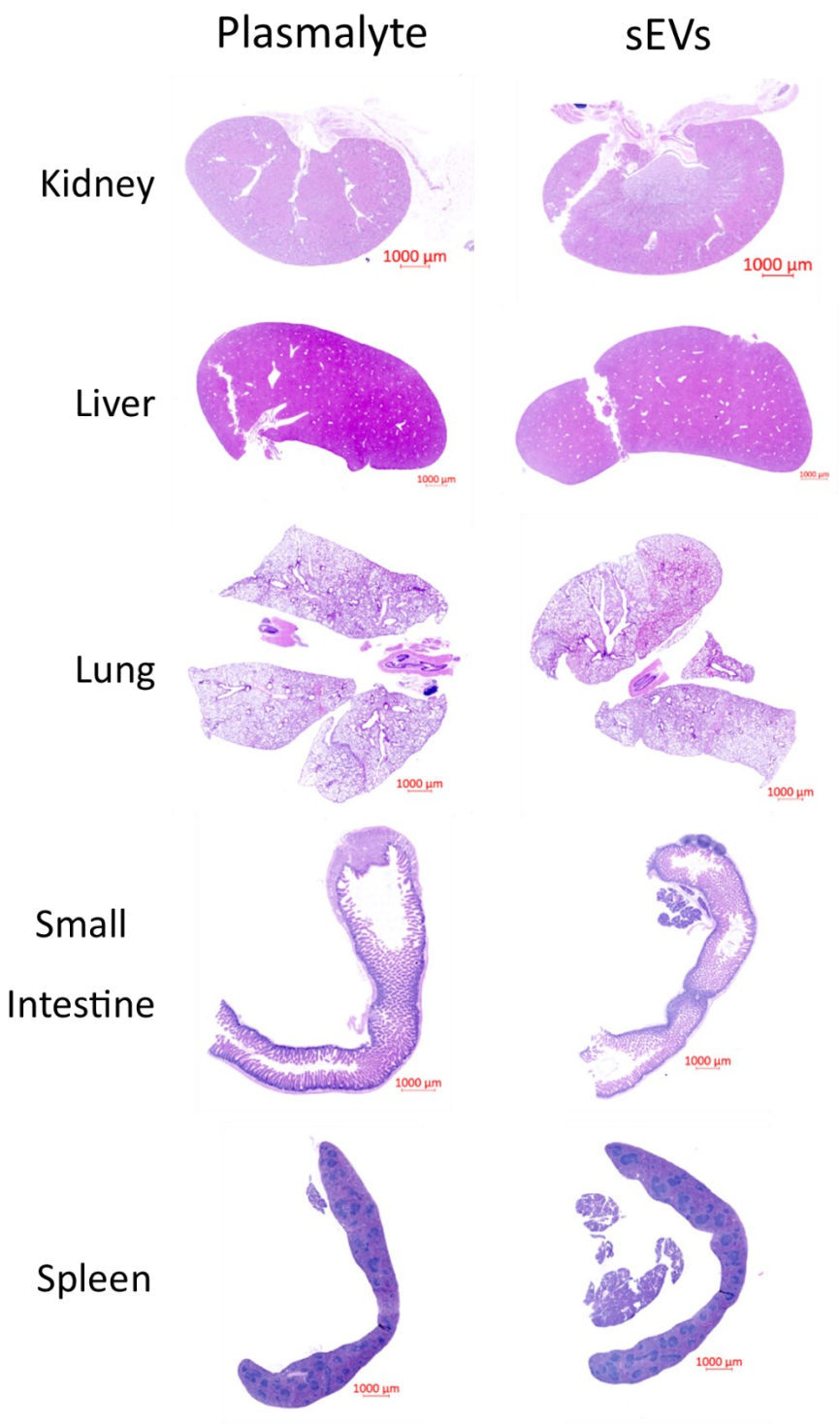

Supplementary Fig. 3.3. TFF-isolated sEVs do not induce gross organ damage in mice. Hematoxylin and eosin staining was performed on sectioned mouse organs 24 hours after mice were injected with a 10-fold higher dose than used to attain maximal target knockdown with siRNA-loaded sEVs. Pathological analysis by a registered veterinary pathologist revealed no observable differences in kidney, liver, lung, small intestine, or spleen between the vehicle (PlasmaLyte) or sEV injected mice. Magnification is 20X; the scale bar represents 1000 µm.

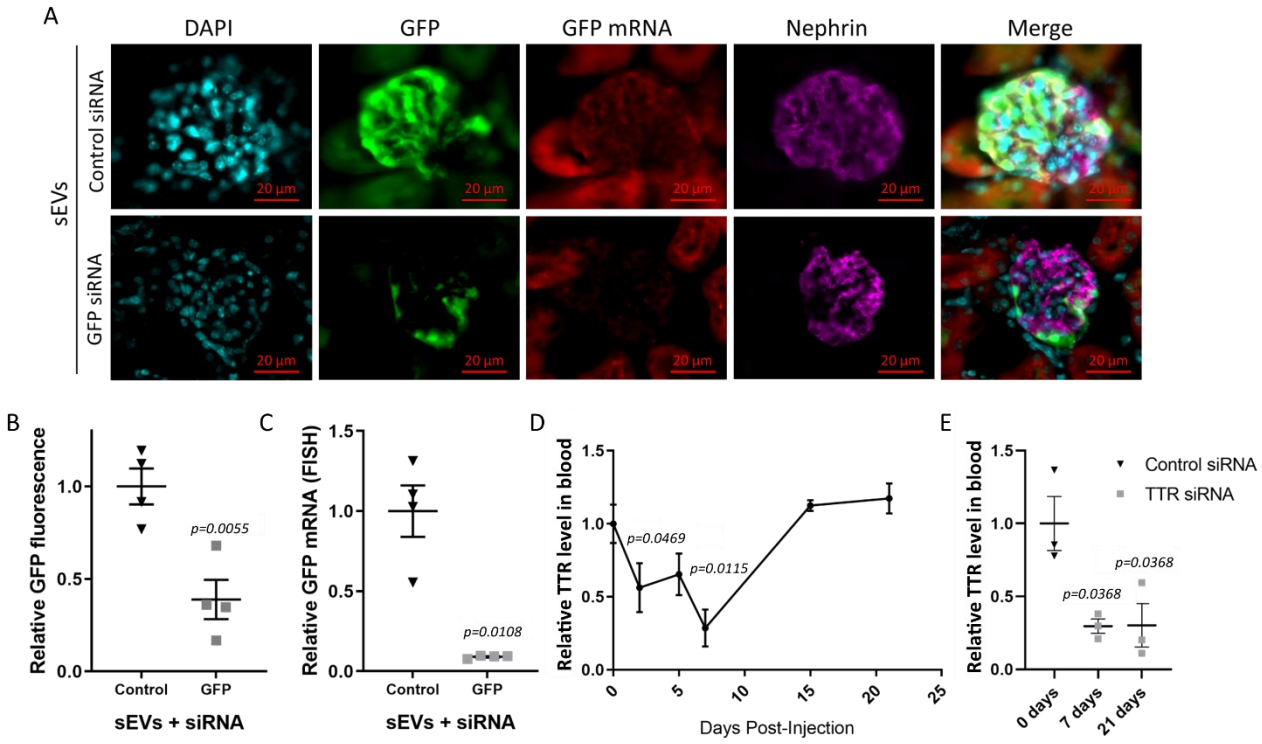

Supplementary Fig. 3.4. siRNA delivered by HEK293T-derived sEVs reduce target expression in the kidney and Ttr in the blood is reduced for extended duration following multiple sEV injections. (**A** to **C**) 10^{11} sEVs containing siRNA targeting *GFP* (or containing an off-target siRNA as control) from HEK293T cells were injected into mice ubiquitously expressing GFP and kidneys were harvested seven days after injection. Immunofluorescence revealed a decrease in GFP expression in Nephrin-positive glomeruli of 60% (A and B) and quantitative FISH revealed a reduction of *GFP* mRNA of 90% (A and C). Magnification is 20X; the scale bar represents 20 µm (n=4). (**D**) Mice were injected with a single injection of 10^{11} fibroblast-derived sEVs containing siRNA against *Ttr* and blood was drawn on days 3, 5, 7, 15, and 21 post-injections to monitor TTR levels. Knockdown peaked at ~70% after 7 days and returned to baseline by day 15 (n=6 for 0,3,5,7h n=3 for 15, 21h). (**E**) Mice were injected with the same 10^{11} dose of *Ttr*-siRNA-loaded sEVs weekly for 3 weeks and TTR levels were reduced by 70% for the full 21 days (n=3). Significant differences between groups were determined by a two-tailed, unpaired t-test with Welch's correction (B and C) or by an ordinary One-Way ANOVA Holm-Šídák's multiple comparisons test (D and E).

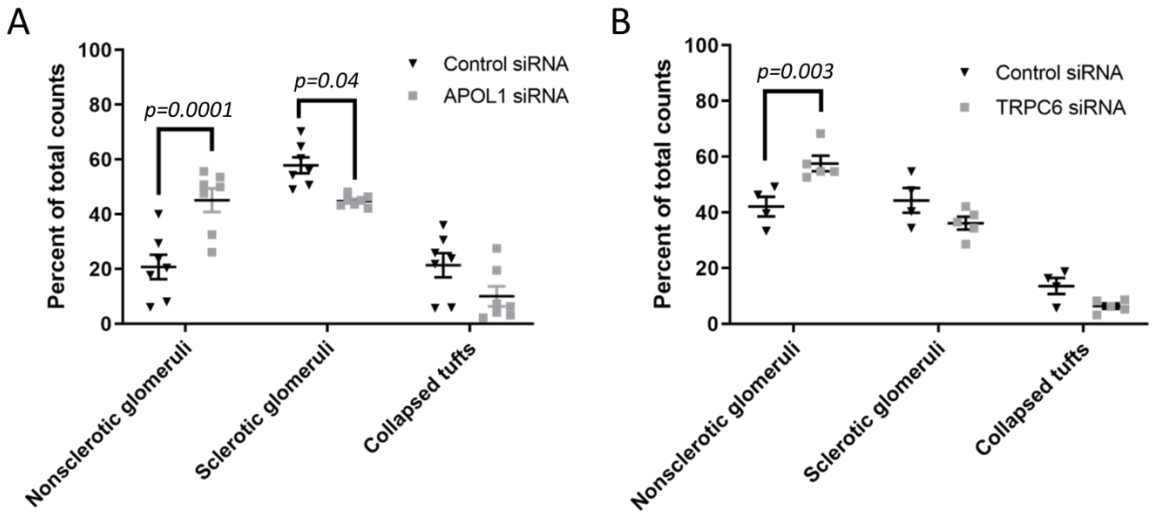

Supplementary Fig. 3.5. Glomerular scoring by a blinded observer shows treatment with siRNA-loaded sEVs reduces the number of damaged glomeruli. (**A** and **B**) PAS staining of kidney sections from control and *APOL1* siRNA (A) or *Trpc6* siRNA (B) treated kidneys with glomerular scoring performed by a blinded, non-expert observer related to figures 3.4h and 3.5f. Significant differences between groups were determined by an ordinary One-Way ANOVA Holm-Šídák's multiple comparisons test.

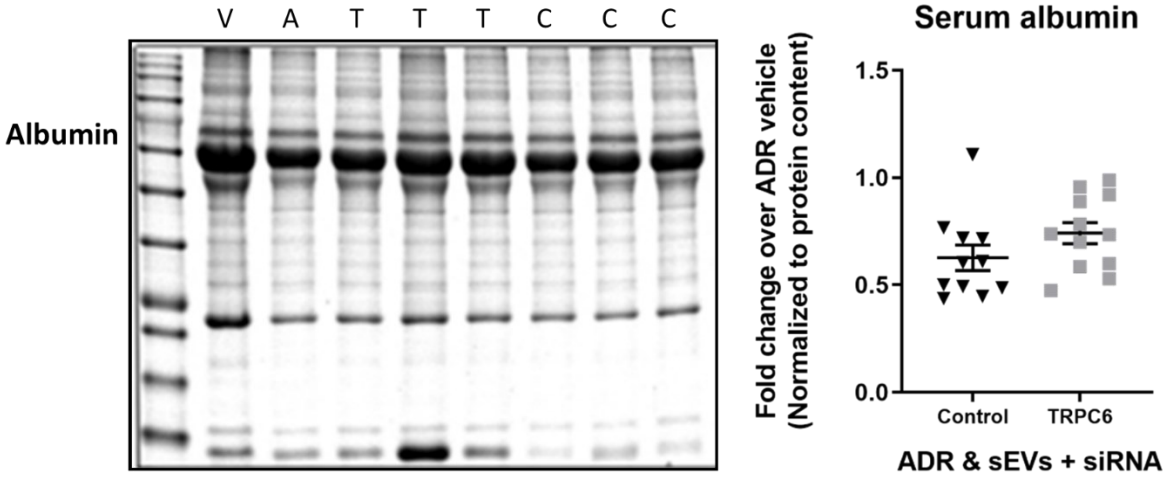

Supplementary Fig. 3.6. sEV-delivered siRNAs cause a trending increase in serum albumin levels in mice treated with Adriamycin, a model of TRPC6-dependent glomerulosclerosis. Representative Coomassie staining of serum samples collected from injected mice post-mortem. Albumin bands were quantified using FIJI. *Trpc6* siRNA-loaded sEV treatment leads to a trend toward increasing serum albumin when compared to mice treated with sEVs containing control siRNA. V=ADR vehicle; A=ADR only; T=ADR+sEVs containing siRNA targeting *Trpc6*; C=ADR+ sEVs containing control siRNA. (n=7 for ADR only, n=11 for control and *Trpc6* siRNA groups).

Chapter 4 - Manuscript #3

Midkine binds pre-miR-451 derivatives for active sorting into small extracellular vesicles

Publication information:

Ryan Reshke, Charlotte Manser, Olanta Negeri and Derrick Gibbings. Midkine binds pre-miR-451 derivatives for active sorting into small extracellular vesicles. Prepared for submission. (2023).

Author Contributions:

Designed experiments: RR, DG. Performed experiments: RR, CM, ON. Analyzed data: RR, CM, DG. Conceived the study: RR, DG. Wrote the manuscript: RR, DG.

RR contributions by figure: Figure 1, Figure 2, Figure 3, Figure 4e-g, Figure 5, Supplementary Figure 1, Supplementary Figure 2, Supplementary Figure 3

Midkine binds pre-miR-451 derivatives for active sorting into small extracellular vesicles

Ryan Reshke[1, 2], Charlotte Manser[1, 2], Olanta Negeri[1,2] and Derrick Gibbings[1, 2*]

[1]Department of Cellular and Molecular Medicine, Faculty of Medicine, University of Ottawa; Ottawa, Canada K1H 8M5.

[2]Eric Poulin Centre for Neuromuscular Disease, Faculty of Medicine, University of Ottawa; Ottawa, Canada, K1H 8M5.

* Corresponding author. Email: gibbings@uottawa.ca

4.1 Abstract

Delivery of cargoes like microRNA (miRNA) into recipient cells is hypothesized to be the primary function of small extracellular vesicles (sEVs) that circulate in the body. The populations of RNAs found in sEVs differ substantially from those in the cells which produce sEVs. This implies that as sEVs form by budding into the late endosome, or from the plasma membrane, mechanisms exist which selectively sort RNAs into them. Across many studies, miR-451 has been identified as one of the most highly enriched miRNAs in sEVs, suggesting it is a primordial example of selective RNA packaging into sEVs. We previously demonstrated that the short stem-loop structure of pre-miR-451 is responsible for its packaging into sEVs. Here, we identified proteins which selectively bind to the pre-miR-451 stem-loop structure and screened these candidates for their impact on packaging of this RNA into sEVs. This identified Midkine. Midkine is present in the cytoplasm and nucleus of cells, and is enriched in the lumen of sEVs. We identify a previously unknown RNA-binding function in Midkine with selectivity for the pre-miR-451 stem-loop, that is likely responsible for its control of RNA packaging into sEVs.

4.2 Introduction

MicroRNAs (miRNA) and short interfering RNAs (siRNA) are short (~22 nucleotide) noncoding RNAs which inhibit gene expression post-transcriptionally. In metazoans, miRNAs which lack perfect complementarity with their mRNA targets inhibit translation and promote mRNA deadenylation and decay. Alternatively, siRNAs can enzymatically cleave mRNA sequences which are perfectly complementary at least in the first 15-17 nucleotides, in a process termed RNA interference (RNAi). Endogenous miRNAs are typically generated through two consecutive cleavage events involving stem loop structures and RNase III enzymes. The first step occurs in the nucleus and involves the RNase III endonuclease Drosha which excises a ~60-120 nucleotide pre-miRNA hairpin from a longer transcript. Following export to the cytoplasm, cleavage by a second RNase III endonuclease, Dicer, produces a double-stranded complex of approximately 22 nucleotides with 2 nucleotide 3' overhangs[2]. These ~22 nucleotide double stranded RNAs are loaded into Argonaute proteins, where one strand is removed. The remaining guide strand is used for targeting mRNA with complementary sequences. When complementarity is perfect, as in the case of siRNA, the target mRNA is cleaved by the silencing activity of Argonaute 2 (Ago2)[292] or, in the case of a specific subset of guide RNAs, Argonaute 3 (Ago3)[34].

Small extracellular vesicles (sEVs) are small (40-120 nm) membrane-bound vesicles formed through one of two main biogenesis mechanisms: the first, via direct budding of the plasma membrane, and the second through inward budding of a late endosome and subsequent release upon its fusion with the plasma membrane[79]. sEVs released from one cell can fuse with another cell to deliver contents, including miRNA, mRNA and proteins, into the cytoplasm to modulate the recipient cell[79, 121, 122, 166, 221, 222]. These findings are fundamental to the hypothesis that the

primary biological role of sEVs is intercellular communication. miRNA delivery by sEVs is now implicated in a myriad of biological processes[168-170, 172, 222, 293].

Given the mounting evidence that sEVs can deliver functional miRNA to target cells, many groups are harnessing sEVs to deliver therapeutic miRNAs and siRNAs in pre-clinical studies[181, 182, 190, 294, 295]. However, the generation of effective sEV-based therapeutics requires efficient packaging of RNAs into the sEVs. It has become clear recently that sEV cargoes do not represent a random assortment of parental cell components[143-145]. Independent studies indicate that between 30-50% of sEV-associated miRNAs are over- or under represented compared to their cells of origin, suggesting the involvement of active mechanisms of miRNA sorting[143-145].

Several mechanisms of active miRNA sorting into sEVs have emerged for different miRNAs and in various cell types. Numerous RNA sequence motifs have been identified that appear to drive miRNAs into sEVs. These RNA motifs are recognized by at least two different RNA binding proteins (RBPs), the heterogeneous nuclear ribonucleoprotein A2B1 (hnRNPA2B1)[147] and synaptotagmin-binding cytoplasmic RNA-interacting protein (SYNCRIP)[148] for sEV sorting in T-lymphocytes or hepatocytes respectively. In both instances, sumoylated RBPs demonstrated direct binding to a variety of target miRNAs containing the identified sequence motifs. Other RBPs that have been shown to bind a specific subset of miRNAs leading to sEV sorting include Human antigen R (HuR) protein that sorts miR-122 into sEVs in hepatocytes[151], Lupus La protein that sorts miR-122 into MDA-MB-231 sEVs[150], the major vault protein (MVP) that was shown to shuttle different miRNAs into sEVs in both HEK293 cells[152] and in colon cancer CT26 cells[153] and the Y-box protein 1 (Ybx1) that shuttles miR-223 into sEVs from HEK293 cells[149]. In the case of YBX-1, the authors suggest that the sorting mechanism may

be mediated by RNA secondary structures and subsequent work demonstrated that YBX-1 binds recurrent hairpins in the 3'-UTR of mRNA transcripts that are sorted into sEVs[296].

Each of the described mechanisms for sorting of miRNA into sEVs is dependent on the direct binding of an RBP to miRNA. In the past, most RBPs were believed to bind RNA using one of a small number of RNA-binding domains including the RNA recognition motif (RRM) domain, zinc fingers, K homology (KH) domain or double stranded RNA binding domains[155]. However, within the past decade many novel RBPs have been identified, most of which have functions independent of RNA-binding and use alternative domains to bind RNAs[156]. Interestingly, SYNCRIP, a canonical RBP, binds miRNAs for sorting into sEVs independent of its canonical RNA recognition domains[157]. This suggests that active sorting of other miRNAs into sEVs could be mediated by novel RBPs with previously unknown RNA binding domains.

miR-451 is one of the most highly enriched miRNAs in sEVs. It is enriched 1,000 to 10,000 fold in sEVs relative to the cells that produce them, suggesting an active sorting mechanism[143, 258]. Pre-miR-451 has a uniquely short stem loop that cannot be processed by Dicer, forcing it through a non-canonical biogenesis pathway. Following cleavage by Drosha and export to the cytoplasm, the pre-miR-451 stem loop binds directly to Ago2, which cuts one strand of the stem. Upon further trimming by exonucleases, mature ~22 nt miR-451 is generated[206-208]. When the sequence of the pre-miR-451 hairpin is altered but the short hairpin structure is retained, those hairpins are also processed through the non-canonical Dicer-independent pathway[223]. Importantly, we showed that alternative sequences in the pre-miR-451 hairpin structure are enriched in sEVs similar to endogenous pre-miR-451, suggesting that the stem-loop structure, rather than the sequence, was critical for packaging into sEVs. The 42 nt stem-loop was also enriched in sEVs as detected using Northern blots, and a RT-qPCR method that differentiates mature miRNAs from their

precursors[258]. This demonstrated that the pre-miR-451 stem loop structure is critical for packaging of these RNAs into sEVs.

We hypothesized that pre-miR-451 sorting into sEVs is mediated by an RBP. Additionally, based on evidence for non-canonical RNA binding domains involved in sEV packaging[157], we did not wish to restrict our search to previously characterized RBPs. To that end, we used biotinylated RNAs to identify proteins which preferentially bind to the pre-miR-451 hairpin structure. We identify Midkine as a factor required for sorting of pre-miR-451 into sEVs, and provide evidence that it accomplishes this through a previously unidentified RNA-binding activity.

4.3 Results

Biotin pulldown identifies proteins that preferentially bind to short RNA hairpins

The hairpin structure of pre-miR-451, rather than its sequence, appears to be critical for its packaging into sEVs. We used RNAs biotinylated on their 3' ends to pulldown putative RBPs. To identify proteins which preferentially bind these hairpin structures, while minimizing the risk of identifying sequence-specific binding, we used two RNAs with the pre-miR-451 structure, but with distinct sequences. These were the 42 nt Drosha-processed pre-miR-451 and an siRNA vs. GFP incorporated in the 42 nt pre-miR-451 structure that we previously reported (Fig. 4.1a)[258]. As negative controls, mature forms of both the GFP siRNA and an abundant miRNA, miR-16, which is present in sEVs from multiple cell sources, were used[297-299].

The 3' biotinylated RNAs were mixed into HEK293T cell lysate and retrieved using streptavidin-conjugated beads. An additional negative control consisted of an equivalent amount of cell lysate that was not incubated with an RNA oligo. Silver staining of the pulldowns showed minimal binding to beads alone, and distinct protein banding patterns for mature 22 nt RNAs and

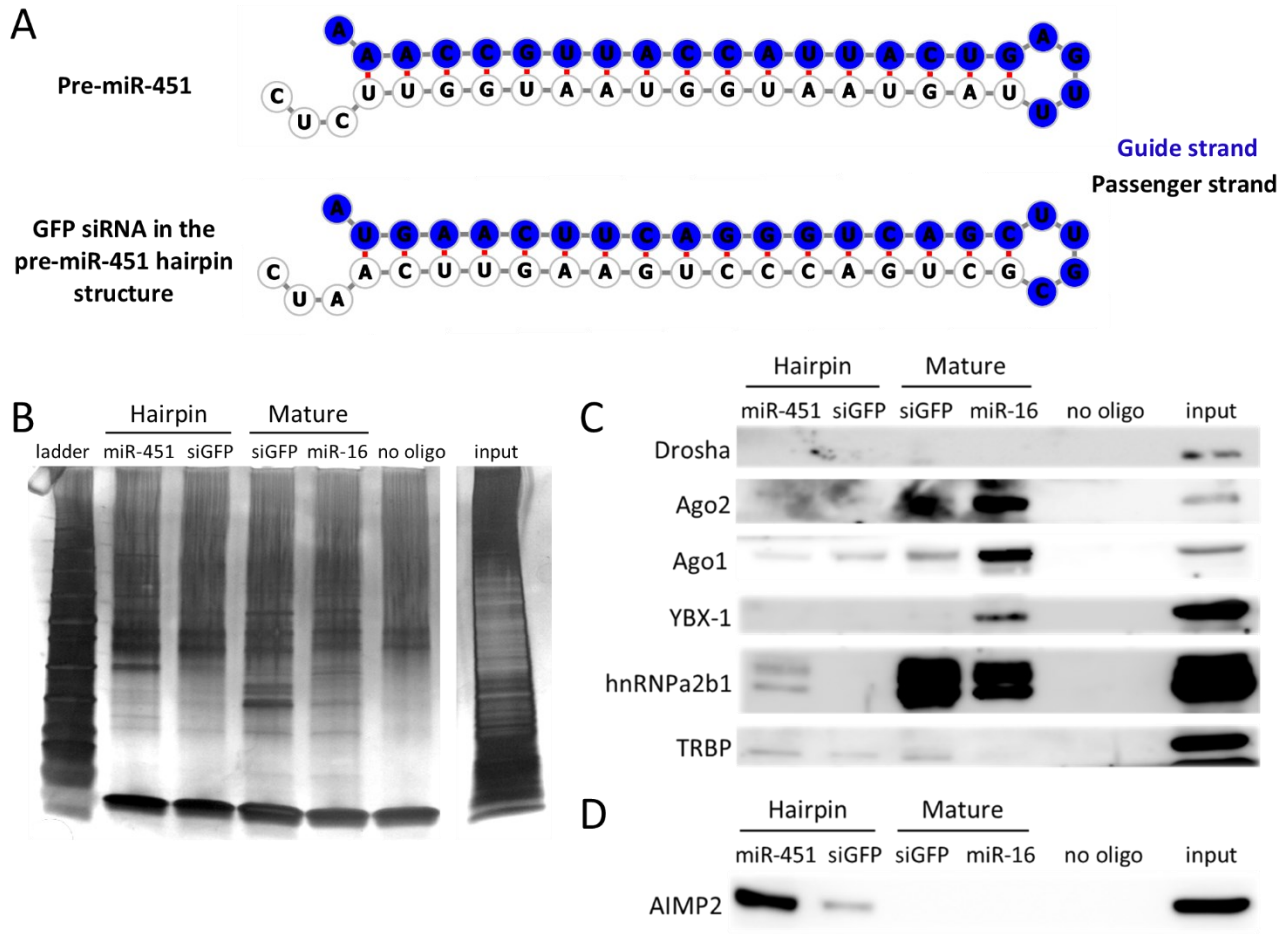

Figure 4.1. Biotin-Streptavidin pulldown identifies proteins that preferentially bind to short RNA hairpins. (**A**) RNAfold[300] schematic of the 42 nt pre-miRNA and GFP siRNA in the pre-miR-451 hairpin structure that were used in biotin-streptavidin pulldown experiments. Blue nucleotides represent the 22 nt mature sequences. (**B**) Silver staining of proteins from pulldown samples performed using biotinylated RNAs mixed into cell lysates and pulled down using streptavidin-bound beads. (siGFP = GFP siRNA in the pre-miR-451 hairpin structure). (**C**) Western blots of protein samples from pulldown samples showing certain RBPs having binding preferences for different RNA species. (**D**) Western blot of an RBP identified by mass spectrometry, AIMP2, in pulldown samples.

42 nt hairpins (Fig. 4.1b). Western blots of these pulldowns showed substantial binding of Ago1 and Ago2 to the mature miRNAs, and low levels of binding to the 42 nt hairpins, as expected. Drosha cleaves longer hairpin RNAs and releases the 42 nt hairpins. As predicted by this, Drosha did not bind to the mature miRNAs nor to the 42 nt hairpins. In contrast, TRBP which binds double-stranded RNA was preferentially pulled down with the 42 nt hairpins (Fig. 4.1c). These

results validate the specificity of the pulldowns and suggest candidate proteins which may be involved in sorting RNAs with the structure of the pre-miR-451 hairpin into sEVs.

To more comprehensively identify proteins bound to the 42 nt hairpins, biological quadruplicates of pulldowns were analyzed by mass spectrometry and a total of 410 proteins were identified. Among identified proteins, we focused on proteins bound to both 42 nt hairpins in at least two of four replicates, and removed proteins which bound to mature miRNA sequences, or the beads alone. This pared the list of candidates to 36 proteins, 67% (24) of which were known RBPs such as ADAR1, IGF2BP2, PTBP1, SND1, SRP9 and STAU1. Another 19% (7) of the identified proteins are predicted novel RNA-binding proteins, according to recent studies[156]. In addition, several of the candidate proteins are known to bind double-stranded RNAs or RNAs containing stem-loop structures (ADAR1, tRNA ligases, STAU1). Validating this proteomics analysis, AIMP2 was strongly enriched in pulldowns with 42 nt hairpins compared to mature miRNAs (Fig. 4.1d). The 36 candidate proteins and their status as known or predicted RBPs are included in Table 4.1.

Table 4.1. Known and predicted RBPs amongst the 36 candidate proteins

Candidate Protein	**RNA binding**
ACTB	No
ADAR	Known
AIMP1	Known
AIMP2	Known
Ashwin	Known
BANF1	Known
DARS	Known
EEF1D	Known
EEF1E1	Known
EPRS	Known
GTF2I	Known
IARS	Known
IGF2BP2	Known
KARS	Known
LARS	Known

MDK	No
MTDH	Predicted
MYH10	Predicted
MYH9	Predicted
MYL12A	No
MYL6	No
MYO18A	Predicted
NPM1	Known
PARP1	Known
PRDX1	Predicted
PRPF19	Known
PTBP1	Known
RARS	Known
SLC25A5	Predicted
SND1	Known
SRP14	Known
SRP9	Known
STAU1	Known
TANC2	No
TRIM25	Predicted
YTHDF2	Known

Reducing levels of Midkine decreases packaging of pre-miR-451 stem loops into sEVs

To facilitate the process of screening, the 36 candidates were tested in pools by knockdown in HEK293T cells. To identify proteins impacting the 42 nt hairpin structure, these experiments were performed in cells expressing endogenous pre-miR-451 and stably transduced to express SOD1 siRNA incorporated in the pre-miR-451 hairpin structure. Many of the siRNA pools did not affect packaging of these RNAs into sEVs, while others affected one of the 42 nt hairpins and not the other (Fig. 4.2a). This could be due to sequence-dependent effects on these RNAs. In several cases, knockdown of candidate proteins like BANF1 and NPM1, or a pool of Myosins, triggered an increase in sEVs of pre-miR-451 products and SOD1 siRNA in the pre-miR-451 structure. These proteins may normally retain these RNAs in cells potentially by directly binding to them. Their depletion may then enable increased packaging of pre-miR-451 derivatives into sEVs.

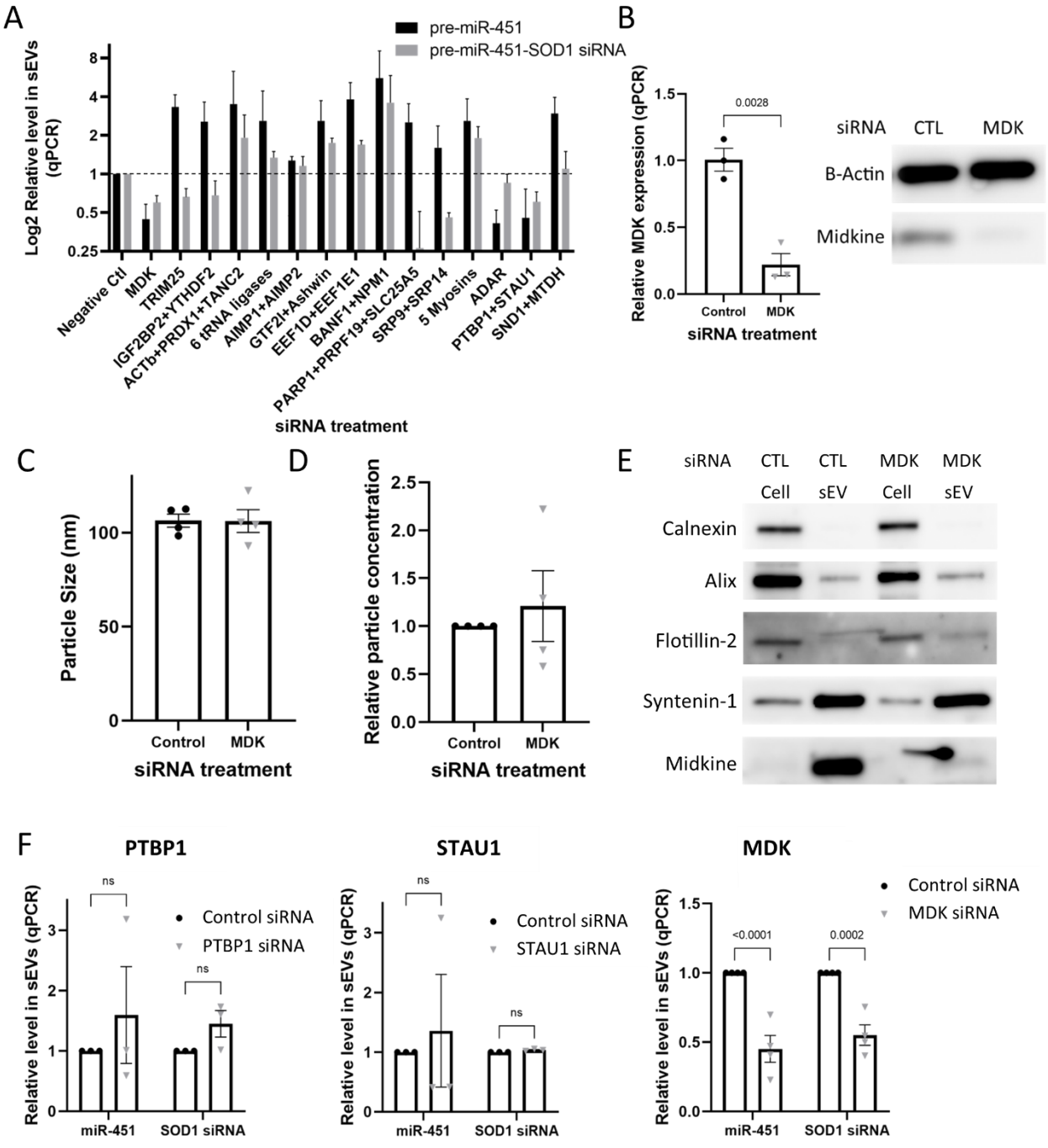

Figure 4.2. Reducing cellular Midkine level leads to reduced sorting into sEVs of pre-miR-451 and SOD1 siRNA in the pre-miR-451 hairpin structure. (**A**) HEK293T cells that express SOD1 siRNA in the pre-miR-451 hairpin structure were transfected with siRNA against sets of RBPs, leading to increases or decreases of pre-miR-451 species in sEVs as quantified by RT-qPCR (n=3). (**B**) Validation of MDK knockdown by siRNA in cells by qPCR (n=3) and Western blot. Reduction of MDK in cells using siRNA does not lead to a significant change in median size (**C**) or relative concentration (**D**) of released sEVs measured by ZetaView NTA (n=4). (**E**) Western blots of cells transfected with negative control or MDK siRNA and their released sEVs, isolated

via differential ultracentrifugation, showing the presence of multiple sEV markers including Alix, Flotillin-2 and Syntenin-1, with the ER-associated protein Calnexin only visible in cell lysates. (**F**) Depletion of cellular PTBP1 or STAU1 by siRNA does not cause a reduction in pre-miR-451 or SOD1 siRNA in the pre-miR-451 hairpin structure packaging into sEVs. Cellular MDK reduction by siRNA leads to a reduction of both species as measured by RT-qPCR. (n=3 for PTBP1 and STAU1, n=4 for MDK). Significant differences between groups were determined by ordinary Two-Way ANOVA Holm-Šídák's multiple comparisons test (F) or by two-tailed, unpaired t-test with Welch's correction (B, C, D).

In contrast, knocking down both Polypyrimidine Tract Binding Protein 1 (PTBP1), a heterogeneous nuclear ribonucleoprotein, and Staufen Double-Stranded RNA Binding Protein 1 (STAU1) led to a decrease in both forms of the pre-miR-451 stem loop in sEVs (Fig. 4.2a). Both STAU1 and PTBP1 have previously been shown to interact with Ago2 within the RISC complex in a miRNA-dependent manner[301, 302], suggesting their potential involvement. However, when tested independently, neither PTBP1 nor STAU1 impacted packaging of the RNA hairpins into sEVs (Fig 4.2f). PTBP1 and STAU1 may participate in packaging the RNA hairpins in the sEVs, but the depletion of one could be compensated for by the other. Changes in cellular levels of pre-miR-451 and SOD1 siRNA in the pre-miR-451 hairpin structure did not correlate with the changing levels in sEVs following candidate protein knockdown, suggesting that candidate knockdown was altering sorting of RNA species into sEVs, and not simply altering cellular expression (Supplementary Fig. 4.1).

Knocking down Midkine (MDK) reduced levels of both RNA hairpins by approximately 50% in sEVs without changing their levels in cells (Fig. 4.2a, f, Supplementary Fig. 4.1). Loss of MDK was confirmed by RT-qPCR and Western blot (Fig. 4.2b). Importantly, sEVs from MDK or control siRNA-treated cells showed characteristic Nanoparticle tracking analysis size distributions of sEVs peaking around 100 nm (Supplementary Fig. 4.2) and MDK depletion did not lead to significant changes in median size (Fig. 4.2c) or concentration (Fig. 4.2d) of the released sEVs. Additionally, Western blot analysis revealed that sEVs from cells treated with control siRNA or

siRNA targeting MDK contained the expected sEV markers including Alix, Flotillin-2 and Syntenin-1, while the ER-associated protein Calnexin was seen only in cell lysates (Fig. 4.2e). This demonstrates that MDK affects packaging of pre-miR-451 stem loops into sEVs independent of effects on sEV numbers.

Increasing cellular Midkine level does not lead to an increase of miR-451 or siRNA sorting into sEVs

Reducing cellular MDK levels with siRNA leads to a decrease in pre-miR-451 levels in sEVs. To investigate whether increased levels of MDK increase pre-miR-451 levels in sEVs, we treated HEK293T cells with retinoic acid, which is known to induce MDK expression. Retinoic acid induced a ~25% increase in MDK expression, measured by RT-qPCR (Fig. 4.3a). sEVs from retinoic acid-treated cells contained a modest (~1.5-fold) but significant increase in the amount of endogenous pre-miR-451, but no significant increase in SOD1 siRNA in the pre-miR-451 hairpin structure in sEVs (Fig. 4.3b). We then transfected an inducible MDK overexpression plasmid into the same HEK293T cells and induced MDK expression using doxycycline. MDK protein levels were increased by approximately five-fold according to Western blot analysis (Fid. 3c) however, this did not lead to a significant increase in the levels of pre-miR-451 species in sEVs (Fig. 4.3d). MDK overexpression also did not change the levels of classic markers on sEVs including Alix, Flotillin-2, and Syntenin-1 (Fig. 4.3e). This data suggests that MDK could be present at a level that saturates the sEV-sorting system, and therefore increasing the level has little to no effect, while reducing it significantly hinders the sorting of pre-miR-451 into sEVs.

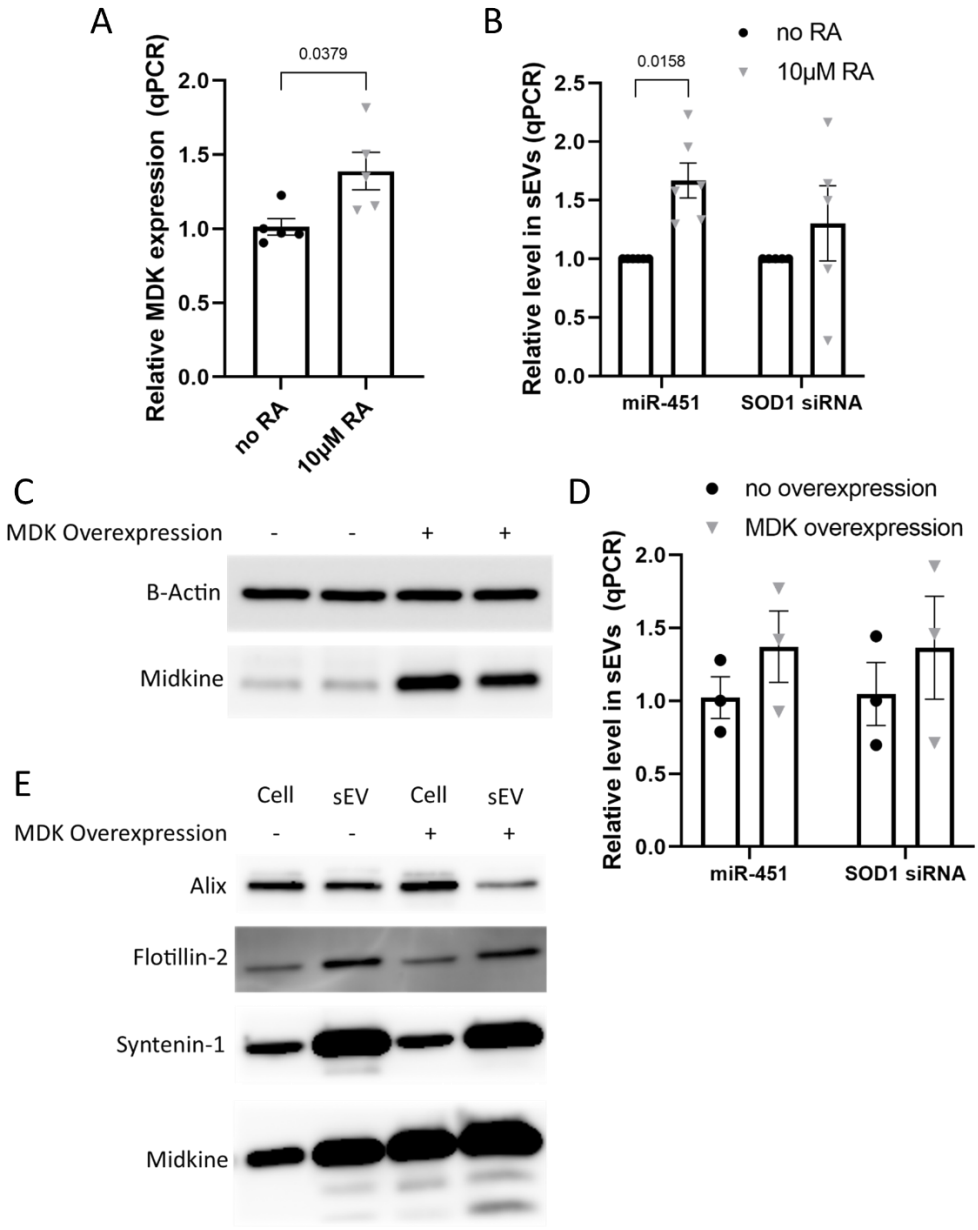

Figure 4.3. Increasing cellular Midkine level does not lead to increased sorting of pre-miR-451 or siRNA in the pre-miR-451 hairpin structure into sEVs. (**A**) Treating HEK293T cells with 10 μM retinoic acid increases the expression of MDK by ~25%, measured by RT-qPCR (n=5, one outlier removed based on Grubbs outlier analysis in GraphPad Prism with alpha = 0.05). (**B**) Following retinoic acid treatment, levels of endogenous pre-miR-451 are significantly increased in sEVs by ~1.5 fold, while levels of SOD1 siRNA in the pre-miR-451 hairpin structure are not significantly affected, (n=6 for miR-451, n=5 for SOD1 siRNA in the pre-miR-451 hairpin structure, one outlier removed based on Grubbs outlier analysis in GraphPad Prism with alpha = 0.05). (**C**) Transfecting an inducible MDK overexpression plasmid into HEK293T cells and inducing with doxycycline over three days leads to an increase in cellular MDK levels as measured by Western blot. (**D**) Levels of endogenous pre-miR-451 or SOD1 siRNA in the pre-miR-451 hairpin structure are not significantly different following MDK overexpression, measured by RT-

qPCR (n=3). (**E**) Western blot of MDK and sEV marker levels in cells and sEVs following MDK overexpression in cells. Significant differences between groups were determined by two-tailed, unpaired t-test with Welch's correction (A) or ordinary Two-Way ANOVA Holm-Šídák's multiple comparisons test (B, D).

Midkine is associated with sEVs

Among the candidates, MDK was the only one that independently controlled packaging of both pre-miR-451 stem loops into sEVs (Fig. 4.2a, f). MDK is a small, secreted, growth factor expressed in many cell types[303, 304]. MDK generally exerts its function through interactions with cell surface ligands including syndecans and other heparin sulfate proteoglycans, integrins, and low-density lipoprotein receptor related protein (LRP) [305, 306], all of which are known to be associated with sEVs[91, 98, 307]. Midkine is involved in numerous pathways and cellular processes including development, cell survival, proliferation and inflammation[303-305]. While the canonical MDK transcript contains a signal peptide, it has also been observed in the nucleus and cytoplasm of cells[308-312]. MDK could impact sorting of RNAs into sEVs by, for example, triggering a receptor on the plasma membrane, or by more directly associating with RNA in the cytoplasm and shepherding it into sEVs. Our pulldowns with biotinylated RNA suggested MDK can associate with RNA and therefore MDK in the cytoplasm, and potentially inside sEVs, could control packaging of pre-miR-451 into sEVs.

To begin to understand how MDK might control pre-miR-451 packaging into sEVs, we first confirmed that MDK is present inside of cells using immunofluorescence (IF) microscopy. The specificity of the MDK antibody used was validated using siRNA knockdown (Fig. 4.4a). MDK exhibited a punctate distribution in the cytoplasm and was also present in the nucleus. 3D rendering of Z-stack images showed MDK signal inside of the nucleus, confirming that MDK is inside of the cells and not simply attached to the surface or resident in endosomes, ER or Golgi (Fig. 4.4b). Immunofluorescence microscopy showed strong colocalization of MDK in the

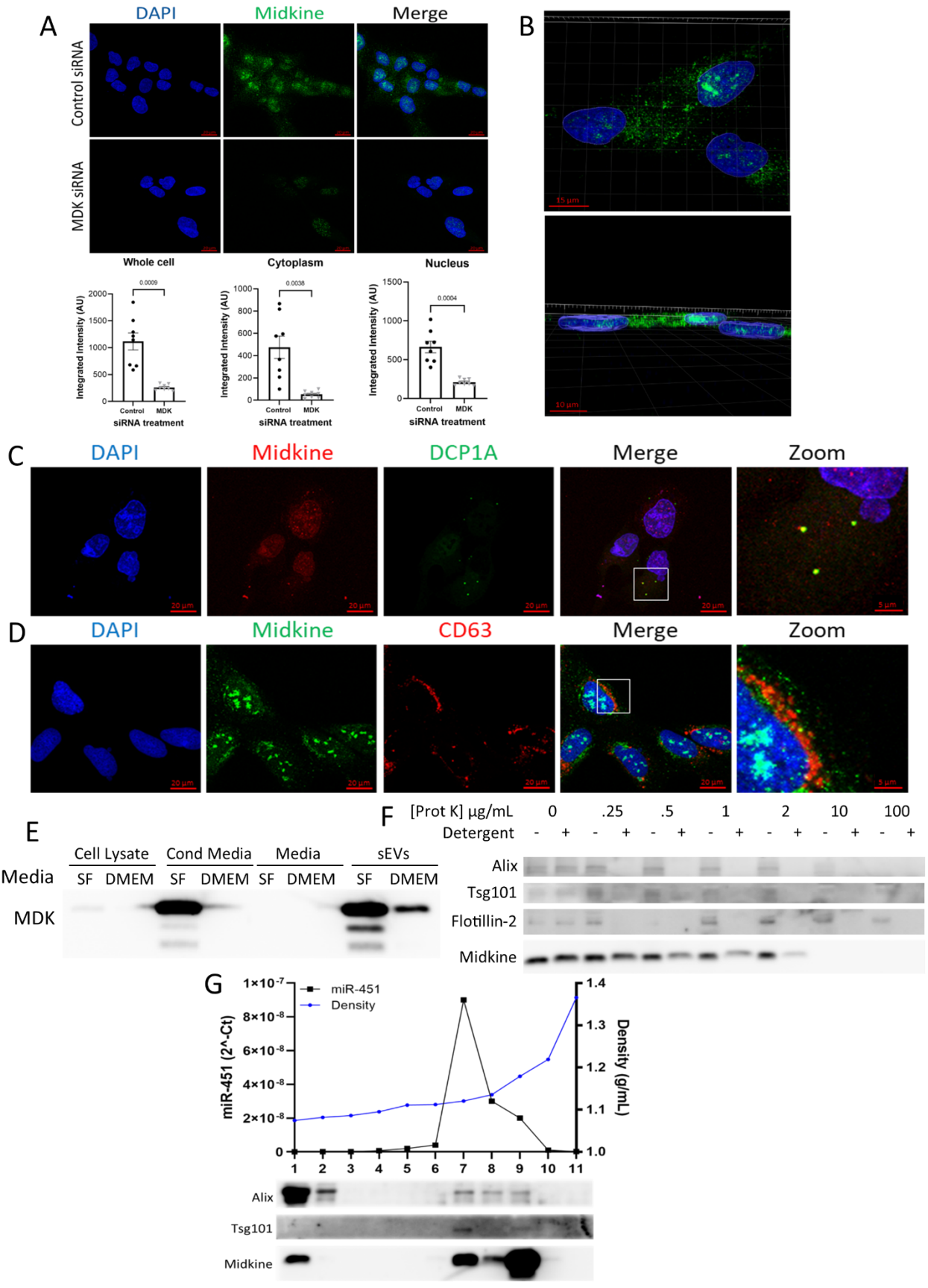
A
DAPI
Midkine
Merge
Control siRNA
MDK siRNA
Whole cell
Cytoplasm
Nucleus
Integrated Intensity (AU)
0.0009
0.0038
0.0004
Control
MDK
siRNA treatment
B
15 µm
10 µm
C
DAPI
Midkine
DCP1A
Merge
Zoom
20 µm
5 µm
D
DAPI
Midkine
CD63
Merge
Zoom
E
Cell Lysate
Cond Media
Media
sEVs
Media
SF
DMEM
MDK
F
[Prot K] µg/mL
0
.25
.5
1
2
10
100
Detergent
Alix
Tsg101
Flotillin-2
Midkine
G
miR-451
Density
miR-451 (2^-Ct)
Density (g/mL)
Alix
Tsg101
Midkine

Figure 4.4. Midkine is associated with sEVs. (**A**) IF microscopy of MDK in U-2 OS cells. Punctate MDK signal in the cytoplasm and nucleus are reduced by MDK siRNA. Z-stacks acquired at 40X magnification and projected into 2D maximum intensity projection images. Scale bar = 20 µm. Quantification is integrated intensity. (**B**) 3D reconstruction of Z-stack images showing top-down (left) and side (right) views showing MDK signal inside the nucleus. Z-stacks acquired at 40X magnification and 3D rendered using Imaris software. Scale bar = 15 µm (left) 10 µm (right). (**C, D**) Immunofluorescence microscopy images showing MDK colocalizing with GFP-tagged DCP1A (C) and with CD63 (D). Z-stacks acquired at 40X magnification and projected into 2D maximum intensity projection images. Scale bar = 5 µm in "Zoom" panel, 20 µm in other panels. (**E**) Western blot of cell and sEV lysates as well as media before and after being conditioned on sEV-producing HEK293T cells [SF = Serum Free media: DMEM supplemented with HL-1 chemically defined FBS substitute (Lonza, catalogue no. 77227). DMEM = complete DMEM containing 10% FBS depleted of sEVs through ultracentrifugation at 100,000 xg for 2 hours and sterile 0.22 µm filtration]. (**F**) Western blots of Proteinase K/detergent experiments on TFF-isolated sEVs show reduction of MDK and sEV-associated proteins Alix, Tsg101 and Flotillin2 by proteinase K only in the presence of detergent. (**G**) Western blot analysis performed on fractions taken from Optiprep density gradients of TFF-isolated HEK293T sEVs shows MDK floats at the expected density of sEVs with sEV markers Alix and Tsg101. Pre-miR-451 levels are most abundant in fractions containing MDK and sEV markers, measured by RT-qPCR on individual fractions.

cytoplasm with GFP-DCP1A, a marker of P-bodies, the locale where miRNA and their target mRNAs accumulate (Fig. 4.4c). A fraction of MDK also co-localizes with CD63, a marker of the late endosome where sEVs are formed (Fig. 4.4d), suggesting it may also be present in sEVs (Fig. 4.3).

Next, we performed experiments to determine whether MDK associates with sEVs. Western blotting revealed that MDK is present in HEK293T cell lysates and cell-conditioned media. sEV preparations were generated by differential ultracentrifugation from cell-conditioned serum-free media or FBS-containing media previously depleted of sEVs (Fig. 4.4e). MDK was much more abundant in sEV preparations than in proteins precipitated from these media. MDK was also not observed in proteins precipitated directly from these two types of media, which had not been exposed to cells, confirming that MDK is not a contaminant of FBS, it is released from cells in culture. sEVs were then isolated from HEK293T cells using tangential flow filtration (TFF), to avoid the damaging forces of ultracentrifugation, and were exposed to proteinase K with

and without detergent to determine if MDK is inside the lumen of the sEVs or bound to their surface (Fig. 4.4f). sEV-associated proteins Alix, Tsg101 and Flotillin-2 are known to be located in the sEV lumen. Alix, Tsg101 and Flotillin-2 in sEVs resisted low doses of Proteinase K digestion. The addition of detergent, or eventually high doses of Proteinase K known to digest cells entirely, caused Alix, Tsg101 and Flotillin-2 degradation. Like these proteins located in the lumen of sEVs, proteinase K had negligible effects on MDK levels in sEVs in the absence of detergent. Similarly, MDK levels were reduced in response to increasing amounts of proteinase K only in the presence of detergent, and at extreme levels of Proteinase K all MDK was lost, as was observed for Alix (Fig. 4.4f). While we cannot exclude that MDK could be embedded within the membrane and thus resistant to Proteinase K, the data collectively is most consistent with a substantial proportion of MDK being in the cytoplasmic-nuclear space of cells (immunofluorescence, Fig. 4.2) and inside of the sEV lumen.

To validate that MDK was inside of sEVs and not a protein complex or other contaminant of ultracentrifuged sEV preparations, we separated sEVs on an Optiprep density gradient. MDK is most abundant in fractions consistent with sEV densities[289], which contain sEV markers Alix and Tsg101 (Fig. 4.4g). Importantly, levels of pre-miR-451 RNA also peak in fractions containing MDK and sEV markers suggesting MDK is found in sEVs with pre-miR-451[258].

Midkine binds RNA

Given that MDK regulates the sorting of pre-miR-451 into sEVs (Fig. 4.2) and is found in the lumen of sEVs (Fig. 4.4), we aimed to determine if MDK can also bind RNA, consistent with MDK physically shuttling pre-miR-451 into sEVs. To this end, we first tested whether MDK immunoprecipitates contain RNA. Western blot analysis confirmed the immunoprecipitation of MDK (Fig. 4.5a). Four different small non-coding RNAs were all found in the MDK

immunoprecipitates at levels several fold higher than in the control IgG IP as measured by RT-qPCR (Fig. 4.5b). Pre-miR-451 and SOD1 siRNA in the pre-miR-451 hairpin structure were enriched in the MDK immunoprecipitate 3.4 and 4.5 fold respectively above their levels in a non-specific IgG immunoprecipitate. To evaluate the preference of MDK for binding RNA species, the level of each RNA in the MDK immunoprecipitates was normalized to its cellular level. This demonstrated that MDK has a preference of several orders of magnitude for pre-miR-451 and SOD1 siRNA in the pre-miR-451 structure compared to its association with miR-16 and U6 (Fig. 4.5c). This suggests that MDK associates with RNAs with a strong preference for structures resembling pre-miR-451.

To evaluate whether MDK can directly bind RNA, we covalently cross-linked RNA to protein using 254 nm UV in intact cells. In this scenario, the protein detected by Western blot on denaturing SDS-PAGE gels should increase in mass if it binds RNA. As a positive control we evaluated the size-shift of HuR, a known RNA-binding protein after UV cross-linking. Higher mass bands and smearing in HuR Western blots were induced by UV and reduced by elevated levels of RNase (Fig. 4.5d bottom). Gentle RNase treatment in Crosslinking immunoprecipitation (CLIP) frequently degrades parts of bound RNA not protected by the RNA-binding protein. Resembling this, gentle RNase treatment of HuR caused the appearance of lower mass bands. UV caused MDK, detected by Western blot, to appear as a new discrete band of approximately 25 kDa, as well as a smear at higher masses (Fig. 4.5d top). The intensity of these size-shifted signals for MDK were reduced upon treatment with high levels of RNase, confirming they were due to RNA binding to MDK. As observed with HuR, Gentle RNase treatment caused lower mass bands to appear, suggesting that MDK directly binds and protects RNA. To confirm that RNA was bound

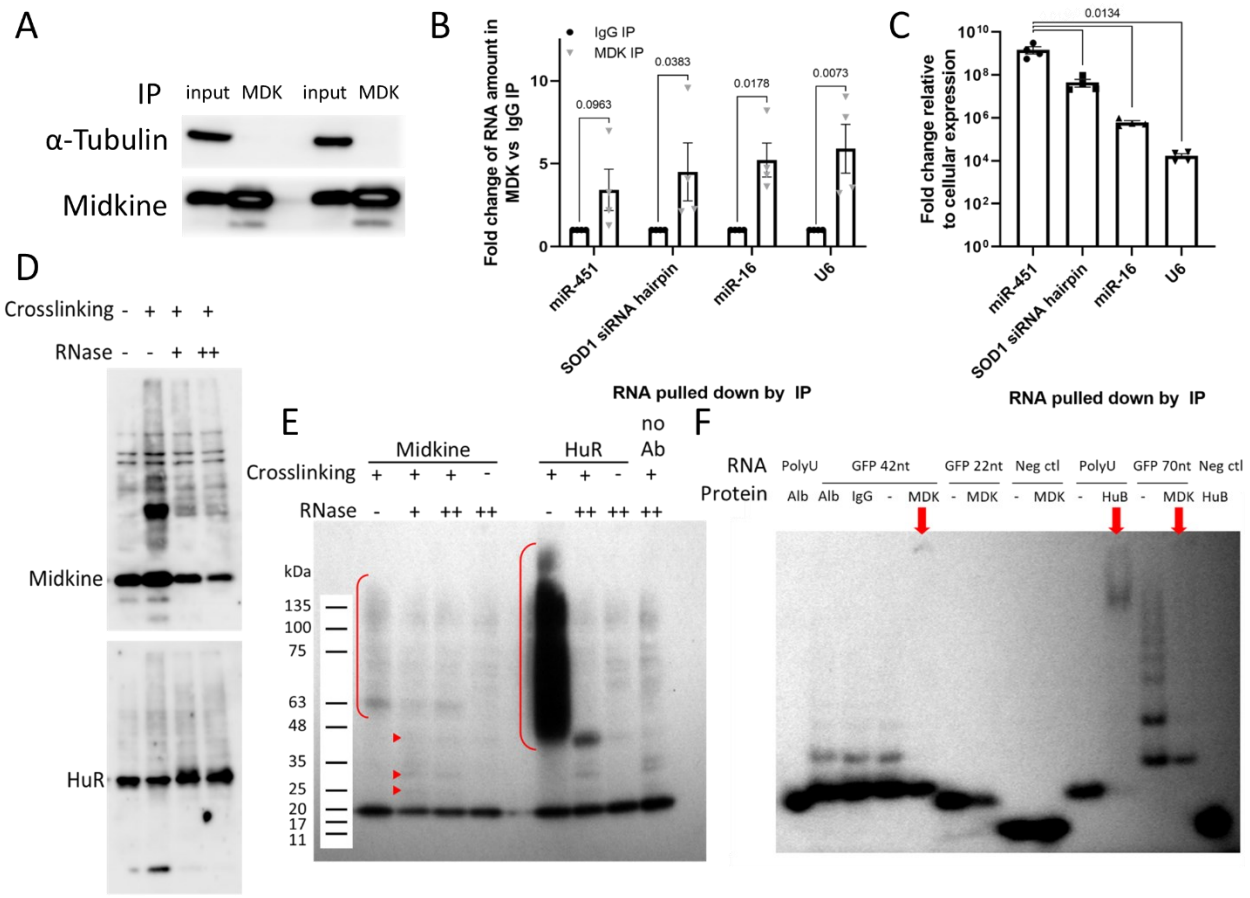

Figure 4.5. Midkine binds RNA inside of cells. (**A-C**) RNA Immunoprecipitation (IP) from HEK293T cells containing SOD1 siRNA in the pre-miR-451 hairpin structure using an antibody against MDK (A) shows that MDK binds to 4 species of small RNA, displayed as fold change of levels in MDK IP over control IgG IP (B) or fold change over control IgG relative to level in total input RNA (C), measured by RT-qPCR (n=4). (**D**) Western blot of crosslinked HEK293T cells that were lysed and treated with RNase shows the appearance of novel MDK (top) or HuR (bottom) bands and smearing with crosslinking that are reduced upon RNase treatment. (**E**) Crosslinking Immunoprecipitation (CLIP) on HEK293T cells shows a reduction of smearing of radio-labeled RNA signal immunoprecipitated by both MDK (left bracket) and HuR (right bracket) antibodies with increasing RNase concentration. Arrow heads show small bands emerging following RNase treatment. (**F**) RNA EMSA analysis of radio-labelled versions of GFP siRNA in the pre-miR-451 hairpin structure of different lengths (GFP 42 nt, GFP 22 nt, GFP 70 nt) showing a size shift in the 42 nt (left arrow) and 70 nt (right arrow) forms when bound by recombinant MDK. PolyU RNA is used as a positive control and a size shift is observed when it is bound by a known binding partner, HuB (middle arrow). A negative control RNA probe (Neg ctl) is not seen to bind to MDK or HuB. Significant differences between groups were determined by ordinary Two-Way (B) or One-Way (C) ANOVA Holm-Šídák's multiple comparisons test.

to MDK, we performed Crosslinking immunoprecipitation (CLIP) and labeled RNA 5' ends with

^{32}P-ATP. To ensure the stringency of MDK pulldown, washes of the immunoprecipitating beads

of up to 1 M NaCl were used. As a positive control, RNA-binding to HuR was detected in CLIP experiments (right bracket) and eliminated by RNase-treatment (Fig. 4.5e). After UV cross-linking of intact cells, followed by stringent washes of MDK immunoprecipitates, a distinct band and smearing of RNA was observed (left bracket). The size of these bands and smears aligned with the bands detected by Western blot for MDK in the same conditions, confirming they are likely MDK. This was dependent on UV cross-linking and eliminated by stringent RNase treatment confirming that it represents RNA bound to MDK in intact cells (Fig. 4.5e). These experiments strongly suggest that MDK directly binds RNA in intact cells.

In pulldowns (Fig. 4.1), MDK was selectively isolated with short hairpin RNAs compared to single-stranded RNAs. To confirm whether MDK has binding preferences for certain RNA structures, recombinant MDK protein was mixed with different radio-labelled RNA species in an electrophoretic mobility shift assay (EMSA) (Fig. 4.5f, Supplementary Fig. 4.3). HuB, a known RBP, was used as a positive control. PolyU RNA, a known binding partner of HuB[313, 314], shifted when incubated with HuB, but not Albumin (middle arrow). No shift is observed when a negative control RNA probe of the same length but composed of random nucleotides was incubated with HuB, validating the specificity of binding in this assay. Recombinant MDK also does not bind the negative control probe used in the HuB assay. MDK exhibited gel shifts when incubated with the 42 nt pre-miR-451 hairpin structure (left arrow). No shift was observed after incubation of this RNA with control proteins bovine albumin or rabbit IgG. A similar, though less intense binding of MDK is observed to a 70 nt RNA containing the pre-miR-451 structure (right arrow). No binding was detected of MDK to a 22 nt mature miRNA version of the pre-miR-451 hairpin, suggesting MDK has a strong binding preference for the 42 nt form, that aligns closely with the binding preferences of MDK in biotinylated-RNA pulldowns (Fig. 4.1). Together, these data

suggest that MDK likely binds to RNA in the cytoplasm with a preference for the 42 nt pre-miR-451 or other RNAs which retain its structure and does not bind, or binds weakly to a mature 22 nt miRNA.

Taken together, our results suggest that MDK binds RNA, is found in the lumen of sEVs and controls the active sorting of pre-miR-451 and other RNAs resembling this structure into sEVs.

4.4 Discussion

MDK was previously identified in a study using computational methods to predict novel RBPs[315]. There are multiple reasons why it was likely not identified in previous empirical efforts to find novel RBPs. First, several of those efforts focused on mRNAs, using oligodT pulldown to identify proteins binding polyadenylated mRNAs, and would be unlikely to purify a protein with a preference for short RNA hairpins. The fact that MDK is not ubiquitously expressed, and that a major proportion of it is released from cells may have also limited its chances of being identified.

Our evidence, using multiple direct and independent methods, demonstrates that MDK can bind RNA. Data using CLIP further demonstrates that RNA binding by MDK is unlikely to be a post-lysis artefact. MDK contains two C-terminal heparin-binding clusters: cluster 1 consists of residues K79, R81 and K102 while cluster two is comprised of residues K86, K87 and R89[316, 317]. We hypothesize that these may be involved in binding to RNA. The positive charge of these clustered lysines may promote interaction with negatively charged RNAs[318]. Regions consisting of large numbers of lysine residues have been shown elsewhere to promote formation of protein/RNA granules like P-bodies[319], suggesting a propensity for interaction with RNA. Similarly, in a recent study that identified a previously unknown RNA binding domain in SYNCRIP that is responsible for binding and shuttling miRNA into sEVs, the novel RNA binding domain was found to centre on a group of positively charged and hydrophobic amino acids[157].

Future work with truncated or mutated versions of MDK may allow us to get a complete picture of the residues responsible for MDK's ability to bind RNA. We are proposing that MDK has a binding preference for a specific structure of RNA, a 42 nt hairpin, consistent with most RBPs having a preference for specific RNA sequences or structures[320, 321].

It should be noted that even though we have shown MDK is capable of binding pre-miR-451 and is physically associated with sEVs (Fig. 4.4, 4.5), this does not completely eliminate the possibility that MDK exerts its role in sEV packaging through a signalling mechanism. We cannot exclude the possibility that secreted MDK interacts with one of its cell-surface receptors and launches a signalling cascade that ultimately leads to pre-miR-451 packaging into sEVs through an unknown mechanism. Future studies expressing MDK without the signal peptide in MDK knockout cells could be used to eliminate this possibility.

This work also indicates that MDK is associated with sEVs (Fig. 4.5). The majority of MDK present in media from cultured cells co-purified with sEVs. Importantly, this was also the case when cells were cultured in media lacking FBS, demonstrating that it is not a contaminant. Some MDK is likely present on the surface of sEVs but a large proportion of the MDK disappeared only in the presence of detergent, suggesting that much of the MDK is inside sEVs or buried within their lipid membrane. The mechanism through which MDK, bound to pre-miR-451, is encapsulated within sEVs remains to be uncovered. However, the literature is pockmarked with examples of proteins containing signal peptides which localize to the cytoplasm or nucleus. This could occur due to alternative splicing variants which lack the signal peptide or inefficiencies in signal peptide processing. Various lines of evidence suggest MDK may have properties of a cell-penetrating peptide that can traverse the plasma membrane to enter cells. MDK has been shown to be internalized by cells following interaction with surface low-density lipoprotein receptor-related

protein (LRP)[308, 309], laminin binding protein precursor (LBP)[322] or nucleolin[310, 323]. Following uptake, in some cases, cytoplasmic MDK is translocated to the nucleus by nucleolin[308, 311]. Alternatively, internalized MDK can remain in the cytoplasm[310, 312] where it interacts with the kinase LKB1 and pseudokinase STRAD to suppress AMP-activated protein kinase (AMPK) activation[312]. In addition, several proteins which are rich in lysines and arginines, like MDK, exhibit cell-penetrating activity[324, 325]. These proteins can traverse the cell membrane from the extracellular space to the cytoplasm. Recently, one of the heparin binding domains of MDK that contains an abundance of lysines and arginines, was used as a cell penetrating peptide (CPP) that, when bound to other proteins, enabled their passage into HeLa and MGC80-3 cells[326]. Furthermore, a recent report demonstrates that supercharging proteins by increasing the abundance of lysines and arginines exposed on their surface allows the proteins to pass through the membrane, and be efficiently loaded into sEVs[327]. MDK contains a similar relative abundance of lysines and arginines as supercharged proteins that can be loaded into sEVs[316, 327], and importantly many of those charged residues are clustered on the surface of the protein[316]. This suggests that MDK can enter the cytoplasm potentially in the manner of a cell-penetrating peptide, binds pre-miR-451 hairpins and sorts them into sEVs.

A number of groups have published work identifying RBPs that are responsible for active packaging of certain miRNA species into sEVs[147-153]. In many of these studies, sequence motifs within the RNA were found to be critical for the RNA sorting by RBPs. We show that MDK is required to sort two distinct miRNA sequences with the same structure into sEVs (Fig. 4.2). We have previously shown that additional RNA sequences incorporated in the pre-miR-451 structure are highly enriched in sEVs[258](chapter 3) suggesting that sequence motifs are not important for MDK to sort the pre-miR-451 hairpins into sEVs. While much work on miRNAs and other RNAs

associated with sEVs has focused on sequences and sequence motifs, our work opens the door for a more thorough investigation of RNA structures that may be actively sorted into sEVs.

As a secreted factor, MDK has been extensively studied for its interaction with a variety of receptors and its role in cancer, inflammation, immunity, angiogenesis, development and cell proliferation[303-306] . Previous work has shown that many different secreted cytokines can be associated with sEVs, either bound to the surface, or found within the lumen[328]. Here we demonstrate that MDK is found within sEVs, suggesting the possibility that encapsulation within sEVs is required for some intercellular effects mediated by MDK. Furthermore, we identify a novel function for MDK; the active sorting of short miRNA hairpins into sEVs though a previously unknown RNA binding capability.

4.5 Materials and Methods

Cell culture

The following cell lines were used: HEK293T (ATCC; catalogue no. CRL-3216), and HEK293T stably expressing SOD1 siRNA in the pre-miR-451 hairpin structure, that we generated previously[258]. All cell culture was performed at 37 °C in 5% CO2 in humidified incubators. Cells were grown in DMEM (Wisent Bioproducts; catalogue no. 319–015-CL; 4.5 g l−1 glucose) with 10% heat-inactivated FBS (Wisent Bioproducts, catalogue no. 080–150) and 1% penicillin-streptomycin (Wisent Bioproducts, catalogue no. 450-201-EL). For production of sEVs, cells were washed once with 1X PBS (Wisent Bioproducts; catalogue no. 311–010-CL) and cultured for up to 72h in sEV-depleted DMEM: DMEM with 10% heat-inactivated FBS and 1% penicillin-streptomycin that was spun at 5,000 g for 30 minutes and subsequently ultracentrifuged at 100,000 g for >2 hours (SW-32Ti rotor, Beckman-Coulter Life Sciences; polycarbonate tubes, catalogue

no. 355631, Beckman-Coulter Life Sciences) prior to being passed through a 0.22 µm bottle-top filtration unit (Thermo-Scientific, catalogue no. 09–741–04).

Biotin-streptavidin pulldown

Biotin-streptavidin pulldown of RBPs was performed using a modified version of a protocol described previously[148]. Briefly, HEK293T cells were washed 3 times in PBS, lysed at room temperature for 10 minutes in hypotonic lysis buffer (10mM Tris, pH 7.4, 20mM KCl, 1.5mM $MgCl_2$, 5mM DTT, 0.5mM EDTA, 5% glycerol, 0.5% NP-40 with protease inhibitor tablets (Millipore Sigma, catalogue no. 4693159001)) and subsequently spun at 10,000 g at 4°C for 10 minutes. Protein was quantified from lysates by colorimetric assay (Bio-Rad) and 250 µg of sample protein was incubated while rotating with 5 nmol synthetic 3'-biotinylated RNA oligonucleotides containing phosphorothioate modifications at the Ago2 cleavage site (Integrated DNA technologies). Table 4.2 contains sequences of synthetic RNA oligonucleotides used in pulldown reactions. Streptavidin Dynabeads (ThermoFisher Scientific, catalogue no. 65601) were blocked in 1 µg/µL yeast RNA extract (Millipore Sigma, catalogue no. R6750) for one hour at 4°C with rotating and 20 µL were then incubated in each pulldown reaction for 90 minutes at 4°C with rotating. Beads were then washed five times with 1 mL of hypotonic lysis buffer and once in PBS using a magnetic stand. Beads were resuspended in a final volume of 25 µL. 10% of the sample was removed for Silver stain and 10% for Western blot analysis and the remainder was prepared for Mass Spectrometry analysis.

Table 4.2. RNA oligos used in biotin-streptavidin pulldown. Related to figure 4.1.

Name	**Sequence with modifications (r-RNA bases, *-phosphorothioate, /3Bio/-3' Biotinylated)**
42 nt miR-451	rArArArCrCrGrUrUrArCrCrArUrUrArCrUrGrArGrUrUrUrArGrUrArArU*rG*rG*rUrArArUrGrGrUrUrCrUrC/3Bio/
42 nt GFP siRNA	rArUrGrArArCrUrUrCrArGrGrGrUrCrArGrCrUrUrGrCrGrCrUrGrArCrC*rC*rU*rGrArArGrUrUrCrArArUrC/3Bio/
22 nt GFP siRNA	rArUrGrArArCrUrUrCrArGrGrGrUrCrArGrCrUrUrGrC/3Bio/
22 nt miR-16	rUrArGrCrArGrCrArCrGrUrArArArUrArUrUrGrGrCrG/3Bio/

Mass spectrometry analysis

Biotin-streptavidin pulldown samples were prepared for Mass spectrometry analysis with an on-bead digestion method. Briefly, a magnetic stand was used to remove liquid from the beads, which were then resuspended in 9 µL of 20mM Tris-HCl pH 8 with 1.6 µL of 25mM DTT and were incubated at room temperature for 30 minutes with gentle shaking. 1.2 µL of 50mM iodoacetamide was added for an additional 10 minutes at room temperature. 10 µL of 100 ng/µL mass-spec grade trypsin (Worthington Biochemical, catalogue no. LS02122) was added to each sample to make a final concentration of 45 ng/µL and was incubated at 37 °C on a rotator overnight (~18 hr). The following day, the beads were removed with a magnetic stand and 500ng of additional trypsin was added to each sample for 4 hours at 37 °C with gentle agitation. Digestion was stopped by adding formic acid (FA) to a final concentration of 2%. Deslating was performed by gravity with Sep-Pak tc18 1cc cartridges (Waters, catalogue no. WAT054960) according to manufacturer instructions. Briefly, cartridges were conditioned in 900 µL of 100% acetonitrile (ACN) followed by 300 µL of 50% ACN, 0.5% acetic acid (HAcO). Cartridges were then equilibrated with 900 µL of 0.1% trifluoroacetic acid (TFA). Samples were adjusted to a final

concentration of 0.4% TFA before being passed through the cartridges. Desalting was performed with 900 µL of 0.1% TFA. Washing was done with 90 µL of 0.5% HAcO and elution with 500 µL of 50% ACN, 0.5% HAcO.

For LCMS Analysis, the Eksigent 2D+ nanoLC system (Dublin, CA) was hooked up with Q-Exactive mass spectrometer (Thermo Electron, Waltham, MA), equipped with a nano-electrospray interface operated in positive ion mode. The solvent system consists of buffer A of 0.1% FA in water, and buffer B of 0.1% FA in 80% ACN. Dried down protein digests were acidified with 0.5% (v/v) formic acid and loaded on a 75 µm I.D. × 150 mm fused silica analytical column packed in-house with 1.9µm ReproSil-Pur C18 beads (100 Å; Dr. Maisch GmbH) at a flow rate of 500 nL/min for 15min. Flow rate was then changed to 200 nL/min to perform the peptide separation in a 1 hour method with a gradient elution set as 5–35% buffer B in 45 min. The spray voltage was set to 2.0 kV and the temperature of heated capillary was 300 °C. The instrument method consisted of one full MS scan from 300 to 1800 m/z followed by data-dependent MS/MS scan of the 12 most intense ions, a dynamic exclusion repeat count of 1 in 30s, and an exclusion duration of 30s. The full mass was scanned in Orbitrap analyzer with R = 70,000 (defined at m/z 400) for MS1 and 17,500 for MS2. To improve the mass accuracy, all the measurements in the orbitrap mass analyzer were performed with a real time internal calibration by the lock mass of background ion 445.120025. The charge state rejection function was enabled, and charge states with unknown and single charge states were excluded for subsequent MS/MS analysis. All data was recorded with Xcalibur software (ThermoFisher Scientific).

The peak lists of the raw files were processed and analyzed with software MaxQuant (Version 1.5.2.8)[329] against the UniProt human protein FASTA database, including commonly observed contaminants. Enzyme specificity was set to trypsin, not allowing for cleavage N-

terminal to proline. Up to two missing cleavages of trypsin were allowed. The precursor ion mass tolerances were 7 ppm, and fragment ion mass tolerance was 20 ppm. Razor and unique peptides were used for LFQ quantification. FDR was set 0.01 on protein, peptide and modification specific site. A minimum length of seven amino acids were used for peptides identification. For protein identification, if the identified peptide sequence of one protein was equal to or contained another protein's peptide set, these two proteins were grouped together by MaxQuant and reported as one protein group.

Silver staining

Silver staining was performed using the GE Healthcare PlusOne Silver Staining Kit, following a modified version of the manufacturer instructions for in-house cast 1mm gels on glass backing, MS compatible. Proteins from pulldown reactions were diluted in 4x Laemmli buffer (Bio-Rad, catalogue no. 161-0747) with 10% 2-mercaptoethanol (Sigma-Aldrich, catalogue no. M3148-100ML) and were incubated for 5 min at 95°C before being loaded on a Mini-PROTEAN TGX Precast Protein Gel (Bio-Rad, catalogue no. 4569033) and run at 150 V. The gel was then moved to a clean glass container and incubations were performed at room temperature with gentle rocking in the following solutions. Fixing solution (30% EtOH, 10% glacial acetic acid) two times for 15 minutes, Sensitizing solution (30% EtOH, 0.2% Sodium thiosulphate (w/v), 6.8% Sodium acetate (w/v)) for 30 minutes, wash solution (distilled water) three times for five minutes, silver solution (0.25% Silver nitrate solution (w/v)) for 20 minutes, wash solution (distilled water) two times for one minute, developing solution (2.5% Sodium carbonate (w/v), 0.03% formaldehyde (w/v)) for as long as required for the desired darkness of bands, stopping solution (1.46% EDTA-Na_2 $2H_2O$ (w/v)) for 10 minutes, and finally washing solution (distilled water) three times for five minutes. Gels were imaged using a Bio-Rad Gel Doc XR+ system.

Western blot

Cell or sEV lysates were diluted in 4x Laemmli buffer (Bio-Rad, catalogue no. 161-0747) with 10% 2-mercaptoethanol (Sigma-Aldrich, catalogue no. M3148-100ML) and were incubated for 5 min at 95°C before being loaded on a 10% polyacrylamide gel. Samples were run at 100 V for 15 minutes followed by 150 V for approximately 1 hour and were then transferred to a PVDF membrane (Millipore Sigma, catalogue no. IPVH00010) using a wet transfer system (Bio-Rad) at 100 V for 1.5 hours at room temperature. The membrane was blocked in 5% skimmed milk (Santa Cruz Biotechnology, catalogue no. sc-2324) in TBST for 1 hour. The membrane was then incubated with primary antibodies diluted in TBST overnight at 4°C and washed three times (10 minutes each) with TBST. Incubation with secondary antibodies diluted at 1:7500 in TBST was done at room temperature for 1 hour. Finally, membranes were washed 3 times (10 minutes each) in TBST and incubated with ECL Western HRP Chemiluminescence Substrates Crescendo (Fisher Scientific, catalogue no. WBLUR0500). The chemiluminescence signal was recorded using a GE ImageQuant LAS4010 system. The membrane was stripped using 0.2N NaOH for 30mins when necessary. Table 4.3 lists the antibodies used.

Table 4.3. List of antibodies used for Western blots

Antibody	**Company**	**Catalogue Number**
β-Actin	Sigma-Aldrich	A5441
α-Tubulin	Sigma-Aldrich	T6199
HuR	Santa Cruz Biotechnology	sc-5261
Ago2	Cell Signaling Technology	2897S
Ago1	Cell Signaling Technology	5053S
Ybx-1	Cell Signaling Technology	9744S
hnRNPa2b1	Abcam	ab31645
TRBP	Abcam	ab42018-100
AIMP2	Proteintech	10424-1-AP
Midkine	Abcam	ab52637
Flotillin2	Cell Signaling Technology	3436S
Tsg101	Genetex	GTX70255

Syntenin-1	Abcam	ab133267
Calnexin	Cell Signaling Technology	2679S
Alix	EMD Millipore	ABC40
Drosha	Cell Signaling Technology	3364S
Anti-Mouse HRP	Jackson ImmunoResearch	115-035-174
Anti-Rabbit HRP	Jackson ImmunoResearch	115-0.35-144

sEV isolation by differential ultracentrifugation

Conditioned media was centrifuged at 300 g for 10 min and supernatants were subsequently centrifuged at 2,000 g for 10 min and 10,000 g for 30 min in 15 mL or 50 mL conical tubes. Supernatants were then poured into ultracentrifuge tubes (Beckman-Coulter Life Sciences catalogue no. 355631 or 331372) and ultracentrifuged at 100,000 g for 2 h (SW-32Ti or SW-41Ti rotor, Beckman-Coulter Life Sciences). sEV pellets were washed by resuspending in 1 ml 1X PBS (Wisent Bioproducts; catalogue no. 311–010-CL) and finally ultracentrifuged at 100,000 g for 30 min (TLA-100.3 rotor, Beckman-Coulter Life Sciences; polypropylene microfuge tubes, catalogue no. 357448, Beckman-Coulter Life Sciences). sEVs pellets were resuspended in 1X PBS.

sEV isolation by tangential flow filtration

Conditioned media was centrifuged at 300 g for 10 min and supernatants were subsequently centrifuged at 2,000 g for 10 min. Supernatants were passed through a 0.22 μm filter (Thermo-Scientific, catalogue no. 09–741–04) and loaded into a bioprocess sample bag (Sartorius Stedim, catalogue no. FFB103547) for TFF concentration. Samples were concentrated 10x using the KR2i tangential flow filtration system (Repligen) with a 75 cm2 modified polyethersulfone hollow fiber column with 500 kDa cut-off (Repligen, catalogue no. D02-E500- 10-S) at a flow rate of 140 ml min−1 and transmembrane pressure 2.5 psi to achieve a shear rate of 2,000 s−1. The concentrated

media underwent 10X buffer exchange in PlasmaLyte A (Baxter, catalogue no. JB2544) to reach a final volume of ~12 mL.

Measurement of miRNA levels in sEVs

RNA was prepared from sEVs using TRIzol reagent (ThermoFisher Scientific, catalogue no. 15596018) as described by the manufacturer, and using 15 μg of GlycoBlue coprecipitant (ThermoFisher Scientific, catalogue no. AM9515) as a carrier in the alcohol precipitation step. RNA was quantified by spectrophotometry and 100 ng were added to a reverse transcription reaction using the miScript II microRNA reverse transcription kit using the Flex buffer option (Qiagen, catalogue no. 218161). Reverse transcription was performed as described by the manufacturer using the miScript SYBR Green PCR kit (Qiagen, catalogue no. 218075). qPCR was performed using the miScript qPCR kit (Qiagen, catalogue no. 218076) on a Bio-Rad CFX-384 instrument using 12.5 μL reaction volumes. Reactions proceeded for 50 cycling steps with melting temperature of 55°C. Relative miRNA levels in sEVs were measured using the ΔΔCt method comparing query miRNA (miR-451 and SOD1 siRNA) levels in sEVs from treated versus control groups relative to miR-16 or U6 reference levels. Table 4.4 contains primer sequences for RT-qPCR.

Measurement of cellular expression levels

RNA was prepared from sEVs using TRIzol reagent (ThermoFisher Scientific, catalogue no. 15596018) as described by the manufacturer, and using 15 μg of GlycoBlue coprecipitant (ThermoFisher Scientific, catalogue no. AM9515) as a carrier in the alcohol precipitation step. RNA was quantified by spectrophotometry and 250 ng were added to a reverse transcription reaction using the M-MuLV enzyme (NEB, catalogue no. M0253S) and 18 nt oligoDT primer

(Integrated DNA technologies, custom synthesis). qPCR was performed using the GoTaq system (Promega) on a Bio-Rad CFX-384 instrument using 10 µL reaction volumes. Reactions proceeded for 40 cycling steps with melting temperature of 60°C. Relative expression level was measured using the ΔΔCt method comparing query mRNA (Midkine) levels in cells from treated versus control groups relative to Actin and Gapdh reference levels. Table 4.4 contains primer sequences for RT-qPCR.

Table 4.4. RT-qPCR primers

Primer target	**Sequence (5'-3')**
miR-451	aaaccgttaccattactgagtt
SOD1 siRNA	ttcagtcagtcctttaatgctt
miR-16	tagcagcacgtaaatattggcg
U6	ttcgtgaagcgttccatatttt
Midkine Forward	caaagcaaaggccaaagccaaga
Midkine Reverse	ggcactggtgggtcacatct
Actin Forward	accacaccttctacaatgagc
Actin Reverse	gatagcacagcctggatagc
Gapdh Forward	tgttgccatcaatgacccctt
Gapdh Reverse	ctccacgacgtactcagcg

siRNA sEV sorting experiments

On day one, $2.5x10^6$ HEK293T cells stably expressing SOD1 siRNA in the pre-miR-451 hairpin structure were plated in 10 cm dishes. The following day, Silencer siRNAs (ThermoFisher Scientific) against one or more candidate proteins, or a negative control scrambled siRNA (ThermoFisher, catalogue no. AM4635) were transfected into the cells using Lipofectamine RNAiMax transfection reagent (ThermoFisher, catalogue no. 13778150) according to manufacturers instructions to a final siRNA concentration of 10 nM. Table 4.5 contains assay IDs for all Silencer siRNAs used in sorting experiments. On day three, media was removed and replaced with sEV-depleted complete DMEM following one wash with 1x PBS. On day four,

media was collected into conical tubes and additional sEV-depleted complete DMEM was added to the plates. On day five, a second media collection was performed and conditioned media were processed through differential ultracentrifugation to isolate sEVs, as described. From each sample, half of the cells were treated with TRIzol reagent for RNA isolation and RT-qPCR analysis and half were lysed (5 mM Tris pH 7.4, 75 mM NaCl, 0.5 mM EDTA, 0.5% Triton X-100) for Western blot. Isolated sEVs were analyzed by nanoparticle tracking analysis, Western blot and RT-qPCR, as described.

Table 4.5. Silencer siRNAs used in sEV sorting studies

Gene Name	**Assay ID (ThermoFisher Scientific)**
ACTB	103857
ADAR	119581
AIMP1	15279
AIMP2	126664
Ashwin	30709
BANF1	6520
DARS	117859
EEF1D	42605
EEF1E1	14464
EPRS	14634
GTF2I	289315
IARS	117878
IGF2BP2	18173
KARS	16507
LARS	28076
MDK	11558
MTDH	128411
MYH10	241476
MYH9	118368
MYL12A	289595
MYL6	118416
MYO18A	290349
NPM1	284660
PARP1	111001
PRDX1	11838
PRPF19	147530
PTBP1	142383
RARS	43343
SLC25A5	119898

SND1	108541
SRP14	142736
SRP9	12893
STAU1	24977
TANC2	263521
TRIM25	118749
YTHDF2	122895

Retinoic acid sEV sorting experiments

sEV sorting experiments with retinoic acid were performed similarly to those performed with siRNA transfection. On day one, $2.5x10^6$ HEK293T cells stably expressing SOD1 siRNA in the pre-miR-451 hairpin structure were plated in 10 cm dishes. The following day, retinoic acid was added to plates to a final concentration of 10 μM. On day three, media was removed and replaced with sEV-depleted complete DMEM with 10 μM retinoic acid following one wash with 1x PBS. On day four, media was collected into conical tubes and additional sEV-depleted complete DMEM with 10 μM retinoic acid was added to the plates. On day five, a second media collection was performed. Cells and conditioned media were processed in the same manner as in the siRNA sEV sorting experiments described above.

MDK overexpression sEV sorting experiments

An inducible Midkine overexpression plasmid was created as a service at the uOttawa Genomic Editing and Molecular biology (GEM) facility by gateway cloning the ORF from the MGC premier human ORFeome Collaboration library into the pINDUCER20 plasmid. On day one, $2.5x10^6$ HEK293T cells stably expressing SOD1 siRNA in the pre-miR-451 hairpin structure were plated in 10 cm dishes. The following day, the inducible MDK overexpression plasmid was transfected into cells using Lipofectamine 2000 transfection reagent (ThermoFisher Scientific, catalogue no. 11668-019) following manufacturer instructions. MDK overexpression was induced

the following day by adding doxycycline to a final concentration of 250 ng/mL. The following day, media was removed and replaced with sEV-depleted complete DMEM with 250 ng/mL doxycycline following one wash with 1x PBS. On day five, media was collected into conical tubes and additional sEV-depleted complete DMEM with 250 ng/mL μM doxycycline was added to the plates. On day six, a second media collection was performed. Cells and conditioned media were processed in the same manner as in the siRNA sEV sorting experiments described above.

Nanoparticle tracking analysis

Nanoparticle tracking analysis was performed on a ZetaView PMX-110 (ParticleMetrix). The instrument was calibrated for experiments following every instrument start-up. Focusing and alignment were performed automatically using 100 nm polystyrene beads (Polysciences, catalogue no. 00876-15). sEV samples were diluted in PBS into the range determined by the instrument to be accurate for measurement. One milliliter of the sample was injected into the machine and allowed to equilibrate until it reached an acceptable level according to the built-in particle-drift sensor. Once the sample fell within the acceptable concentration range, video acquisition and analysis were performed using the following pre-acquisition parameters: Sensitivity 85, shutter speed 40, frame rate 30 fps, resolution highest, camera gain 770, positions measured 11, and the following post-acquisition parameters: minimum brightness 15, minimum size 10 pixels, maximum size 500 pixels. Undiluted concentration and median size based on concentration are reported.

Proteinase K/detergent experiments

sEVs for proteinase K/detergent experiments were produced via tangential flow filtration. 140 μg of sEV protein was added into two tubes. One tube received Triton X-100 and SDS to a

final concentration of 0.5% each. The other tube, the "no detergent" tube received an equivalent volume of PBS. Tubes were incubated at room temperature for five minutes, then split into seven tubes each such that each tube contained 20 µg of TFF-prepared sEVs. Tubes received proteinase K (ThermoFisher Scientific, catalogue no. AM2546) to a final concentration of 0, 0.25, 0.5, 1, 2, 10 or 100 µg/mL. Proteinase K digestion was performed at 37 °C for ten minutes and was stopped by adding PMSF to a final concentration of 5 mM for 10 minutes at room temperature. Samples were then prepared for Western blot as described.

Density gradients

Optiprep gradients were performed as described previously[289]. Briefly, 1 mL of TFF-purified sEVs were mixed with 3 mL of 60% iodixanol (Millipore Sigma, catalogue no. D1556-250ML) and this solution was added to the bottom of a 12 mL ultracentrifuge tube. Iodixanol solutions of 30% (3 mL), 23% (2 mL) and 18% (2 mL) were layered on top, and finally 2 mL of PBS was added to the top of the gradient. Tubes were ultracentrifuged for 16 h at 150,000 g in a SW41Ti swinging bucket rotor (Beckman-Coulter). Eleven fractions were collected following the spin. Density of all fractions was measured using a refractometer. Half of each fraction was taken through RNA isolation by TRIzol and RT-qPCR as described to quantify miR-451 levels. The other half of the fraction was diluted in 30 mL of PBS and ultracentrifuged in a SW32Ti swinging bucket rotor (Beckman-Coulter) for two hours at 100,000 g and sEV pellets were analyzed by Western blot, as described.

RNA immunoprecipitation

~80% confluent cells were washed twice in ice-cold PBS and were lysed in IP lysis buffer (50 mM Tris pH 7.5, 150 mM NaCl, 1% NP-40, protease inhibitor tablet (Millipore Sigma,

catalogue no. 4693159001)). Lysed cells were scraped from plates using a cell scraper and tumbled for 20 minutes at 4°C. Lysates were then spun at 5000 g for 10 minutes and supernatants were transferred to new tubes. To pre-clear the lysates, 10 µL of Protein G Dynabeads (ThermoFisher Scientific, catalogue no. 10004D) were washed three times in 500 µL wash buffer (50 mM Tris pH 7.5, 150 mM NaCl, 0.1% NP-40), were resuspended in 100 µL wash buffer and were added to the spun lysates, which were tumbled for 20 minutes at 4°C. Protein concentration was estimated by colorimetric assay (Bio-Rad) and 1000 µg of protein was added to two tubes per sample, one for MDK IP, and one for IgG control IP. 1 µg of antibody (Midkine: Abcam, catalogue no. ab52637, Rabbit IgG: GeneTex, catalogue no. GTX35035) was added and tubes were tumbled for 3 hours at 4°C. 20 µL of beads per sample were then washed three times in cold wash buffer and were added to the antibody tubes for an additional one hour. Supernatants were then removed from the tubes and the beads were washed four times in cold wash buffer, tumbling for five minutes at 4°C for each wash step. 10% of the sample was then prepared for Western Blot analysis, as described, and the remainder was taken through TRIzol RNA isolation and RT-qPCR, as described.

Crosslinking Western blots

Cells were grown to ~80% confluence in 15 cm plates. For UV crosslinking, cells were washed twice in ice-cold PBS and 6 mL of ice-cold PBS was added to plates prior to irradiation with 600 mJ three times. Cells were removed from the plates using a cell scraper and centrifuged at 22,000 g for 10 seconds. Pellets were resuspended in 500 µL of lysis buffer (5 mM Tris pH 7.4, 75 mM NaCl, 0.5 mM EDTA, 0.5% Triton X-100) and 5 µL of RNaseA (ThermoFisher Scientific, catalogue no. EN0531) was added to the high RNase sample, and 5 µL of a 1/10 dilution of RNase was added to the low RNase sample. Samples were incubated for 10 minutes at 37 °C and then

centrifuged at 22,000 g for 10 minutes. Protein was quantified by colorimetric assay (Bio-Rad) and 10 µg of protein per sample was prepared for Western blot, as described.

Crosslinking Immunoprecipitation (CLIP)

CLIP experiments were performed following the previously published iCLIP protocol[330]. Cells were grown to ~80% confluence in 15 cm plates. For UV crosslinking, cells were washed twice in ice-cold PBS and 6 mL of ice-cold PBS was added to plates prior to irradiation with 150 mJ/cm^2 at 254 nm in a Fisherbrand UV Crosslinker (Fisher Scientific). Cells were then scraped into tubes and spun at 500 g for one minute and were resuspended in 1 mL of lysis buffer (50 mM Tris pH 7.5, 100 mM NaCl, 1% Tergitol, 0.1% SDS, 0.5% sodium deoxycholate, protease inhibitor tablet). 2 µL of DNase (Promega, catalogue no. M610A) was added to each tube and increasing amounts of RNase was added to the appropriate samples. Low RNase consisted of 10 µL of a 1/250 dilution of RNaseA (ThermoFisher Scientific, catalogue no. EN0531), while high RNase concentration consisted of 10 µL of a 1/50 dilution and the highest concentration, 10 µL undiluted RNaseA. Samples were incubated at 37 °C for three minutes with shaking and were then placed on ice. They were then centrifuged for 10 minutes at 22,000 g at 4°C and supernatants were collected into new tubes. 100 µg of Protein G Dynabeads (ThermoFisher Scientific, catalogue no. 10004D) were washed twice with lysis buffer and resuspended in 100 µL of lysis buffer with 1 µg of antibody (Midkine: Abcam, catalogue no. ab52637, HuR: Santa Cruz Biotechnology, catalogue no. sc-5261) and tumbled for 30 minutes at room temperate before being washed an additional three times in lysis buffer. Beads were then added to the lysates and rotated at room temperature for one hour, then placed on a magnetic stand and washed twice in high salt wash buffer (50 mM Tris pH 7.5, 1 M NaCl, 1 mM EDTA, 1% tergitol, 0.1% SDS, 0.5% sodium deoxycholate) and twice in PNK buffer (20 mM Tris pH 7.5, 10 mM $MgCl_2$, 0.2% Tween-20) for 5 minutes each

with tumbling at 4°C. 20% of the beads were then radiolabeled in hot PNK solution (0.2 µL PNK, 0.4 µL γ-^{32}P-ATP, 0.4 µL 10x T4 PNK buffer, 3 µL H_2O) for five minutes at 37 °C with shaking. Supernatants were then discarded, 20 µL of 1x NuPAGE loading buffer (ThermoFisher Scientific, catalogue no. NP0007) was added to the beads and this mixture was then added to the remaining cold beads, incubated at 70°C for five minutes and loaded into a 4-12% NuPAGE Bis-Tris gel (ThermoFisher Scientific, catalogue no. NP0321BOX). Gels were run at 180 V for 50 minutes in 1x MOPS running buffer (ThermoFisher Scientific, catalogue no. NP0001) before being transferred to a Protran Nitrocellulose membrane at 30 V for 70 minutes. Membranes were wrapped in plastic and exposed to an X-ray film (Denville Scientific, catalogue no. DV-E3018) for up to two weeks. Films were developed in a Konica Minolta SRX-101A film processor.

Electrophoretic mobility shift assay

Probes were radiolabelled in the following reaction: 1 µL RNA (100pmol), 2 µL 10x T4 PNK buffer, 8 µL γ-^{32}P-ATP, 2 µL T4 PNK, 7 µL H_2O for 30 minutes at 37 °C. Hot probes were measured by Geiger counter and 20,000 cpm was added into a binding reaction with 10 µL 2X binding buffer (20 mM Tris pH 7.4, 1 mM EDTA, 100 mM KCl, 1 mM DTT, 5% glycerol), 120 ng of recombinant protein (Midkine: R&D Systems, catalogue no. 258-MD-010, HuR: made in-house) and 7 µL of H_2O. Binding reactions were incubated for 30 minutes at room temperature while 4% acrylamide:bisacrylamid (29:1) gels were pre-run for one hour at 90 V. 2.5 µL of sample loading buffer (100 mM Tris pH 7.4, 10 mM EDTA, 50% glycerol, 0.1% Xylene cyanol, 0.1% bromophenol blue) was added to the binding reactions and 10 µL was loaded into the pre-run gel. Electrophoresis was run for 30 minutes at 100 V in 1X TBE. Gels were dried onto Whatman 3MM filter paper in a Bio-Rad Model 583 gel dryer for two hours and were exposed to X-ray film for

24 hours and for two weeks. Films were developed in a Konica Minolta SRX-101A film processor. Table 4.6 lists the RNA probes used in gel shift experiments.

Table 4.6. RNA probes used in gel shift experiments

RNA probe	Sequence 5'-3' (r-RNA bases, *-phosphorothioate, /3Bio/-3' Biotinylated)
42 nt GFP siRNA	rArUrGrArArCrUrUrCrArGrGrGrUrCrArGrCrUrUrGrCrGrCrUrGrArCrC*rC*rU*rGrArArGrUrUrCrArArUrC/3Bio/
22 nt GFP siRNA	rArUrGrArArCrUrUrCrArGrGrGrUrCrArGrCrUrUrGrC/3Bio/
70 nt GFP siRNA	rUrUrGrGrGrArArUrGrGrCrArArGrGrArUrGrArArCrUrUrCrArGrGrGrUrCrArGrCrUrUrGrCrGrUrUrGrArCrC*rC*rU*rGrArArGrUrUrCrArArUrCrUrUrGrCrUrArUrArCrCrCrArG/3Bio/
polyU	rUrUrUrUrUrUrUrUrUrUrUrUrUrUrU
scramble	rArCrGrUrGrArCrCrUrArArCrGrUrCrA

Immunofluorescence microscopy

U-2 OS cells were transfected with Silencer siRNAs targeting MDK (ThermoFisher scientific, assay ID 11558) or a negative control scrambled siRNA (ThermoFisher Scientific, catalogue no. AM4635) using Lipofectamine RNAiMax transfection reagent (ThermoFisher, catalogue no. 13778150) according to manufacturers instructions for reverse transfection to a final siRNA concentration of 10 nM. Immunofluorescence experiments were carried out 72-hours post-transfection. For transient transfection with DNA, Lipofectamine2000 (ThermoFisher Scientific, catalogue no. 11668-019) was used to reverse transfect 1.6 µg pT7-EGFP-C1-HsDCP1a plasmid DNA according to manufacturers instructions. Media was changed 4-hours post-transfection and immunofluorescence experiments were carried out 48-hours post-transfection. pT7-EGFP-C1-HsDCP1a was a gift from Elisa Izaurralde (Addgene plasmid # 25030 ; http://n2t.net/addgene:25030 ; RRID:Addgene_25030)[331].

For immunofluorescence, U-2 OS cells were seeded onto #1.5 coverslips in a 12-well plate at density of 1.2 x 10^6 cells/mL and allowed to rest overnight. The following day, coverslips were fixed with 4% formaldehyde for 10 minutes at room temperature. Coverslips were then rinsed with PBS and permeabilized with 0.2% Triton X-100 with 2mM NH_4Cl_2 for 10 minutes and blocked with 10% goat serum albumin for 1 hour at room temperature. Coverslips were incubated with primary antibody for 1 hour at room temperature [rabbit anti-MDK (1:50, Abcam, catalogue no. ab52637), mouse anti-β-actin (1:500, Sigma Aldrich, catalogue no. A5441-100UL), mouse anti-CD63 (1:100, Santa Cruz Biotechnology, catalogue no. sc-5275)]. Secondary antibodies [Alexa Fluor anti-rabbit-IgG 488 (1:750, ThermoFisher Scientific, catalogue no. A11034), Alexa Fluor anti-mouse 546 (1:750, ThermoFisher Scientific, catalogue no. A11030)] were incubated on coverslips for 1 hour in the dark at room temperature. Coverslips were then mounted onto slides with Vectashield mounting medium containing 4'-6' diamidino-2-phenylindole (DAPI) (Vector Laboratories, catalogue no. H1200-10). Fluorescence images were obtained using a Zeiss LSM 880 Confocal Laser Scanning microscope. Z-stacks were acquired at 40X magnification and projected into 2D maximum intensity projection images using Zeiss Zen Black software. A minimum of five fields of view were obtained per condition. 3D renderings of Z-stacks were acquired using Imaris software.

Statistics

Sample size is noted in the figure legends with n denoting measurements taken from distinct samples. Statistical analyses performed are listed in figure legends and were calculated in GraphPad Prism. In cases where two groups are compared, a two-tailed, unpaired t-test with Welch's correction was performed. Where more than two groups were compared, an ordinary One-

or Two-Way ANOVA Holm-Šídák's multiple comparisons test was performed. Significant P values are shown. Error bars indicate s.e.m.

4.6 Acknowledgements

The authors acknowledge the University of Ottawa Faculty of Medicine Cell Biology and Image Acquisition core facility, the University of Ottawa Faculty of Medicine Genome Editing and Molecular biology Facility and the University of Ottawa Proteomics Resource Center. We would specifically like to thank Dr. Zhibin Ning for his guidance with mass spectrometry sample preparation and analysis.

Funding

This work was funded through a Natural Sciences and Engineering Research Council of Canada (NSERC) Postgraduate Scholarship-Doctoral to RR and NSERC Discovery grant and NSERC Discovery Accelerator Supplement to DG.

Author Contributions

RR performed all non-microscopy experiments, analyzed and visualized data, and wrote the manuscript. CM performed IF microscopy experiments, image acquisition and analysis. ON made recombinant HuB protein and assisted with EMSA experiments. DG conceptualized the study and reviewed and edited the manuscript.

Competing Interests

DG is an inventor on a filed patent that claims the use of the pre-miR-451 backbone for the enrichment of small RNAs in sEVs. The remaining authors declare no competing interests.

Data and materials availability

Data supporting the results of this study are available within the paper and its Supplementary Information. Raw and analysed datasets can be obtained for research purposes from the corresponding author on reasonable request.

4.7 Supplementary Figures

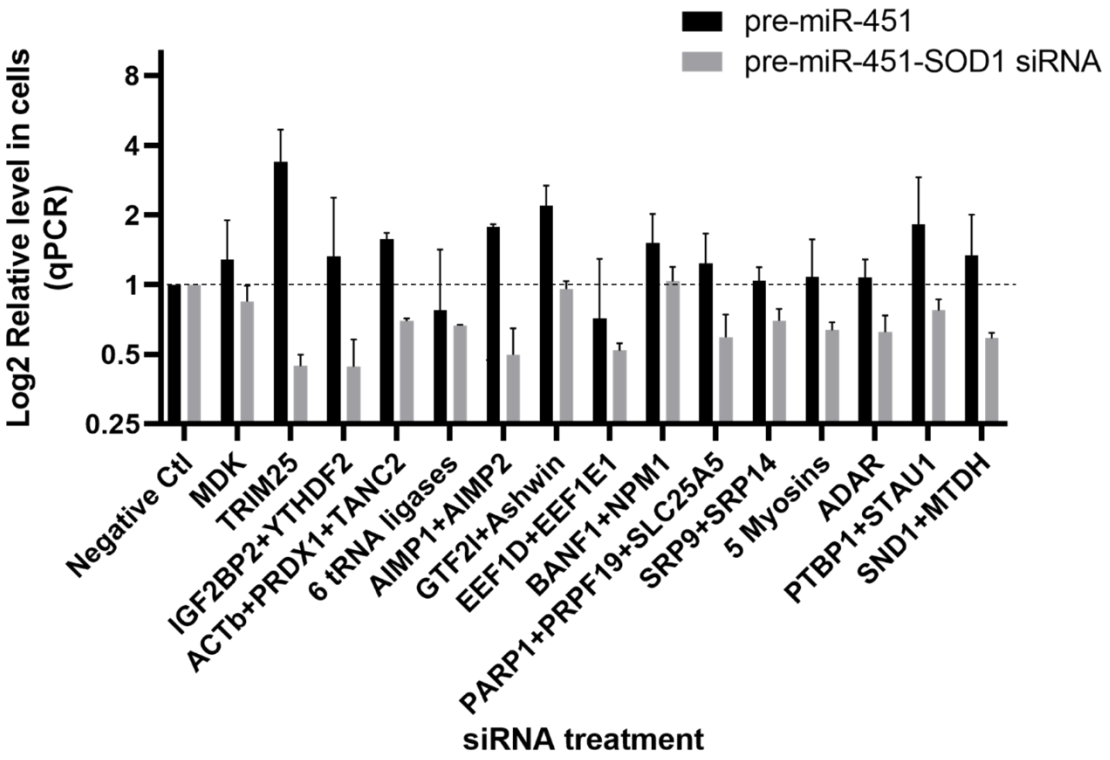

Supplementary Fig. 4.1. Cellular levels of pre-miR-451 species following siRNA knockdown of candidate RBPs. HEK293T cells that express SOD1 siRNA in the pre-miR-451 hairpin structure were transfected with siRNA against sets of RBPs, leading to increases or decreases of cellular pre-miR-451 species, quantified by RT-qPCR, that do not correlate with changes in sEV levels in Fig. 4.2a (n=3).

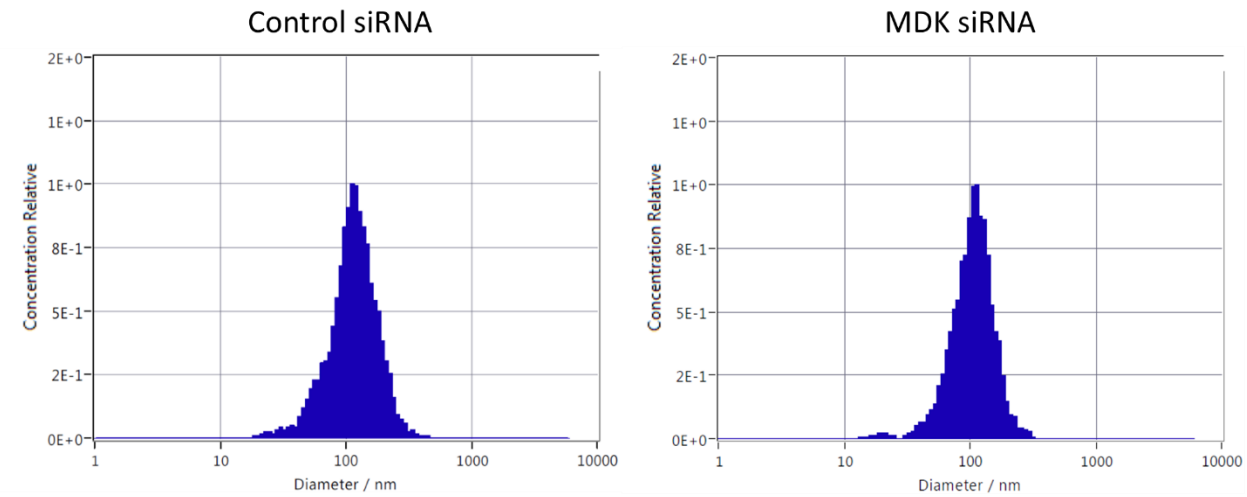

Supplementary Fig. 4.2. ZetaView NTA size histograms related to Fig. 4.2. Size histograms produced by the Zetaview NTA instrument show similar size distributions and peaks of sEVs from HEK293T cells transfected with control (left) or MDK (right) siRNA.

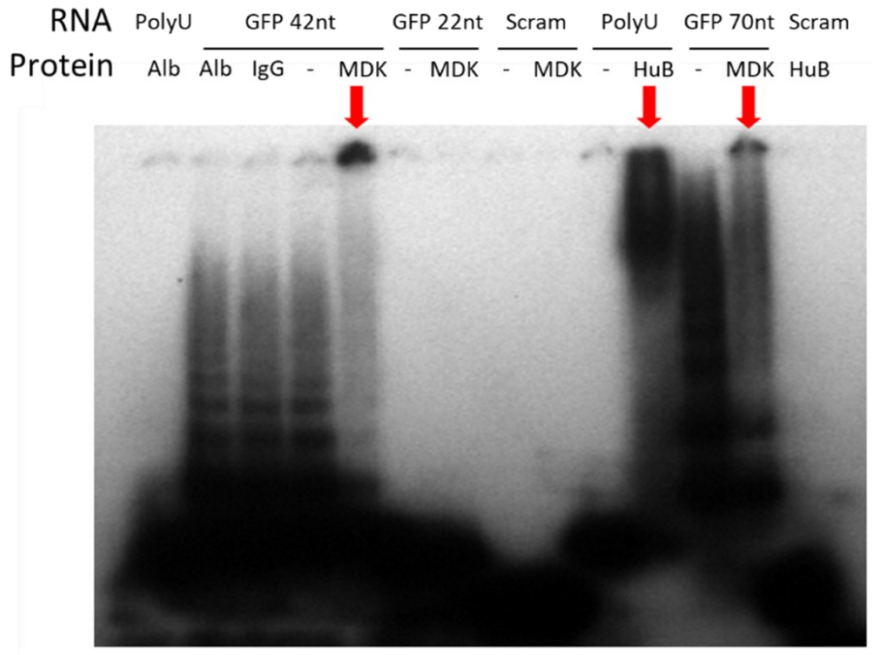

Supplementary Fig. 4.3. Darker exposure of RNA EMSA from Fig. 4.5. RNA EMSA from Fig. 4.5f subject to additional exposure to show shifted bands more clearly in the indicated lanes.

Chapter 5 - General Discussion

The three manuscripts that comprise this thesis, chapters 2, 3, and 4 respectively, each focus on a different angle of the same story: packaging siRNA into sEVs by reprogramming pre-miR-451 to create a potential novel therapeutic. Chapter two demonstrates the feasibility of packaging siRNA into sEVs by harnessing the natural propensity for pre-miR-451 to be sorted into sEVs, and compares sEVs loaded with siRNA in this fashion to competing technologies. Chapter three explores manufacturing, safety, and scalability of these sEVs and their efficacy in pre-clinical models of kidney disease. Finally, chapter four examines the mechanism that facilitates pre-miR-451 packaging into sEVs and uncovers a novel RBP that is involved in the process.

Pre-miR-451 reprogramming provides a platform that should enable the packaging of virtually any siRNA sequence into sEVs. This could, in theory, allow for the production of new therapeutics for a myriad of previously untreatable genetic disorders, provided that sEVs are able to deliver those siRNAs into the cells that express disease-associated mRNAs. With that in mind, it is important to position this technology in the context of the overall siRNA therapeutic landscape.

5.1 sEVs loaded with siRNA via the pre-miR-451 hairpin versus other RNA and sEV technologies

There are multiple siRNA therapeutics currently on the market, in clinical trials and in pre-clinical development based on GalNAc conjugation and LNP encapsulation. Furthermore, various technologies for loading siRNAs into sEVs are emerging and moving rapidly toward the clinic. Here, sEVs loaded with siRNA using the pre-miR-451 hairpin are compared with the leading competition in terms of their ability to reduce target expression, safety profiles and ability to function in tissues and cells of interest.

5.1.1 siRNA loading and delivery

sEVs loaded with siRNA using the pre-miR-451 hairpin contain approximately 1-30 copies of siRNA per sEV, when accounting for RNA recovery (Fig. 2.2g, Supplementary Fig. 2.4c), which is in line with the most abundant, naturally occurring, miRNAs in sEVs shown here (Fig. 2.1d) and elsewhere[199]. Notably, it is possible to load a significantly higher number of siRNAs into each sEV using other loading strategies than is achievable with pre-miR-451 reprogramming. For example, a recent study showed that cholesterol-mediated loading of siRNA into previously purified sEVs allows for up to 18,000 siRNA copies to be loaded into each sEV[191]. However, having a drastically increased number of siRNA present per vesicle is only useful if they can be successfully delivered into the cytoplasm of target cells. Work with sEVs loaded with siRNA using cholesterol modification showed that sEVs containing 3,000 siRNAs per vesicle delivered cargoes more effectively than those containing 18,000 siRNAs[191]. When dosing those sEVs containing 3,000 siRNA per vesicle onto recipient cells *in vitro*, approximately 240,000 siRNAs per cell had to be delivered to reach target knockdown of about 50%[191]. In contrast, here we show that it takes 1,000-30,000 siRNAs, carried by sEVs loaded via the pre-miR-451 hairpin, to knock down targets *in vitro* by 50%, suggesting delivery by pre-miR-451 hairpin-loaded sEVs is roughly 10 to 200 times more efficient (Fig. 2.3). This improved delivery efficiency can likely be attributed to the fact that siRNA loading via the pre-miR-451 hairpin does not require any modification to the sEVs following isolation. In other words, the protein and lipid content and arrangement of their surface remains in the natural state that has evolved over time to make sEVs such an efficient intercellular delivery vehicle.

Similarly, sEVs can be loaded with significant amounts of siRNA using electroporation[181, 182]. Electroporation causes aggregation of sEVs and of naked siRNA which leads to difficulties in

deconvoluting the effects of aggregated siRNAs versus those contained within sEVs[195]. Further to this, we performed a head-to-head comparison of sEVs loaded with siRNA via the pre-miR-451 backbone or through electroporation. sEVs loaded via electroporation were unable to reduce targets in mouse liver (Fig. 2.5e) at the same dose that allowed sEVs loaded via the pre-miR-451 hairpin to reach 50% target knock down (Fig. 2.5a). In a similar experiment, sEVs loaded via the pre-miR-451 hairpin that were able to reduce targets in mouse liver and small intestine, lost their function following electroporation with published conditions[181] (Fig. 2.5i, j). Again, this data suggests that any perturbation of the sEV membrane likely inhibits functional delivery of cargoes due to alterations to the lipids of the membrane and the proteins found there; an issue not encountered when loading sEVs using the pre-miR-451 hairpin. Nevertheless, a novel therapeutic based on siRNA-loaded sEVs using electroporation is currently in clinical trials[194]. Results associated with this therapeutic show successful reduction of tumour size and metastasis as well as increased survival in multiple pancreatic cancer models[181, 187], however results presented here suggest that the siRNA dose required using this technology is likely significantly higher than what could be achieved via the pre-miR-451 hairpin, though we have not specifically explored therapeutic delivery in the pancreas.

Another siRNA loading technology, LNP encapsulation, was used for the development of the first FDA approved siRNA therapeutic, Onpattro. Here, we experimentally compared sEVs loaded via the pre-miR-451 hairpin against C12-200 LNPs (Fig. 2.5d). An siRNA dose 10-300 times higher was required to elicit similar levels of knock down when administered via LNP, demonstrating the improved delivery ability of sEVs. Similarly, we injected sEVs loaded with siRNA against *Ttr*, the mRNA target of Onpattro, and obtained similar levels of knockdown achieved by Onpattro, while using siRNA doses at least three orders of magnitude lower[47] (Fig.

2.8c, d). This finding is in agreement with previous studies that show sEVs are internalized by recipient cells more efficiently than LNPs[332] and confirms the hypothesis that they deliver their cargoes into the cytoplasm more efficiently than LNPs, which enable less than 1% of their RNA cargoes to enter the cytoplasm[218].

While we did not perform a direct experimental comparison with GalNAc-conjugated siRNAs or ASOs, similar conclusions can be drawn from the published literature. siRNA doses ranging from 0.5-300 mg kg^{-1} of GalNAc-conjugated siRNAs were required to achieve clinically relevant levels of target knockdown in the liver in multiple studies, as opposed to 10-300 ng kg^{-1} doses required with sEVs loaded via the pre-miR-451 hairpin seen here[74, 78, 333]. To compare efficacy of sEVs with ASOs, we dosed sEVs containing siRNA against *APOL1* into the same podocyte-specific *G2APOL1* mice that have previously been used in studies using ASOs[215]. In one study, to model treatment in animals with pre-established kidney disease, *APOL1* transgene expression was induced via doxycycline diet three days prior to ASO treatment. Animals were injected with 50 mg kg^{-1} ASO doses on days 3, 6 and 9 prior to euthanasia on day 10 following the start of doxycycline diet. *APOL1* mRNA expression in the kidney was reduced by ~50% and urine albumin/creatinine ratio and serum BUN levels were reduced by ~40% and 25%, respectively[215]. In our study using the same mouse model, sEV doses of 10-300 ng kg^{-1} were injected into mice on days 2, 3, 9, 10, 16 and 17 after commencing doxycycline diet and euthanasia was on day 22 (Fig. 3.4a). *APOL1* mRNA expression in the kidney was reduced by >90% and urine albumin/creatinine ratio and serum BUN levels were reduced by >90% and ~60%, respectively (Fig. 3.4c, g). While significant target reduction and improved kidney function metrics were achieved in both studies, and though study designs were not identical, superior effects

were obtained with sEVs using siRNA doses several orders of magnitude lower, demonstrating their improved functionality.

Results presented here demonstrate that sEVs loaded via the pre-miR-451 hairpin deliver siRNA into the liver more effectively than LNPs, and suggest the same is true for GalNAc conjugates. Meanwhile, based on their size, structure and/or modes of action, both LNP-encapsulated- and GalNAc conjugated siRNAs are currently only able to deliver siRNA into cells in the liver. Our work confirms other recent studies that injected sEVs from multiple cell types can distribute to a wide range of organs including the liver, spleen, lungs, kidney, heart, and intestines amongst others[180] (Fig. 2.4a, b, Fig. 3.2e). We have shown that sEVs can deliver functional siRNA to reduce targets in multiple organs beyond the liver including the small intestine (Fig. 2.4 c, d, Fig. 2.5 b, Fig. 2.7a-c) and the kidney (Fig. 2.7, Fig. 3.3-3.7), a feat that current FDA-approved siRNA therapeutics have not achieved to date, and this can be accomplished with significantly lower doses than required with other RNA therapeutics such as ASOs.

5.1.2 Safety

The requirement for higher siRNA doses to achieve target knockdown associated with the aforementioned delivery technologies can pose safety concerns. For example, there was a problematically high number of deaths associated with Revusiran, the first GalNAc-conjugated siRNA therapeutic brought to phase 3 clinical trials, leading to rapid termination of the trial[51]. It is not evident if those deaths were caused by drug-associated liver toxicity, induction of immune response related to the high dose of siRNA, the result of sequence specific off target knockdown, or off target knockdown of DNA repair genes that can be targeted by certain chemically modified siRNAs[51, 334]. Since then, newer GalNAc-conjugated siRNAs have received FDA approval, but concerns still remain, including increased serum creatinine levels associated with decreased

glomerular filtration rate in 15% of patients receiving Givosiran during its phase III clinical trial[256]. Meanwhile, Onpattro, the FDA-approved LNP-encapsulated siRNA, requires pre-treatment with a corticosteroid due to its inherent immunogenicity[51].

Here, we demonstrate the safety of sEVs loaded with siRNA via the pre-miR-451 hairpin. Notably, a dose of sEVs 10 times higher than that needed to achieve clinically relevant levels of target knockdown did not induce meaningful signs of immune response when incubated with human blood in culture (Fig. 3.2b) or when injected into mice (Fig. 3.2c). IL-6 was the only cytokine significantly increased over vehicle treated mice, yet its level was more than an order of magnitude lower than levels induced by siRNAs with known immunostimulatory properties, even at this high dose[335]. Additionally, no signs of organ toxicity or gross pathological abnormalities were observed (Fig. 3.2f, Supplementary Fig. 3.2, 3.3). Injecting mice multiple times with sEVs allowed for strong target knockdown and resulted in no obvious adverse effects (Fig. 3.4-3.6). An allogenic immune response is one where T cells of the immune system recognizes nonself elements on cells, tissues or organs in the body. This can lead to severe, cascading immune reactions that cause rejection of transplanted organs, for example[336]. Similarly, a xenogeneic response is an immune response initiated by nonself recognition of elements transplanted across members of different species. Here, sEVs do not appear to induce an allogenic response as evidenced by the lack of immune activation in cultured human blood treated with sEVs of human origin (Fig. 3.2b), or a xenogeneic response following injection of human cell-derived sEVs into mice, rats or rabbits, even following up to six distinct injections over nearly three weeks. Considering that human blood contains an abundance of sEVs and thousands of blood transfusions occur every day, these results were not surprising. These results support other studies where repeated injections of human cell-

derived sEVs into mice over several weeks showed no significant signs of immune activation or toxicity[181, 185].

It should be noted, however, that we did not perform a full safety profile following repeated injections in mice over several weeks. The full impact of this type of dosing schedule remains unknown. sEVs are less complex than cells and when isolated from healthy cells, they typically present reduced levels of immunostimulatory proteins like the Major histocompatibility complex (MHC) on their surfaces, making them less likely to activate an adverse immune response[337]. In contrast, sEVs derived from certain tumour cells or primed immune cells have been used to intentionally activate the immune system to target tumour cells[338, 339], and sEVs have been shown to support cancer metastasis[160]. Furthermore, in addition to the intended therapeutic siRNA, sEVs contain many other components including miRNAs and proteins that could potentially have off-target affects. As such, a complete, long term safety profile of sEVs derived from each different cell type being used as a delivery vehicle will need to be established before clinical use to ensure they are non immunogenic, non toxic, devoid of cancer-associated activity and do not cause other unintended, off-target effects.

5.2 The future of siRNA-loaded sEVs in kidney disease and beyond

siRNA delivered into the kidneys by sEVs can reduce targets in three different models of CKD, leading to improved kidney function and pathology (Fig. 3.4-3.6). Furthermore, sEV-delivered treatment is readily scaled into larger animal models in a predictable manner: doses required to reduce targets in rat liver and rabbit kidneys were half of the calculated dose that would be required if it were directly proportional to the body mass of the recipient animal (Fig. 3.7). For example, a dose only 100 times higher than that required to reach 75% target knockdown in mice was required to reach the same level of knockdown in a rabbit that was 200 times larger (Fig. 3.7d-

i). Considering this finding, we might expect the required sEV dose to reduce kidney targets in an 80kg human patient to be approximately $2x10^{14}$ sEVs containing 10-30 siRNA copies.

There are several factors to consider that will impact the feasibility of manufacturing sEVs loaded with siRNA using the pre-miR-451 hairpin at a clinical scale. These include cell growth conditions, isolation methods, producing cell types, storage conditions and potentially engineering vesicles. Here, we showed that processing conditioned media to generate an sEV product by TFF increases yields by 10-fold when compared to ultracentrifugation (Fig. 3.1b) and that these sEVs are significantly more effective in delivering functional siRNA cargo than their ultracentrifuged counterparts (Fig. 3.1c). The TFF process is also more rapid than ultracentrifugation, especially where larger volumes of media are being processed, since the process is highly scalable. This, along with the process sterility and reproducibility seen here and elsewhere[108, 110-113], suggest that TFF is an ideal method for production of therapeutic sEVs since larger volumes of media must be processed for applications in human patients. Using TFF we were able to generate sufficient quantities of sEVs from cells grown in flatware to inject multiple rabbits. Meanwhile, growing cells in 3D cultures in bioreactors can increase cell density and cell viability as well as the duration that they can be kept in culture[340] and multiple studies have demonstrated that cells grown in bioreactors produce large amounts of sEVs[111, 112, 187, 341]. Thus, moving forward, a combination of cell growth in bioreactors and media processing by TFF is likely to represent the most effective approach for mass manufacturing of sEVs loaded with siRNA via the pre-miR-451 hairpin.

To facilitate the transition to clinical applications of sEV-based siRNA therapeutics, long term storage conditions for sEVs must be optimized. Here, sEVs were isolated using TFF and were stored in PlasmaLyte A, an isotonic solution with similar salt content to serum, for up to one week at 4°C prior to animal injections. Long term storage was not tested here, though published studies

suggest that long term storage at -80°C in PlasmaLyte A may be the ideal storage condition[113, 187, 342], potentially with addition of cryopreservatives like trehalose, which was shown to protect sEVs during cryopreservation[343]. Moving forward, long term storage of siRNA loaded sEVs using the pre-miR-451 hairpin will be tested.

Careful consideration of the cell type(s) to be used for generating sEV-based therapeutics will be required moving forward. We have shown that sEVs from a mouse cell line, NSC-34 (Fig. 2.7) and two human cell lines, HEK293T (Supplementary Fig. 3.4a-c) and dermal fibroblasts (Fig. 3.3-3.7) can all deliver siRNA into kidney cells to reduce target mRNA expression in the glomeruli. We also demonstrated that sEVs do not deliver functional cargo in every organ where they accumulate following injection. For example, no knockdown was observed by siRNA-loaded sEVs in heart, lungs and brown fat despite accumulation of fluorescently labeled sEVs in those tissues (Fig. 2.4a,b). Furthermore, even within a tissue where functional siRNA delivery by sEVs is observed, delivery is limited to certain areas and cell types. For example, in liver, effective target knockdown was achieved in hepatocytes and macrophages, but not stellate cells (Fig. 2.7d-i) and in kidney, knockdown is observed in glomeruli and, to a lesser extent, in proximal tubules, while no significant knockdown is observed in distal tubules (Fig. 3.7d-i). These phenomena can be explained at the tissue level and at the cellular level. Many biological barriers exist within the body to keep certain components isolated from each other. For example, in the brain, the blood brain barrier (BBB) is formed by a network of endothelial cells with unique properties that form the walls of the blood vessels of the central nervous system[344]. The BBB limits more than 98% of small molecule drugs from entering the brain[345]. Similarly, in the kidney, the glomerular barrier is composed of specialized endothelial cells, a basement membrane and a layer of specialized podocyte cells and is responsible for filtering water and salts from the blood stream while

restricting passage of large macromolecules like proteins[346]. These types of barriers exist throughout the body and can restrict the passage of relatively large therapeutics, like LNPs and potentially sEVs, into certain regions. Numerous studies have demonstrated that certain sEVs possess the ability to cross the BBB[182, 347] and our findings that sEVs can deliver functional cargoes into podocytes within kidney glomeruli as well as in the proximal tubules suggest active transport mechanisms involving cell surface receptor interactions may allow sEVs to pass through these barriers. Still, it remains possible that sEVs from only a subset of cell types would possess the ability to pass different biological barriers. At the cellular level, there is mounting evidence that interactions between surface components of sEVs and their recipient cells determine how and if sEVs can be internalized for cargo delivery[158, 165]. Identifying the cell types that release siRNA-loaded sEVs via the pre-miR-451 hairpin that are best able to accumulate in tissues of interest, and deliver their cargoes into cells at those locations will be of paramount importance. This could expand the technology to reach previously inaccessible tissues and could also reduce the sEV dose required to achieve target knockdown, and therefore the amount of conditioned media that requires processing to produce a therapeutic.

Engineering sEVs to display different surface markers has the potential to make delivery more efficient. For example, displaying CD47 on the sEV surface increases time in circulation[181], and fusing peptides like the rabies viral glycoprotein peptide or iRGD peptide with Lamp2b allows them to be displayed on the sEV surface, promoting brain[182] and tumour[348] targeting, respectively. Similarly, display of different integrins on the sEV surface has been shown to cause them to specifically accumulate in different tissues including the brain, lungs or liver[160]. Chemical modifications like conversion of amine groups to alkynes and insertion of amphipathic molecules into sEV membranes can also be used to attach different peptides to the surface of sEVs that have

been shown to promote organ and tumour specific tropism[349]. However, critical care must be taken to ensure that any changes to sEV surface biology and chemistry does not negatively affect the natural ability for sEVs to effectively deliver their cargoes.

5.3 RNA binding proteins for engineering therapeutic sEVs

While we have shown that sEVs are highly efficient in delivering their siRNA cargoes into recipient cells, finding ways to increase the functional siRNA load per sEV is an area of ongoing study in the field, and could allow for the development of even more potent therapeutics. In the pre-miR-451 hairpin loading system outlined herein, siRNA loading is governed by the natural packaging mechanism of pre-miR-451 into sEVs. By co-opting this mechanism, 1-30 copies of siRNA can be loaded into each sEV, a similar level to the most abundant naturally occurring miRNAs in sEVs. We have determined that the protein MDK is involved in this loading process, and it exerts its function through a direct RNA binding mechanism (chapter 4). Many other RBPs have previously been shown to be involved in miRNA sorting into sEVs[147-153], however there is limited or no published evidence that overexpressing these RBPs can be used to improve miRNA packaging into sEVs. In accordance with this, we found no convincing evidence that overexpressing MDK in cells stably expressing an siRNA sequence in the pre-miR-451 hairpin increases loading of the endogenous pre-miR-451 or the siRNA sequence into sEVs in HEK293T cells (Fig. 4.3). It is unclear if this is simply because these RBPs are typically identified using pulldown methods, as was the case here (Fig. 4.1), and as such are likely highly abundant in the cells being studied in each case. Therefore, these RBPs could be present at saturating levels meaning that increasing their levels has no affect on packaging, even while reducing their levels greatly reduces packaging, as is the case with MDK (Fig. 4.2, Fig. 4.3). Exploring the ability for each of these RBPs, including MDK, to increase packaging of miRNAs in other cell types where

their expression is lower warrants investigation as it could lead to novel ways to increase the number of therapeutic siRNA copies per sEV.

The discovery that MDK was involved in pre-miR-451 sorting into sEVs was surprising. Since we were employing a direct pulldown method with biotinylated RNA hairpins, we expected to identify a well characterized RBP involved in this process, as has been the case with other sEV-sorted miRNAs[147-153]. However, it is becoming clear in the field that novel RBDs exist that are distinct from canonical domains like the RRM, KH domain, and zinc fingers and that many unconventional RBPs exist that bind RNA through these domains[156]. Our findings demonstrate that MDK can bind RNA, with a preference for short hairpin structures (Fig. 4.5) and it accomplishes this through a non-canonical RNA binding domain, as it does not possess a traditional RBD. We hypothesize that the binding occurs at the region canonically associated with heparan binding that is rich in lysine and arginine residues.

Two recent studies provide intriguing possibilities for how MDK is able to package bound RNA into sEVs. First, a study published in 2022 demonstrated that one of the heparin binding domains of MDK can be used as a cell penetrating peptide (CPP)[326], and was able to drive proteins across the cell membrane into the cytoplasm. Additionally, a second study published in 2022 demonstrated that increasing the lysine and arginine content of proteins, especially on their solvent-exposed surface, allows them to pass through membranes and be loaded inside of the sEV lumen without the need for electroporation or chemical transfection[327]. Similarly, MDK is rich in lysine and arginine residues on its solvent exposed surface[316], leading us to hypothesize that it binds pre-miR-451 hairpins and could sort them into sEVs through a membrane penetrating mechanism. Alternatively, intracellular MDK has been shown to be ubiquitinated[309], suggesting

that following binding to pre-miR-451 it could be sorted into forming sEVs via the ESCRT-dependent protein sorting pathway[79]

The cell penetrating ability of MDK provides an exciting possibility for a new mechanism for loading chemically modified siRNAs into sEVs. As discussed earlier, chemically modified siRNAs possess numerous advantages over traditional siRNAs, such as increased half life, increased potency and improved duration of target knockdown. Since the pre-miR-451 packaging system is based on co-opting endogenous sorting mechanisms, it cannot be used to sort chemically modified siRNAs. sEVs produced with this method are extremely effective at delivering their cargoes into cells, likely achieved in part due to the lack of any alterations to the sEV membranes. However, levels of the target mRNA return to pre-treatment levels after approximately two weeks (Supplementary Fig. 3.4d), while chemically modified siRNAs were able to reduce targets for over 6 months with a single injection[46, 47]. Exogenous MDK may be able to bind chemically modified siRNAs in the short pre-miR-451 hairpin structure and drive them through sEV membranes without damaging them, allowing us to combine the benefits of unaltered sEVs with chemically modified siRNAs. Along the same lines, MDK could potentially be used as a lipid-free transfection reagent to put miRNAs or siRNAs into cells. These possibilities warrant further investigation.

The recent finding that SYNCRIP sorts miRNAs into sEVs through a non-canonical RNA binding domain[157], in addition to findings presented here (chapter 4) suggest that it may not be uncommon for RNAs to be sorted into sEVs by unconventional RBPs. We have also shown that MDK, traditionally thought to be a secreted cytokine, is, at least in part, encapsulated within secreted sEVs (Fig. 4.4). Many studies have performed proteomic analysis on sEVs isolated using a variety of methods, and have identified proteins associated with sEVs. However, the location of those proteins, inside versus outside versus simply copurifying with sEVs, has not been verified

in many cases. The MDK finding provides another opportunity for reflection, in this case on which assumed sEV cargoes are in fact cargoes, and what roles outside of the obvious ones they might be playing in sEV biology. This could help shed light on how cargo is sorted into sEVs, much of which remains poorly understood, how sEVs deliver their cargoes, and could unlock new ways to engineer cells and sEVs in the future to improve their therapeutic potential.

5.4 Conclusions and future directions

We have demonstrated the safe and effective delivery of siRNAs by sEVs loaded via the pre-miR-451 hairpin in multiple tissues, in three different animal models and established their therapeutic potential in pre-clinical models of kidney disease. We performed head-to-head comparisons, which highlight the advantages of sEVs loaded with siRNA via the pre-miR-451 hairpin as compared to other RNA and sEV technologies. In doing so, we have provided support for the idea that sEVs have evolved to be highly efficient delivery vehicles for RNA cargoes. Work presented here suggests that this technology will be functional in larger animals and manufacturing will be readily scalable. By carefully considering the sEV-producing cell types, surface engineering and cell culture conditions we expect to continue progressing toward the development of therapeutics for *Trpc6* and *Apol1* associated CKD, and at the same time plan to expand this technology to target an array of disease-associated genes in multiple tissues in human patients, not limited to the liver or even the kidney, that other siRNA therapies cannot currently treat. Selection of specific mRNA targets will depend on which tissues and organs are best targeted by sEVs from diverse cellular origins, and within those tissues, which cells can effectively have siRNA delivered into their cytoplasm. The brain presents an exciting potential target since sEVs can cross the BBB and deliver cargoes into brain cells. A myriad of genetic disorders with limited or no treatment

options caused by brain-associated disease gene expression could potentially be treated with this technology.

In this study, we uncovered a protein involved in active sEV sorting of pre-miR-451, one of the most highly enriched miRNAs in sEVs. This secreted cytokine, Midkine, was found to have a previously unidentified RNA binding ability and a preference for binding short RNA hairpins. This has allowed us to speculate that RBPs with unconventional RNA binding domains could be involved in other miRNA sorting into sEVs.

Moving forward, we intend to identify other RNAs that can be bound by MDK and determine if they are also preferentially sorted into sEVs and also work toward fully understanding the mechanism through which MDK binds RNA and sorts it into sEVs, potentially through a membrane penetrating function. This will fill knowledge gaps in the areas of sEV cargo sorting as well as novel RBP biology, and can potentially be applied to the engineering of cells or sEVs to improve the therapeutic potency of siRNA-loaded sEVs.

References

1. Lee, R.C., Feinbaum, R.L. & Ambros, V. The C. elegans heterochronic gene lin-4 encodes small RNAs with antisense complementarity to lin-14. *Cell* **75**, 843-854 (1993).
2. Bartel, D.P. MicroRNAs: genomics, biogenesis, mechanism, and function. *Cell* **116**, 281-297 (2004).
3. Fire, A. et al. Potent and specific genetic interference by double-stranded RNA in Caenorhabditis elegans. *Nature* **391**, 806-811 (1998).
4. Mello, C.C. & Conte, D., Jr. Revealing the world of RNA interference. *Nature* **431**, 338-342 (2004).
5. Carthew, R.W. & Sontheimer, E.J. Origins and Mechanisms of miRNAs and siRNAs. *Cell* **136**, 642-655 (2009).
6. Yi, R., Qin, Y., Macara, I.G. & Cullen, B.R. Exportin-5 mediates the nuclear export of pre-microRNAs and short hairpin RNAs. *Genes Dev* **17**, 3011-3016 (2003).
7. Kim, Y.K., Kim, B. & Kim, V.N. Re-evaluation of the roles of DROSHA, Export in 5, and DICER in microRNA biogenesis. *Proc Natl Acad Sci U S A* **113**, E1881-1889 (2016).
8. Ha, M. & Kim, V.N. Regulation of microRNA biogenesis. *Nat Rev Mol Cell Biol* **15**, 509-524 (2014).
9. Fareh, M. et al. TRBP ensures efficient Dicer processing of precursor microRNA in RNA-crowded environments. *Nat Commun* **7**, 13694 (2016).
10. Meister, G. et al. Human Argonaute2 mediates RNA cleavage targeted by miRNAs and siRNAs. *Mol Cell* **15**, 185-197 (2004).
11. Wang, B. et al. Distinct passenger strand and mRNA cleavage activities of human Argonaute proteins. *Nat Struct Mol Biol* **16**, 1259-1266 (2009).
12. Schwarz, D.S. et al. Asymmetry in the assembly of the RNAi enzyme complex. *Cell* **115**, 199-208 (2003).
13. Huntzinger, E. & Izaurralde, E. Gene silencing by microRNAs: contributions of translational repression and mRNA decay. *Nat Rev Genet* **12**, 99-110 (2011).
14. Petersen, C.P., Bordeleau, M.E., Pelletier, J. & Sharp, P.A. Short RNAs repress translation after initiation in mammalian cells. *Mol Cell* **21**, 533-542 (2006).
15. Maroney, P.A., Yu, Y., Fisher, J. & Nilsen, T.W. Evidence that microRNAs are associated with translating messenger RNAs in human cells. *Nat Struct Mol Biol* **13**, 1102-1107 (2006).
16. Kong, Y.W. et al. The mechanism of micro-RNA-mediated translation repression is determined by the promoter of the target gene. *Proc Natl Acad Sci U S A* **105**, 8866-8871 (2008).
17. Behm-Ansmant, I. et al. mRNA degradation by miRNAs and GW182 requires both CCR4:NOT deadenylase and DCP1:DCP2 decapping complexes. *Genes Dev* **20**, 1885-1898 (2006).
18. Filipowicz, W., Bhattacharyya, S.N. & Sonenberg, N. Mechanisms of post-transcriptional regulation by microRNAs: are the answers in sight? *Nat Rev Genet* **9**, 102-114 (2008).
19. Guo, H., Ingolia, N.T., Weissman, J.S. & Bartel, D.P. Mammalian microRNAs predominantly act to decrease target mRNA levels. *Nature* **466**, 835-840 (2010).

20. Friedman, R.C., Farh, K.K., Burge, C.B. & Bartel, D.P. Most mammalian mRNAs are conserved targets of microRNAs. *Genome Res* **19**, 92-105 (2009).
21. Wightman, B., Ha, I. & Ruvkun, G. Posttranscriptional regulation of the heterochronic gene lin-14 by lin-4 mediates temporal pattern formation in C. elegans. *Cell* **75**, 855-862 (1993).
22. Ebert, M.S. & Sharp, P.A. Roles for microRNAs in conferring robustness to biological processes. *Cell* **149**, 515-524 (2012).
23. Fazi, F. et al. A minicircuitry comprised of microRNA-223 and transcription factors NFI-A and C/EBPalpha regulates human granulopoiesis. *Cell* **123**, 819-831 (2005).
24. Baek, D. et al. The impact of microRNAs on protein output. *Nature* **455**, 64-71 (2008).
25. Poy, M.N. et al. A pancreatic islet-specific microRNA regulates insulin secretion. *Nature* **432**, 226-230 (2004).
26. Vidigal, J.A. & Ventura, A. The biological functions of miRNAs: lessons from in vivo studies. *Trends Cell Biol* **25**, 137-147 (2015).
27. Juźwik, C.A. et al. microRNA dysregulation in neurodegenerative diseases: A systematic review. *Prog Neurobiol* **182**, 101664 (2019).
28. Croce, C.M. Causes and consequences of microRNA dysregulation in cancer. *Nat Rev Genet* **10**, 704-714 (2009).
29. Watanabe, T. et al. Endogenous siRNAs from naturally formed dsRNAs regulate transcripts in mouse oocytes. *Nature* **453**, 539-543 (2008).
30. Golden, D.E., Gerbasi, V.R. & Sontheimer, E.J. An inside job for siRNAs. *Mol Cell* **31**, 309-312 (2008).
31. Waterhouse, P.M., Wang, M.B. & Lough, T. Gene silencing as an adaptive defence against viruses. *Nature* **411**, 834-842 (2001).
32. Meister, G. & Tuschl, T. Mechanisms of gene silencing by double-stranded RNA. *Nature* **431**, 343-349 (2004).
33. Schiffelers, R.M., Woodle, M.C. & Scaria, P. Pharmaceutical prospects for RNA interference. *Pharm Res* **21**, 1-7 (2004).
34. Park, M.S. et al. Human Argonaute3 has slicer activity. *Nucleic Acids Res* **45**, 11867-11877 (2017).
35. Park, M.S., Sim, G., Kehling, A.C. & Nakanishi, K. Human Argonaute2 and Argonaute3 are catalytically activated by different lengths of guide RNA. *Proc Natl Acad Sci U S A* **117**, 28576-28578 (2020).
36. Chakraborty, C., Sharma, A.R., Sharma, G., Doss, C.G.P. & Lee, S.S. Therapeutic miRNA and siRNA: Moving from Bench to Clinic as Next Generation Medicine. *Mol Ther Nucleic Acids* **8**, 132-143 (2017).
37. Wittrup, A. & Lieberman, J. Knocking down disease: a progress report on siRNA therapeutics. *Nat Rev Genet* **16**, 543-552 (2015).
38. Zogg, H., Singh, R. & Ro, S. Current Advances in RNA Therapeutics for Human Diseases. *Int J Mol Sci* **23** (2022).
39. Kulkarni, J.A. et al. The current landscape of nucleic acid therapeutics. *Nat Nanotechnol* **16**, 630-643 (2021).
40. Rinaldi, C. & Wood, M.J.A. Antisense oligonucleotides: the next frontier for treatment of neurological disorders. *Nat Rev Neurol* **14**, 9-21 (2018).
41. Muntoni, F. & Wood, M.J. Targeting RNA to treat neuromuscular disease. *Nat Rev Drug Discov* **10**, 621-637 (2011).

42. Gagliardi, M. & Ashizawa, A.T. The Challenges and Strategies of Antisense Oligonucleotide Drug Delivery. *Biomedicines* **9** (2021).
43. van Poelgeest, E.P. et al. Antisense-mediated reduction of proprotein convertase subtilisin/kexin type 9 (PCSK9): a first-in-human randomized, placebo-controlled trial. *Br J Clin Pharmacol* **80**, 1350-1361 (2015).
44. Frazier, K.S. & Obert, L.A. Drug-induced Glomerulonephritis: The Spectre of Biotherapeutic and Antisense Oligonucleotide Immune Activation in the Kidney. *Toxicol Pathol* **46**, 904-917 (2018).
45. Stephenson, M.L. & Zamecnik, P.C. Inhibition of Rous sarcoma viral RNA translation by a specific oligodeoxyribonucleotide. *Proc Natl Acad Sci U S A* **75**, 285-288 (1978).
46. Fitzgerald, K. et al. A Highly Durable RNAi Therapeutic Inhibitor of PCSK9. *N Engl J Med* **376**, 41-51 (2017).
47. Coelho, T. et al. Safety and efficacy of RNAi therapy for transthyretin amyloidosis. *N Engl J Med* **369**, 819-829 (2013).
48. Elliott, P. et al. Long-Term Survival With Tafamidis in Patients With Transthyretin Amyloid Cardiomyopathy. *Circ Heart Fail* **15**, e008193 (2022).
49. Maurer, M.S. et al. Tafamidis Treatment for Patients with Transthyretin Amyloid Cardiomyopathy. *N Engl J Med* **379**, 1007-1016 (2018).
50. Ozcan, G., Ozpolat, B., Coleman, R.L., Sood, A.K. & Lopez-Berestein, G. Preclinical and clinical development of siRNA-based therapeutics. *Adv Drug Deliv Rev* **87**, 108-119 (2015).
51. Garber, K. Alnylam terminates revusiran program, stock plunges. *Nat Biotechnol* **34**, 1213-1214 (2016).
52. Wittrup, A. et al. Visualizing lipid-formulated siRNA release from endosomes and target gene knockdown. *Nat Biotechnol* **33**, 870-876 (2015).
53. Pei, Y. et al. Quantitative evaluation of siRNA delivery in vivo. *Rna* **16**, 2553-2563 (2010).
54. Veldhoen, S., Laufer, S.D., Trampe, A. & Restle, T. Cellular delivery of small interfering RNA by a non-covalently attached cell-penetrating peptide: quantitative analysis of uptake and biological effect. *Nucleic Acids Res* **34**, 6561-6573 (2006).
55. Kaczmarek, J.C., Kowalski, P.S. & Anderson, D.G. Advances in the delivery of RNA therapeutics: from concept to clinical reality. *Genome Med* **9**, 60 (2017).
56. Tatiparti, K., Sau, S., Kashaw, S.K. & Iyer, A.K. siRNA Delivery Strategies: A Comprehensive Review of Recent Developments. *Nanomaterials (Basel)* **7** (2017).
57. Hu, B. et al. Therapeutic siRNA: state of the art. *Signal Transduct Target Ther* **5**, 101 (2020).
58. Schott, J.W., Morgan, M., Galla, M. & Schambach, A. Viral and Synthetic RNA Vector Technologies and Applications. *Mol Ther* **24**, 1513-1527 (2016).
59. Singha, K., Namgung, R. & Kim, W.J. Polymers in small-interfering RNA delivery. *Nucleic Acid Ther* **21**, 133-147 (2011).
60. Schroeder, A., Levins, C.G., Cortez, C., Langer, R. & Anderson, D.G. Lipid-based nanotherapeutics for siRNA delivery. *J Intern Med* **267**, 9-21 (2010).
61. Mahon, K.P. et al. Combinatorial approach to determine functional group effects on lipidoid-mediated siRNA delivery. *Bioconjug Chem* **21**, 1448-1454 (2010).
62. Kanasty, R., Dorkin, J.R., Vegas, A. & Anderson, D. Delivery materials for siRNA therapeutics. *Nat Mater* **12**, 967-977 (2013).

63. Semple, S.C. et al. Rational design of cationic lipids for siRNA delivery. *Nat Biotechnol* **28**, 172-176 (2010).
64. Bao, Y. et al. Effect of PEGylation on biodistribution and gene silencing of siRNA/lipid nanoparticle complexes. *Pharm Res* **30**, 342-351 (2013).
65. Herrera, M., Kim, J., Eygeris, Y., Jozic, A. & Sahay, G. Illuminating endosomal escape of polymorphic lipid nanoparticles that boost mRNA delivery. *Biomater Sci* **9**, 4289-4300 (2021).
66. Sato, Y. et al. Resolution of liver cirrhosis using vitamin A-coupled liposomes to deliver siRNA against a collagen-specific chaperone. *Nat Biotechnol* **26**, 431-442 (2008).
67. Estapé Senti, M. et al. Anti-PEG antibodies compromise the integrity of PEGylated lipid-based nanoparticles via complement. *J Control Release* **341**, 475-486 (2022).
68. Kedmi, R., Ben-Arie, N. & Peer, D. The systemic toxicity of positively charged lipid nanoparticles and the role of Toll-like receptor 4 in immune activation. *Biomaterials* **31**, 6867-6875 (2010).
69. Garber, K. Alnylam launches era of RNAi drugs. *Nat Biotechnol* **36**, 777-778 (2018).
70. Lorenzer, C., Dirin, M., Winkler, A.M., Baumann, V. & Winkler, J. Going beyond the liver: progress and challenges of targeted delivery of siRNA therapeutics. *J Control Release* **203**, 1-15 (2015).
71. Tsoi, K.M. et al. Mechanism of hard-nanomaterial clearance by the liver. *Nat Mater* **15**, 1212-1221 (2016).
72. Gilleron, J. et al. Image-based analysis of lipid nanoparticle-mediated siRNA delivery, intracellular trafficking and endosomal escape. *Nat Biotechnol* **31**, 638-646 (2013).
73. Dowdy, S.F. Overcoming cellular barriers for RNA therapeutics. *Nat Biotechnol* **35**, 222-229 (2017).
74. Springer, A.D. & Dowdy, S.F. GalNAc-siRNA Conjugates: Leading the Way for Delivery of RNAi Therapeutics. *Nucleic Acid Ther* **28**, 109-118 (2018).
75. Baenziger, J.U. & Fiete, D. Galactose and N-acetylgalactosamine-specific endocytosis of glycopeptides by isolated rat hepatocytes. *Cell* **22**, 611-620 (1980).
76. Seymour, L.W. et al. Hepatic drug targeting: phase I evaluation of polymer-bound doxorubicin. *J Clin Oncol* **20**, 1668-1676 (2002).
77. Prakash, T.P. et al. Targeted delivery of antisense oligonucleotides to hepatocytes using triantennary N-acetyl galactosamine improves potency 10-fold in mice. *Nucleic Acids Res* **42**, 8796-8807 (2014).
78. Nair, J.K. et al. Multivalent N-acetylgalactosamine-conjugated siRNA localizes in hepatocytes and elicits robust RNAi-mediated gene silencing. *J Am Chem Soc* **136**, 16958-16961 (2014).
79. Colombo, M., Raposo, G. & Thery, C. Biogenesis, secretion, and intercellular interactions of exosomes and other extracellular vesicles. *Annu Rev Cell Dev Biol* **30**, 255-289 (2014).
80. Crescitelli, R. et al. Distinct RNA profiles in subpopulations of extracellular vesicles: apoptotic bodies, microvesicles and exosomes. *J Extracell Vesicles* **2** (2013).
81. Willms, E., Cabañas, C., Mäger, I., Wood, M.J.A. & Vader, P. Extracellular Vesicle Heterogeneity: Subpopulations, Isolation Techniques, and Diverse Functions in Cancer Progression. *Front Immunol* **9**, 738 (2018).

82. Nabhan, J.F., Hu, R., Oh, R.S., Cohen, S.N. & Lu, Q. Formation and release of arrestin domain-containing protein 1-mediated microvesicles (ARMMs) at plasma membrane by recruitment of TSG101 protein. *Proc Natl Acad Sci U S A* **109**, 4146-4151 (2012).
83. Sheta, M., Taha, E.A., Lu, Y. & Eguchi, T. Extracellular Vesicles: New Classification and Tumor Immunosuppression. *Biology (Basel)* **12** (2023).
84. Jeppesen, D.K. et al. Reassessment of Exosome Composition. *Cell* **177**, 428-445.e418 (2019).
85. Rilla, K. et al. Extracellular vesicles are integral and functional components of the extracellular matrix. *Matrix Biol* **75-76**, 201-219 (2019).
86. Zhang, H. et al. Identification of distinct nanoparticles and subsets of extracellular vesicles by asymmetric flow field-flow fractionation. *Nat Cell Biol* **20**, 332-343 (2018).
87. Zhang, Q. et al. Transfer of Functional Cargo in Exomeres. *Cell Rep* **27**, 940-954.e946 (2019).
88. Théry, C. et al. Minimal information for studies of extracellular vesicles 2018 (MISEV2018): a position statement of the International Society for Extracellular Vesicles and update of the MISEV2014 guidelines. *J Extracell Vesicles* **7**, 1535750 (2018).
89. Witwer, K.W. & Théry, C. in J Extracell Vesicles, Vol. 8 1648167 (United States; 2019).
90. Colombo, M. et al. Analysis of ESCRT functions in exosome biogenesis, composition and secretion highlights the heterogeneity of extracellular vesicles. *J Cell Sci* **126**, 5553-5565 (2013).
91. Gurung, S., Perocheau, D., Touramanidou, L. & Baruteau, J. The exosome journey: from biogenesis to uptake and intracellular signalling. *Cell Commun Signal* **19**, 47 (2021).
92. Larios, J., Mercier, V., Roux, A. & Gruenberg, J. ALIX- and ESCRT-III-dependent sorting of tetraspanins to exosomes. *J Cell Biol* **219** (2020).
93. Nickerson, D.P., West, M. & Odorizzi, G. Did2 coordinates Vps4-mediated dissociation of ESCRT-III from endosomes. *J Cell Biol* **175**, 715-720 (2006).
94. Stuffers, S., Sem Wegner, C., Stenmark, H. & Brech, A. Multivesicular endosome biogenesis in the absence of ESCRTs. *Traffic* **10**, 925-937 (2009).
95. Trajkovic, K. et al. Ceramide triggers budding of exosome vesicles into multivesicular endosomes. *Science* **319**, 1244-1247 (2008).
96. Edgar, J.R., Eden, E.R. & Futter, C.E. Hrs- and CD63-dependent competing mechanisms make different sized endosomal intraluminal vesicles. *Traffic* **15**, 197-211 (2014).
97. Willms, E. et al. Cells release subpopulations of exosomes with distinct molecular and biological properties. *Sci Rep* **6**, 22519 (2016).
98. Baietti, M.F. et al. Syndecan-syntenin-ALIX regulates the biogenesis of exosomes. *Nat Cell Biol* **14**, 677-685 (2012).
99. Ostrowski, M. et al. Rab27a and Rab27b control different steps of the exosome secretion pathway. *Nat Cell Biol* **12**, 19-30; sup pp 11-13 (2010).
100. Han, J., Pluhackova, K. & Böckmann, R.A. The Multifaceted Role of SNARE Proteins in Membrane Fusion. *Front Physiol* **8**, 5 (2017).
101. Hugel, B., Martínez, M.C., Kunzelmann, C. & Freyssinet, J.M. Membrane microparticles: two sides of the coin. *Physiology (Bethesda)* **20**, 22-27 (2005).
102. Muralidharan-Chari, V. et al. ARF6-regulated shedding of tumor cell-derived plasma membrane microvesicles. *Curr Biol* **19**, 1875-1885 (2009).
103. Gardiner, C. et al. Techniques used for the isolation and characterization of extracellular vesicles: results of a worldwide survey. *J Extracell Vesicles* **5**, 32945 (2016).

104. Cvjetkovic, A., Lotvall, J. & Lasser, C. The influence of rotor type and centrifugation time on the yield and purity of extracellular vesicles. *J Extracell Vesicles* **3** (2014).
105. Linares, R., Tan, S., Gounou, C., Arraud, N. & Brisson, A.R. in J Extracell Vesicles, Vol. 4 (2015).
106. Greening, D.W., Xu, R., Ji, H., Tauro, B.J. & Simpson, R.J. A protocol for exosome isolation and characterization: evaluation of ultracentrifugation, density-gradient separation, and immunoaffinity capture methods. *Methods Mol Biol* **1295**, 179-209 (2015).
107. Lamparski, H.G. et al. Production and characterization of clinical grade exosomes derived from dendritic cells. *J Immunol Methods* **270**, 211-226 (2002).
108. Busatto, S. et al. Tangential Flow Filtration for Highly Efficient Concentration of Extracellular Vesicles from Large Volumes of Fluid. *Cells* **7** (2018).
109. Nordin, J.Z. et al. Ultrafiltration with size-exclusion liquid chromatography for high yield isolation of extracellular vesicles preserving intact biophysical and functional properties. *Nanomedicine* **11**, 879-883 (2015).
110. Gimona, M., Pachler, K., Laner-Plamberger, S., Schallmoser, K. & Rohde, E. Manufacturing of Human Extracellular Vesicle-Based Therapeutics for Clinical Use. *Int J Mol Sci* **18** (2017).
111. Haraszti, R.A. et al. Exosomes Produced from 3D Cultures of MSCs by Tangential Flow Filtration Show Higher Yield and Improved Activity. *Mol Ther* **26**, 2838-2847 (2018).
112. Watson, D.C. et al. Scalable, cGMP-compatible purification of extracellular vesicles carrying bioactive human heterodimeric IL-15/lactadherin complexes. *J Extracell Vesicles* **7**, 1442088 (2018).
113. Andriolo, G. et al. Exosomes From Human Cardiac Progenitor Cells for Therapeutic Applications: Development of a GMP-Grade Manufacturing Method. *Front Physiol* **9**, 1169 (2018).
114. Weng, Y. et al. Effective isolation of exosomes with polyethylene glycol from cell culture supernatant for in-depth proteome profiling. *Analyst* **141**, 4640-4646 (2016).
115. Sidhom, K., Obi, P.O. & Saleem, A. A Review of Exosomal Isolation Methods: Is Size Exclusion Chromatography the Best Option? *Int J Mol Sci* **21** (2020).
116. Böing, A.N. et al. Single-step isolation of extracellular vesicles by size-exclusion chromatography. *J Extracell Vesicles* **3** (2014).
117. Lobb, R.J. et al. Optimized exosome isolation protocol for cell culture supernatant and human plasma. *J Extracell Vesicles* **4**, 27031 (2015).
118. Théry, C. et al. Proteomic analysis of dendritic cell-derived exosomes: a secreted subcellular compartment distinct from apoptotic vesicles. *J Immunol* **166**, 7309-7318 (2001).
119. Skotland, T., Hessvik, N.P., Sandvig, K. & Llorente, A. Exosomal lipid composition and the role of ether lipids and phosphoinositides in exosome biology. *J Lipid Res* **60**, 9-18 (2019).
120. Thakur, B.K. et al. in Cell Res, Vol. 24 766-769 (England; 2014).
121. Valadi, H. et al. Exosome-mediated transfer of mRNAs and microRNAs is a novel mechanism of genetic exchange between cells. *Nat Cell Biol* **9**, 654-659 (2007).
122. Pegtel, D.M. et al. Functional delivery of viral miRNAs via exosomes. *Proc Natl Acad Sci U S A* **107**, 6328-6333 (2010).

123. Chen, Y., Zhao, Y., Yin, Y., Jia, X. & Mao, L. Mechanism of cargo sorting into small extracellular vesicles. *Bioengineered* **12**, 8186-8201 (2021).
124. Moreno-Gonzalo, O., Fernandez-Delgado, I. & Sanchez-Madrid, F. in Cell Mol Life Sci, Vol. 75 1-19 (Switzerland; 2018).
125. Raiborg, C. & Stenmark, H. The ESCRT machinery in endosomal sorting of ubiquitylated membrane proteins. *Nature* **458**, 445-452 (2009).
126. Kunadt, M. et al. Extracellular vesicle sorting of α-Synuclein is regulated by sumoylation. *Acta Neuropathol* **129**, 695-713 (2015).
127. Villarroya-Beltri, C. et al. ISGylation controls exosome secretion by promoting lysosomal degradation of MVB proteins. *Nat Commun* **7**, 13588 (2016).
128. de Gassart, A., Geminard, C., Fevrier, B., Raposo, G. & Vidal, M. Lipid raft-associated protein sorting in exosomes. *Blood* **102**, 4336-4344 (2003).
129. Skotland, T., Sandvig, K. & Llorente, A. Lipids in exosomes: Current knowledge and the way forward. *Prog Lipid Res* **66**, 30-41 (2017).
130. Haraszti, R.A. et al. High-resolution proteomic and lipidomic analysis of exosomes and microvesicles from different cell sources. *J Extracell Vesicles* **5**, 32570 (2016).
131. Elzanowska, J., Semira, C. & Costa-Silva, B. DNA in extracellular vesicles: biological and clinical aspects. *Mol Oncol* **15**, 1701-1714 (2021).
132. Fernando, M.R., Jiang, C., Krzyzanowski, G.D. & Ryan, W.L. New evidence that a large proportion of human blood plasma cell-free DNA is localized in exosomes. *PLoS One* **12**, e0183915 (2017).
133. Kahlert, C. et al. Identification of double-stranded genomic DNA spanning all chromosomes with mutated KRAS and p53 DNA in the serum exosomes of patients with pancreatic cancer. *J Biol Chem* **289**, 3869-3875 (2014).
134. Yokoi, A. et al. Mechanisms of nuclear content loading to exosomes. *Sci Adv* **5**, eaax8849 (2019).
135. Takahashi, A. et al. Exosomes maintain cellular homeostasis by excreting harmful DNA from cells. *Nat Commun* **8**, 15287 (2017).
136. Cai, J. et al. Extracellular vesicle-mediated transfer of donor genomic DNA to recipient cells is a novel mechanism for genetic influence between cells. *J Mol Cell Biol* **5**, 227-238 (2013).
137. O'Grady, T. et al. Sorting and packaging of RNA into extracellular vesicles shape intracellular transcript levels. *BMC Biol* **20**, 72 (2022).
138. Bolukbasi, M.F. et al. miR-1289 and "Zipcode"-like Sequence Enrich mRNAs in Microvesicles. *Mol Ther Nucleic Acids* **1**, e10 (2012).
139. Baglio, S.R. et al. Human bone marrow- and adipose-mesenchymal stem cells secrete exosomes enriched in distinctive miRNA and tRNA species. *Stem Cell Res Ther* **6**, 127 (2015).
140. Chiou, N.T., Kageyama, R. & Ansel, K.M. Selective Export into Extracellular Vesicles and Function of tRNA Fragments during T Cell Activation. *Cell Rep* **25**, 3356-3370.e3354 (2018).
141. Cambier, L. et al. Y RNA fragment in extracellular vesicles confers cardioprotection via modulation of IL-10 expression and secretion. *EMBO Mol Med* **9**, 337-352 (2017).
142. Nolte-'t Hoen, E.N. et al. Deep sequencing of RNA from immune cell-derived vesicles uncovers the selective incorporation of small non-coding RNA biotypes with potential regulatory functions. *Nucleic Acids Res* **40**, 9272-9285 (2012).

143. Guduric-Fuchs, J. et al. Selective extracellular vesicle-mediated export of an overlapping set of microRNAs from multiple cell types. *BMC Genomics* **13**, 357 (2012).
144. Pigati, L. et al. Selective release of microRNA species from normal and malignant mammary epithelial cells. *PLoS One* **5**, e13515 (2010).
145. van Balkom, B.W., Eisele, A.S., Pegtel, D.M., Bervoets, S. & Verhaar, M.C. Quantitative and qualitative analysis of small RNAs in human endothelial cells and exosomes provides insights into localized RNA processing, degradation and sorting. *J Extracell Vesicles* **4**, 26760 (2015).
146. Kosaka, N. et al. Secretory mechanisms and intercellular transfer of microRNAs in living cells. *J Biol Chem* **285**, 17442-17452 (2010).
147. Villarroya-Beltri, C. et al. Sumoylated hnRNPA2B1 controls the sorting of miRNAs into exosomes through binding to specific motifs. *Nat Commun* **4**, 2980 (2013).
148. Santangelo, L. et al. The RNA-Binding Protein SYNCRIP Is a Component of the Hepatocyte Exosomal Machinery Controlling MicroRNA Sorting. *Cell Rep* **17**, 799-808 (2016).
149. Shurtleff, M.J., Temoche-Diaz, M.M., Karfilis, K.V., Ri, S. & Schekman, R. Y-box protein 1 is required to sort microRNAs into exosomes in cells and in a cell-free reaction. *Elife* **5** (2016).
150. Temoche-Diaz, M.M. et al. Distinct mechanisms of microRNA sorting into cancer cell-derived extracellular vesicle subtypes. *Elife* **8** (2019).
151. Mukherjee, K. et al. Reversible HuR-microRNA binding controls extracellular export of miR-122 and augments stress response. *EMBO Rep* **17**, 1184-1203 (2016).
152. Statello, L. et al. Identification of RNA-binding proteins in exosomes capable of interacting with different types of RNA: RBP-facilitated transport of RNAs into exosomes. *PLoS One* **13**, e0195969 (2018).
153. Teng, Y. et al. MVP-mediated exosomal sorting of miR-193a promotes colon cancer progression. *Nat Commun* **8**, 14448 (2017).
154. Sork, H. et al. Heterogeneity and interplay of the extracellular vesicle small RNA transcriptome and proteome. *Sci Rep* **8**, 10813 (2018).
155. Lunde, B.M., Moore, C. & Varani, G. RNA-binding proteins: modular design for efficient function. *Nat Rev Mol Cell Biol* **8**, 479-490 (2007).
156. Hentze, M.W., Castello, A., Schwarzl, T. & Preiss, T. A brave new world of RNA-binding proteins. *Nat Rev Mol Cell Biol* **19**, 327-341 (2018).
157. Hobor, F. et al. A cryptic RNA-binding domain mediates Syncrip recognition and exosomal partitioning of miRNA targets. *Nat Commun* **9**, 831 (2018).
158. Mathieu, M., Martin-Jaular, L., Lavieu, G. & Théry, C. Specificities of secretion and uptake of exosomes and other extracellular vesicles for cell-to-cell communication. *Nat Cell Biol* **21**, 9-17 (2019).
159. Morelli, A.E. et al. Endocytosis, intracellular sorting, and processing of exosomes by dendritic cells. *Blood* **104**, 3257-3266 (2004).
160. Hoshino, A. et al. Tumour exosome integrins determine organotropic metastasis. *Nature* **527**, 329-335 (2015).
161. Christianson, H.C., Svensson, K.J., van Kuppevelt, T.H., Li, J.P. & Belting, M. Cancer cell exosomes depend on cell-surface heparan sulfate proteoglycans for their internalization and functional activity. *Proc Natl Acad Sci U S A* **110**, 17380-17385 (2013).

162. Prada, I. & Meldolesi, J. Binding and Fusion of Extracellular Vesicles to the Plasma Membrane of Their Cell Targets. *Int J Mol Sci* **17** (2016).
163. Parolini, I. et al. Microenvironmental pH is a key factor for exosome traffic in tumor cells. *J Biol Chem* **284**, 34211-34222 (2009).
164. Kourembanas, S. Exosomes: vehicles of intercellular signaling, biomarkers, and vectors of cell therapy. *Annu Rev Physiol* **77**, 13-27 (2015).
165. Horibe, S., Tanahashi, T., Kawauchi, S., Murakami, Y. & Rikitake, Y. Mechanism of recipient cell-dependent differences in exosome uptake. *BMC Cancer* **18**, 47 (2018).
166. Joshi, B.S., de Beer, M.A., Giepmans, B.N.G. & Zuhorn, I.S. Endocytosis of Extracellular Vesicles and Release of Their Cargo from Endosomes. *ACS Nano* **14**, 4444-4455 (2020).
167. O'Brien, K., Ughetto, S., Mahjoum, S., Nair, A.V. & Breakefield, X.O. Uptake, functionality, and re-release of extracellular vesicle-encapsulated cargo. *Cell Rep* **39**, 110651 (2022).
168. Thomou, T. et al. Adipose-derived circulating miRNAs regulate gene expression in other tissues. *Nature* **542**, 450-455 (2017).
169. Hergenreider, E. et al. Atheroprotective communication between endothelial cells and smooth muscle cells through miRNAs. *Nat Cell Biol* **14**, 249-256 (2012).
170. Xin, H. et al. Exosome-mediated transfer of miR-133b from multipotent mesenchymal stromal cells to neural cells contributes to neurite outgrowth. *Stem Cells* **30**, 1556-1564 (2012).
171. Lou, G. et al. Exosomes derived from miR-122-modified adipose tissue-derived MSCs increase chemosensitivity of hepatocellular carcinoma. *J Hematol Oncol* **8**, 122 (2015).
172. Mittelbrunn, M. et al. Unidirectional transfer of microRNA-loaded exosomes from T cells to antigen-presenting cells. *Nat Commun* **2**, 282 (2011).
173. Moghadasi, S. et al. A paradigm shift in cell-free approach: the emerging role of MSCs-derived exosomes in regenerative medicine. *J Transl Med* **19**, 302 (2021).
174. Tieu, A. et al. An Analysis of Mesenchymal Stem Cell-Derived Extracellular Vesicles for Preclinical Use. *ACS Nano* **14**, 9728-9743 (2020).
175. Zhang, G. et al. Mesenchymal Stromal Cell-Derived Extracellular Vesicles Protect Against Acute Kidney Injury Through Anti-Oxidation by Enhancing Nrf2/ARE Activation in Rats. *Kidney Blood Press Res* **41**, 119-128 (2016).
176. Eirin, A. et al. Mesenchymal stem cell-derived extracellular vesicles attenuate kidney inflammation. *Kidney Int* **92**, 114-124 (2017).
177. Mardpour, S. et al. Hydrogel-Mediated Sustained Systemic Delivery of Mesenchymal Stem Cell-Derived Extracellular Vesicles Improves Hepatic Regeneration in Chronic Liver Failure. *ACS Appl Mater Interfaces* **11**, 37421-37433 (2019).
178. Li, J.W., Wei, L., Han, Z. & Chen, Z. Mesenchymal stromal cells-derived exosomes alleviate ischemia/reperfusion injury in mouse lung by transporting anti-apoptotic miR-21-5p. *Eur J Pharmacol* **852**, 68-76 (2019).
179. Doeppner, T.R. et al. Extracellular Vesicles Improve Post-Stroke Neuroregeneration and Prevent Postischemic Immunosuppression. *Stem Cells Transl Med* **4**, 1131-1143 (2015).
180. Wiklander, O.P. et al. Extracellular vesicle in vivo biodistribution is determined by cell source, route of administration and targeting. *J Extracell Vesicles* **4**, 26316 (2015).
181. Kamerkar, S. et al. Exosomes facilitate therapeutic targeting of oncogenic KRAS in pancreatic cancer. *Nature* **546**, 498-503 (2017).

182. Alvarez-Erviti, L. et al. Delivery of siRNA to the mouse brain by systemic injection of targeted exosomes. *Nat Biotechnol* **29**, 341-345 (2011).
183. Saleh, A.F. et al. Extracellular vesicles induce minimal hepatotoxicity and immunogenicity. *Nanoscale* **11**, 6990-7001 (2019).
184. Sun, L. et al. Safety evaluation of exosomes derived from human umbilical cord mesenchymal stromal cell. *Cytotherapy* **18**, 413-422 (2016).
185. Zhu, X. et al. Comprehensive toxicity and immunogenicity studies reveal minimal effects in mice following sustained dosing of extracellular vesicles derived from HEK293T cells. *J Extracell Vesicles* **6**, 1324730 (2017).
186. Matsuda, A. et al. Safety of bovine milk derived extracellular vesicles used for delivery of RNA therapeutics in zebrafish and mice. *J Appl Toxicol* **40**, 706-718 (2020).
187. Mendt, M. et al. Generation and testing of clinical-grade exosomes for pancreatic cancer. *JCI Insight* **3** (2018).
188. Ingato, D., Edson, J.A., Zakharian, M. & Kwon, Y.J. Cancer Cell-Derived, Drug-Loaded Nanovesicles Induced by Sulfhydryl-Blocking for Effective and Safe Cancer Therapy. *ACS Nano* **12**, 9568-9577 (2018).
189. Carobolante, G., Mantaj, J., Ferrari, E. & Vllasaliu, D. Cow Milk and Intestinal Epithelial Cell-derived Extracellular Vesicles as Systems for Enhancing Oral Drug Delivery. *Pharmaceutics* **12** (2020).
190. Didiot, M.C. et al. Exosome-mediated Delivery of Hydrophobically Modified siRNA for Huntingtin mRNA Silencing. *Mol Ther* **24**, 1836-1847 (2016).
191. Haraszti, R.A. et al. Optimized Cholesterol-siRNA Chemistry Improves Productive Loading onto Extracellular Vesicles. *Mol Ther* **26**, 1973-1982 (2018).
192. Liao, K. et al. Intranasal Delivery of lincRNA-Cox2 siRNA Loaded Extracellular Vesicles Decreases Lipopolysaccharide-Induced Microglial Proliferation in Mice. *J Neuroimmune Pharmacol* **15**, 390-399 (2020).
193. Xu, L. et al. Exosome-mediated RNAi of PAK4 prolongs survival of pancreatic cancer mouse model after loco-regional treatment. *Biomaterials* **264**, 120369 (2021).
194. Surana, R. et al. Phase I study of mesenchymal stem cell (MSC)-derived exosomes with KRASG12D siRNA in patients with metastatic pancreatic cancer harboring a KRASG12D mutation. *Journal of Clinical Oncology* **40**, TPS633-TPS633 (2022).
195. Kooijmans, S.A.A. et al. Electroporation-induced siRNA precipitation obscures the efficiency of siRNA loading into extracellular vesicles. *J Control Release* **172**, 229-238 (2013).
196. McCann, J. et al. Contaminating transfection complexes can masquerade as small extracellular vesicles and impair their delivery of RNA. *J Extracell Vesicles* **11**, e12220 (2022).
197. Zhou, Y. et al. Tumor-specific delivery of KRAS siRNA with iRGD-exosomes efficiently inhibits tumor growth. *ExRNA* **1**, 28 (2019).
198. Zhang, Q. et al. Exosome-Delivered c-Met siRNA Could Reverse Chemoresistance to Cisplatin in Gastric Cancer. *Int J Nanomedicine* **15**, 2323-2335 (2020).
199. Chevillet, J.R. et al. Quantitative and stoichiometric analysis of the microRNA content of exosomes. *Proc Natl Acad Sci U S A* **111**, 14888-14893 (2014).
200. Kim, M. et al. MIR144 and MIR451 regulate human erythropoiesis via RAB14. *Br J Haematol* **168**, 583-597 (2015).

201. Rasmussen, K.D. et al. The miR-144/451 locus is required for erythroid homeostasis. *J Exp Med* **207**, 1351-1358 (2010).
202. Patrick, D.M. et al. Defective erythroid differentiation in miR-451 mutant mice mediated by 14-3-3zeta. *Genes Dev* **24**, 1614-1619 (2010).
203. de Rie, D. et al. An integrated expression atlas of miRNAs and their promoters in human and mouse. *Nat Biotechnol* **35**, 872-878 (2017).
204. Grant, J.S. et al. Transient but not genetic loss of miR-451 is protective in the development of pulmonary arterial hypertension. *Pulm Circ* **3**, 840-850 (2013).
205. Wang, X. et al. Loss of the miR-144/451 cluster impairs ischaemic preconditioning-mediated cardioprotection by targeting Rac-1. *Cardiovasc Res* **94**, 379-390 (2012).
206. Cifuentes, D. et al. A novel miRNA processing pathway independent of Dicer requires Argonaute2 catalytic activity. *Science* **328**, 1694-1698 (2010).
207. Cheloufi, S., Dos Santos, C.O., Chong, M.M. & Hannon, G.J. A dicer-independent miRNA biogenesis pathway that requires Ago catalysis. *Nature* **465**, 584-589 (2010).
208. Yang, J.S. et al. Conserved vertebrate mir-451 provides a platform for Dicer-independent, Ago2-mediated microRNA biogenesis. *Proc Natl Acad Sci U S A* **107**, 15163-15168 (2010).
209. Freedman, B.I. et al. Differential effects of MYH9 and APOL1 risk variants on FRMD3 Association with Diabetic ESRD in African Americans. *PLoS Genet* **7**, e1002150 (2011).
210. Yusuf, A.A., Govender, M.A., Brandenburg, J.T. & Winkler, C.A. Kidney disease and APOL1. *Hum Mol Genet* **30**, R129-r137 (2021).
211. Winn, M.P. et al. A mutation in the TRPC6 cation channel causes familial focal segmental glomerulosclerosis. *Science* **308**, 1801-1804 (2005).
212. Hall, G., Wang, L. & Spurney, R.F. TRPC Channels in Proteinuric Kidney Diseases. *Cells* **9** (2019).
213. Reiser, J. et al. TRPC6 is a glomerular slit diaphragm-associated channel required for normal renal function. *Nat Genet* **37**, 739-744 (2005).
214. Aghajan, M. et al. Antisense oligonucleotide treatment ameliorates IFN-γ-induced proteinuria in APOL1-transgenic mice. *JCI Insight* **4** (2019).
215. Yang, Y.W. et al. Antisense oligonucleotides ameliorate kidney dysfunction in podocyte-specific APOL1 risk variant mice. *Mol Ther* (2022).
216. Eckel, J. et al. TRPC6 enhances angiotensin II-induced albuminuria. *J Am Soc Nephrol* **22**, 526-535 (2011).
217. Whitehead, K.A., Langer, R. & Anderson, D.G. Knocking down barriers: advances in siRNA delivery. *Nat Rev Drug Discov* **8**, 129-138 (2009).
218. Gilleron, J. et al. Image-based analysis of lipid nanoparticle-mediated siRNA delivery, intracellular trafficking and endosomal escape. *Nat Biotechnol* **31**, 638-646 (2013).
219. Masciopinto, F. et al. Association of hepatitis C virus envelope proteins with exosomes. *Eur J Immunol* **34**, 2834-2842 (2004).
220. Baj-Krzyworzeka, M. et al. Tumour-derived microvesicles carry several surface determinants and mRNA of tumour cells and transfer some of these determinants to monocytes. *Cancer Immunol Immunother* **55**, 808-818 (2006).
221. Ratajczak, J. et al. Embryonic stem cell-derived microvesicles reprogram hematopoietic progenitors: evidence for horizontal transfer of mRNA and protein delivery. *Leukemia* **20**, 847-856 (2006).

222. Skog, J. et al. Glioblastoma microvesicles transport RNA and proteins that promote tumour growth and provide diagnostic biomarkers. *Nat Cell Biol* **10**, 1470-1476 (2008).
223. Yang, J.S. & Lai, E.C. Alternative miRNA biogenesis pathways and the interpretation of core miRNA pathway mutants. *Mol Cell* **43**, 892-903 (2011).
224. Stevanato, L., Thanabalasundaram, L., Vysokov, N. & Sinden, J.D. Investigation of Content, Stoichiometry and Transfer of miRNA from Human Neural Stem Cell Line Derived Exosomes. *PLoS One* **11**, e0146353 (2016).
225. Shelke, G.V., Lässer, C., Gho, Y.S. & Lötvall, J. Importance of exosome depletion protocols to eliminate functional and RNA-containing extracellular vesicles from fetal bovine serum. *J Extracell Vesicles* **3** (2014).
226. Wei, Z., Batagov, A.O., Carter, D.R. & Krichevsky, A.M. Fetal Bovine Serum RNA Interferes with the Cell Culture derived Extracellular RNA. *Sci Rep* **6**, 31175 (2016).
227. McKenzie, A.J. et al. KRAS-MEK Signaling Controls Ago2 Sorting into Exosomes. *Cell Rep* **15**, 978-987 (2016).
228. Melo, S.A. et al. Cancer exosomes perform cell-independent microRNA biogenesis and promote tumorigenesis. *Cancer Cell* **26**, 707-721 (2014).
229. Eldh, M., Lötvall, J., Malmhäll, C. & Ekström, K. Importance of RNA isolation methods for analysis of exosomal RNA: evaluation of different methods. *Mol Immunol* **50**, 278-286 (2012).
230. Meerson, A. & Ploug, T. Assessment of six commercial plasma small RNA isolation kits using qRT-PCR and electrophoretic separation: higher recovery of microRNA following ultracentrifugation. *Biol Methods Protoc* **1**, bpw003 (2016).
231. Gantier, M.P. et al. Analysis of microRNA turnover in mammalian cells following Dicer1 ablation. *Nucleic Acids Res* **39**, 5692-5703 (2011).
232. Bartlett, D.W. & Davis, M.E. Insights into the kinetics of siRNA-mediated gene silencing from live-cell and live-animal bioluminescent imaging. *Nucleic Acids Res* **34**, 322-333 (2006).
233. Furuyama, K. et al. Continuous cell supply from a Sox9-expressing progenitor zone in adult liver, exocrine pancreas and intestine. *Nat Genet* **43**, 34-41 (2011).
234. Bobrie, A., Colombo, M., Krumeich, S., Raposo, G. & Thery, C. Diverse subpopulations of vesicles secreted by different intracellular mechanisms are present in exosome preparations obtained by differential ultracentrifugation. *J Extracell Vesicles* **1** (2012).
235. Kowal, J. et al. Proteomic comparison defines novel markers to characterize heterogeneous populations of extracellular vesicle subtypes. *Proc Natl Acad Sci U S A* **113**, E968-977 (2016).
236. Théry, C., Amigorena, S., Raposo, G. & Clayton, A. Isolation and characterization of exosomes from cell culture supernatants and biological fluids. *Curr Protoc Cell Biol* **Chapter 3**, Unit 3.22 (2006).
237. Okabe, M., Ikawa, M., Kominami, K., Nakanishi, T. & Nishimune, Y. 'Green mice' as a source of ubiquitous green cells. *FEBS Lett* **407**, 313-319 (1997).
238. Gurney, M.E. et al. Motor neuron degeneration in mice that express a human Cu,Zn superoxide dismutase mutation. *Science* **264**, 1772-1775 (1994).
239. Miller, V.M., Gouvion, C.M., Davidson, B.L. & Paulson, H.L. Targeting Alzheimer's disease genes with RNA interference: an efficient strategy for silencing mutant alleles. *Nucleic Acids Res* **32**, 661-668 (2004).

240. Foust, K.D. et al. Therapeutic AAV9-mediated suppression of mutant SOD1 slows disease progression and extends survival in models of inherited ALS. *Mol Ther* **21**, 2148-2159 (2013).
241. Lin, X. et al. A robust in vivo positive-readout system for monitoring siRNA delivery to xenograft tumors. *Rna* **17**, 603-612 (2011).
242. Taylor, S.C., Carbonneau, J., Shelton, D.N. & Boivin, G. Optimization of Droplet Digital PCR from RNA and DNA extracts with direct comparison to RT-qPCR: Clinical implications for quantification of Oseltamivir-resistant subpopulations. *J Virol Methods* **224**, 58-66 (2015).
243. Love, K.T. et al. Lipid-like materials for low-dose, in vivo gene silencing. *Proc Natl Acad Sci U S A* **107**, 1864-1869 (2010).
244. Webster, A.C., Nagler, E.V., Morton, R.L. & Masson, P. Chronic Kidney Disease. *Lancet* **389**, 1238-1252 (2017).
245. Kalantar-Zadeh, K., Jafar, T.H., Nitsch, D., Neuen, B.L. & Perkovic, V. Chronic kidney disease. *Lancet* **398**, 786-802 (2021).
246. Global, regional, and national burden of chronic kidney disease, 1990-2017: a systematic analysis for the Global Burden of Disease Study 2017. *Lancet* **395**, 709-733 (2020).
247. Rosenberg, A.Z. & Kopp, J.B. Focal Segmental Glomerulosclerosis. *Clin J Am Soc Nephrol* **12**, 502-517 (2017).
248. Xie, X. et al. Renin-Angiotensin System Inhibitors and Kidney and Cardiovascular Outcomes in Patients With CKD: A Bayesian Network Meta-analysis of Randomized Clinical Trials. *Am J Kidney Dis* **67**, 728-741 (2016).
249. Beckerman, P. et al. Transgenic expression of human APOL1 risk variants in podocytes induces kidney disease in mice. *Nat Med* **23**, 429-438 (2017).
250. Guo, W. et al. Structural mechanism of human TRPC3 and TRPC6 channel regulation by their intracellular calcium-binding sites. *Neuron* **110**, 1023-1035.e1025 (2022).
251. Brown, B.J., Boekell, K.L., Stotter, B.R., Talbot, B.E. & Schlondorff, J.S. Gain-of-function, focal segmental glomerulosclerosis Trpc6 mutation minimally affects susceptibility to renal injury in several mouse models. *bioRxiv*, 2022.2002.2011.479954 (2022).
252. Canales, C.P. et al. Characterization of a Trpc6 Transgenic Mouse Associated with Early Onset FSGS. *Br J Med Med Res* **5**, 1198-2012 (2015).
253. Möller, C.C. et al. Induction of TRPC6 channel in acquired forms of proteinuric kidney disease. *J Am Soc Nephrol* **18**, 29-36 (2007).
254. Staffel, J. et al. Natriuretic Peptide Receptor Guanylyl Cyclase-A in Podocytes is Renoprotective but Dispensable for Physiologic Renal Function. *J Am Soc Nephrol* **28**, 260-277 (2017).
255. Henry, S.P. et al. (2007).
256. Scott, L.J. Givosiran: First Approval. *Drugs* **80**, 335-339 (2020).
257. van Poelgeest, E.P. et al. Acute kidney injury during therapy with an antisense oligonucleotide directed against PCSK9. *Am J Kidney Dis* **62**, 796-800 (2013).
258. Reshke, R. et al. Reduction of the therapeutic dose of silencing RNA by packaging it in extracellular vesicles via a pre-microRNA backbone. *Nat Biomed Eng* **4**, 52-68 (2020).
259. Sharma, V. & McNeill, J.H. To scale or not to scale: the principles of dose extrapolation. *Br J Pharmacol* **157**, 907-921 (2009).

260. Tóth, E. et al. Formation of a protein corona on the surface of extracellular vesicles in blood plasma. *J Extracell Vesicles* **10**, e12140 (2021).
261. Wolf, M. et al. A functional corona around extracellular vesicles enhances angiogenesis during skin regeneration and signals in immune cells. *bioRxiv*, 808808 (2021).
262. Segura, E., Guérin, C., Hogg, N., Amigorena, S. & Théry, C. CD8+ dendritic cells use LFA-1 to capture MHC-peptide complexes from exosomes in vivo. *J Immunol* **179**, 1489-1496 (2007).
263. Pisitkun, T., Shen, R.F. & Knepper, M.A. Identification and proteomic profiling of exosomes in human urine. *Proc Natl Acad Sci U S A* **101**, 13368-13373 (2004).
264. Zhu, Q. et al. The genetic source tracking of human urinary exosomes. *Proc Natl Acad Sci U S A* **118** (2021).
265. Tsai, P.S. et al. Correlations of neuronal and microvascular densities in murine cortex revealed by direct counting and colocalization of nuclei and vessels. *J Neurosci* **29**, 14553-14570 (2009).
266. Lindström, N.O. et al. Conserved and Divergent Features of Human and Mouse Kidney Organogenesis. *J Am Soc Nephrol* **29**, 785-805 (2018).
267. Jameson, S.C. & Masopust, D. What Is the Predictive Value of Animal Models for Vaccine Efficacy in Humans? Reevaluating the Potential of Mouse Models for the Human Immune System. *Cold Spring Harb Perspect Biol* **10** (2018).
268. Hinderer, C. et al. Severe Toxicity in Nonhuman Primates and Piglets Following High-Dose Intravenous Administration of an Adeno-Associated Virus Vector Expressing Human SMN. *Hum Gene Ther* **29**, 285-298 (2018).
269. Chen, N., Sun, K., Chemuturi, N.V., Cho, H. & Xia, C.Q. The Perspective of DMPK on Recombinant Adeno-Associated Virus-Based Gene Therapy: Past Learning, Current Support, and Future Contribution. *Aaps j* **24**, 31 (2022).
270. Zitvogel, L. et al. Eradication of established murine tumors using a novel cell-free vaccine: dendritic cell-derived exosomes. *Nat Med* **4**, 594-600 (1998).
271. Damas, P. et al. Cytokine serum level during severe sepsis in human IL-6 as a marker of severity. *Ann Surg* **215**, 356-362 (1992).
272. Voit, T. et al. Safety and efficacy of drisapersen for the treatment of Duchenne muscular dystrophy (DEMAND II): an exploratory, randomised, placebo-controlled phase 2 study. *Lancet Neurol* **13**, 987-996 (2014).
273. Janas, M.M. et al. The Nonclinical Safety Profile of GalNAc-conjugated RNAi Therapeutics in Subacute Studies. *Toxicol Pathol* **46**, 735-745 (2018).
274. Zhang, H.T. et al. The mTORC2/Akt/NFκB Pathway-Mediated Activation of TRPC6 Participates in Adriamycin-Induced Podocyte Apoptosis. *Cell Physiol Biochem* **40**, 1079-1093 (2016).
275. Zhang, L., Chen, X.P., Qin, H., Jiang, L. & Qin, Y.H. ATRA attenuate proteinuria via downregulation of TRPC6 in glomerulosclerosis rats induced by adriamycin. *Ren Fail* **40**, 266-272 (2018).
276. Lee, V.W. & Harris, D.C. Adriamycin nephropathy: a model of focal segmental glomerulosclerosis. *Nephrology (Carlton)* **16**, 30-38 (2011).
277. DeVos, S.L. et al. Tau reduction prevents neuronal loss and reverses pathological tau deposition and seeding in mice with tauopathy. *Sci Transl Med* **9** (2017).
278. Murphy, D.E. et al. Natural or Synthetic RNA Delivery: A Stoichiometric Comparison of Extracellular Vesicles and Synthetic Nanoparticles. *Nano Lett* **21**, 1888-1895 (2021).

279. Sviben, D., Forčić, D., Kurtović, T., Halassy, B. & Brgles, M. Stability, biophysical properties and effect of ultracentrifugation and diafiltration on measles virus and mumps virus. *Arch Virol* **161**, 1455-1467 (2016).
280. Burns, J.C., Friedmann, T., Driever, W., Burrascano, M. & Yee, J.K. Vesicular stomatitis virus G glycoprotein pseudotyped retroviral vectors: concentration to very high titer and efficient gene transfer into mammalian and nonmammalian cells. *Proc Natl Acad Sci U S A* **90**, 8033-8037 (1993).
281. Mestas, J. & Hughes, C.C. Of mice and not men: differences between mouse and human immunology. *J Immunol* **172**, 2731-2738 (2004).
282. Zhao, Z., Wijerathne, H., Godwin, A.K. & Soper, S.A. Isolation and analysis methods of extracellular vesicles (EVs). *Extracell Vesicles Circ Nucl Acids* **2**, 80-103 (2021).
283. Li, Y. & Boraschi, D. Endotoxin contamination: a key element in the interpretation of nanosafety studies. *Nanomedicine (Lond)* **11**, 269-287 (2016).
284. LeClaire, M., Gimzewski, J. & Sharma, S. A review of the biomechanical properties of single extracellular vesicles. *Nano Select* **2**, 1-15 (2021).
285. Colella, P., Ronzitti, G. & Mingozzi, F. Emerging Issues in AAV-Mediated In Vivo Gene Therapy. *Mol Ther Methods Clin Dev* **8**, 87-104 (2018).
286. Wu, J. et al. APOL1 risk variants in individuals of African genetic ancestry drive endothelial cell defects that exacerbate sepsis. *Immunity* **54**, 2632-2649.e2636 (2021).
287. Wu, J. et al. The key role of NLRP3 and STING in APOL1-associated podocytopathy. *J Clin Invest* **131** (2021).
288. Hesketh, E.E. et al. A murine model of irreversible and reversible unilateral ureteric obstruction. *J Vis Exp* (2014).
289. Dooley, K. et al. A versatile platform for generating engineered extracellular vesicles with defined therapeutic properties. *Mol Ther* **29**, 1729-1743 (2021).
290. Wang, F. et al. RNAscope: a novel in situ RNA analysis platform for formalin-fixed, paraffin-embedded tissues. *J Mol Diagn* **14**, 22-29 (2012).
291. D'Agati, V.D., Kaskel, F.J. & Falk, R.J. Focal segmental glomerulosclerosis. *N Engl J Med* **365**, 2398-2411 (2011).
292. Lam, J.K., Chow, M.Y., Zhang, Y. & Leung, S.W. siRNA Versus miRNA as Therapeutics for Gene Silencing. *Mol Ther Nucleic Acids* **4**, e252 (2015).
293. Terlecki-Zaniewicz, L. et al. Small extracellular vesicles and their miRNA cargo are anti-apoptotic members of the senescence-associated secretory phenotype. *Aging (Albany NY)* **10**, 1103-1132 (2018).
294. Ohno, S. et al. Systemically injected exosomes targeted to EGFR deliver antitumor microRNA to breast cancer cells. *Mol Ther* **21**, 185-191 (2013).
295. Mahati, S., Fu, X., Ma, X., Zhang, H. & Xiao, L. Delivery of miR-26a Using an Exosomes-Based Nanosystem Inhibited Proliferation of Hepatocellular Carcinoma. *Front Mol Biosci* **8**, 738219 (2021).
296. Yanshina, D.D. et al. Structural features of the interaction of the 3'-untranslated region of mRNA containing exosomal RNA-specific motifs with YB-1, a potential mediator of mRNA sorting. *Biochimie* **144**, 134-143 (2018).
297. Palma, J. et al. MicroRNAs are exported from malignant cells in customized particles. *Nucleic Acids Res* **40**, 9125-9138 (2012).

298. Hagiwara, K., Katsuda, T., Gailhouste, L., Kosaka, N. & Ochiya, T. Commitment of Annexin A2 in recruitment of microRNAs into extracellular vesicles. *FEBS Lett* **589**, 4071-4078 (2015).
299. Das, A. et al. Inhibition of extracellular vesicle-associated MMP2 abrogates intercellular hepatic miR-122 transfer to liver macrophages and curtails inflammation. *iScience* **24**, 103428 (2021).
300. Gruber, A.R., Lorenz, R., Bernhart, S.H., Neuböck, R. & Hofacker, I.L. The Vienna RNA websuite. *Nucleic Acids Res* **36**, W70-74 (2008).
301. Engels, B., Jannot, G., Remenyi, J., Simard, M.J. & Hutvagner, G. Polypyrimidine tract binding protein (hnRNP I) is possibly a conserved modulator of miRNA-mediated gene regulation. *PLoS One* **7**, e33144 (2012).
302. Peredo, J., Villacé, P., Ortín, J. & de Lucas, S. Human Staufen1 associates to miRNAs involved in neuronal cell differentiation and is required for correct dendritic formation. *PLoS One* **9**, e113704 (2014).
303. Filippou, P.S., Karagiannis, G.S. & Constantinidou, A. Midkine (MDK) growth factor: a key player in cancer progression and a promising therapeutic target. *Oncogene* **39**, 2040-2054 (2020).
304. Ross-Munro, E. et al. Midkine: The Who, What, Where, and When of a Promising Neurotrophic Therapy for Perinatal Brain Injury. *Front Neurol* **11**, 568814 (2020).
305. Xu, C., Zhu, S., Wu, M., Han, W. & Yu, Y. Functional receptors and intracellular signal pathways of midkine (MK) and pleiotrophin (PTN). *Biol Pharm Bull* **37**, 511-520 (2014).
306. Kadomatsu, K., Kishida, S. & Tsubota, S. The heparin-binding growth factor midkine: the biological activities and candidate receptors. *J Biochem* **153**, 511-521 (2013).
307. Shayista Akbar and Shahnaz Qadri and Sarmadia Ashraf and Aijaz Parray and Afsheen Raza and Wafa Abualainin and Said Dermime and Yousef, H. Expression of CD91 in extracellular vesicles: A potential biomarker for the diagnosis of non-small cell lung cancer. *Advances in Cancer Biology - Metastasis* **4**, 100046 (2022).
308. Shibata, Y. et al. Nuclear targeting by the growth factor midkine. *Mol Cell Biol* **22**, 6788-6796 (2002).
309. Suzuki, N. et al. Proteasomal degradation of the nuclear targeting growth factor midkine. *J Biol Chem* **279**, 17785-17791 (2004).
310. Said, E.A. et al. The anti-HIV cytokine midkine binds the cell surface-expressed nucleolin as a low affinity receptor. *J Biol Chem* **277**, 37492-37502 (2002).
311. Dai, L.C. et al. Midkine accumulated in nucleolus of HepG2 cells involved in rRNA transcription. *World J Gastroenterol* **14**, 6249-6253 (2008).
312. Xia, T. et al. Midkine noncanonically suppresses AMPK activation through disrupting the LKB1-STRAD-Mo25 complex. *Cell Death Dis* **13**, 414 (2022).
313. Ince-Dunn, G. et al. Neuronal Elav-like (Hu) proteins regulate RNA splicing and abundance to control glutamate levels and neuronal excitability. *Neuron* **75**, 1067-1080 (2012).
314. Cook, K.B. et al. RNAcompete-S: Combined RNA sequence/structure preferences for RNA binding proteins derived from a single-step in vitro selection. *Methods* **126**, 18-28 (2017).
315. Brannan, K.W. et al. SONAR Discovers RNA-Binding Proteins from Analysis of Large-Scale Protein-Protein Interactomes. *Mol Cell* **64**, 282-293 (2016).

316. Iwasaki, W. et al. Solution structure of midkine, a new heparin-binding growth factor. *Embo j* **16**, 6936-6946 (1997).
317. Muramatsu, T. Structure and function of midkine as the basis of its pharmacological effects. *Br J Pharmacol* **171**, 814-826 (2014).
318. Terribilini, M. et al. Prediction of RNA binding sites in proteins from amino acid sequence. *Rna* **12**, 1450-1462 (2006).
319. Ukmar-Godec, T. et al. Lysine/RNA-interactions drive and regulate biomolecular condensation. *Nat Commun* **10**, 2909 (2019).
320. Jolma, A. et al. Binding specificities of human RNA-binding proteins toward structured and linear RNA sequences. *Genome Res* **30**, 962-973 (2020).
321. Corley, M., Burns, M.C. & Yeo, G.W. How RNA-Binding Proteins Interact with RNA: Molecules and Mechanisms. *Mol Cell* **78**, 9-29 (2020).
322. Salama, R.H. et al. Midkine binds to 37-kDa laminin binding protein precursor, leading to nuclear transport of the complex. *Exp Cell Res* **270**, 13-20 (2001).
323. Take, M. et al. Identification of nucleolin as a binding protein for midkine (MK) and heparin-binding growth associated molecule (HB-GAM). *J Biochem* **116**, 1063-1068 (1994).
324. Gratton, J.P. et al. Cell-permeable peptides improve cellular uptake and therapeutic gene delivery of replication-deficient viruses in cells and in vivo. *Nat Med* **9**, 357-362 (2003).
325. Su, Y., Doherty, T., Waring, A.J., Ruchala, P. & Hong, M. Roles of arginine and lysine residues in the translocation of a cell-penetrating peptide from (13)C, (31)P, and (19)F solid-state NMR. *Biochemistry* **48**, 4587-4595 (2009).
326. Chen, Y., Li, S., Zhao, J., Cao, X. & Wang, F. Efficient drug delivery by novel cell-penetrating peptide derived from Midkine, with two heparin binding sites braced by a length-specific helix. *J Drug Target* **30**, 326-333 (2022).
327. Breyne, K. et al. Exogenous loading of extracellular vesicles, virus-like particles, and lentiviral vectors with supercharged proteins. *Commun Biol* **5**, 485 (2022).
328. Fitzgerald, W. et al. A System of Cytokines Encapsulated in ExtraCellular Vesicles. *Sci Rep* **8**, 8973 (2018).
329. Cox, J. & Mann, M. MaxQuant enables high peptide identification rates, individualized p.p.b.-range mass accuracies and proteome-wide protein quantification. *Nat Biotechnol* **26**, 1367-1372 (2008).
330. Huppertz, I. et al. iCLIP: protein-RNA interactions at nucleotide resolution. *Methods* **65**, 274-287 (2014).
331. Tritschler, F. et al. DCP1 forms asymmetric trimers to assemble into active mRNA decapping complexes in metazoa. *Proc Natl Acad Sci U S A* **106**, 21591-21596 (2009).
332. Heusermann, W. et al. Exosomes surf on filopodia to enter cells at endocytic hot spots, traffic within endosomes, and are targeted to the ER. *J Cell Biol* **213**, 173-184 (2016).
333. Foster, D.J. et al. Advanced siRNA Designs Further Improve In Vivo Performance of GalNAc-siRNA Conjugates. *Mol Ther* **26**, 708-717 (2018).
334. Shen, W., Liang, X.H., Sun, H. & Crooke, S.T. 2'-Fluoro-modified phosphorothioate oligonucleotide can cause rapid degradation of P54nrb and PSF. *Nucleic Acids Res* **43**, 4569-4578 (2015).
335. Xue, W. et al. Small RNA combination therapy for lung cancer. *Proc Natl Acad Sci U S A* **111**, E3553-3561 (2014).

336. Lakkis, F.G. & Lechler, R.I. Origin and biology of the allogeneic response. *Cold Spring Harb Perspect Med* **3** (2013).
337. Elsharkasy, O.M. et al. Extracellular vesicles as drug delivery systems: Why and how? *Adv Drug Deliv Rev* **159**, 332-343 (2020).
338. Robbins, P.D. & Morelli, A.E. Regulation of immune responses by extracellular vesicles. *Nat Rev Immunol* **14**, 195-208 (2014).
339. Dai, S. et al. Phase I clinical trial of autologous ascites-derived exosomes combined with GM-CSF for colorectal cancer. *Mol Ther* **16**, 782-790 (2008).
340. Antoni, D., Burckel, H., Josset, E. & Noel, G. Three-dimensional cell culture: a breakthrough in vivo. *Int J Mol Sci* **16**, 5517-5527 (2015).
341. Patel, D.B., Luthers, C.R., Lerman, M.J., Fisher, J.P. & Jay, S.M. Enhanced extracellular vesicle production and ethanol-mediated vascularization bioactivity via a 3D-printed scaffold-perfusion bioreactor system. *Acta Biomater* **95**, 236-244 (2019).
342. Witwer, K.W. et al. Standardization of sample collection, isolation and analysis methods in extracellular vesicle research. *J Extracell Vesicles* **2** (2013).
343. Bosch, S. et al. Trehalose prevents aggregation of exosomes and cryodamage. *Sci Rep* **6**, 36162 (2016).
344. Daneman, R. & Prat, A. The blood-brain barrier. *Cold Spring Harb Perspect Biol* **7**, a020412 (2015).
345. Pardridge, W.M. The blood-brain barrier: bottleneck in brain drug development. *NeuroRx* **2**, 3-14 (2005).
346. Daehn, I.S. & Duffield, J.S. The glomerular filtration barrier: a structural target for novel kidney therapies. *Nat Rev Drug Discov* **20**, 770-788 (2021).
347. Liu, Y. et al. Targeted exosome-mediated delivery of opioid receptor Mu siRNA for the treatment of morphine relapse. *Sci Rep* **5**, 17543 (2015).
348. Tian, Y. et al. A doxorubicin delivery platform using engineered natural membrane vesicle exosomes for targeted tumor therapy. *Biomaterials* **35**, 2383-2390 (2014).
349. Liang, Y., Duan, L., Lu, J. & Xia, J. Engineering exosomes for targeted drug delivery. *Theranostics* **11**, 3183-3195 (2021).